DESIGN AND DEVELOPMENT OF MODIFIED SELF-COMMUTATING CSI-FED INDUCTION MOTOR DRIVE

A THESIS

Submitted in fulfilment of the
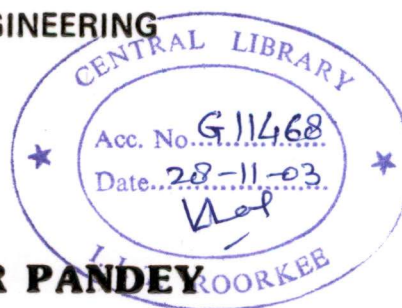*requirements for the award of the degree*
of

DOCTOR OF PHILOSOPHY

in

ELECTRICAL ENGINEERING

By

ASHOK KUMAR PANDEY

DEPARTMENT OF ELECTRICAL ENGINEERING
INDIAN INSTITUTE OF TECHNOLOGY ROORKEE
ROORKEE–247 667 (INDIA)

JANUARY, 2003

INDIAN INSTITUTE OF TECHNOLOGY ROORKEE
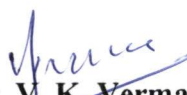## ROORKEE

CANDIDATE'S DECLARATION

I hereby certify that the work which is being presented in the thesis entitled **DESIGN AND DEVELOPMENT OF MODIFIED SELF-COMMUTATING CSI-FED INDUCTION MOTOR DRIVE** in fulfilment of the requirement for the award of the Degree of **Doctor of Philosophy** and submitted in the **Department of Electrical Engineering** of the Institute is an authentic record of my own work carried out during a period from July 1998 to January 2003 under the supervision of **Dr. V. K. Verma**, Professor (Retd.) and **Dr. Pramod Agarwal**, Associate Professor, Department of Electrical Engineering, Indian Institute of Technology Roorkee, Roorkee.
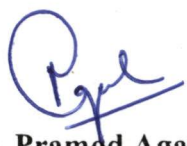
The matter presented in this thesis has not been submitted by me for the award of any other degree of this or any other Institute/University.
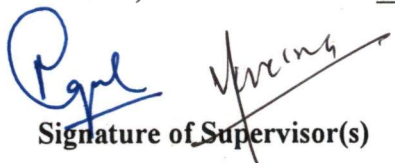
(ASHOK KUMAR PANDEY)

This is to certify that the above statement made by the candidate is correct to the best of my (our) knowledge.
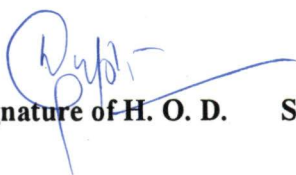
Date : January 3, 2003

(Dr. V. K. Verma)
Professor (Retd.)
EED, IITR

(Dr. Pramod Agarwal)
Associate Professor
EED, IITR

The Ph. D. Viva-Voce examination of **Ashok Kumar Pandey**, Research Scholar, has been held on 10.10.2003.

Signature of Supervisor(s)   Signature of H. O. D.   Signature of External Examiner

ABSTRACT

Variable speed drive is the main requirement of any industry. Among the various AC/DC motors, the statically controlled d.c. motor easily achieves this capability and hence it was a probable choice for the industry. The motor is powered from both d.c.or a.c. supply, and variable d.c. voltage is applied to the armature through chopper or converter, but because of mechanical commutators, high cost, noise and frequent maintenance of carbon brushes; hence these motors are not reliable and economical for industrial applications. Due to these limitations of d.c. drives, a.c. drives have gained preference over the d.c. drives. Among the a.c. drives, variable speed squirrel cage induction motor drive is preferred over the synchronous motor drive, because of its robust construction without slip ring and carbon brushes. Induction motor is having hard torque-slip characteristics; hence only a small range speed control is possible when it is operated from a constant frequency supply. The precise wide range speed control is possible only with the variable frequency a.c. source. With the latest development in the semi-conductor technology, it is easily achieved with the variable frequency power semi controllers. To operate the machine at rated flux, the terminal voltage is also controlled in accordance with the frequency. Variable frequency operation of the induction motor is possible with the help of either voltage source inverter or current source inverter. The current source inverter is having the regeneration capability without an extra cost and it is having inherent over current protection because of its controlled current operation. The conventional CSI-fed induction motor drive line currents are stepped in nature and have dominant low order harmonics. These harmonics give rise to torque pulsation, however the line to line voltage is nearly sinusoidal with transient voltage spikes.

i

To overcome the problem associated with the conventional CSI-fed induction motor drive, lots of work has been carried out such as: implementation of PWM technique in front-end current source as well as in motor- end current source inverter, for better input displacement factor and line currents respectively. PWM operation in front-end converter also reduces the size of d.c.link inductor required.

In the light of above works, a modified self commutating CSI-fed induction motor drive is designed and developed so that the motor line voltages and currents are nearly sinusoidal over the wide range of the speed control, with smooth drive operation. The input supply voltage and current of front-end rectifier is also sinusoidal and hence the size of d.c. link inductor is drastically reduced.

The modified current source inverter fed induction motor drives consists of two converters coupled through a d.c. link inductor. The front-end converter is equal PWM converter and it acts as a current source, with d.c link current feed back. The current source inverter is space vector PWM inverter, and it regulates d.c. link current into a variable frequency a.c. current. Both converter and inverter make use of MOSFET as self-commutating devices. At the terminals of induction motor, a 3-phase capacitor is connected, which removes the harmonics from the machine voltages and currents at almost every operating frequency. For better dynamic characteristics of the drive two PI controllers are used, one in outer speed feed back loop and other in inner current feed back loop. The speed PI controller compares the reference speed with actual speed and sets the reference slip speed ($\omega_{sl}*$). To maintain the motor flux at rated value a slip regulator is also used in the feed back loop. The reference value of stator active current (I_{act}) and the stator reactive current (I_{react}) are obtained, from slip regulator characteristics. These characteristics are obtained experimentally at rated voltage and frequency, by

loading the motor till rated load. Two characteristic curves (I_{act} vs. ω_{sl}) and (I_{react} vs. ω_{sl}) are drawn. These characteristic curves are defined as slip regulator, characteristics in the present work. The synchronous speed is obtained by adding actual speed and reference slip speed. The desired capacitor current (I_c) is calculated at the operating frequency for constant (V/f) control of the drive. The reference values of stator active current, reactive current and capacitor current are used to obtain the reference d.c. link current (I_{ref}). The current PI controller acts on d.c. link current error between reference d.c. link current and actual d.c. link current. The current PI controller sets the T_{on}/T_{off} periods of PWM pulses, of the front-end converter and hence d.c. link voltage for regulating the d.c. link current.

To analyze the performance of drive in steady state and dynamic conditions, a mathematical model of complete drive system is developed in synchronously rotating (q^e - d^e) reference frame, by considering only fundamental component and neglecting the effect of core loss, saturation and switching transients. To study the steady state performance, mathematical expressions are derived for torque developed, power output, stator voltage per phase, stator current per phase, power loss, efficiency, d.c. link voltage. The performance characteristics of the drive are drawn for different operating conditions; (i) Variable capacitance at the motor terminals, fixed operating frequency, fixed d.c. link current. (ii) Fixed capacitance, variable frequency. fixed d.c. link current. (iii) Fixed capacitance, fixed frequency, variable d.c. link current. (iv) Without capacitance at the motor terminals, fixed d.c. link current, variable operating frequency. (v) Fixed capacitance, fixed d.c. link current, fixed load torque. (vi) Fixed capacitance, fixed d.c. link current, linearly varying load torque. The simulated results and practical waveforms decide the value of capacitor, which is to be connected across the motor terminals. With the selected value of capacitance, simulated steady state curves shows that at some value

of frequency resonance is taking place, and hence at the resonance frequency and in the vicinity of resonance frequency experimentation is not possible.

To improve the performance of the front-end converter a 3-phase PWM converter of equal pulse width modulation type is applied, which gives almost ripple free d.c. link current with small d.c. link inductance, and input power factor is almost unity. Firing signals for the converter are generated through a dedicated 8031 micro controller based card, which relives the personal computer for processing the speed and current errors and generation of pulses for the inverter. The control to the pulse width modulated rectifier is applied through the personal computer, which serially communicates with the 8031 micro controller. The personal computer serially send the pulse width information to control the output voltage of the rectifier, and hence current. The 3-phase inverter connected to the PWM rectifier through d.c. link is also pulse width modulated type and firing commands for the PWM operation of inverter are generated using a space vector technique for the different operating frequency ranges. At low value of operating frequency number of crossing points of modulating signal and reference signals are more and at high value of operating frequency the number of crossing points are less, due to the switching frequency consideration of power devices. The firing pulses for pulse width modulated inverter is generated through personal computer using Add on cards. The reference speed is given through keyboard of the personal computer.

The d.c. link current is measured through the Hall effect current sensor, and rotor speed is measured through incremental rotary pulse encoder. The d.c. link current is digitized through A/D converter for processing. The speed error PI processing is carried out at every 10 ms, while the current error PI processing is done at every 1 ms. A timer is used to generate the interrupt at an interval of 1m sec for current and 10 m sec for speed

PI processing respectively. Both PI controllers are implemented through software. The slip regulator characteristics are stored in the memory and used to read the stator active and reactive currents.

The use of PI controllers in the speed loop and current feed back loop improves the dynamic performance of the drive. With the proper design of controller parameters, the response of the system is fast and over shoots within the defined limits of (5% tolerance). Proper design of controllers also enable the drive to over-come external disturbances. For the design of controller parameters D - partitioning technique is used. The inner current loop is designed first and outer speed controller later as the electrical time constant is much smaller than mechanical time constant. The system governing equations are basically non-linear in nature; therefore these equations are linearized using small perturbation method around a steady state operating point. The characteristic equations are derived in terms of the current controller parameters for synthesis. The probable stable region in parametric plane is obtained with the help of D-partitioning technique. The stability of the region is confirmed by frequency scanning. To get the region of better stability, relative stability boundaries are drawn for the different value of (σ and ξ). As these values increase from their minimum values of zero, the better stability regions are achieved which keep on shrinking. After certain values of (σ and ξ) relative stability in parametric plane regions completely vanish. The final selection of current controller parameters is carried out by the transient response of current loop. With the pre-estimated parameters of current controllers, parameters of speed controllers are designed with the help of D-partitioning technique, followed by frequency scanning. Final decision of controller parameters is obtained by the transient response of the complete drive.

The steady state and dynamic performance of the drive is thoroughly investigated in steps. The performance investigation of PWM rectifier is carried out first by operating it alone with R-L load. Various signals, such as zero crossing, quantizers, and firing pulses of switching devices are recorded. Output voltage, output current, input voltage and input current waveforms of rectifier are also recorded at the different duty cycles with R-L loads. Fundamental current is found to be in phase with the input voltage. Performance of PWM inverter is investigated by recording the firing pulses of the devices at the different operating frequencies. Inverter output current, motor current, terminal voltage waveforms, with/without capacitor at the motor terminals are also recorded.

With the selected value of capacitance, extensive experimentation is carried out in open loop as well as closed loop. The open loop experiment is carried out at the various operating frequencies at a fixed value of d.c. link current, and closed loop experiment is carried out at linearly varying load torque on the motor using a coupled dc generator. The experimental open loop and closed loop results are compared with the simulated results. They are quite close to each other, except at the resonance frequency, and in the vicinity of the resonance frequency. The transient performance of the drive is also investigated experimentally for linearly varying load torque on the machine, and it is found to be quite satisfactory.

To summarize a practical model of modified CSI-fed induction motor drive is designed and developed. The equal pulse width modulated technique is employed in the front-end rectifier and space vector PWM technique is employed in the inverter. Firing signals for the converter is generated through a dedicated 8031 micro controller based card, which serially communicates with personal computer. The open loop experiment is carried out at the different operating frequency for a fixed value of d.c. link current and at

the different values of capacitance connected across the motor terminals and the value of capacitor is selected. Various voltages and current waveforms of the inverter and converter are recorded. The line voltages and currents of motor are nearly sinusoidal at each operating speed. The input power factor of the converter is almost unity and the size of coupling d.c. link inductor is drastically reduced.

The mathematical model of complete drive system is developed and steady state analysis of the drive is carried out at different operating conditions. D-partitioning technique is applied to continuous-data drive model to obtain the controller parameters. The closed control of the drive is implemented through personal computer. The performance of the drive is investigated experimentally with the designed controller parameters. Extensive experiments are carried out in the open loop and closed loop. The performance characteristics are drawn at various operating conditions. The experimental results are compared with the simulated results over the wide range of operating speed and they are quite close to each other.

ACKNOWLEDGEMENT

I take this opportunity to express my sincere gratitude towards my guides **Dr. V.K. Verma (Prof. Retd.) and Dr. P. Agarwal (Assoc. Prof.)**, Department of Electrical Engineering, Indian Institute of Technology Roorkee, Roorkee for their guidance, advice, and encouragement, which were the constant source of inspiration for the completion of this research work. Their painstaking support and exhaustive involvement in preparation of manuscript, conduction of the experimental investigations and simulation studies are gratefully acknowledged. I humbly acknowledge a lifetime's gratitude to them.

I express my deep sense of gratitude to Head, Electrical Engineering Department, Indian Institute of Technology Roorkee, for providing the excellent laboratory and computing facilities of the department during my research work.

My sincere thanks are also due to Prof. S.P. Gupta, Prof. S.C. Saxena, Dr. S.P. Srivastava, Dr. R.S. Anand, Dr. Vinay Pant, Dr. R.P. Maheshwari, Mr. Y.P. Singh, Dr. Indra Gupta, Mr. E. Fernandez for useful discussions and providing help in preparing the report.

I acknowledge my sincere gratitude to the Quality Improvement Program of Govt. of India. This work is carried out under this scheme. I thankfully acknowledge my appreciation to Prof. S.C. Handa, Co-ordinator, QIP Centre, Indian Institute of Technology Roorkee for his kind co-operation and support.

I would like to express my sincere thanks to **Dr. P.K. Garg, Assoc. Prof.,** Civil Engg, IIT Roorkee and his wife **Mrs. Seema Garg** for providing the constant help and support during the completion of the work.

I thankfully acknowledge my friends Mr. Rajeev Verma and his wife for extending their support for the completion of this work. My special thanks goes to Mr. Manoj and his wife Mrs. Ashu for providing the necessary support during the completion of this work.
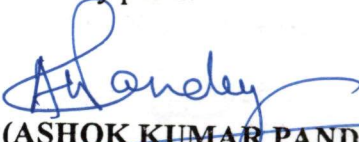
My heartful gratitude and indebtedness are due to my parents for their constant encouragement and blessing.

My special appreciation goes to **Mr. K.N. Pathak, my Father-in-Law** for his keen interest and support rendered to my family members during the completion of this work.

I am specially lucky to get the helping hand from my wife Madhu and kids Akriti, Paribhasha and Ekagra. Even though they have missed me a lot during my research work, they waited patiently for the completion of the work. I appreciate them for their kind cooperation and support extended. No words can adequately express my gratitude to them.

Thanks are also due to those who helped me directly and indirectly in preparing the thesis.

Acknowledge Him in all Thy ways and He shall direct Thy paths.

(ASHOK KUMAR PANDEY)

x

CONTENTS

5. **CONTROL TECHNIQUE AND SOFTWARE DEVELOPMENT**

Symbol	Description
d, q	Direct axis and quardrature axis
i_{as}, i_{bs}, i_{cs}	Line currents of the PWM inverter
v_{ds}^e, i_{ds}^e	Voltage and current in d-axis stator winding in synchronous rotating reference frame
v_{qs}^e, i_{qs}^e	Voltage and current in q-axis stator winding in synchronous rotating reference frame
i_{dr}^e, i_{qr}^e	Current in d axis and q axis of the rotor winding in synchronous rotating reference frame
I_{act}	Active component of stator current
I_{act}^*	Reference active component of stator current
I_{react}	Reactive component of stator current
I_{react}^*	Reference reactive component of stator current
I_s^*	Reference stator current
ω_e	Synchronous speed of the induction motor
ω_r	Rotor speed of induction motor
ω_{sl}	Slip speed of the induction motor
ω_{sl}^*	Reference slip speed
I_c	rms value of capacitor current
θ_e	Angular position of synchronous reference frame
I_{dc}	d.c. link current
t_e	Electromagnetic torque

t_l	Load torque
t_L	Rated load torque
I_{ref}	Reference d.c. link current
K (is a frequency dependent factor)	$= \dfrac{\text{Maximum value of fundamental inverter line current}}{\text{D.C. Link current}\,(I_{dc})}$
V_{inv}	Input voltage of the inverter
I_{inv}	Input current of the inverter
V_r	Rectifier output voltage
r_f	Resistance of d.c. link inductor
l_f	Inductance of d.c. link inductor
l_{ss}, r_s	Self inductance and resistance of stator winding per phase
l_{rr}, r_r	Self inductance and resistance of rotor winding per phase
l_m	Mutual inductance per phase
l_l	$l_s\, l_r - l_m^2$
c	Capacitance per phase
ω_r^*	Reference speed
J	Moment of inertia in kg-m^2
B	Viscous friction coefficient
β	Pulse width of PWM rectifier
V_{LL}	Line to line input voltage of the rectifier
P	No. of poles
i_c	Instantaneous phase current of capacitor
v_s	Instantaneous stator phase voltage
i_{cd}^e	Capacitor current in d axis winding in synchronously rotating reference frame

i_{cq}^e	Capacitor current in q axis winding in synchronously rotating reference frame
k_{p_i}, k_{i_i}	Proportional and integral gains of current controller parameters
k_{p_s}, k_{i_s}	Proportional and integral gains of speed controller parameters
T_{s_s}	Sampling time of speed controller
T_{i_s}	Sampling time of current controller
Suffix 0	Represents a variable in steady state conditions
p	Differential operator d/dt or complex frequency
σ	Degree of relative stability
ξ	Damping ratio
$i_{d(inv)}^e, i_{q(inv)}^e$	Inverter direct axis current and quadrature axis current in synchronously rotating reference frame
ω	Natural frequency
m	Modulation index
PWM	Pulse width modulation
CSI	Current source inverter
VSI	Voltage source inverter
k_1	Slope of stator active current (I_{act}) vs. slip speed (ω_{sl})
k_2	Slope of stator reactive current vs. slip speed (ω_{sl})
k_{11}	$\dfrac{\text{Rated value of capacitor current per phase}}{(\text{Rated angular frequency } (\omega_e))^2}$
ψ_s	Flux linkage of stator winding
ψ_r	Flux linkage of rotor winding
ψ_{sd}, ψ_{sq}	Flux linkages of d - q axes of the stator windings
ψ_{rd}, ψ_{rq}	Flux linkage of d and q axis of the rotor winding

INTRODUCTION

1.1   GENERAL

The most outstanding features of electric drive is their amazing, almost universal, ability to adopt to the widest possible variety of tasks. The spectrum ranges from the miniature mechanism in a wrist watch to the motor in a pumped storage hydroelectric station which is hundred million times powerful; from rolling mill drives running at speeds of about 60 rpm to ultra centrifuges running at 100000 rpm. Unlike internal combustion engines, electric motors are always ready for immediate services and can withstand high over loads for short periods. Since they cause no environmental pollution at the point of use and produce very little vibration or noise, they are ideally suited for integration into production mechanism [1].

Electric motors are the principal workhorse of any electric drives system used in the industrial application. Electric drive system provides a wide speed control range for small as well as large size motors [2]. The rotating electric drive used in most of the industries is either a.c. or d.c. When these motors are operated directly from the normal power supply, the inherent speed torque characteristic of the motor and load torque characteristics decides the operating point. Motors are provided with control equipment, to operate the motor at desired speed demanded by the load. The conventional control techniques are slow, less efficient, limited range of control, noisy, poor transient response, less precise control. The latest demand of the modern industrial drives is fast and smooth speed control, good transient behavior, less maintenance, high efficiency.

With the advances in both power electronics and microelectronics, the electric drives have gained the new dimensions as a variable speed drives in the industrial applications. Static control of the drives have been possible using power semiconductor devices and it is preferred over the conventional control because of the less cost, space saving, elimination of large audio noise, less maintenance, improved reliability, high quality performance [3]. The statically controlled d.c. drives have been widely used as variable speed drives due to easy implementation of torque control loop. The d.c. motor is having a decoupled structure, hence the armature current and field current can be controlled independently. Since at constant air gap flux, torque is proportional to the armature current, fast acting armature current loop gives effective torque control .It also protects the power converter and motor from over current during fast transient and steady state over loads. The speed of the motor can be controlled statically either through phase controlled converters or choppers [4]. Precise and smooth speed control can be obtained, by adoption of closed feed back loops. Inspite of the above advantages, it suffers from the certain disadvantages, such as: higher cost, higher rotor inertia, maintenance problem with carbon brushes and mechanical commutators. Commutators and brushes, in addition, limit the machine speed at peak current, cause EMI problem and do not permit to operate in dirty and explosive environments. Therefore the d.c. motor is not best-suited adjustable speed drive for all the applications in the industries [5].

The induction motor, in particular the squirrel cage induction motor, has many inherent advantages for industrial applications because of its, ruggedness, simplicity, low-inertia rotor, low cost, robust construction, absence of sliding electrical contacts, high power/weight ratio, maintenance free operation, availability in ratings over the wide range, efficient operation, capacity to work in the hazardous environment. Inspite of the

2

above merits, the motor possesses a hard torque speed characteristics, i.e. its speed is almost constant with the torque, and hence it is normally a constant speed machine, and its speed control over a wide range in smooth and step -less manner is a problem. Unlike the d.c. motor, it is having a coupled structure therefore the separate control of the field and armature is not easily possible. Its rotor current cannot be sensed. The researchers have proposed the other methods to meet the requirements. These methods have been discussed in the literature in detail [6- 13].

The draw back of almost constant speed with the load torque associated with the induction motor can be over come by varying the frequency of a.c. power source. Due to rapid growth in the technology of power semiconductor devices in the recent years, static frequency converters are available at easily acceptable prices, therefore by feeding the induction motor through static frequency converters, it can be easily used as a variable speed drive. This method of speed control of the induction motor also helps in saving energy losses in the large fans, pumps, blowers, and compressor etc. [7].

The static frequency conversion is achieved either in single stage using cycloconverters or in two stages using d.c. link converters. Phase controlled cycloconverters are best suited for very low speed operation as their output frequency is limited to normally one-third of the supply frequency. However the output voltage of cycloconverters contains large harmonics, which increases the losses and decreases the efficiency of the drive therefore derating of the motor. The control and power circuit of the cycloconverter is very complex; therefore drive is not much popular in general applications [14]. The research in variable speed drive has shown that the d.c. link

converters, voltage source and current source can be effectively used for smooth and step -less control of drive over a wide range.

Voltage source inverters based on thyristors requiring forced commutation, thus limits the frequency of operation [15]. With the invention of fast power semi conductor switching devices as power transistors, MOSFET, IGBT, GTOs, the operating frequency of the inverter has been increase to several kilo Hz and the problem of commutation is also rectified. Various control techniques are proposed to maintain constant flux even at low frequency of operation. However for regeneration, an essential requirement of the drive system one extra converter is required, which increase the cost, and reduces the reliability of the drive.

The other d.c. link converter is a current source inverter introduced by ward E.E. in 1964 [16]. In which the adjustable d.c. voltage from phase controlled rectifier is converted to an adjustable but load independent current source by connecting large inductor. Unlike the voltage source inverter, the CSI is having the natural regeneration capability without an extra cost and it protects the devices from over current, because of its controlled current operation. The conventional, CSI has the six step output current which is the dual of six step voltage waveform of VSI and having dominant lower order harmonics. These harmonics give rise to objectionable torque pulsation and heating due to harmonic losses under low speed operation of the drive. The motor terminal voltage is nearly sinusoidal with superimposed voltage spikes due to commutation transients. The CSI finds application in high power motor applications for pump and fan loads, stainless steel recoiling lines, paper mills, traction etc. [17,18,19].

The performance of the current source inverters has been improved drastically in the past several years. The state of the art has been reviewed in detail by Chattophadhyay,

A.K. [20]. Inspite of the several advantages of CSI-fed induction motor drive, it suffers with the certain limitations such as: complex commutating circuit, limited frequency range of operation and it is unable to operate at no load. The commutation is affected by machine leakage inductance. The response of the drive is sluggish because of large inductance in series and tends to give a stability problem at light load and speed.

The problem associated with the conventional CSI fed induction motor drive can be over come by replacing the forced commutating devices by self commutating devices at high switching frequencies such as, MOSFETs, IGBTs .PWM technique can be easily employed for the better quality of line currents. The current source may employ PWM technique can be easily employed for reduction of d.c.link inductor. It will also improve the transient performance of the drive. The digital control techniques such as microprocessor, microcontroller and DSP must be employed for fast control of the drive. To maintain the rated flux in the entire operating frequency region, slip regulator loop must be incorporated in the feed back loop. The capacitor bank can be connected at the terminals of the CSI- fed induction motor, so that the reactive power requirement of the motor is met by the capacitor. Lots of researches have been carried out on PWM inverter drives, which concerns one or more of the following aspects.

- Different pulse width modulation techniques for inverter drives.
- Steady state and transient analysis of current source inverter fed induction motor drive.
- Improvement in modulation and control techniques used in the inverter fed drive.
- Micro computer and DSP based control schemes

- Closed loop analysis of the drive.

- Minimization of the size of inductor.

- Design of controller parameters used in feed back loop

The selected literature on the above aspect of conventional current source inverter and PWM current source inverters is reviewed by the author.

1.2   LITERATURE REVIEW

During the past several years, several attempts have been made by the researchers to improve the performance of the current source inverter. After the inception of current source inverter in 1964, Philips [21] for the first time in 1972 introduced the concept of Auto Sequentially Commutated Current Source Inverter (ASCI). Philips has introduced the employment of current source concepts in thyristor converter to obtain the adjustable firing angle and adjustable current waveforms. He has also explained the use of d.c. filter cho ke and current feedback loop to produce a regulated current source. Simplified inverter commutation circuit is made possible for the current source inverter is also discussed.

After introduction of the concept of ASCI, research has been carried out in the direction of analysis of ACSI. A simplified analysis neglecting stator resistance, parameters of the d.c. link inductor and the variation of the motor back e.m.f. during commutation interval was presented by Farrer and Miskin using per phase series equivalent circuit of the induction motor [22]. It has been shown that if a squirrel cage induction motor is fed with a quasi-sine wave current, the motor terminal voltage is near to sinusoidal. The commutation was neglected in the analysis. A comparison of the ASCI with an auxiliary commutated CSI fed induction motor was made in [23]. A new model of

6

induction motor fed from the ASCI including saturation of magnetizing circuit and leakage reactance was proposed in [24].

The research work has been carried out by the different authors for the suitable design of the component of CSI and suitable guidelines were presented for the design of component. For the ripple free current source, a large value of inductor is required at the output of the converter. Large value of inductor makes the system costly and makes the transient response of the drive sluggish. The effect of inductor is investigated in [30] and a design criterion is presented for inductor. The requirement of d.c. source applied to the converter side for the reduction of size of inductor is discussed in [26, 27].

The steady state analysis of the controlled current source inverter fed induction motor was done by the several authors. Lipo and Cornell [35] has analyzed the steady state operating controlled current induction motor drive fed from an ideal current source inverter. The equations, which have been derived, are also applicable for transient analysis and can be extended to include the effect of source impedance. The effect of saturation has been discussed. Investigation of operating points indicates that if the motor is to remain unsaturated, feedback control is required to achieve stable operation. The steady state characteristics and instability of an induction motor driven by the current and voltage source are compared [29]. The analysis shows that the steady state characteristics of an induction motor fed with the current source inverter for variable frequency differ considerably from those for the some motor fed with the voltage source inverter some experimental results are also presented, which show agreement with the simulated results.

A modified steady state analysis of the current source inverter fed squirrel cage induction motor has been given in [31]. The analysis includes the effect of the variation of

ac back EMF and the phase-shift of the fundamental component of the line current during commutations but neglecting the rotor resistance and d.c. filter. It was shown that the effective leakage inductance of the machine during commutation can be measured by performing the block rotor test with low frequency square wave current from the CSI. All the investigations are confined to the operation of the drive at low output frequencies.

In [32] Singh et al presented the operating principle as well as steady state analysis of a three-phase induction motor fed by a d.c. link inverter commutated by machine induced e.m.f. The active power requirement of the motor is met by the d.c. link while the necessary reactive power is supplied by a capacitor connected across the motor terminals. A generalized analytical model is developed for no load as well as loaded condition of the motor. The steady state performance of the motor is analytically evaluated. The computed results are compared with the experimental results. The analytically obtained results are in good agreement with the experimental results.

Song et. al. [33] presented a systematic study for the induction motor drive using a load commutated current source inverter [LCCSI]. The steady state characteristics of LCCSI are shown to be the intermediate characteristics between the voltage source inverter (VSI) and the Auto Sequentially Commutated Current Source Inverter (ASCI) system.

The steady state analysis of the current source inverter fed induction motor drive has been carried out by Agarwal and Verma [34]. The stability analysis of CSI fed induction motor drive shows that open loop stable operation of the drive is possible at a very low value of slip. At high value of slip, the operation of the drive is inherently unstable and leads to saturation, increased losses, therefore, closed loop operation of the drive is

8

essential to operate the drive at high value of slip. Through closed loop the flux in the air gap can be maintained to rated value in the entire range of operating slip. Rated value of flux is maintained by incorporating the slip regulation characteristics in the closed loop. A constant flux operation using air gap voltage as a feed back variable is discussed in [36].

At the low value of the operating frequency, the pulsating mode, the pulsating torque problem become serious in ASCI. Several techniques like pulse width modulation (PWM), multiple inverter scheme, current amplitude modulation are used to improve the current wave form and eliminate the torque pulsation [37- 46] .The contributions made by some of the researchers are presented below.

Hombu et al presented [39] a new current source GTO inverter to which PWM control technique were applied was developed. The developed inverter has both output voltage and output current sinusoidal. The commutating capacitor requirement is considerably reduced than the conventional thyristor type current source inverter.
Nonka and Neba [40] presented a new GTO current source inverter, in which two auxiliary GTO's are added to the basic inverter circuit, which consists of six GTO's and three capacitors. The inverter can supply both sinusoidal output voltage and current. The experimental and analytical results have been presented by feeding the induction motor through proposed CSI. The same author (s) have presented a new current source inverter [43], employing GTO as a switching device. The inverter can supply both the sinusoidal voltage and current to the induction motor. Experimental and analytical results are presented when the induction motor is drive by this inverter. The experiment on the induction motor shows that inverter can drive motor smoothly over a wide frequency range.

Nabe et al [41] presented a high performance current controlled inverter, having quick response in transient state and low harmonic current in steady state. A novel control scheme is proposed which is based on the current deviation vector. Experimental results show good agreement with the theoretical results.

With the fast development in the power semiconductor devices and microelectronics technology, lots of work has been carried out to improve the performance of the current source inverter such as, replacement of line- commutating devices thyristors with the self- commutating devices Power MOSFETs, IGBTs etc, implementation of the PWM techniques in the front end converter to reduce the requirement of d.c.link inductor, PWM operation in motor-end inverter for better quality of supply to the motor and implementation of micro processor based control. The selected research works are presented below:

The Konishi et al presents [57] a digital speed regulator. They have given an expression to calculate the sampling time required for a processor for a thyristor drive microprocessor based regulator system. A software based speed regulator for motor drives is proposed by Kumbo et al [58]. The regulator can be applied to any type of motor drive by simply changing the software. Agarwal and Verma [61] have proposed a microprocessor based firing pulse generation for PWM current source inverter operating under variable frequency, it requires less memory space and less computation time, the response of the processor is fast.

The problem of reducing the pulsating torque in current source inverter fed induction motor system is investigated by Chin and Tomita [52]. They have given the general criteria for judging the torque ripple.

An analytical design is presented of the control system of slip controlled current source inverter induction motor drive by Bolognani and Buja [63]. The current and speed controller are designed and their analytical expressions are given. Two function generators are synthesized and incorporated in the speed loop to obtain constant rotor flux operation.

An application of modern control theory for the control of current source inverter fed induction motor drive is presented by Prakash et al [64]. A linearly quadratic Gaussian [L QG] control scheme is developed in which Kalman filter is tuned for high robustness by a method of Doyic and Stein.

Hombu and Ueda [42] presented a GTO based current source inverter capable of producing sinusoidal input voltage and current. The pulse width modulation technique is applied in the front converter and motor and inverter. The PWM control employed in the front and converter greatly reduces the d.c. link inductor requirement.

A novel scheme is presented by Bolognani and Buja [67] to control the d.c. link current of a current source inverter induction motor drive, which greatly enhances the current response, and overall performance of the drive. The scheme incorporates the function generator to compensate for the motor back emf seen by the d.c. link.

Bowes and Bullough [44] presented an optimal PWM switching strategies for the CSI fed induction motor drive. The PWM strategies are designed to minimize rotor speed ripple and rotor position error. The developed strategies are applicable in a closed loop. The optimal PWM strategies are dependent upon the motor operating conditions principally slip frequency or phase angle between flux and current. Boost et al [54] presented a critical evaluation of the state of art of the PWM techniques on the basis of

11

application, there by giving the guidelines for selection of the best techniques for each area of application.

Mutho et al [66] have described a new control method that suppresses oscillations generated when induction motor is driven by PWM inverters. The suppression is done by correcting the power direction based on the period of the negative component of the inverter input current. This system can be applied to individual motor drive systems driven by general-purpose inverters because oscillation can be suppressed regardless of the type of motors.

Zargari and Xiao [49], proposed a simple control scheme for near input displacement factor operation of the three phase current source type PWM rectifiers. The rectifier is operated by a conventional Simple harmonic elimination (SHE) with 420 Hz switching frequency, which is feasible for GTO switches used in high power applications. The operation of proposed scheme is verified under various conditions including steady state and d.c. link current / load transients.

A PWM pulse pattern optimization method using the pulse frequency modulation (PFM) is presented by Iwaji and Fukuda in 1992 [72]. In the conventional PWM's, the pulse frequency is kept constant. In the proposed PFM, pulse frequency is adjusted. The technique improves the current distortion and torque pulsations of drive motors. A method of realizing PFM by single chip microprocessor is described.

An induction motor drive system, which is composed of current output type converter and current source inverter with sinusoidal input and output voltage is presented by Nonka and Neba [73]. PWM strategies with GTO's are applied to the converter and inverter section from the point of view of reduction of the current harmonics and

suppression of the motor torque pulsations. A simple method for quick regulation of a.c. output current amplitude is presented, which is applied to the PWM inverter section. The experimental results of steady state and dynamic operations of the motor are shown.

A unified modulation algorithm for VSI and CSI has been discussed Holmes [55] in 1992. The algorithm is based on a.c– a.c. matrix converter theory and algorithm is equally applicable for current source as well as voltage source inverters. The proposed strategies capable of being computed on line by a single chip microprocessor at switching frequencies up to several kilo Hz. The theoretical and experimental results are shown in the paper.

A modified PWM current source inverter that can operate with varying modulation index has been presented by Joos et al [77]. Any standard VSI PWM pattern can be used with this inverter. This feature is obtained without comprising the converter system efficiency and power factor, and at the cost of only one auxiliary switch. Steady state performance equations have been derived. The performance of the inverter was verified by experimental and analytical analysis.

Karshenas et al [83] have presented a generalized techniques for selective harmonic elimination and current magnitude modulation for current source inverter and converter. Generalized equations and tables which show the relationship of various PWM-SHEM parameters to the shape and location of short circuit pulses and the number of Chops per 30° have been provided and discussed.

Chakrabarti et al [100] have presented a method of driving switching instants of different space vectors in direct torque control of induction motor drives using pulse width modulated voltage source inverter.

A new feed back current controller for three phase PWM inverter is presented by Martins et al [104] in 1998. The scheme is based on a current loop with two non-linear three level hysteresis controller. It requires the measurements of only two-phase currents and with the accurate choice of the output voltage vectors, offers advantage over the types of control without increasing significantly the hardware complexity.

Jacobina et al [107] presented a digital PWM method based on scalar as well as vector modulation approach. The paper shows the complete relation to obtain the equivalence between vector and scalar digital modulation approach. From this equivalence it was proposed a simple software algorithm to generate the space vector modulation from the scalar implementation. The simulated experimental results are presented for the validation of the method.

The relationship between regular sampled pulse width modulation (PWM) and space vector modulation was defined by Bowes and Lai [110] and it was shown that under certain circumstances the two approaches are equivalent. The various possibility of adding a zero-sequence component to the regular sampled sinusoidal modulating waves is explored. This approach simplifies the microprocessor implementation.

Espinoza and Joos [91] have presented an on line PWM pattern generators for current source rectifiers and inverters, offer a number of control advantages over off line optimized patterns. However when implemented using the principles which apply to voltage source inverter, PWM pattern generators, the switching frequency equal to (i) the carrier frequency in standard carried based implementation, (ii) a function of cycle frequency, sequence of space vector and selection of zero space vector in space vector implementations. The paper shows that this frequency can be reduced to one half of the

respective frequencies. Espinoza and Joos [92], have proposed a PWM control strategy for current source inverter fed induction motor drive. The control strategy allows the operation of the inverter at constant modulation index in steady state regardless of the load speed and torque. The strategy achieves this goal by minimizing the steady state d.c. link current. In addition to the inherent advantages of current source topology (short circuit protection, low output dv/dt and regeneration capabilities), the proposed control schemes adds the advantages such as; fixed and reduced motor voltage distortion, minimized d.c. bus and switch conduction loss, elimination of motor circuit resonance through instant output voltage control. Experimental results based on a DSP implementation confirm these features.

Yin and Yu [93] presented a new electric drive system topology, based on PWM current source inverter. The purpose of the new drive system is to reduce both line and load harmonics, as well as the voltage rate of rising due to the PWM high-frequency switching based on the PWM – CSI drive, a further harmonic reduction is achieved by modifying the drive rectifier control circuit. The new drive system based on the PWM-CSI currently has certain limitations due to the cost of components, however if the industry became more concerned about the problem of harmonic and voltage rate of rising, the concept of PWM CSI can be implemented to update the currently dominated PWM-VSI fed drives.

Bowes and Grewal [97] proposed a novel space vector PWM control strategy. They have review the (0-60°) regular sampled HE PWM strategy together with the space vector modulation technique for the development of a novel SVM-based harmonic elimination PWM [HE PWM] technique. The advantage of this method is that it uses only space vector concepts for the calculations of the vector states and the vector times. A

15

regular sampled HE PWM strategy has been presented which closely approximated the switching angles of the offline of 0-90°. HE PWM family of switching angle solution sets. Both HE PWM strategies can be implemented in real time on a DSP. This technique can be applicable for drive application, uninterrupted power supply and static frequency converter.

Loh, P.C.; and Holmes ,D.G. [101] presented an integrated approach to the closed-loop control of output voltage for a VSI and output current for a current source inverter, using hysteresis with a rectangular bounding box in the synchronous d-q reference frame, and a simple switching rules. The modulator is constrained to only select from the two nearest active space vectors to the targeted reference, and hence achieves a significantly improved harmonic performance compared to sigma-delta and other stationary frame hysteresis modulators.

Bendre et al [95] presents a new PWM current source inverter topology using one gate off switch and six SCRs is presented. The converter uses active commutation to realize PWM techniques in a conventional SCR based current source inverter. Modulation technique for the proposed inverter, simulation and experimental results are discussed.

From the literature survey it is observed that problem of sinusoidal voltage and non sinusoidal line currents associated with the CSI can be overcome by implementing the PWM techniques in the inverter and by connecting the capacitor at the terminals of the inverter. By using GTOs as a switching devices and by putting the capacitor at the terminals of the PWM inverter, several attempts has been made to make the voltage and current of the inverter sinusoidal [40,42,43]. The purpose of the capacitor is to work as a filter and to help in commutations. But due to switching frequency limitations of the

devices, scheme is not applicable at high frequency. With the availability of fast self-commutating switching devices such as: Power MOSFETs, IGBTs the above scheme can be applied at high frequencies of operation. Here the requirement of the capacitor connected across the terminals of the inverter is to act as a filter only. Therefore the requirement of the capacitor is considerably reduced. Limited papers are available on the PWM CSI having self commutating devices and capacitor at the terminals of inverter. Proper selection of the capacitor and their effects on the steady state performance of the drive is not discussed in detail. Closed loop is a mandatory requirement of the CSI –fed drive, there is no direct method available to design the speed PI and current PI controller parameters of the drive, a method is required for the design of the controller parameters.

The author has made an attempt to design and develop a modified self-commutating PWM current source inverter, having capacitor at the output terminal, feeding power to the induction motor. The closed loop control of the drive is implemented digitally by using PC (8088 processor based) and 8031 microcontroller.

1.3   AUTHOR'S CONTRIBUTION

After reviewing the literature on PWM current source inverter fed induction motor drive, an attempt has been made in present thesis to design and develop a Modified self-commutating current source inverter fed induction motor drive. The complete drive system consists of a three phase PWM front – end converter, current source inverter, coupled through d.c.link inductor, three phase induction motor, three phase capacitor bank connected at the at the terminals of the induction motor. The front-end converter operates in closed loop with d.c.link current feed back to maintain the d.c.link current demanded by the load. The motor-end current source inverter is PWM inverter,

17

employing space vector modulation technique .For the stable operation of the drive under all operating condition; drive is operated in closed loop. The two PI controllers are used; one in speed feed back loop and other in current feedback loop. The rated air gap flux is maintained at each operating frequency with the use of slip regulator. The synchronous speed is determined by adding actual speed and reference slip speed.

The mathematical modeling of the complete drive system is developed in synchronously rotating reference frame and is used for the steady state and transient analysis of the drive. The steady state equations are derived for the steady state analysis of the drive for the various operating conditions such as (i) Variable operating frequency, fixed d.c.link current and fixed capacitance (ii) Fixed frequency, constant d.c. link current and variable capacitance per phase (iii) Variable frequency, constant d.c. link current, fixed capacitance per phase (iv) Variable d.c. link current, fixed frequency, fixed capacitance per phase (iv) Constant load torque, fixed capacitance per phase, fixed d.c. link current (v) Linearly varying load torque, fixed capacitance per phase, fixed d.c. link current. The value of capacitor to be connected across the machine terminal is decided by the analytically determined steady state performance of the drive and then confirmed by experimental investigation.

The complete hardware of the drive is developed in the laboratory. Hardware includes power, control, protection, quantizer, zero crossing, snubber, speed and current measurement circuits The front– end PWM converter employs three self-commutating devices as MOSFETs and three line commutated devices as thyristors. The motor – end PWM inverter employs six self-commutating devices as MOSFETs.

18

The software of the drive system is developed in 'C' language, which consists of the main program, ISS for timers and subroutines for firing pulse generation of converter and inverter, current measurement, speed measurement, speed PI processing, current PI processing etc. The details of the software are shown in the form of flow charts and discussed. Equal pulse width modulation technique is used in the converter and space vector pulse width modulation technique in the motor-end inverter. At low and medium value of operating frequency the number of firing commands issued to the devices are more than at high value of operating frequency due to the consideration of the switching frequency of the devices. The PWM firing commands for the front-end converters are generated through 8031 microcontroller based system, which communicates serially with the PC-AT to get the firing commands. The firing pulses for the inverter are generated using ADD-ON cards in personal computer (8088 processor based) and sent to the switching devices after amplification.

The actual d.c.link current required for the PI processing of the inner controller (current controller) is sensed, using Hall effect current sensor. The output of the Hall effect current sensor is in terms of current and it is converted to voltage signal. A low pass R-C filter is used to filter the ripples from the output current. The actual rotor speed needed for the speed PI processing is measured through the rotatory incremental pulse encoder. These signals are digitized through a 12 bit high resolution ADD-ON card for digital control implementation. The developed hardware is tested using the software developed and various control and power signals are recorded through X-Y recorder.

The transient stability of the system depends upon the speed and current controller parameters. The mathematical model of the drive already derived is used for the design of current and speed controller parameters. The system equations are non--linear. These

equations are linearized for the small perturbations about the rated steady state operating point in order to develop the characteristic equation. Using the characteristic equation of the closed loop drive, the parameters of the speed and current controllers are designed. The inner control loop, being fast is considered first to design current controller. Later, the parameters of speed controllers are designed. Both the controller parameters are designed for high degree of relative stability and good damping. This ensures the fast and stable operation of the drive.

The D–partition technique is employed to determine the probable stable region in parametric plane. The probable stable region is obtained by D- partition technique. The frequency scanning technique is used for confirming the stability of the point. This method of determining the controller parameters is superior to other conventional method, because it requires less computational effort. Although root locus is the best method of synthesis, but it selects a single parameter, where as the D- partition method directly gives a stable region in the parameter of the two planes. The final selection of the controller parameters are decided by the transient response of the drive for 5% step change in reference current and speed respectively using state equations of the drive. The parameter, which gives minimum overshoot and minimum settling time, is finally selected.

The developed modified current source inverter supplies sinusoidal voltage and current at almost each operating frequency. The input displacement factor of front- end converter is found to be almost unity, therefore the d.c.link inductor requirement is considerably reduced and transient response of the drive is found to be fast. An attempt to made the digital closed loop control of the drive using 8088 processor /8031 microcontoller is found to be successful. All the experimental results are verified with the simulation results and they are in good agreement to each other.

20

The performance of the developed drive is investigated experimentally in open loop under different operating conditions and compared with the analytical result obtained in open loop through simulation. Both the performances are found to be in good agreement to each other.

The performance of the developed drive is investigated experimentally in closed loop for the designed value of the controller parameters. The performance of the drive in closed loop is also obtained analytically. The transient response of the drive (d.c.link current, speed) for the step change in reference speed is experimentally recorded and also determined through computer simulation. Experimental results obtained in closed loop and under transient condition are in good agreement to the analytically obtained results.

The conclusion of the developed system, D-partitioning and frequency scanning techniques used for controller parameters estimation, motor specifications and the various components used for the development of the hardware are given in the appendices. A detailed bibliography of literature related to this work is appended at the end.

MATHEMATICAL MODELING OF MODIFIED SELF-COMMUTATING CSI-FED INDUCTION MOTOR DRIVE

As reviewed from the literature survey the speed control of induction motor is possible over a wide range by feeding the motor through a variable frequency source. Current source inverter converts the regulated dc link current into variable frequency ac current. Due to controlled current operation of the inverter, slip regulated current source inverter is preferred over voltage source inverter. The slip regulator maintains the rated flux in machine at its rated value by regulating slip. The current source at the front end makes the inverter converter arrangements naturally capable of power regeneration [4,11,30,35]

This chapter deals with the mathematical equations describing the behaviour of modified self-commutating CSI-fed Induction motor drive. The suitability of any drive for an application depends upon its behaviour under steady state and transient conditions. In order to study the behaviour of drive over a complete speed range, a mathematical modeling of the drive is required. A closed loop control scheme incorporating speed and current controllers for the modified CSI-fed induction motor is described. The mathematical modeling of the system is developed in synchronously rotating (d^e-q^e) reference frame.

2.1 INTRODUCTION

With the help of variable frequency a.c. supply the speed of an induction motor can be controlled very smoothly. The voltage source and current source inverter can give

a variable frequency a.c. source. In the present work current source inverter is used for variable frequency a.c. supply; the current source inverter is slip regulated. The slip regulator maintains the flux in the machine at its rated value by regulating the slip.

The developed model is used in later chapters for steady state, designing of speed , current controller parameters and transient analysis.

2.2   SYSTEM CONFIGURATION

The system consists of a 3 phase a.c. power source, a 3 phase PWM rectifier incorporating equal pulse width modulation, a three phase pulse width modulated inverter using space vector technique, a dc link inductor, a three phase squirrel cage induction motor and 3 phase capacitor bank as shown in Fig 2.1. In the CSI-fed induction motor, air gap flux saturates at a very low value of slip; motor can not be operated in this region because of excess iron loss. To operate the machine at a normal value of air gap flux, the motor is operated in statically unstable region of torque-slip characteristics. Hence closed loop operation of the drive is mandatory. The present work makes use of speed and current controllers of PI type.

The actual speed of induction motor is measured by pulse encoder and compared with the reference speed set via the computer keyboard. The speed error is processed in the speed control loop to obtain the reference slip speed (ω_{sl}^*).Using reference slip speed (ω_{sl}^*) and the slip regulator characteristics, the value of reference active stator current of the induction motor (I_{act}^*) and reference reactive current (I_{react}^*) are determined.

23
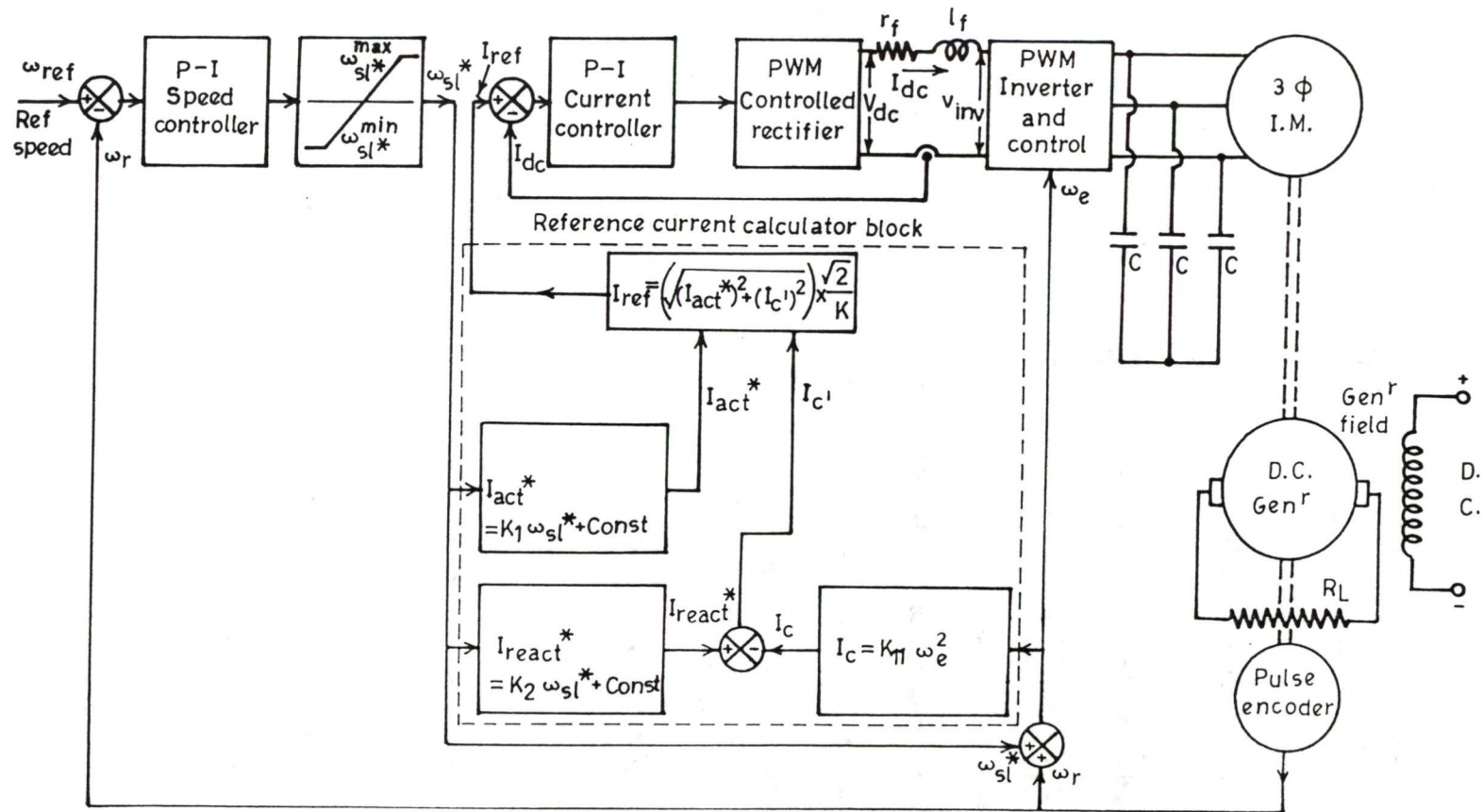
Fig.2.1. Variable speed modified current source inverter fed induction motor drive.

For the determination of reference current (I_{ref}), the stator active reference current (I_{act}^*), the stator reactive reference current (I_{react}^*) and capacitor current (I_c) are required as shown in the Fig. 2.1. The reference stator current vs slip speed and reference reactive stator current vs slip speed plots are treated as slip regulator characteristics in the present work and are experimentally determined. Using reference active current (I_{act}^*), capacitor r.m.s. current (I_c) and stator reference reactive current (I_{react}^*), stator reference current (I_s^*) is determined. Which is transformed to the d.c link side to obtain the reference d.c. link current (I_{ref}). The reference slip speed (ω_{sl}^*) is added to the actual rotor speed (ω_r) to obtain the switching frequency of the inverter (ω_e).

2.3   MATHEMATICAL MODELING OF THE COMPLETE DRIVE SYSTEM

The modeling of the complete drive system is carried out in synchronously rotating $q^e - d^e$ reference frame.

2.3.1   System Equations in M.K.S.

The mathematical modeling of the drive system is carried out for the following component of the drive in $q^e - d^e$ reference frame.

(i)   Three Phase PWM Rectifier

(ii)   Three Phase Pulse Width Modulated Inverter

(iii)   D.C. Link

(iv)   Three Phase Induction Motor With Load

(v)   Three Phase Capacitor Bank

25

(i)   Three Phase PWM Rectifier

Three phase PWM rectifier output voltage depends upon the number of pulses per cycle and their width. The converter is modeled for twelve numbers of equal pulses per cycle. It leads to a two pulse per 60° each of β width. Fig.2.2 shows the pulse width modulated waveform for 60° period. The output voltage of the rectifier can be expressed with the following expressions.

$$V_r = \frac{\sqrt{2}\ V_{LL}}{\pi/3} \left[\int_{\alpha}^{\alpha+\beta} \sin{(\omega t + \pi/3)} + \int_{\alpha+\beta+2\alpha}^{\alpha+\beta+2\alpha+\beta} \sin{(\omega t + \pi/3)}\ d(\omega t) \right] \qquad (2.1)$$

$$V_r = \frac{3\sqrt{2}}{\pi}\ V_{LL}\ (4\sin{\frac{5\pi}{12}})\ \sin{\frac{\beta}{2}} \qquad (2.2)$$

Since β is varied from 10% to 90% of $\frac{\pi}{6}$ radians, it can be approximated as

$$\sin{\frac{\beta}{2}} \approx \frac{\beta}{2}$$

$$V_r = \frac{3\sqrt{2}}{\pi}\ V_{LL}\ (4\sin{\frac{5\pi}{12}})\ \frac{\beta}{2}$$

$$V_r = 5.218\ V_{LL}\ \frac{\beta}{2}$$

where,

V$_{LL}$ is the line to line input voltage

(ii)   Three Phase Pulse Width Modulated Inverter

If I_{dc} is the current in d.c.link , then the fundamental component of line currents of the 3-phase pulse width modulated inverter $i_{as,}\ i_{bs,}\ i_{cs}$ forms a balanced set of 3-phase currents with a maximum value as $I_{as(max)}$
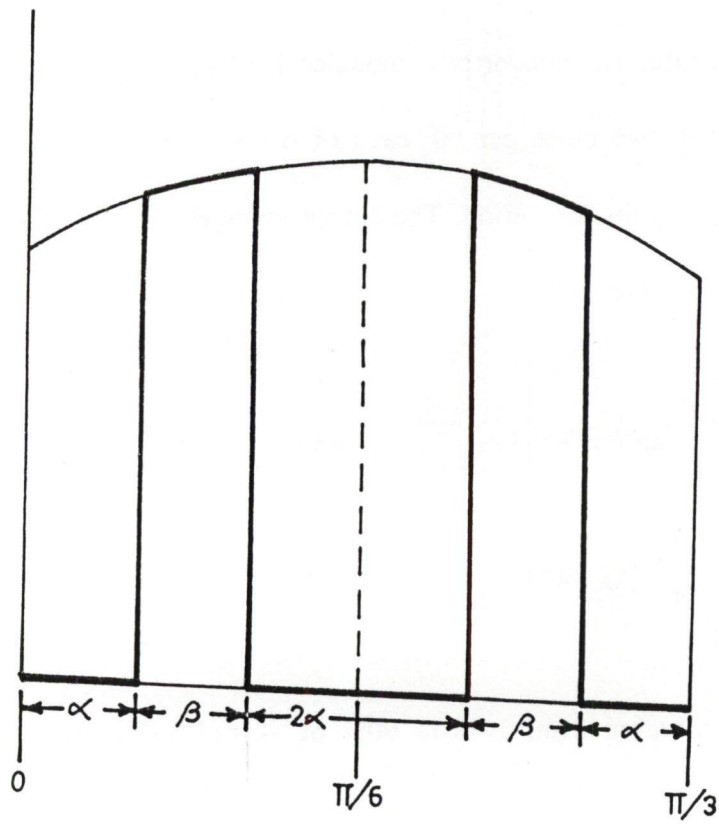
Fig.2.2. PWM Waveform of rectifier over 60° period.

$$I_{as(max)} = k\, I_{dc} \tag{2.3}$$

The value of k is obtained with the help of Fourier analysis of inverter line current waveforms and it is given by:

$$k = \frac{\text{maximum value of fundamental inverter line current}}{\text{d.c.link current } (I_{dc})} \tag{2.4}$$

The value of k depends upon the operating frequencies of the inverter and it varies from 0.8485 to 0.9970 for variation in operating frequencies from 10 Hz to 50 Hz.

The line currents of three phase pulse width modulated inverter can be expressed in terms of d-q variables, either in a stationary or a rotating $d-q$ reference frame (rotating at a synchronous electrical angular velocity ω_e). The synchronously rotating reference frame provides an advantage that with sinusoidal excitation the variables appear as dc quantities in steady state condition. In the present work synchronously rotating reference frame ($q^e - d^e$) is considered for the modeling of the drive. The q^e axis of the rotating reference frame is assumed to coincide with the stator a-axis at $t = 0$ as shown in Fig. 2.3. It will advance by an angle θ_e such that $\dfrac{d\theta_e}{dt} = \omega_e$.

Since inverter output fundamental current peak is taken along the q-axis of the reference frame, the transformed phase current equations in the $q^e - d^e$ reference frame are:

$$i_{0s}{}^e = 0$$

$$i_{qs}{}^e = k\, I_{dc}$$

28
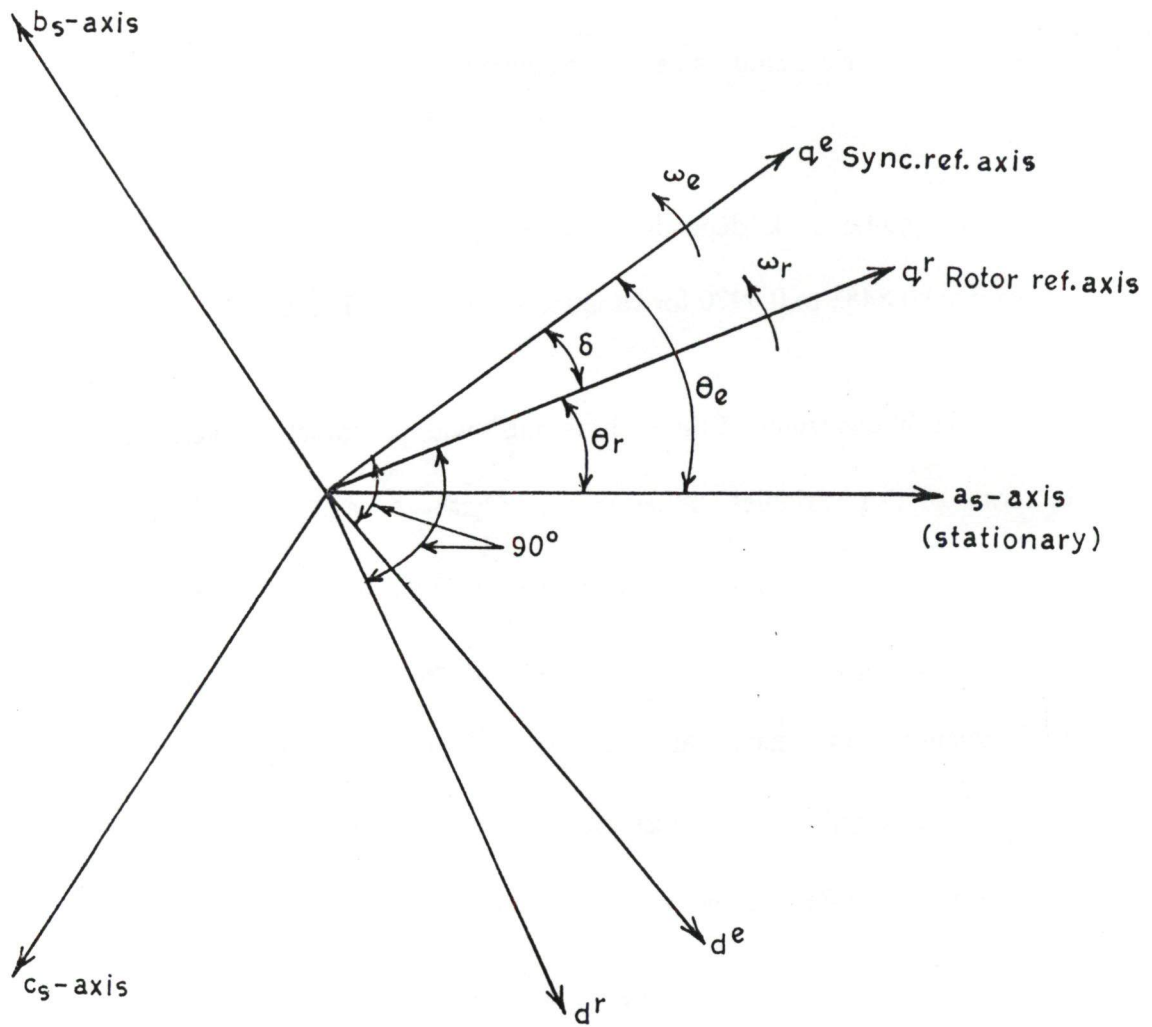
Fig.2.3. d-q reference frame .

$$i_{ds}^{\,e} = 0 \tag{2.5}$$

Applying the power invariance principle across the inverter i.e. no power loss in the inverter.

$$\text{Inverter input power} = \text{Inverter output power}$$

$$V_{inv} I_{inv} = v_{as} i_{as} + v_{bs} i_{bs} + v_{cs} i_{cs}$$

$$= \frac{3}{2}\left(v_{qs}^{\,e} i_{qs}^{\,e} + v_{ds}^{\,e} i_{ds}^{\,e}\right) \tag{2.6}$$

Substituting the values of $i_{qs}^{\,e}$ and $i_{ds}^{\,e}$ from equation 2.5 with the value of $I_{inv} = I_{dc}$, following equations are obtained.

$$V_{inv} I_{dc} = 3/2 \, k \, v_{qs}^{\,e} \, I_{dc}$$

$$V_{inv} = 1.5 \, k \, v_{qs}^{\,e} \tag{2.7}$$

(iii) D. C. link

The rectifier output votage V_r is related with the PWM inverter input dc voltage V_{inv} as:

$$V_r = V_{inv} + \left(r_f + p l_f\right) I_{dc} \tag{2.8}$$

where,

$$p = \frac{d}{dt}$$

$r_f = $ resistance of d.c. link inductor

$l_f = $ inductance of d.c. link inductor

Substituting the value of V_{inv} from equation (2.7) into the equation (2.8)

$$V_r = 1.5 \text{ k } V_{qs}{}^e + (r_f + pl_f) I_{dc} \qquad (2.9)$$

(iv) Three Phase Induction Motor With Load

The induction motor can be modeled in $(q^e - d^e)$ reference frame using the following assumptions.

(i)   The three phase stator windings of the motor are balanced and sinusoidally distributed in space.

(ii) The d.c. link current is ripple free.

(iii) The switching transients in the inverter are ignored.

(iv) There is no core loss in the induction machine.

The motor can be described by the following fourth-order matrix equation in $(q^e - d^e)$ reference frame .

$$\begin{bmatrix} v_{qs}^e \\ v_{ds}^e \\ 0 \\ 0 \end{bmatrix} = \begin{bmatrix} r_s + pl_{ss} & \omega_e l_{ss} & pl_m & \omega_e l_m \\ -\omega_e l_{ss} & r_s + pl_{ss} & -\omega_e l_m & pl_m \\ pl_m & \omega_{sl} l_m & r_r + pl_{rr} & \omega_{sl} l_{rr} \\ -\omega_{sl} l_m & pl_m & -\omega_{sl} l_{rr} & r_r + pl_{rr} \end{bmatrix} \begin{bmatrix} i_{qs}^e \\ i_{ds}^e \\ i_{qr}^e \\ i_{dr}^e \end{bmatrix} \qquad (2.10)$$

The slip speed (ω_{sl}) in electrical rad/sec is given by the following equation

$$\omega_{sl} = \omega_e - \omega_r \qquad (2.11)$$

The electromagnetic torque equation of the motor is given by the following expression.

$$t_e = \frac{3}{2} \cdot \frac{P}{2} \cdot l_m \left(i_{qs}{}^e i_{dr}{}^e - i_{qr}{}^e i_{ds}{}^e \right) \qquad (2.12)$$

Motional equation of the drive is given by the following expression.

31

$$t_e = t_1 + J\frac{d\omega_r}{dt} + B\,\omega_r \qquad (2.13)$$

Neglecting the effect of viscous friction, and converting the angular speed from electrical radian/sec. to mechanical radian/sec, following equation is obtained.

$$t_e - t_1 = \left(2J\middle/p\right)\frac{d\omega_r}{dt} \qquad (2.14)$$

The induction motor is coupled to a d.c. generator (operated at rated field flux) feeding power to a fixed load resistance, decided by the rated load torque of the machine. Therefore the load torque equation is given by:

$$t_1 = t_L \cdot \left(\frac{\omega_r}{\omega_{base}}\right) \qquad (2.15)$$

where,

t_L = Load torque equivalent to the rated torque of the motor.

ω_{base} = Rated angular speed in radian/second of the motor.

ω_r = Speed at which drive is running

P = No. of poles

(v) Three Phase Capacitor Bank

The capacitor current is related to stator voltage of induction motor as shown below:

$$i_c = c\frac{dv_s}{dt} \qquad (2.16)$$

where,

i_c = capacitor phase current

$$c \quad = \quad \text{capacitance/phase in star}$$

$$v_s \quad = \quad \text{stator phase voltage}$$

Transforming the equation (2.16) in the synchronously rotating ($q^e - d^e$) reference frame as show below:

$$\left(i_{cd}^e \cos\omega_e t - i_{cq}^e \sin\omega_e t\right) = c\frac{d}{dt}\left(v_{ds}^e \cos\omega_e t - v_{qs}^e \sin\omega_e t\right)$$

$$\left.\begin{aligned} i_{cd}^e &= c\,(pv_{ds}^e - \omega_e v_{qs}^e) \\ i_{cq}^e &= c\,(pv_{qs}^e + \omega_e v_{ds}^e) \end{aligned}\right\} \qquad (2.17)$$

2.4 CONTROL STRATEGIES

The d.c.link current is regulated by controlling the pulse width of the PWM rectifier pulses, which in turn controls the rectifier output voltage. Two proportional and integral controllers (PI) are used for speed and current loop, respectively for controlling the speed and current at different operating conditions. Hall effect current sensor is used for measurement of actual d.c. link current needed for the current feed back. The pulse encoder is used for measurement of actual rotor speed, which is needed for the speed feed back. The slip regulator maintains constant flux in the machine at almost every frequency (except at very low frequency).

(i) Slip Regulator

The slip regulator characteristics are experimentally determined by performing the load test on induction motor at rated voltage and frequency .The motor is loaded till rated load and various readings are noted (power input, stator current, speed). From the noted value of power input, stator current, stator voltage and speed, power factor and slip speed

33

is calculated at each load. The stator active and reactive currents are calculated at each value of load from stator current and power factor of the machine .Two curves are plotted (i) stator active current vs slip speed (ii) stator reactive current vs slip speed as shown in Fig 2.4 and 2.5 respectively. These curves are called slip regulator characteristics.

With the slope of slip regulator characteristics (I_{act} vs ω_{sl}) and (I_{react} vs ω_{sl}), the values of constants (k_1) and (k_2) are determined respectively, which are needed for the calculation of (I^*_{act}) and (I^*_{react}) respectively.

(ii)   Speed Controller

The speed PI controller decides the reference slip speed (ω^*_{sl}), which is required to estimate the reference stator active current (I^*_{act}) and reference stator reactive current (I^*_{react}) of the induction motor. It is also used in the calculation of switching frequency (ω_e) of the inverter. The following mathematical expressions are used to obtain the various operating variables.

$$\omega^*_{sl} = k_{p_s}\left(\omega_{ref} - \omega_r\right) + \frac{k_{i_s}}{T_{s_s}} \int_0^\infty \left(\omega_{ref} - \omega_r\right).dt \tag{2.18}$$

$$\left.\begin{aligned} I^*_{act} &= k_1\, \omega^*_{sl} + \text{cons tant} \\ I^*_{react} &= k_{1_1}\, \omega^*_{sl} + \text{cons tant} \end{aligned}\right\} \tag{2.19}$$

$$\omega_e \quad = \omega_r + \omega^*_{sl} \tag{2.20}$$

(iii)   Determination of capacitor current

The stator reactive current (I_{react}) of induction motor is constant over entire operating frequency range; in order to maintain the rated air gap flux in the motor. This
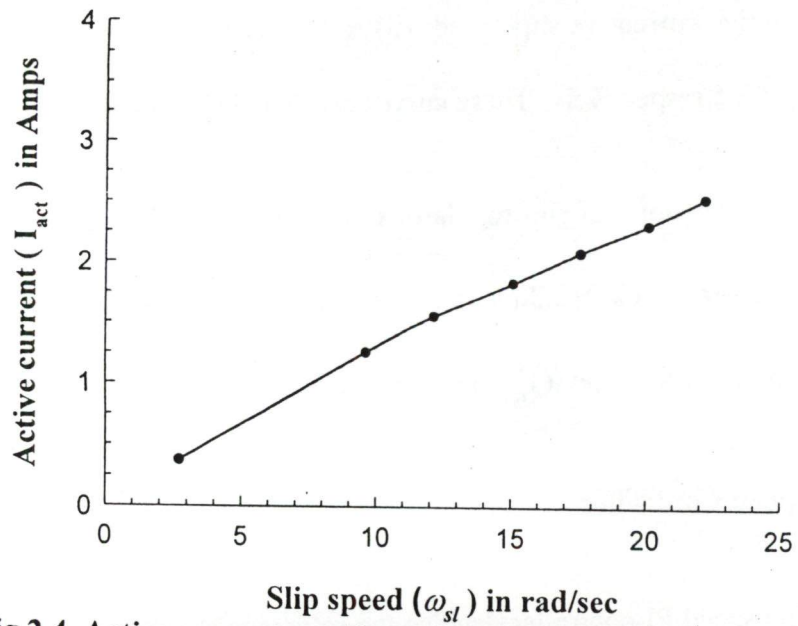
Fig 2.4. Active current vs. slip speed characteristics
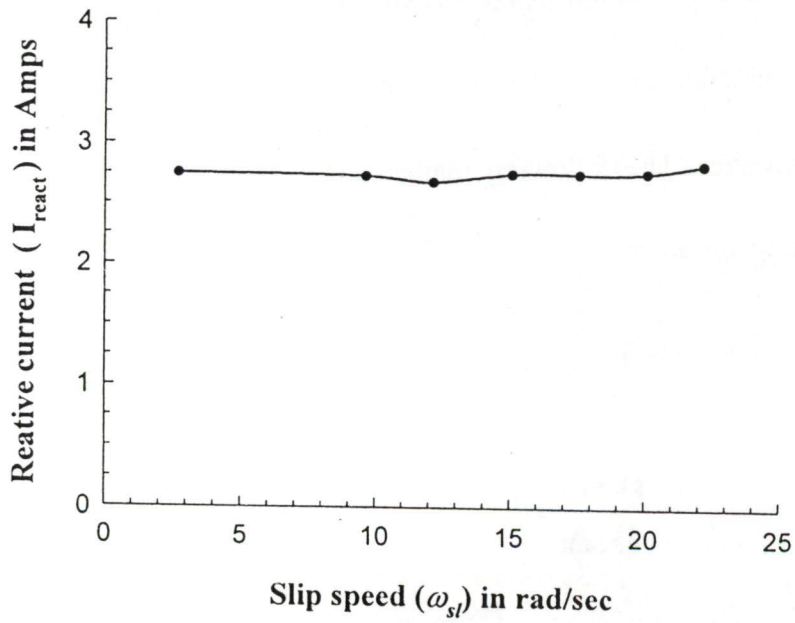
Fig 2.5. Reactive current vs. slip speed characteristics

leads to $\left(\dfrac{V}{f_e}\right)$ operation of the drive; therefore capacitor rms current per phase is determined from the following equations

$$I_c = k_{11}\, \omega_e^2 \tag{2.21}$$

where,

$$k_{11} = \frac{\text{rated value of capacitor current per phase}}{(\text{rated angular frequency})^2} \tag{2.22}$$

(iv)   Current Controller

The current PI controller is used to regulate the error between the reference d.c. link current and actual d.c. link current. The output of current PI controller decides the pulse widths of the PWM rectifier pulses and hence controls the output voltage of the pulse width modulated rectifier, which in turn controls the d.c. link current. The output voltage of the rectifier in terms of current controller parameter is given by the following expression.

$$V_r = k_{p_i}\left(I_{ref} - I_{dc}\right) + \frac{k_{i_i}}{T_{i_i}}\int_0^\infty \left(I_{ref} - I_{dc}\right) dt \tag{2.23}$$

The reference d.c. link current is determined using I_{act}^*, I_{react}^* and I_c according to the following equation.

$$I_{ref} = \left(\sqrt{\left(I_{act}^*\right)^2 + \left(I_{react}^* - I_c\right)^2}\right) \cdot \left(\frac{\sqrt{2}}{k}\right) \tag{2.24}$$

36

2.5   CONCLUSION

The mathematical modeling of the three phase PWM rectifier, three phase pulse width modulated inverter, 3-phase induction motor, d.c. link, 3-phase capacitor, is developed in synchronously rotating ($d-q$) reference frame. The overall control strategy has been discussed, which consists of two PI regulators, one PI regulator for current loop, and other PI regulator for speed loop. It also uses a slip regulator to maintain the rated airgap flux in the motor at almost every frequency.

The current PI controller regulates the d. c. link current in such a way that it is always equal to reference d. c. link current. The speed PI regulator processes the speed error and gives the reference slip speed. This reference slip speed is used for the determination of reference active and reactive current components of the induction motor current. The synchronous angular speed (ω_e) in radian/sec. is obtained with the help of actual speed of the rotor and reference slip speed.

The rms value of capacitor current is calculated as function of switching frequency of the inverter. The reference d.c. link current is estimated with the help of stator active, reactive and capacitor r.m.s. currents.

STEADY STATE ANALYSIS OF THE DRIVE

This chapter deals with the steady state analysis of modified self-commutating current source inverter fed induction motor drive. Using mathematical model developed in chapter 2, performance characteristics of drive under various operating conditions are obtained.

3.1   INTRODUCTION

The use of variable speed cage rotor induction motor fed from variable voltage and variable frequency source for a particular application depends upon its steady state performance over the complete speed range. The knowledge of the steady state behaviour of the drive is necessary, for improvement in its performance, and in optimization of the system for meeting the desired specifications. Therefore, the steady state performance of the drive is obtained before fabricating it. The steady state analysis of the CSI fed drive is reported in the literature [31-34].

In the present analysis pulse width modulated current supply is assumed as the input to the induction motor. Two PI regulators are used, one for speed loop and other for current loop. The mathematical expressions are developed for torque, phase voltage, phase current, d.c. link voltage, total loss, efficiency and power factor. Core loss is neglected. A computer program in 'C' language is developed to study the effect of capacitance connected across motor terminals, stator frequency, d.c. link current, fixed load and variable load.

3.2 STEADY STATE PERFORMANCE EQUATIONS

The steady state performance of the modified self-commutating current source inverter fed induction motor drive is obtained using the mathematical model of the drive developed in chapter 2. The various mathematical equations used in the analysis are derived using the assumptions, such as 3-phase balanced stator windings, ripple free d.c. link current, rated flux and loss less capacitor connected across the terminals of the stator. Further only fundamental components of winding currents are considered, neglecting the effect of all the harmonics. The speed controller sets the reference slip speed, that is required to calculate the reference stator active current (I_{act}^*) and reference reactive current (I_{react}^*). These currents determine the reference d.c. link current (I_{ref}). The current controller sets the d.c. link current, equal to the reference d.c. link current. The slip regulator maintains the constant flux. Reference slip speed is added to the actual steady state speed of the rotor of the motor to obtain the steady state synchronous speed of motor and hence frequency.

Under steady state condition the machine, capacitor and d.c. link variables (voltage and current) are constant in $q^e - d^e$ reference frame. Hence, differential terms in the equations, derived in chapter 2, are set to zero. The various steady state equations are as show below:

$$V_{r(0)} = V_{inv(0)} + r_f\ I_{dc(0)} \tag{3.1}$$

$$V_{inv(0)} = \frac{3}{2}\ k\ v_{qs(0)}^e \tag{3.2}$$

Substituting (3.2) in (3.1), the steady state d.c. link voltage equation is as shown below:

$$V_{r(0)} = 1.5 \, k \, v_{qs(0)}^e + r_f \, I_{dc(0)} \tag{3.3}$$

The steady state inverter current, machine current and capacitor current are related according to the following equations in ($q^e - d^e$) reference frame.

$$i_{invd(0)}^e = i_{dc(0)}^e + i_{ds(0)}^e \tag{3.4}$$

$$i_{invq(0)}^e = i_{qc(0)}^e + i_{qs(0)}^e \tag{3.5}$$

Since inverter output fundamental current peak is taken along the q-axis of the reference frame, therefore,

$$i_{invd(0)}^e = 0 \tag{3.6}$$

$$i_{invq(0)}^e = k \, I_{dc(0)} \tag{3.7}$$

Capacitor current is expressed in ($q^e - d^e$) reference frame as shown below:

$$i_{dc(0)}^e = -c \, \omega_e \, v_{qs(0)}^e \tag{3.8}$$

$$i_{qc(0)}^e = c \, \omega_e \, v_{ds(0)}^e \tag{3.9}$$

Substituting (3.6) to (3.9) in equations (3.4) and (3.5), the steady state stator current equations in ($q^e - d^e$) reference frame are given by the following expressions.

$$i_{ds(0)}^e = c \, \omega_e \, v_{qs(0)}^e \tag{3.10}$$

$$i_{qs(0)}^e = k \, I_{dc} - c \, \omega_e \, v_{ds(0)}^e \tag{3.11}$$

40

The steady state equation of the machine in $(q^e - d^e)$ reference frame are as shown below:

$$\begin{bmatrix} v^e_{qs(0)} \\ v^e_{ds(0)} \\ 0 \\ 0 \end{bmatrix} = \begin{bmatrix} r_s & \omega_e l_{ss} & 0 & \omega_e l_m \\ -\omega_e l_{ss} & r_s & -\omega_e l_m & 0 \\ 0 & \omega_{sl} l_m & r_r & \omega_{sl} l_{rr} \\ -\omega_{sl} l_m & 0 & -\omega_{sl} l_{rr} & r_r \end{bmatrix} \begin{bmatrix} i^e_{qs(0)} \\ i^e_{ds(0)} \\ i^e_{qr(0)} \\ i^e_{dr(0)} \end{bmatrix} \qquad (3.12)$$

Under steady state condition, torque developed by the motor is equal to the load torque hence,

$$t_e = \frac{3}{2} \cdot \frac{P}{2} \cdot l_m \left(i^e_{qs(0)} \, i^e_{dr(0)} \right) = t_l \qquad (3.13)$$

From equations (3.1) to (3.12)

$$v^e_{qs(0)} = r_s i^e_{qs(0)} + \omega_e l_{ss} i^e_{ds(0)} + \omega_e l_m i^e_{dr(0)} \qquad (3.14)$$

$$v^e_{ds(0)} = r_s i^e_{ds(0)} - \omega_e l_{ss} i^e_{qs(0)} - \omega_e l_m i^e_{qr(0)} \qquad (3.15)$$

$$0 = \omega_{sl} l_m i^e_{ds(0)} + r_r i^e_{qr(0)} + \omega_{sl} l_{rr} i^e_{dr(0)} \qquad (3.16)$$

$$0 = -\omega_{sl} l_m i^e_{qs(0)} + r_r i^e_{dr(0)} - \omega_{sl} l_{rr} i^e_{qr(0)} \qquad (3.17)$$

Solving equation (3.14) and (3.17) and substituting the value of $v^e_{ds(0)}$ from equation (3.11) result in

$$k\, I_{dc} \omega_{sl} l_m = \left(1 - c\omega_e^2 l_{ss} \right) \omega_{sl} l_m i^e_{qs(0)} + \left(-c\omega_e^2 \omega_{sl} l_m{}^2 - c\omega_e r_s r_r \right) i^e_{qr(0)} - c\omega_e \omega_{sl} l_{rr} r_s i^e_{dr(0)} \qquad (3.18)$$

Solving equation (3.14) and (3.16) and substituting the value $v^e_{qs(0)}$ from equation (3.10) result in:

$$0 = \left(c\omega_e^2 l_{ss} - 1 \right) i^e_{ds(0)} + c\omega_e r_s \, i^e_{qs(0)} + c\omega_e^2 l_m i^e_{dr(0)} \qquad (3.19)$$

41

Finally solving equations (3.17), (3.18), (3.19) results in

$$i^e_{dr(0)} = \frac{kI_{dc}\omega_{sl}l_m(-c\omega_e\omega_{sl}l_{rr}r_s - c\omega_e^2 l_{ss}r_r + r_r)}{((-c\omega_e\omega_{sl}l_{rr}r_s + r_r - c\omega_e^2 l_{ss}r_r)^2 + (c\omega_e^2\omega_{sl}l_1 - c\omega_e r_s r_r - \omega_{sl}l_{rr})^2)} \qquad (3.20)$$

Define,

$$l_1 = l_{ss}l_{rr} - l_m^2$$

$$i^e_{qr(0)} = \frac{-i^e_{dr(0)}(c\omega_e r_s r_r - c\omega_e^2\omega_{sl}l_1 + \omega_{sl}l_{rr})}{(-c\omega_e\omega_{sl}l_{rr}r_s - c\omega_e^2 l_{ss}r_r + r_r)} \qquad (3.21)$$

$$i^e_{ds(0)} = \frac{-r_r i^e_{qr(0)} - \omega_{sl}l_{rr}i^e_{dr(0)}}{\omega_{sl}l_m} \qquad (3.22)$$

$$i^e_{qs(0)} = \frac{r_r i^e_{dr(0)} - \omega_{sl}l_{rr}i^e_{qr(0)}}{\omega_{sl}l_m} \qquad (3.23)$$

$$V_{r(0)} = r_f I_{dc(0)} + \frac{3}{2} k\, v^e_{qs(0)} \qquad (3.24)$$

Torque developed by the motor can be obtained by substituting the values of $i^e_{dr(0)}$ and $i^e_{qs(0)}$ from equation (3.20) and (3.23) in equation (3.13).

$$t_e = \frac{3}{2}\cdot\frac{P}{2}\cdot l_m\left[\frac{kI_{dc}\omega_{sl}l_m(-c\omega_e\omega_{sl}l_{rr}r_s - c\omega_e^2 l_{ss}r_r + r_r)}{\{(c - c\omega_e\omega_{sl}l_{rr}r_s + r_r - c\omega_e^2 l_{ss}r_r)^2 + (c\omega_e^2\omega_{sl}l_1 - c\omega_e r_s r_r - \omega_{sl}l_{rr})^2\}}\right. $$
$$\left. *\left(\frac{-r_r i^e_{qr(0)} - \omega_{sl}l_{rr}i^e_{dr(0)}}{\omega_{sl}l_m}\right)\right] \qquad (3.25)$$

Copper losses in induction motor stator $= \dfrac{3}{2}\cdot r_s((i^e_{qs(0)})^2 + (i^e_{ds(o)})^2) \qquad (3.26)$

Copper losses in induction motor rotor $= \dfrac{3}{2}\cdot r_r((i^e_{qr(0)})^2 + (i^e_{dr(o)})^2) \qquad (3.27)$

Losses in the d.c link $\qquad\qquad = r_f I_{dc(0)}^2 \qquad (3.28)$

Ignoring the core, friction and windage losses, total loss in the drive is given by the following expression:

Total loss = Losses in induction motor stator + Losses in induction motor rotor

+Losses in d.c link

$$= \frac{3}{2}\left[r_s((i^e_{qs(0)})^2 + (i^e_{ds(0)})^2) + r_r.((i^e_{qr(0)})^2 + (i^e_{dr(0)})^2)\right] + r_f I_{dc(0)}^2 \quad (3.29)$$

$$\text{Power factor (lag)} = \cos\left[\left(\tan^{-1}\left(\frac{v^e_{qs(0)}}{v^e_{ds(0)}}\right) - \tan^{-1}\left(\frac{i^e_{qs(0)}}{i^e_{ds(0)}}\right)\right)\right] \quad (3.30)$$

Define,

$$\omega_r = \omega_e - \omega_{sl} \quad (3.31)$$

$$\text{Power out put} = t_e.\omega_r(\text{mech}) \quad (3.32)$$

$$= t_e.\omega_r(\text{elect}).\left(\frac{2}{P}\right) \quad (3.33)$$

$$\text{Efficiency of the drive} = \frac{\text{Power output}}{\text{Power output} + \text{Losses}} \quad (3.34)$$

3.3 COMPUTATION, RESULTS AND DISCUSSIONS

3.3.1 Steady State Performance

The steady state performance under various operating conditions is obtained by simulating the steady state equations 3.14 to 3.34 on digital computer. Computer program is developed to get the performance of the drive. To check the validity of developed program, the performance characteristics of the drive is determined for the following conditions.

(i)   In the original program the value of c is substituted as zero and some of the performance curves are drawn, as shown in Fig 3.1 to 3.4.

(ii)   A new program is written for normal pulse width modulated current source inverter drive (without capacitance at the terminals) and the same performance characteristics are determined [34].

From both the programs similar performance characteristics are obtained. This partially confirms the validity of the developed program. The steady state performance of the drive is studied for the following conditions and the performance curves are drawn under all operating conditions.

(i)   Fixed frequency, Constant d.c. link current, Variable capacitance per phase.

(ii)   Variable frequency, Constant d.c. link current, Fixed capacitance per phase.

(iii)   Variable d.c. link current, Fixed frequency, Fixed capacitance per phase

(iv)   Constant load torque, Fixed capacitance per phase, Fixed d.c. link current

(v)   Linearly varying load torque, Fixed capacitance per phase, Fixed d.c. link current.

3.3.1.1 Constant D.C. Link current, Fixed frequency, Variable capacitance per Phase

The steady state performance curves for fixed value of d.c. link current, fixed frequency and variable capacitance per phase can be obtained by computing the value of torque developed by the motor, power output, stator voltage per phase, stator current, power factor, power loss efficiency, d.c. link voltage by varying the slip from 0 to 1. The d.c. link current is fixed at 4A. The operating frequency is fixed at $\omega_e = 314$ rad/sec. The performance of the drive is obtained for four values of capacitance $c = 90\mu F/phase, 150\mu F/phase, 180\mu F/phase, 210\mu F/phase$. From the calculation it is

44

Characterstic curves without capacitance at the machine terminals
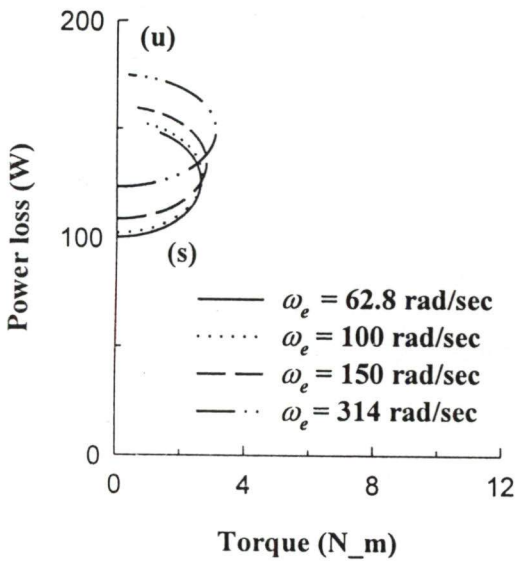
Fig 3.1. Power loss vs. torque characteristics
(I_{dc}= 4.0 A)
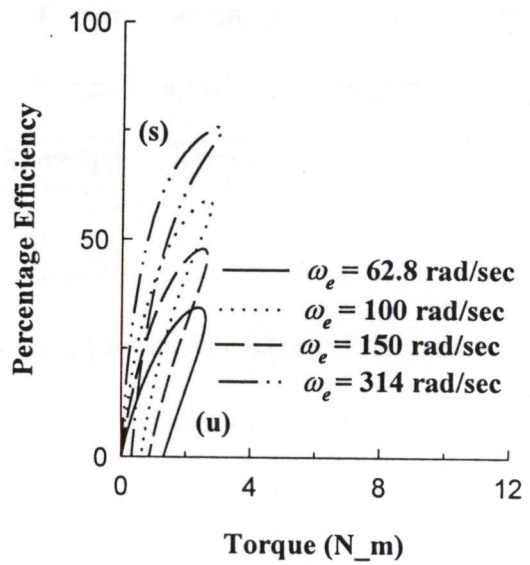
Fig 3.2. Efficiency vs. torque characteristics
(I_{dc}= 4.0 A)
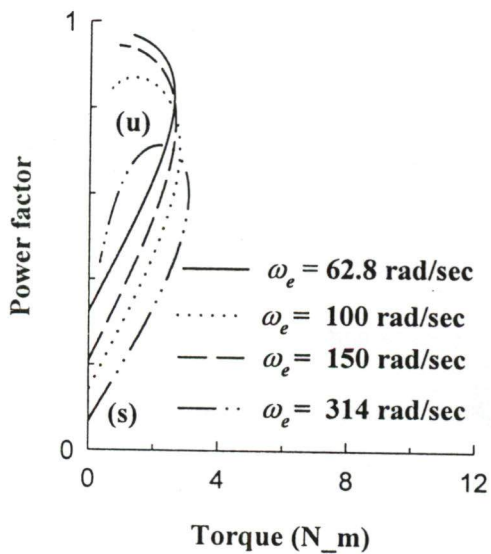
Fig 3.3. Power factor vs. torque characteristics
(I_{dc}= 4.0 A)
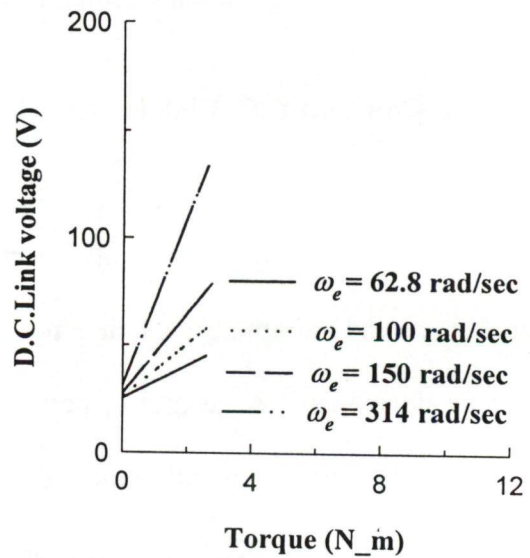
Fig 3.4. D.C.Link voltage vs. torque characteristics
(I_{dc}= 4.0 A)

found that corresponding to full load slip and the rated operating frequency $\omega_e = 314 \, \text{rad/sec}$, the resonance takes place in the machine at the capacitance $c = 55 \, \mu\text{F/phase}$. The magnetization and rotor current variation with torque are shown in the Fig 3.5. These curves are drawn to explain some of the performance characteristics. All the performance characteristics are drawn with respect to torque as shown in Figs. (3.6 to 3.13). At the operating frequency $\omega_e = 314 \, \text{rad/sec}$ and $c = 90 \, \mu\text{F/phase}$, slip-torque characteristic shows that the torque developed by the machine is affected by the resonance. At this value of capacitance only slip-torque characteristics is plotted, with broken lines, other performance characteristics are not plotted at this value of capacitance.

(i)   Slip vs Torque

Slip vs torque characteristic curves are drawn in Fig. 3.6. Each curve is characterized by two regions, a stable region and an unstable region. In stable region as the capacitance increases, the slip increases for any value of torque. The peak value of torque decreases with the increase in capacitance while the slip corresponding to peak value of torque increases with the increase in capacitance. The variation of slip with torque is very clear from the rotor current vs torque variation curves drawn in Fig. 3.5 With the increase in capacitance, rotor current increases with the torque i.e. slip increases with the torque. The value of starting torque is high at higher value of capacitance. As obvious the torque at any value of slip in unstable region is less than the torque in stable region at any value of slip, at each value of capacitance.

(ii)   Power output vs torque characteristics

The power output vs torque curves are shown in Fig. 3.7. Each curve has two regions, a stable region and unstable region. In the stable region at lower capacitance,
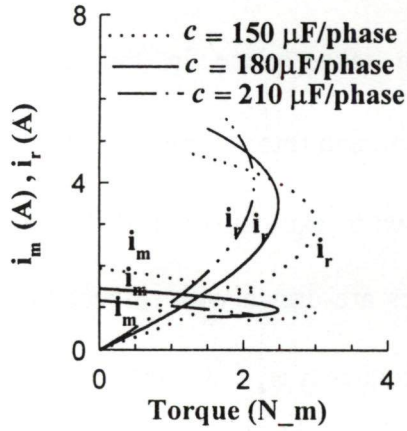
Fig 3.5. i_m, i_r vs. torque characteristics
(I_{dc} = 4.0 A, ω_e = 314 rad/sec)
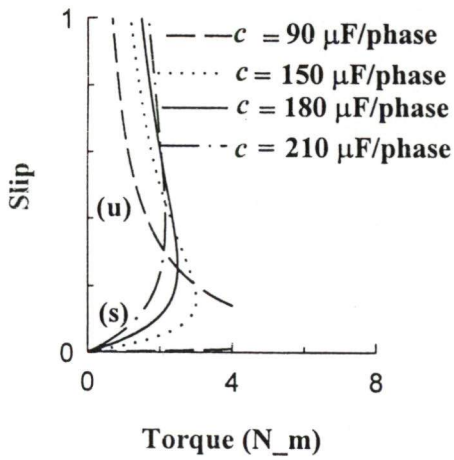
Fig 3.6. Slip vs. torque characteristics
(I_{dc} = 4.0 A, ω_e = 314 rad/sec)
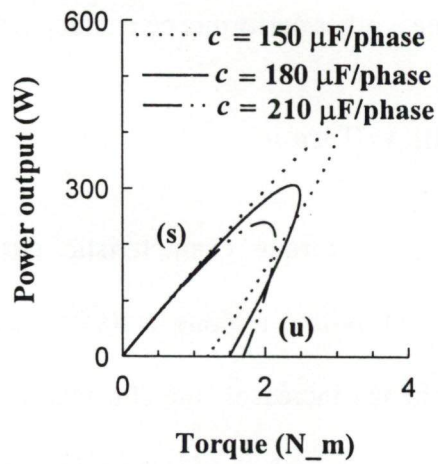
Fig 3.7. Power output vs. torque characteristics
(I_{dc} = 4.0 A, ω_e = 314 rad/sec)
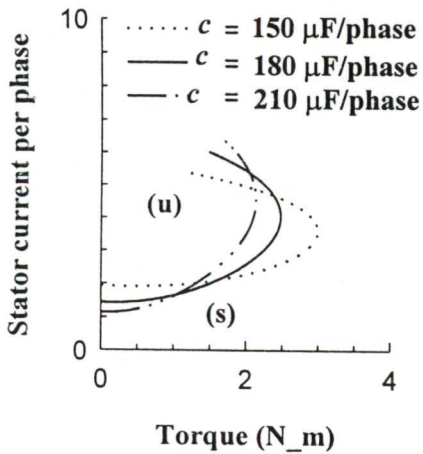
Fig 3.8. Stator current vs. torque characteristics
(I_{dc} = 4.0 A, ω_e = 314 rad/sec)
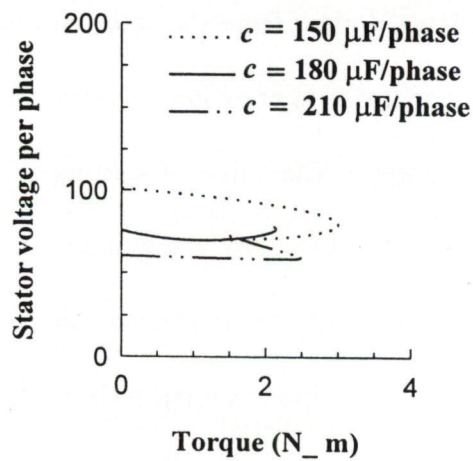
Fig 3.9. Stator voltage vs. torque characteristics
(I_{dc} = 4.0 A, ω_e = 314 rad/sec)

47

higher torque occurs at small value of slip. Therefore corresponding power output is high. The maximum value of power output reduces with the increase in capacitance. Power output decreases with decrease in torque, in unstable region at each value of capacitance, because of low torque and high value of slip.

(iii)   Stator current vs Torque

The relevant curves are plotted in Fig. 3.8. The stator current increases with increase in torque, in stable region, corresponding to each value of capacitance. The stator current is the phasor sum of the magnetization and the rotor currents. As it is clear from the curves drawn in Fig. 3.5 the magnetization current is nearly constant with respect to torque at any value of capacitance while rotor current varies widely with respect to torque. In the stable region at low value of slip, magnetization current is large in comparison to the rotor current; therefore stator current varies according to the variation of magnetization current. At high value of slip, rotor current is large in comparison to the magnetization current, therefore stator current varies according to the variation of the stator current. In the unstable region stator current increases with the decrease in torque corresponding to each value of capacitance because of high value of rotor current.

(iv)   Stator voltage Per Phase vs Torque

The variations of stator voltage vs torque curves are shown in Fig. 3.9. The stator voltage depends upon the product of stator current and net impedance of the machine (including stator impedance, magnetizing impedance, rotor impedance). As obvious the net impedance of the machine decreases with the increase in the torque; while stator current increases with the increase in torque. The product of the two vary in such a way that in the stable region voltage decreases with the increase in capacitance. Corresponding

48

to each value of capacitance the voltage is maximum at zero value of slip. In unstable region at medium and high value of capacitance stator voltage increases with the torque while at the low value of capacitance it decreases with decrease in torque.

(v)   Power Loss vs Torque

Power loss vs torque variations plots are shown in Fig. 3.10. Each curve is characterized by two regions, a stable region, and an unstable region. Corresponding to each value of capacitance, the power loss is low in stable region, and high in unstable region. In stable region power loss increases slowly with increase in torque because of slow increase in stator and rotor currents ,while in unstable region power loss increases rapidly with decrease in torque because of large increments in stator and rotor currents. In unstable region, power loss is more due to increased rotor copper loss .

(vi)   Percentage efficiency vs Torque

The plots are shown in Fig. 3.11. Each curve is characterized in the two regions, stable and unstable. Efficiency of the drive is more in stable region, than in unstable region at each value of capacitance. Efficiency of the drive is poor in unstable region because of low power output and high loss. In the stable region at low value of torque efficiency of the drive is almost same at each value of capacitance because of almost same power output and same power losses; at high value of torque, efficiency increases with the increase in torque. The maximum value of efficiency decreases with the increase in capacitance. In unstable region efficiency decreases with the decrease in torque at each value of capacitance.
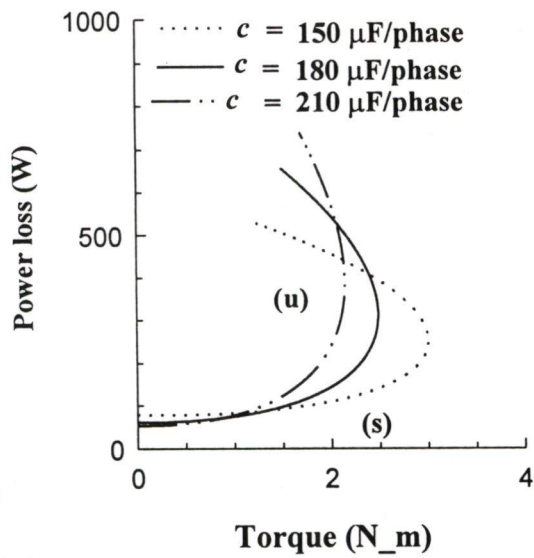
Fig 3.10. Power loss vs. torque characteristics
($\omega_e = 314$ rad/sec, $I_{dc} = 4.0$ A)
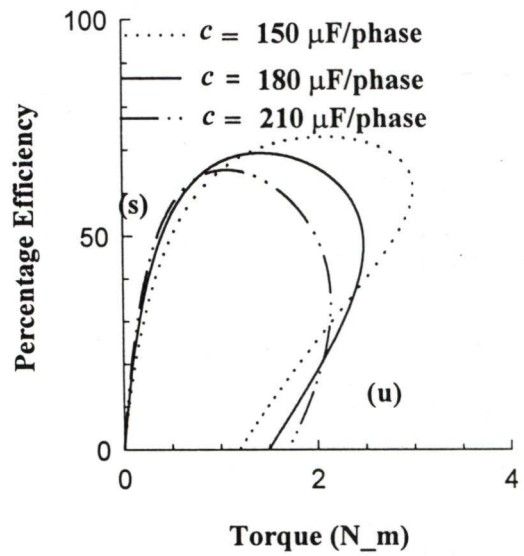
Fig 3.11. Efficiency vs. torque characteristics
($\omega_e = 314$ rad/sec, $I_{dc} = 4.0$ A)
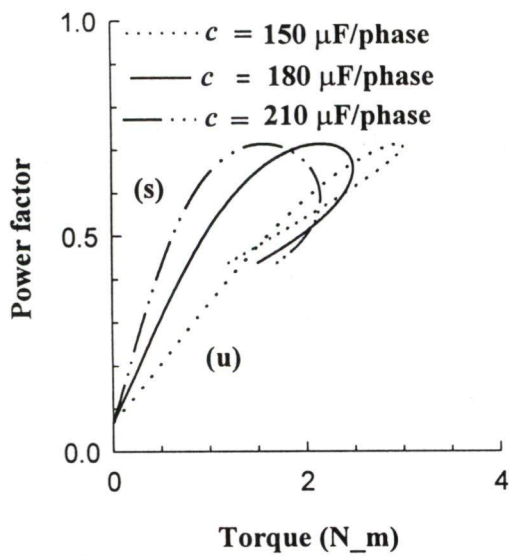
Fig 3.12. Power factor vs. torque characteristics
($I_{dc} = 4.0$ A, $\omega_e = 314$ rad/sec)
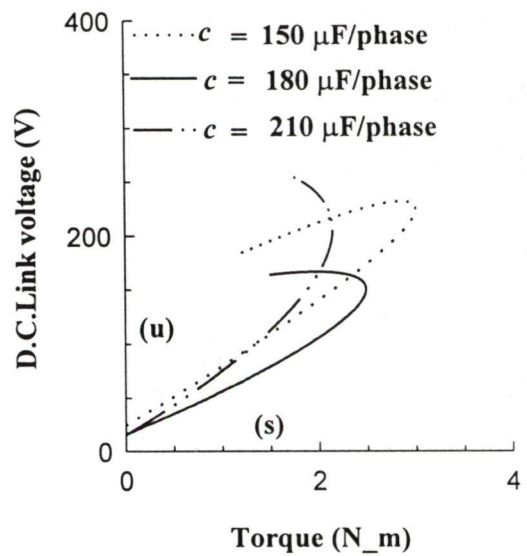
Fig 3.13. D.C.Link voltage vs. torque characteristics
($I_{dc} = 4.0$ A, $\omega_e = 314$ rad/sec)

50

(vii)   Power Factor vs Torque

The characteristics are shown in Fig. 3.12. The power factor   variation depends upon the machine parameters, slip and operating frequency. It does not depend upon the capacitance connected across machine terminals. Hence the minimum and maximum value of power factor are same for all the three values of capacitance. With the increase in slip, power factor increases up to a certain value then it decreases with the increase in slip. Since the slip, corresponding to torque changes with the capacitance connected across machine terminals, hence the power factor of the machine also changes with respect to torque at each value of capacitance. The variation of slip is more with torque at high value of capacitance and hence the power factor variation is more at high value of capacitance. In the unstable region power factor decreases with the decrease in torque .

(viii)   D.C. Link Voltage vs Torque

The d.c. link voltage vs torque characteristics are shown in Fig. 3.13. Since the d.c.link current is assumed constant, therefore, the power output of the inverter is directly proportional to d.c.link voltage neglecting the losses within the inverter. The power output increases with the torque and hence d.c.link voltage also increases with the torque. The d.c.link voltage increases linearly with the torque at each value of capacitance. In the unstable region d.c.link voltage decreases with the torque at low value of capacitance, while it increases with the torque at medium and high value of capacitance.

The performance characteristics show that at the machine terminals capacitance of $150\,\mu F/phase$, the performance of the drive is better. The experimental investigations are also carried out in open loop with the different values of capacitance across motor terminals, and it is found that the open loop performance of the drive is found to be the

51

best at the capacitance value of $150\,\mu F\,/\,phase$. Hence this value of capacitance is selected for the simulation at the different operating conditions, discussed below, and for practical investigations of the drive.

3.3.1.2 Fixed d.c. link Current , Variable Frequency, Fixed Capacitance per phase

After selecting the capacitance as $150\,\mu F\,/\,phase$ across motor terminals, the steady state performance characteristics of the drive are obtained by determining the torque, power output, stator current, stator voltage, power loss, efficiency, power factor and d.c. link voltage for variation in the slip from 0 to 1. The performance characteristics of the drive are drawn with respect to torque at fixed $I_{dc} = 4.0$ A , variable frequency, and fixed capacitance per phase $c = 150\,\mu F\,/\,phase$. The magnetization and rotor current variation with torque shown in the Fig 3.14. These curves are drawn to explain some of the performance characteristics The performance characteristics are shown in Figs.3.15 to 3.22. At the operating frequency $\omega_e = 150\,rad\,/\,sec$ and c = 150 μF/phase, slip- torque characteristic shows that the torque developed by the machine is affected by the resonance. At this operating frequency only slip – torque characteristics of the drive is shown with the broken line, other performance characteristics are not shown at this operating frequency.

(i)   Slip vs Torque

Slip vs torque characteristics are drawn at the operating frequencies, $\omega_e = 62.8\,rad\,/\,sec, 100\,rad\,/\,sec, 150\,rad\,/\,sec, 314\,rad\,/\,sec$, as shown in Fig.3.15. Each curve is characterized by the two regions, a stable and an unstable region. In the stable region, slip increases slowly with the increase in torque at each operating frequency. At medium
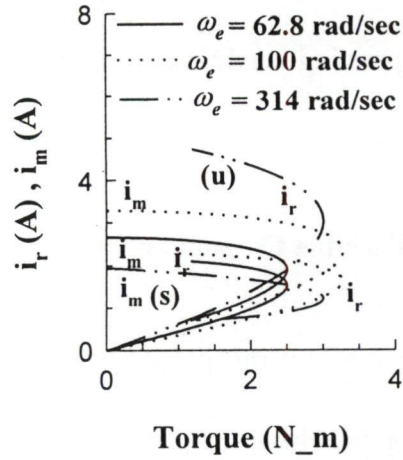
Fig 3.14. i_m , i_r **vs. torque characteristics**
$(I_{dc} = 4.0$ A, $c = 150$ μF/phase $)$
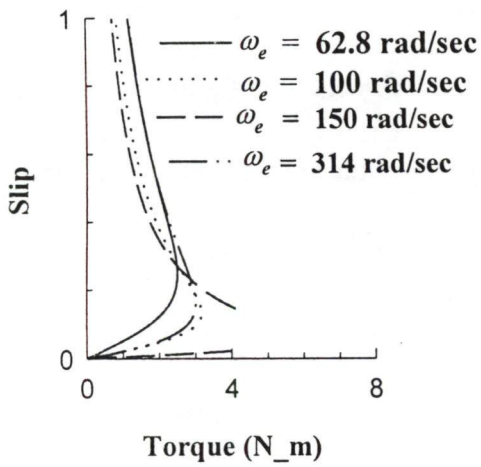
Fig 3.15. Slip vs. torque characteristics
$(I_{dc} = 4.0$ A, $c = 150$ μF/phase$)$
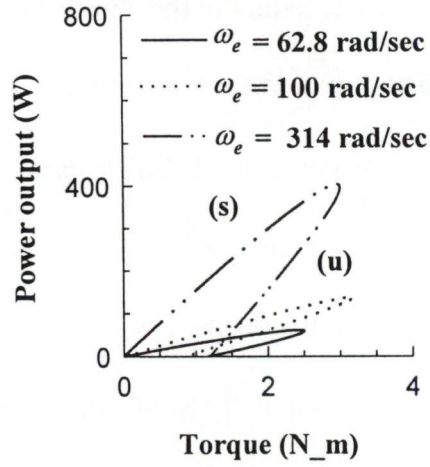
Fig 3.16. Power output vs. torque characteristics
$(I_{dc} = 4.0$ A, $c = 150$ μF/phase$)$
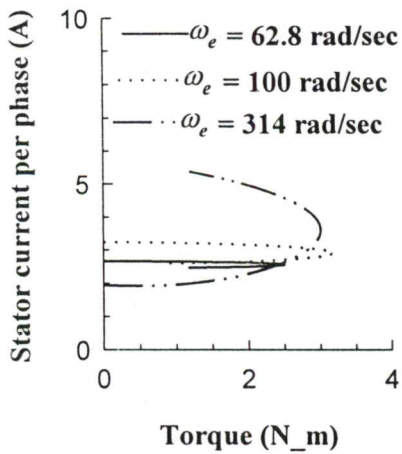
Fig 3.17. Stator current vs. torque characteristics
$(I_{dc} = 4.0$ A, $c = 150$ μF/phase$)$
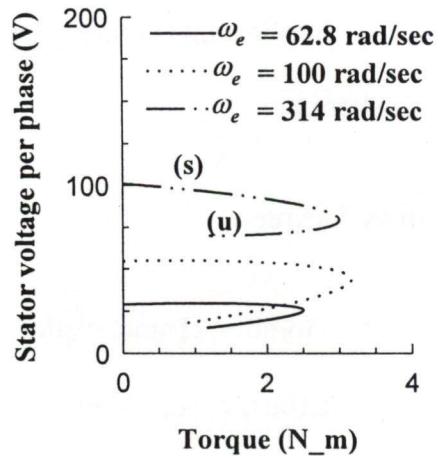
Fig 3.18. Stator voltage vs. torque characteristics
$(I_{dc} = 4.0$ A, $c = 150$ μF/phase$)$

and high values of operating frequency, the peak torque is almost same and it occurs almost at the same value of the slip. At low value of the operating frequency $\omega_e = 62.8 \, \text{rad/sec}$, the peak value of the torque occurs at high value of slip and its magnitude is also less in comparison to values of peak torque at medium and high value of the operating frequencies.

(ii)   Power output vs Torque

The required characteristics are plotted in Fig. 3.16. Each curve is characterized by the two regions, a stable region and an unstable region. As expected the power out put at any value of torque is more at higher frequency of the operation. At any value of operating frequency power output in unstable region is less in comparison to the power output in the stable region because of increased rotor copper loss. Core, friction and windage losses are neglected.

(iii)   Stator Current vs Torque

The stator current vs torque plots are shown in Fig. 3.17. The stator current is the phasor sum of the rotor current and magnetizing current. As shown in the Fig 3.14 ,the value of magnetizing current is quite high in comparison to the rotor current at low and medium value of operating frequencies and its variation is also very small with respect to torque in the stable region. Therefore the stator current is almost constant with the torque in the stable slip- torque region at low and medium values of operating frequencies. At high value of operating frequency, as shown in the Fig. 3.14 the value of rotor current varies rapidly with the torque in the stable region and after a certain value of the torque rotor current exceeds the value of the magnetizing current. Hence the stator current

variation with torque is mainly decided by the variation of rotor current with the torque and it increases slowly with the torque. In the unstable region the stator current decreases with the decrease in torque at low and medium value of operating frequencies, while it increases with decrease in torque at high frequency of operation.

(iv)   Stator Voltage vs Torque

Stator voltage vs torque curves are shown in Fig. 3.18. The stator voltage depends upon the product of stator current and net machine impedance. In stable region at low and medium values of operating frequencies, net impedance of the machine is almost constant because of small value of slip variation. At high value of operating frequency, the net impedance of the machine is high and varies widely with respect to torque, the net impedance of the machine decreases with the increase in torque. Therefore the stator voltage in stable region at low and medium value of operating frequencies are almost constant, while it decreases slightly with the torque at high value of operating frequency. At all the operating frequencies the stator voltage decreases with the decrease in torque in the unstable region.

(v)   Power Loss vs Torque

Power loss vs torque characteristics are shown in Fig. 3.19. Each curve is characterized by two regions, a stable region and an unstable region. Corresponding to each value of operating frequency, the power loss is low in stable region, and high in unstable region. In stable region power loss is almost constant with increase in torque, at low and medium value of operating frequencies, while at high value of operating frequency power loss increases slowly with increase in torque. At low value of operating frequency, the power loss is same in both the regions. In unstable region at medium and
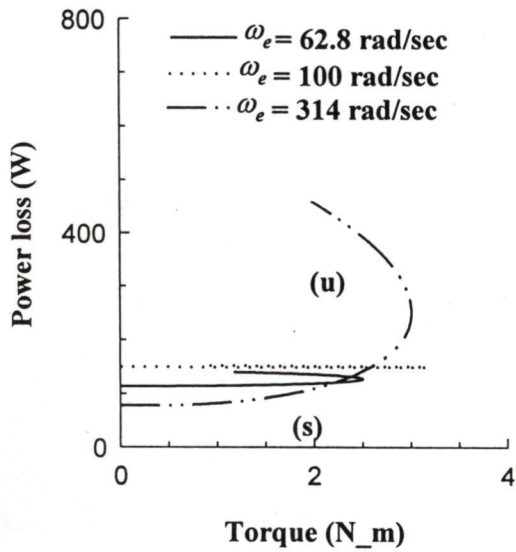
Fig 3.19. Power loss vs. torque characteristics
$(I_{dc} = 4.0$ A, $c = 150$ μF/phase$)$
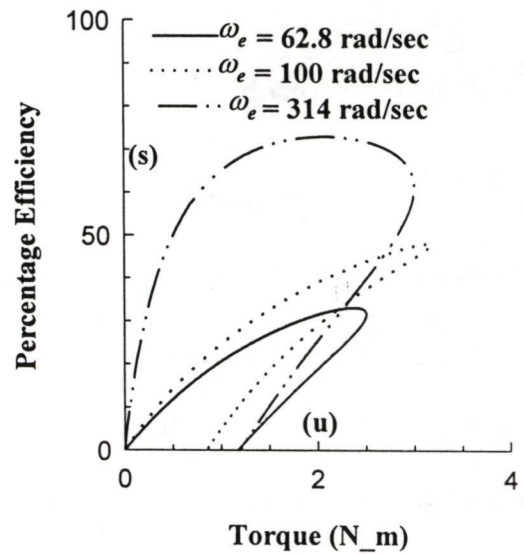
Fig 3.20. Efficiency vs. torque characteristics
$(I_{dc} = 4.0$ A, $c = 150$ μF/phase$)$
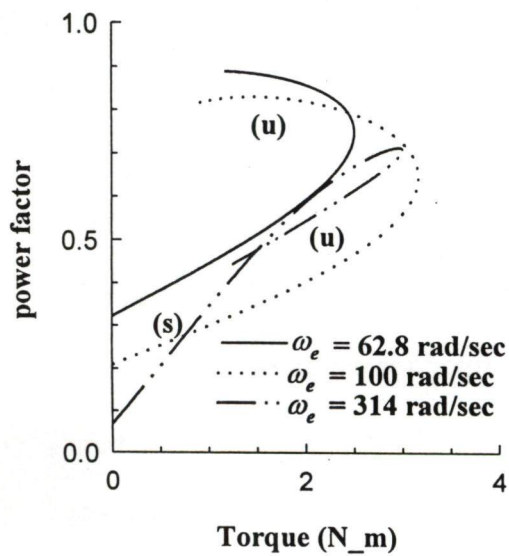
Fig 3.21. Power factor vs. torque characteristics
$(I_{dc} = 4.0$ A, $c = 150$ μF/phase$)$
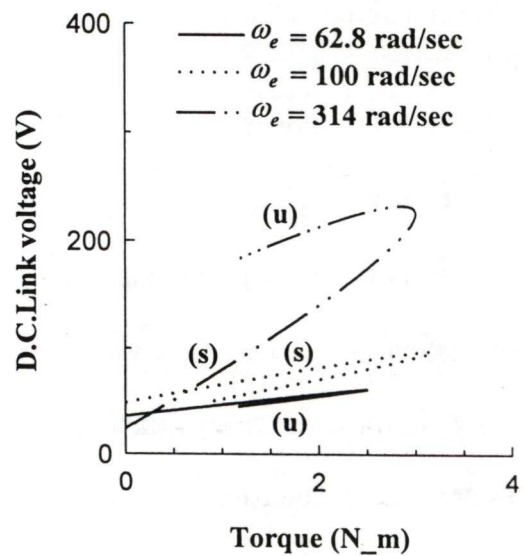
Fig 3.22. D.C.Link voltage vs. torque characteristics
$(I_{dc} = 4.0$ A, $c = 150$ μF/phase$)$

high value of operating frequencies, power loss is more in comparison to the stable region. At medium frequency of operation, power loss in both the regions are not much different.

(vi) Efficiency vs Torque

The efficiency vs torque characteristics are shown in Fig. 3.20. Each curve is characterized in the two regions, a stable and an unstable. Efficiency of the drive is more in stable region, than unstable region at each value of operating frequency. Efficiency of the drive is poor in unstable region, because of low power output and high loss. As expected in the stable region at each value of operating frequency, the efficiency increases with the increase in torque. The maximum value of efficiency is obtained at high frequency of operation because of high power output and low value of losses. In unstable region efficiency decreases with decrease in torque at each value of capacitance because of low power output and increased copper loss.

(vii) Power Factor vs Torque

The plots are shown in Fig. 3.21. The power factor increases with the increase in torque in the stable region at each operating frequency just like an ordinary induction motor. As the operating frequency increases the power factor decreases with the torque in the stable region because of high value of stator and rotor reactance. In the unstable region power factor is better than stable region at any value of torque at low and medium value of operating frequencies. At high value of operating frequency the power factor is poor than stable region at any value of torque.

(viii) D.C. Link Voltage vs Torque

D.C. link voltage vs torque plots are shown in Fig. 3.22. At constant value of d.c.link current the d.c. link voltage depends upon the power output of the inverter neglecting the losses in the inverter. In stable region at each value of operating frequency the power output of the machine increases with the torque, hence the d.c.link voltage increases with the increase in torque in the stable region. As the operating frequency increases the d.c.link voltage increases because of high power output. In the unstable region the d.c. link voltage decreases with the decrease in torque at low and medium value of operating frequencies, because of low power output. At high value of operating frequency though the power output decreases with decrease in torque in the unstable region, the d.c.link voltage increases due to high motor copper loss.

3.3.1.3 Variable d.c. link current, Fixed frequency, Fixed capacitance per phase.

The performance characteristics for the above conditions are drawn in Figs. 3.23 to 3.30. The performance characteristics are drawn at the three values of d.c. link currents, $I_{dc} = 2.0A, 4.0A, 6.0A$, at a fixed operating frequency $\omega_e = 314 \text{rad/sec},$ and capaci $\tan ce \ c = 150 \mu F/phase$ across machine terminals.

(i) Slip vs Torque

The slip vs torque characteristics for different d.c.link currents are shown in Fig. 3.23. At a fixed operating frequency, the rotor and magnetizing currents are directly proportional to the d.c.link current at a slip and hence torque developed at any slip is proportional to the square of the d.c.link current. Therefore as the d.c.link current increases torque developed by the machine increases in both the regions. At a fixed

58
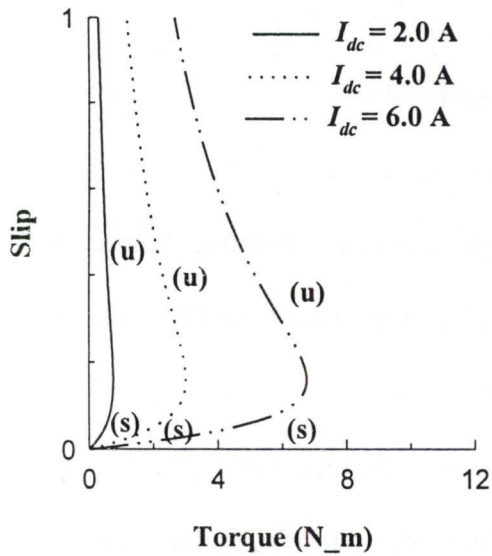
Fig 3.23. Slip vs. torque characteristics
($c = 150\mu$F/phase, $\omega_e = 314$ rad/sec)
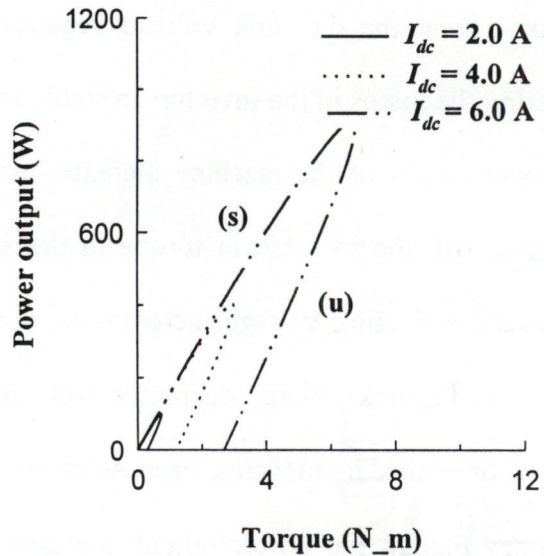
Fig 3.24. Power output vs. torque characteristics
($c = 150\mu$F/phase, $\omega_e = 314$ rad/sec)
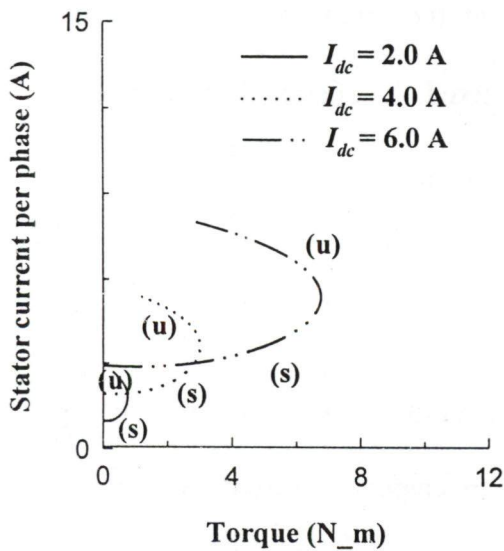
Fig 3.25. Stator current vs. torque characteristics
($c = 150\mu$F/phase, $\omega_e = 314$ rad/sec)
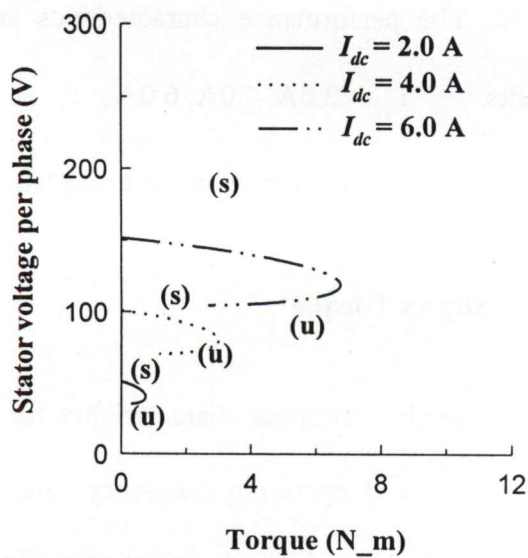
Fig 3.26. Stator voltage vs. torque characteristics
($c = 150\mu$F/phase, $\omega_e = 314$ rad/sec)

operating frequency the slip corresponding to peak torque occurs at the same value of slip in all the cases and its magnitude is proportional to the square of the d.c.link current. In unstable region slip increases with the decrease in torque at each value of d.c.link current.

(ii) Power Output vs Torque

Power output vs torque plots are shown in Fig. 3.24. Each curve has two regions, a stable region and an unstable region.. At fixed operating frequency corresponding to each value of d.c.link current, the power output increases linearly with the increase in torque in stable region of slip-torque curve. In the stable region peak torque, occurring at the same value of slip, is large at high value of d.c.link current than the low and medium values of d.c. link currents ; therefore the power output is large at high value of d.c.link current than the low and medium values of d.c. link currents. In the unstable region power output decreases with the decrease in torque at each value of d.c.link current because of high value of copper losses.

(iii) Stator Current vs Torque

The stator current vs torque characteristics are shown in Fig. 3.25. The nature of stator current variation with torque is similar at each value of d.c.link current in the stable region, although their magnitudes are different. The stator current is the phasor sum of magnetization and rotor currents. Corresponding to each value of d.c.link current, in stable region, at low value of torque, the magnetization current is very large than the rotor current and it is almost constant; hence the stator current is mainly due to magnetization current and it is almost constant. After a certain value of torque, the rotor current is more than the magnetization current and hence the stator current is mainly due to rotor current

and it increases due to increase in torque. As the d.c.link current increases, the magnetization and rotor both current increases, therefore the stator current at any value of slip increases with the increase in d.c.link current. At each value of d.c.link current stator current at any value of torque is more than its value in the stable region because of increased value of rotor current at high value of slip.

(iv) Stator voltage per phase vs Torque

The stator voltages per phase vs torque characteristics are shown in Fig. 3.26. The stator voltage per phase, depends upon the product of stator current and net impedance of the machine. Machine impedance decreases with the increase in torque in the both the region. At high value of d.c.link current the net impedance variation of machine with the torque is slow. In the stable region at high value of d.c. link current, the stator current increases very slowly with the increase in torque. The net effect is stator voltage decreases with increase in torque. In stable region at low and medium value of d.c.link currents the stator currents and net impedance of the machine varies faster with torque than the high value of d.c.link current. The net effect is stator voltage decreases fast with the torque at low and medium value of d.c.link currents. The stator voltage is less in unstable region at any value of torque than the value in stable region at each value of d.c.link current. The variation of stator voltage with the torque is less at each value of d.c.link currents in the unstable region.

(v) Power Loss vs Torque

The desired characteristics are shown in Fig. 3.27. At each value of d.c. link current, the power loss increases with the increase in torque due to increase in stator and rotor currents. At high value of d.c. link current power loss is more because of higher
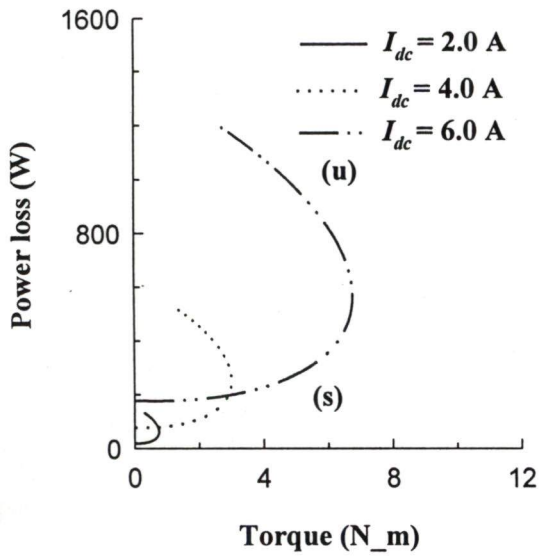
Fig 3.27. Power loss vs. torque characteristics
($c = 150 \ \mu$F/phase , $\omega_e = 314$ rad/sec)
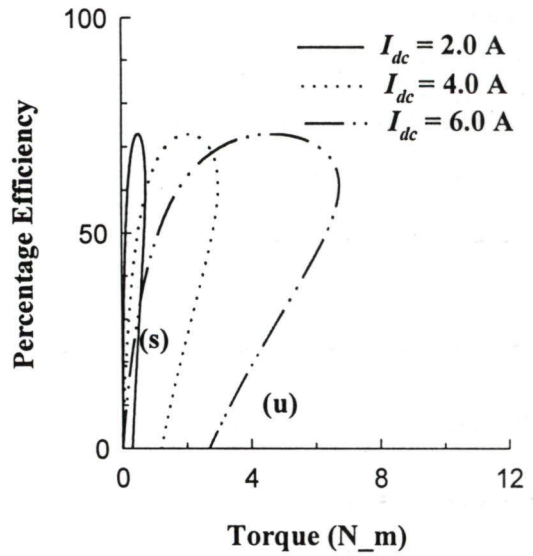
Fig 3.28. Efficiency vs. torque characteristics
($c = 150 \ \mu$F/phase , $\omega_e = 314$ rad/sec)
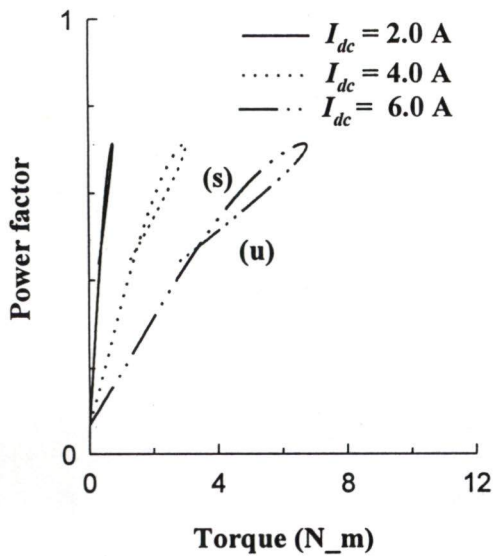
Fig 3.29. Power factor vs. torque characteristics
(c =150μF/phase, ω_e = 314 rad/sec)
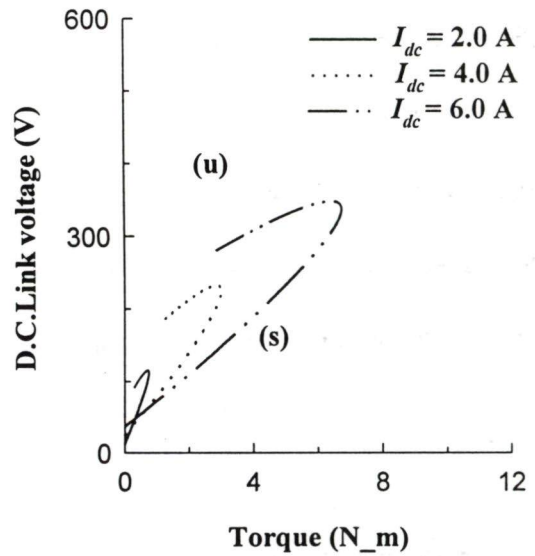
Fig 3.30. D.C.Link voltage vs. torque characteristics
(c =150μF/phase, ω_e = 314 rad/sec)

value of stator and rotor currents. In the unstable region power losses are more than stable region at each value of d.c.link current because of increased rotor copper loss.

(vi)   Percentage Efficiency vs Torque

The relevant curves are plotted in the Fig. 3.28. Each curve is characterized by the two regions, a stable and an unstable. As expected in the stable region with the increase in torque efficiency increases up to a maximum value at each value of d.c.link currents. At a fixed operating frequency the variation of efficiency and its maximum value with slip is same at each value of d.c.link currents. Hence the maximum efficiency at each value of d.c.link current is same , although it occurs at the different values of torque. As the d.c.link current increases the torque corresponding to maximum efficiency increases. In unstable region at each value of operating frequency, efficiency of the drive decreases with decrease in torque. At each value of d.c.link current efficiency of the drive is poor in unstable region, because of low power outputs and high losses.

(vii)   Power Factor vs Torque

Power factor vs torque plots are shown in Fig.3.29. The power factor of the machine does not depend upon the input d.c.link currents; hence the minimum and maximum value of the power factor is same at each value of d.c.link current. For fixed machine parameters and fixed operating frequency, power factor depends upon the slip variation. At each value of d.c.link current slip- torque variation is different therefore the power factor vs torque variation is different in all the three cases. In the stable region as the torque increases power factor also increases at each value of d.c.link currents. As the d.c.link current increases, the power factor vs torque variation decreases because of slow

variation of slip with torque. In unstable region power factor decreases with the decrease in torque at each value of d.c.link current.

(viii) D.C. link Voltage vs Torque

The d.c. link voltage variation vs. torque plots are shown in Fig 3.30. In the stable region the d.c.link current increases with the input power demand by the drive increases because of increased power output. To meet out the input power requirement of the drive the d.c.link voltage increases with the increase in torque in the stable region at each value of d.c.link current. In the unstable region corresponding to each value of torque input power demand of the drive increases with the decrease in torque because of high copper loss; therefore the d.c.link voltage increases with the decrease in the torque.

3.3.1.4 Constant Load Torque, Fixed D.C. Link current , Fixed Capacitance per Phase, Variable Speed

The performance characteristics, of the drive at a constant load torque of 0.8 times the rated value are determined. The operating frequency of the drive is increased from a minimum value to the rated value, with the d.c. link current fixed at its rated value of $I_{dc} = 5.5A$. The performance characteristics of the drive are drawn with respect to speed as shown in Figs. 3.31 to 3.38. Nearly at the angular speed $(\omega_r) = 135$ rad/sec, the phenomenon of resonance is observed. The effect of resonance is observed up to the angular speed $(\omega_r) = 245$ rad/sec, hence the performance characteristics of the drive are discussed before the occurrence of the resonance. The performance characteristic of the drive in the resonance affected region is shown with the dotted line.

(i)   Torque vs Speed

The torque vs speed curve is shown in Fig. 3.31. Since the load torque is kept constant, hence torque developed by the drive is also constant with respect to speed. The torque required for friction and windage losses are neglected in the analysis.

(ii)   Power Output vs Speed

Power output vs speed curve is shown in Fig. 3.32. Power output depends upon the torque and speed. Since load torque is fixed at all the operating speeds, hence power output is proportional to speed.

(iii)   Stator Current vs Speed

Stator current per phase vs speed variation is shown in Fig 3.33. With the increase in speed operating frequency increases and slip decreases. Therefore stator current increases with the increase in speed.

(iv)   Stator Voltage vs Speed

Stator voltage vs speed variation is shown in Fig3.34. Stator voltage depends upon the product of stator current and net impedance of the machine. At constant load torque, the operating frequency and slip both changes; although the slip variation is small, hence net impedance of the machine changes mainly due to change in operating frequency. As the speed increases, the machine impedance continuously increases with the increase in speed, stator current also increases continuously with the speed of the machine. Therefore stator voltage continuously increases with the increase in speed.
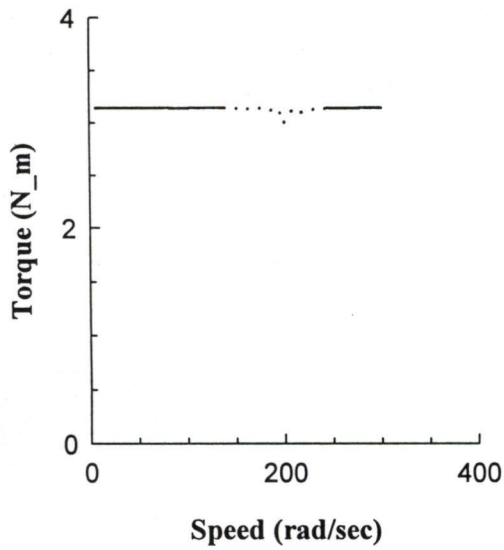
Fig 3.31. Torque vs. speed characteristics $(I_{dc}= 5.5$ A, $t_l= .8\,t_L$, $c = 150\ \mu$F/phase)
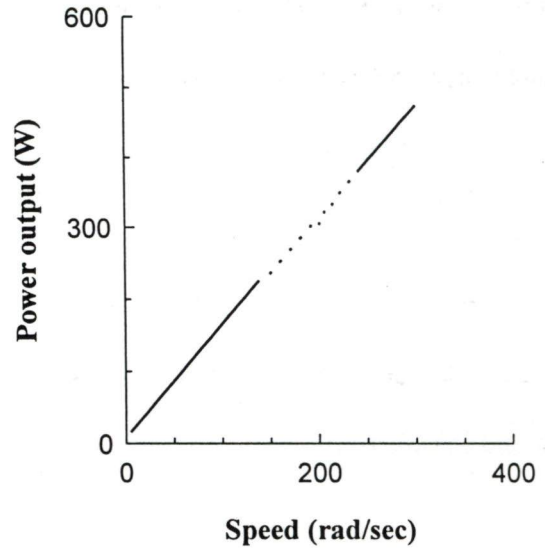
Fig 3.32. Power output vs. speed characteristics $(I_{dc}= 5.5$ A, $t_l= .8\,t_L$, $c = 150\ \mu$F/phase)
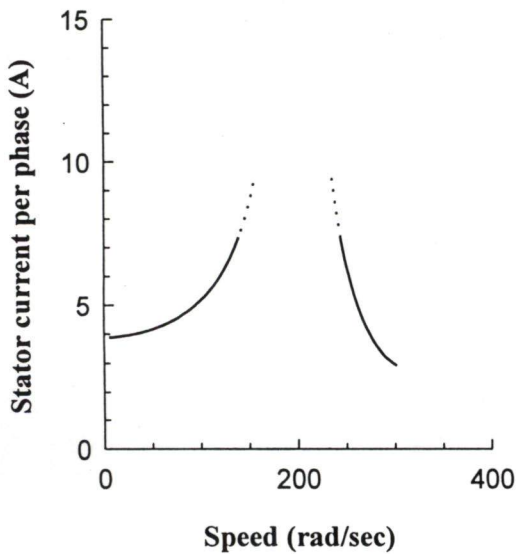
Fig 3.33. Stator current vs. speed characteristics $(I_{dc}= 5.5$ A, $t_l= .8\,t_L$, $c = 150\ \mu$F/phase)
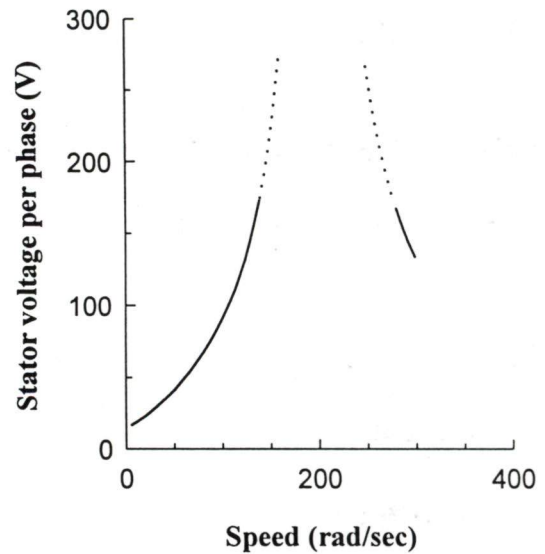
Fig 3.34. Stator voltage vs. speed characteristics $(I_{dc}= 5.5$ A, $t_l= .8\,t_L$, $c = 150\ \mu$F/phase)

(v) Power Loss vs Speed

Power loss vs speed curve is shown in Fig 3.35. Power loss increases with the increase in speed. As the speed increases, current drawn by the drive increases with the increase in speed, resulting in higher copper losses. Iron, friction and windage losses are not considered in the analysis.

(vi) Percentage Efficiency vs Speed

The plot is shown in Fig 3.36. The efficiency of the drive depends on power output and losses. Initially the efficiency of the drive increase linearly with the increase in speed because of linear increase in power output with the speed, while power loss is almost constant with the increase in speed. After a certain value of speed, power loss increases faster than the power output with the increase in speed; hence efficiency decreases with the increase in speed.

(vii) Power Factor vs Speed

Power factor vs speed curve is drawn in Fig 3.37. With the increase in operating frequency, power factor decreases.

(viii) D.C. Link Voltage vs Speed

D.C. Link voltage vs speed plot is shown in Fig 3.38. At constant d.c. link current, the d.c.link voltage depends upon input power demand of the machine. With the increase in speed, power input of the drive increases, hence d.c. link voltage increases with the increase in speed.
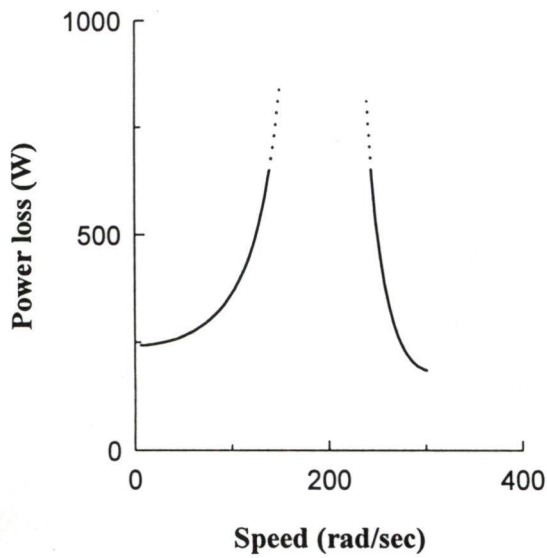
Fig 3.35. Power loss vs. speed characteristics
$(I_{dc} = 5.5 \text{ A}, t_l = .8 \, t_L, c = 150 \, \mu\text{F/phase})$
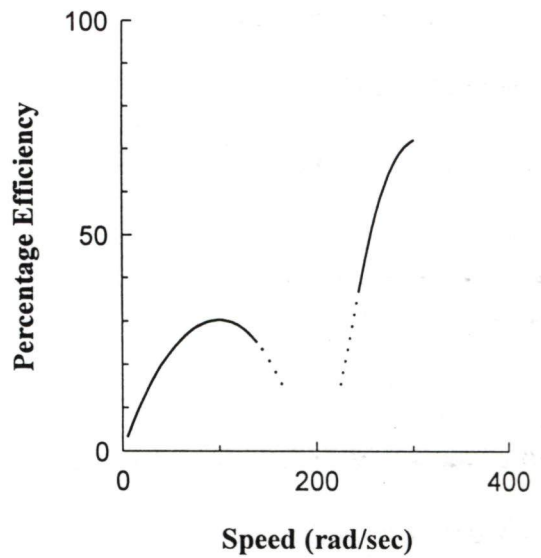
Fig 3.36. Efficiency vs. speed characteristics
$(I_{dc} = 5.5 \text{ A}, t_l = .8 \, t_L, c = 150 \, \mu\text{F/phase})$
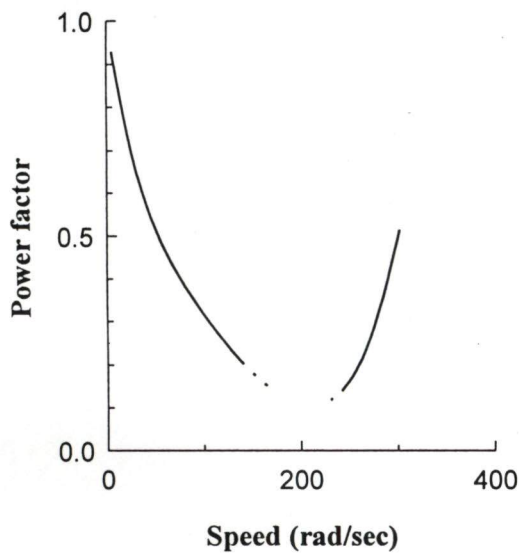
Fig 3.37. Power factor vs. speed characteristics
$(I_{dc} = 5.5 \text{ A}, t_l = .8 \, t_L, c = 150 \, \mu\text{F/phase})$
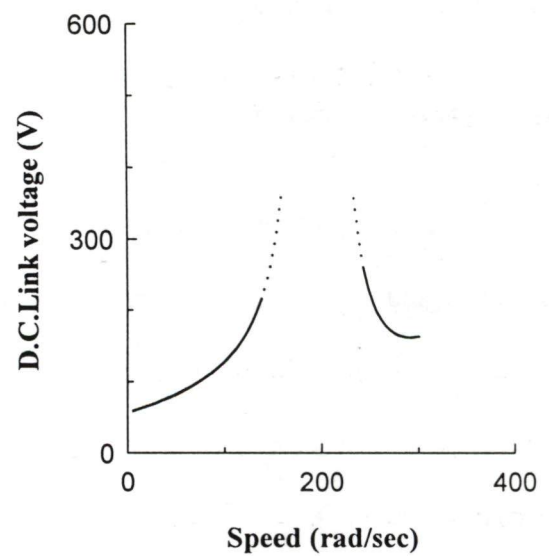
Fig 3.38. D.C.Link volage vs. speed characteristics
$(I_{dc} = 5.5 \text{ A}, t_l = .8 \, t_L, c = 150 \, \mu\text{F/phase})$

3.3.1.5 Linearly Varying Load Torque, Fixed d.c. link Current, Fixed Capacitance per phase

The performance characteristics are drawn at a load torque $\left(t_l = T_L * \left(\frac{\omega_r}{\omega_b} \right) \right)$

where $T_L = 3.93$ N_m and $\omega_r = 314$ rad/sec, linearly varying with the speed at a fixed d.c. link current $I_{dc} = 5.5$ A and fixed $c = 150\mu F/phase$. The motor is run at different speeds by changing the operating frequency and the performance of the drive is evaluated. The performance characteristics are plotted against torque. The phenomena of resonance is observed in the speed range 130 rad/sec to 248 rad/sec corresponding torque (1.6 N_m, to 3.10 N_m). The performance curves in this region of torque are shown with the dotted line and the behavior of the performance curves are discussed before the occurrence of the resonance. The performance curves are shown in Figs. 3.39 to 3.46.

(i)   Speed vs torque

Speed vs torque curve is shown in Fig 3.39. Since load torque is varying linearly with the speed of the motor, hence electrical torque also varies linearly with the speed.

(ii)   Power output vs Torque

Power output vs torque curve is shown in Fig 3.40. Power output depends upon the torque and speed; hence power output increases in square proportion of the increase in torque.

(iii)   Stator current per phase vs Torque

The stator current vs torque plot is shown in Fig 3.41. With the increase in torque demand, there is increase in stator current.
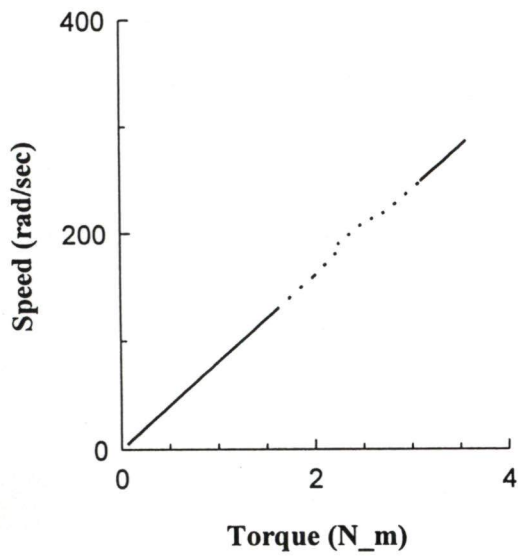
Fig 3.39. Speed vs. torque characteristics
$(I_{dc} = 5.5$ A, $t_l = t_L*(\omega_r/\omega_b)$, $c = 150$ μF/phase)
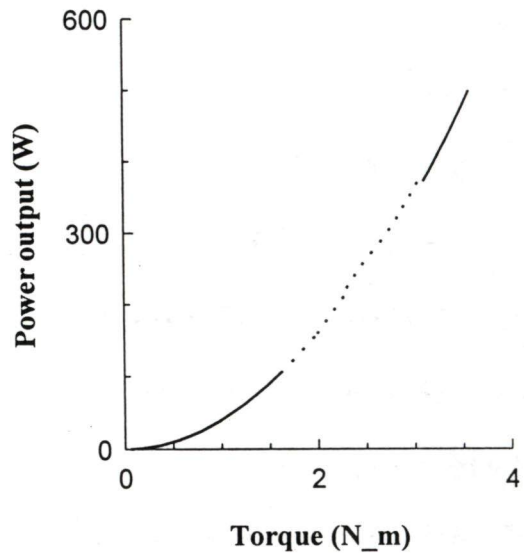
Fig 3.40. Power output vs. torque characteristics
$(I_{dc} = 5.5$ A, $t_l = t_L*(\omega_r/\omega_b)$, $c = 150$ μF/phase)
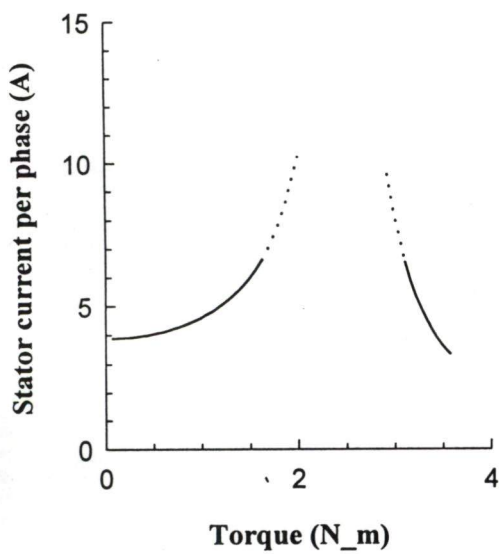
Fig 3.41. Stator current vs. torque characteristics
$(I_{dc} = 5.5$ A, $t_l = t_L*(\omega_r/\omega_b)$, $c = 150$ μF/phase)
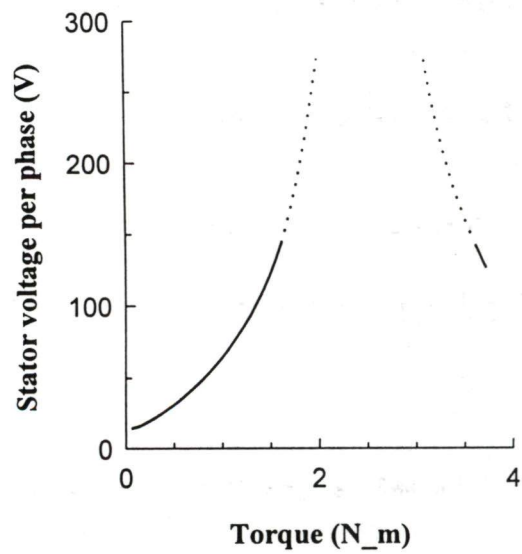
Fig 3.42. Stator voltage vs. torque characteristics
$(I_{dc} = 5.5$ A, $t_l = t_L*(\omega_r/\omega_b)$, $c = 150$ μF/phase)

(iv) Stator Voltage vs Torque

The stator voltage vs torque curve is shown in Fig 3.42. Stator voltage depends upon the stator current and net impedance of the machine. For fixed machine parameters, the net impedance of the machine depends upon the operating frequency and slip. As the load torque on the drive increases, the operating frequency increases and slip of the drive decreases. The variation in slip is quite small with torque , hence net impedance of the drive mainly depends upon operating frequency variation. The stator current increases with the torque and net impedance also increases with the torque; therefore stator voltage increases with the torque.

(v) Power loss vs Torque

Power loss vs torque plot is shown in Fig. 3.43. Power loss increases with the increase in torque. As the torque increases, current drawn by the drive increases with the increase in torque; hence ohmic losses increases with the increase in torque.

(vi) Percentage Efficiency vs Torque

Percentage efficiency vs torque curve is shown in Fig 3.44. Efficiency variation depends upon the variation of power output and losses. Initially the power loss of the drive varies very slowly with the increase in torque, while power output increases with the increase in torque; therefore the efficiency of the drive increase with the increase in torque and reaches to a maximum value. After a certain value of torque, power loss increases faster with the increase in speed, in comparison to the increase in power output with the increase in torque, hence efficiency of the drive decreases with the increase in speed.
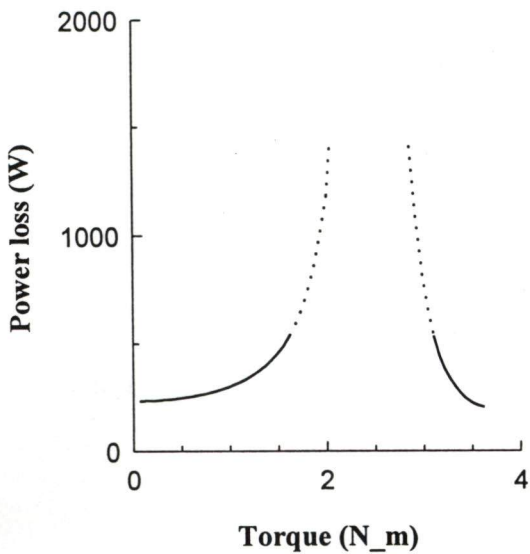
Fig 3.43. Power loss vs. torque characteristics
(I_{dc}= 5.5 A, $t_l = t_L{}^*(\omega_r\,/\omega_b)$, c = 150 μF/phase)
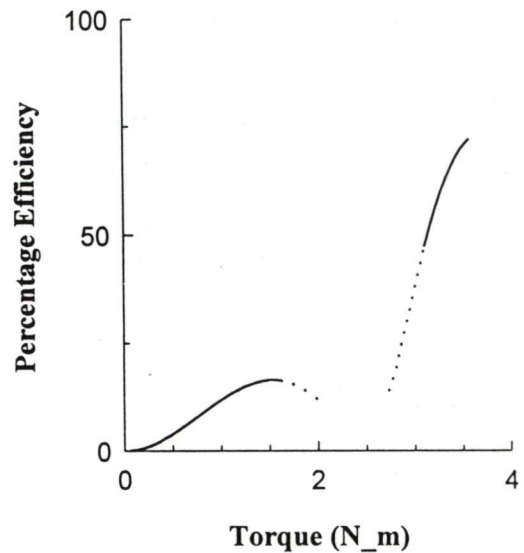
Fig 3.44. Efficiency vs. torque characteristics
(I_{dc}= 5.5 A, $t_l = t_L{}^*(\omega_r\,/\omega_b)$, c = 150 μF/phase)
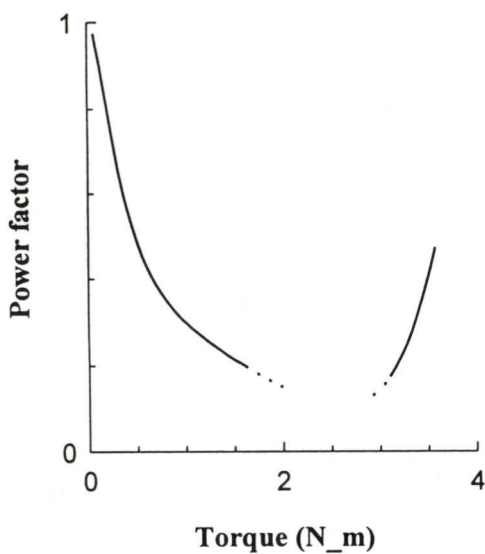
Fig 3.45. Power factor vs. torque characteristics
(I_{dc}= 5.5 A, $t_l = t_L{}^*(\omega_r\,/\omega_b)$, c = 150 μF/phase)
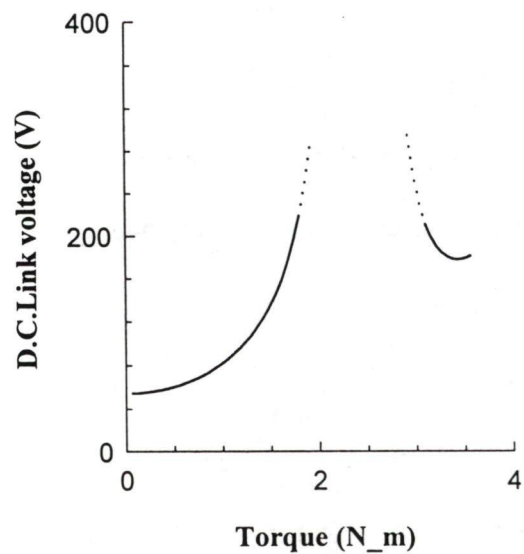
Fig 3.46. D.C.Link voltage vs. torque characteristics
(I_{dc}= 5.5 A, $t_l = t_L{}^*(\omega_r\,/\omega_b)$, c = 150 μF/phase)

72

(vii) Power factor vs Torque

Power factor vs torque curve is shown in Fig 3.45. The power factor decreases with the increase in torque .

(viii) D.C. Link Voltage vs Torque

D.C. Link voltage vs torque curve is shown in Fig 3.46. With the increase in torque power input of the drive increases; hence at constant d.c. link current d.c. link voltage increases with the increase in speed to meet the increased input power demand of the drive.

3.4 CONCLUSION

An analytical technique is described for determination of the steady state performance of the drive under various operating conditions. The value of capacitor connected across motor terminals has been finalized as 150 μF/phase. Two regions were identified in the performance characteristics, one stable and other unstable. At each operating condition, the efficiency of the drive is found to be poor in the unstable region, because of excess loss. The phenomenon of resonance and its effect has been observed at some frequencies under loading condition of the drive. The performance results at some operating conditions are described in the following paragraphs.

For fixed operating frequency, fixed d.c. link current and variable capacitance, the torque developed by the drive increases, as the capacitance across motor terminals are reduced, in the stable region .At low value of capacitance, the peak value of torque occurs at low value of slip. Stator current, stator voltage, power output, power loss, d.c. link

voltage and maximum value of efficiency increase with the reduction of capacitance connected across motor terminals in the stable region of torque- slip curve.

For fixed value of capacitance across motor terminals, fixed d.c.link current and variable operating frequency, torque developed by the drive increases in the stable region, as the operating frequency of the drive increases. At high value of operating frequency, the peak value of torque occurs at low value of slip. Stator voltage, power output, d.c. link voltage and maximum value of efficiency increase with the increase in operating frequency, while stator current, power loss and power factor decrease.

For fixed value of capacitance across motor terminals, fixed operating frequency and variable d.c. link current, the torque developed by the drive increases in the stable region, as the d.c.link current increases. At each value of d.c.link current, the peak value of torque occurs at same value of slip. Stator voltage, stator current, power output, power loss and d.c. link voltage increase with the increase in d.c.link current. The maximum value of efficiency is same at each value of d.c.link current. The minimum and maximum value of power factor is same at each value of d.c.link current.

SYSTEM DESCRIPTION AND HARDWARE DEVELOPMENT

4.1 INTRODUCTION

Current source inverters are more popular as compared to the voltage source inverter for the speed control of large rating induction motor [17,18,19]. One of the main advantage of a controlled current source at the front- end is to provide the natural protection to the switching devices from the short circuit condition. In the present work a 3- phase modified current source inverter is designed and developed. Space vector PWM technique is used to control the current source inverter. It reduces the harmonics present in the output current of the inverter. Equal pulse width modulation technique is employed to control the front-end input PWM converter used to develop a current source. The induction motor drive is run in closed loop for better speed regulation and dynamic performance. This above closed loop system is implemented with the help of a personal computer, based on 8088 processor, and an 8031 microcontroller based system.

The present chapter deals with the development of hardware for the control of modified self - commutating current source inverter fed induction motor drive. The hardware of complete system includes a three phase pulse width modulated converter, a three phase PWM inverter, an 8031 microcontroller based system, zero crossing detection circuit, pulse amplification circuit for the converter and inverter devices and necessary hardware for d.c.link current and speed measurement.

4.2   SYSTEM DESCRIPTION

The schematic diagram of the complete drive system is shown in Fig 4.1. The modified self – commutating current source inverter fed induction motor drive consists of controlled current source, three phase PWM current source inverter, connected through a d.c.link inductor and a three phase delta connected squirrel cage induction motor. The current source is developed using three phase PWM rectifier. A three phase capacitor bank is connected at the terminals of the machine, so that the line currents and voltages of the motor are almost sinusoidal at all values of operating frequency. The closed loop system consists of two loops, outer speed loop and inner current loop. The outer speed loop is used to obtain the reference d.c.link current from slip speed. A slip regulator as described in chapter 2, is used to calculate the reference active and reactive components of stator current. It also maintains the rated air gap flux in the drive. The inner current loop regulates the d.c.link current according to the reference d.c. link current demand. The PWM firing pulses for the inverter is generated using ADD- ON cards in personal computer and sent to the switching devices after amplification. To remove the burden on the personal computer (less interrupts handling), the pulses for the pulse width modulated converter are generated using 8031 microcontroller. The d.c.link current is sensed using Hall effect current sensor and digitized through a 12-bit analog to digital converter (ADC). The rotor speed is measured using incremental rotary pulse encoder. Zero crossing detection circuit generates short duration pulses at every zero crossing of line to line a.c.supply voltages and are used to synchronize the firing pulses of the pulse width modulated converter with the supply line- line voltages. Three quantizer signals which represents the positive and negative half cycles of each input line-line voltage are also generated. These signals are phase shifted by 120° as the line voltages and are used to
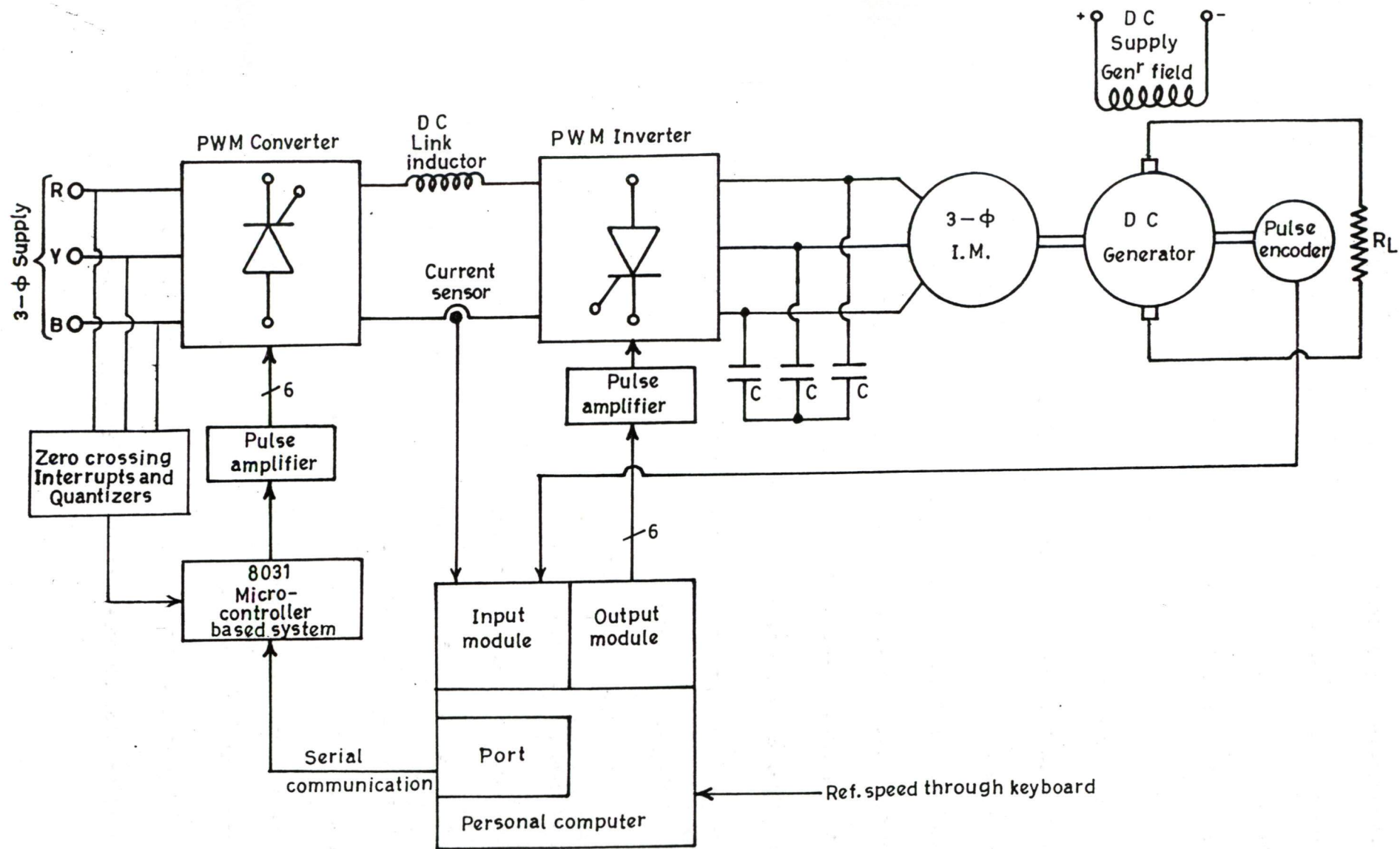
Fig.4.1. Schematic diagram of the drive system.

identify 60° intervals. Based on the status of the quantizer signals the microcontroller generates the firing pulses for converter devices. A PC- AT with ADD- ON card is used to read the reference speed, actual speed and d.c.link current. It processes the speed and current errors, and computes the operating frequency of the inverter and pulse widths of the pulse width modulated converter. The microcontroller communicates serially to the PC-AT to get the pulse widths of the converter. Firing pulses for inverter are generated through PC-AT. The various peripherals interfaced with PC-AT are 8255- Programmable Peripheral Interface (PPI), 8259- Programmable Interrupt Controller (PIC), 8253- Programmable Interval Timer (PIT) and 12- bit ADC are as shown in Fig 4.2. Provisions are made to amplify the firing signals obtained from the microcontroller and computer to trigger the converter and inverter semi-conductor power devices, as these signals are not strong enough to trigger these devices.

4.3 DEVELOPMENT OF THREE PHASE PULSE WIDTH MODULATED CONVERTER

The conventional phase-angle controlled converter has inherent shortcoming as both the displacement factor and input power factor decrease at lower output voltage and the converter introduces harmonics in the supply. To overcome these shortcomings the pulse width modulated AC-DC converter has been developed which makes the displacement factor near unity. The schematic diagram of three- phase fully controlled pulse width modulated converter is shown in Fig 4.3. The three-phase pulse width modulated converter consists of three MOSFETS as self – commutating switches in the upper half. To provide the reverse voltage blocking capability of the self – commutating devices, three fast recovery diodes are connected in series with the MOSFETS. Three
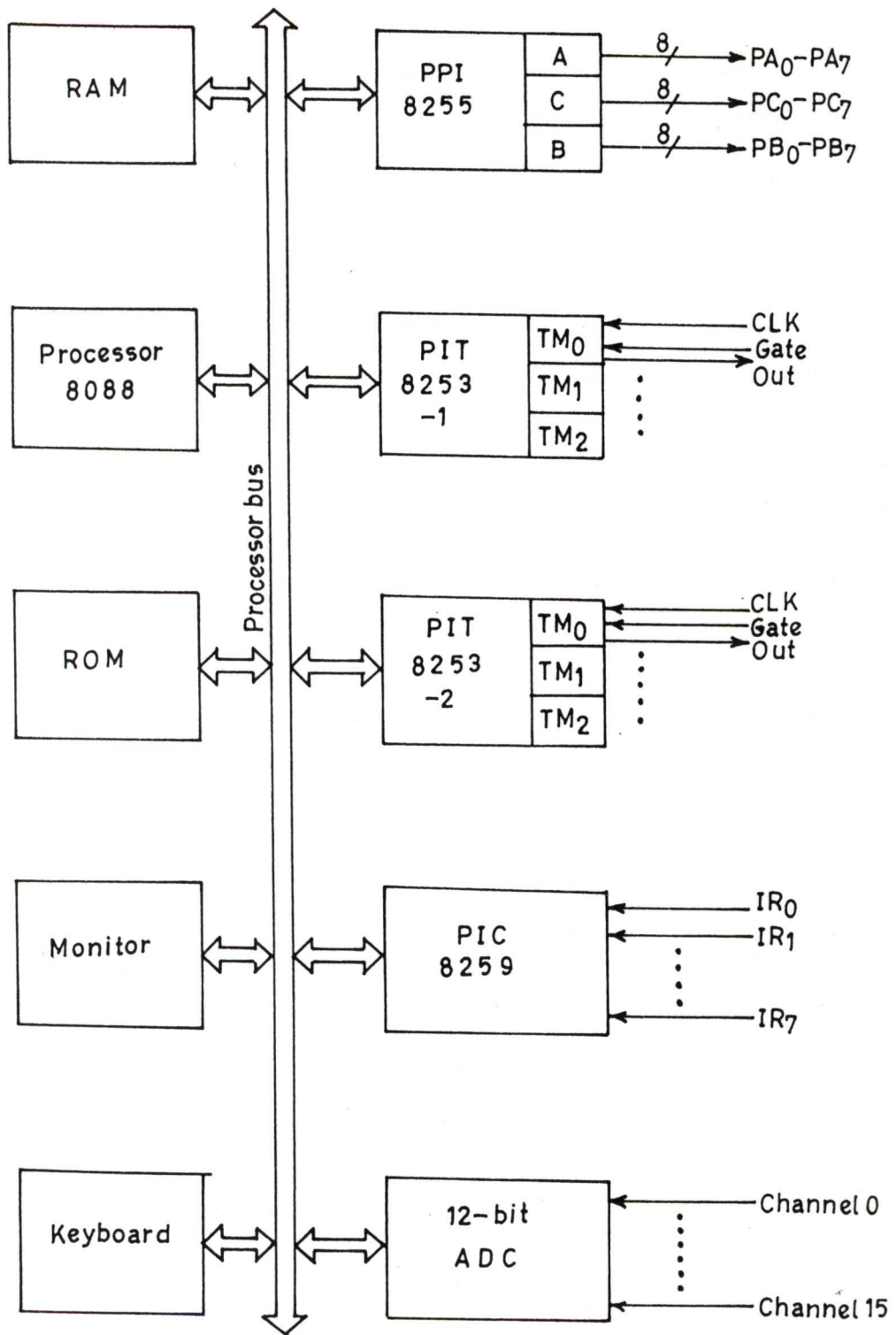
Fig. 4.2. PC-AT Microcomputer system.
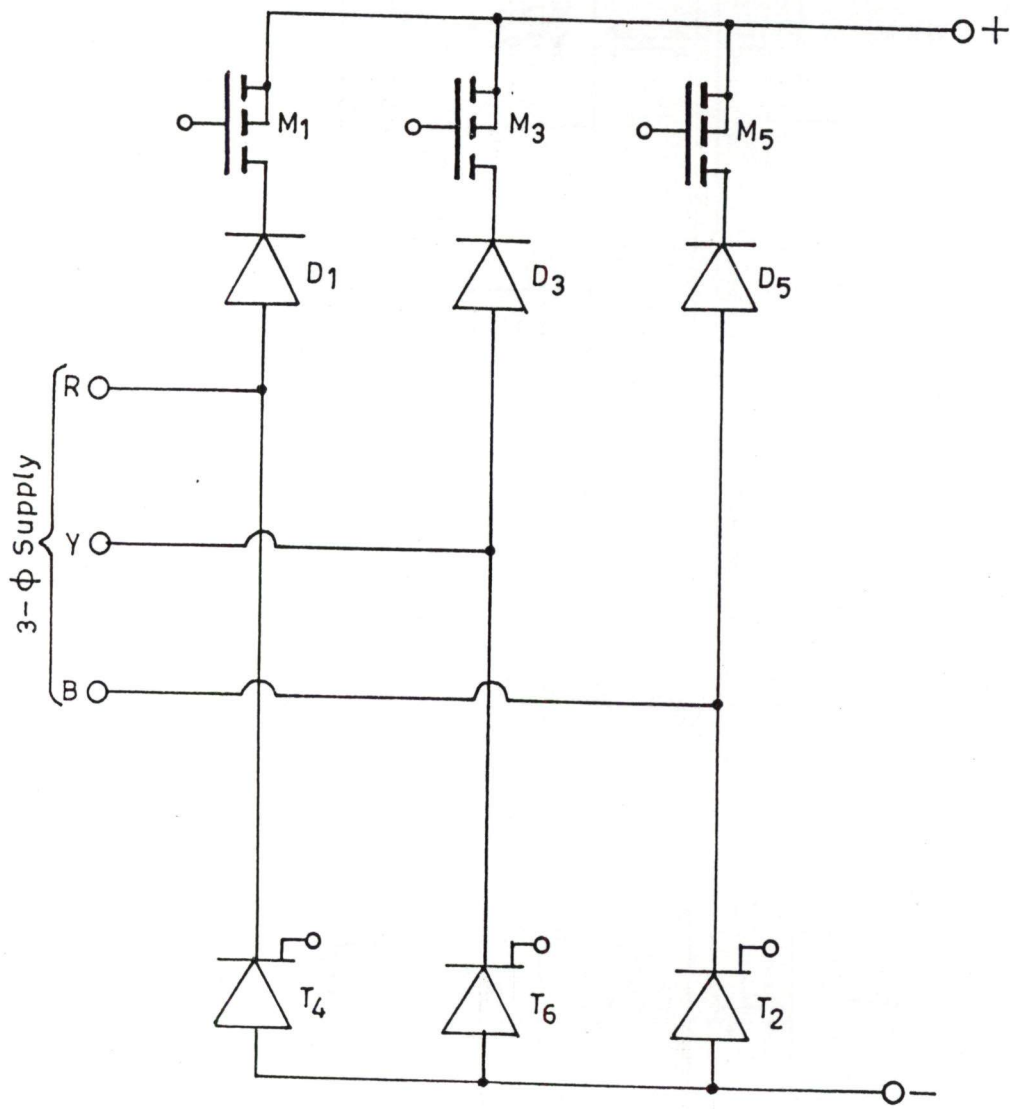
Fig. 4.3. 3-ØFront-end converter .

line- commutated thyristors are used as switching devices in the lower half of the converter.

The pulse width modulation can be achieved by several techniques such as equal pulse width modulation, sinusoidal pulse width modulation, trapezoidal modulation and square wave modulation. The commonly used modulation techniques are equal pulse width modulation and sinusoidal pulse width modulation techniques. Although sinusoidal pulse width modulation reduces the input harmonics to a great extent, its implementation is complex using microcontroller. In the present work equal pulse width modulation technique is employed to control the pulse width modulated converter used as a current source. The input harmonics in this technique is more as compared to sinusoidal pulse width modulation, but its microcontroller implementation is easier.

4.3.1 Development of Power Circuit of the PWM Converter

The power circuit of PWM converter is designed on the basis of maximum d.c.link current requirement for motor and the input supply voltage. Suitable rating all the switching devices are selected. The ratings of all the devices are shown in Appendix B.

It is necessary to connect a snubber circuit across the thyristor and MOSFET to protect the device from supply and load side transients. Snubber circuit reduces the off state and reapplied dv/dt magnitude of peak reverse voltage and device switching loss. Fig 4.4 shows the snubber circuit for the thyristor. The selection of R and C in the snubber circuit ensures that the dv/dt across the capacitor during its charging is less than the specified dv/dt rating of the thyristor and discharge current at the turn off of the thyristor is within reasonable limit. The values of R and C selected for the snubber circuit of the thyristor are given in Appendix B.

PC- AT. The microcontroller with I/O activities performed by it and its serial communication with the personal computer is shown in the Fig 4.6.

4.3.3 Quantizers and Zero Crossing Interrupts

To synchronize the firing signals of the front- end converter with the input power supply, three quantizers are used along with zero crossing interrupts as shown in Fig 4.7. The three-phase line to line voltage is stepped down and is fed to low offset voltage comparator used as a zero crossing detector. The outputs of comparators are used to trigger the positive edge triggered and negative edge triggered monoshots. Outputs of all the monoshots are combined to achieve zero crossing signals (ZOI) at every $60°$. The zero crossing signals are connected to an interrupt line of the microcontroller (INT0). The comparator outputs are inverted to get quantizer signals (ϕ_R, ϕ_Y, ϕ_B), which are logic 1 during positive half cycle of input voltage and logic 0 in the negative half of the input cycle. The status of the quantizer signals is read via a port. Using the status of these quantizer signals, the controller issues the firing pulses through a port of microcontroller.

4.3.4 Pulse Amplification Circuit for MOSFET

The pulse amplification circuit for MOSFET is shown in Fig 4.8. The pulses issued from the microcontroller port are not strong enough to turn on the MOSFETs. Since MOSFET is a voltage operated device, the voltage level of the pulses are amplified using pulse amplification circuit. The gate to source voltage is clipped to 12 volts by zener diode. To protect the devices used in the microcontroller based system, an isolation between power circuit and control circuit is provided with the help of opto-coupler MCT 2E.

line- commutated thyristors are used as switching devices in the lower half of the converter.

The pulse width modulation can be achieved by several techniques such as equal pulse width modulation, sinusoidal pulse width modulation, trapezoidal modulation and square wave modulation. The commonly used modulation techniques are equal pulse width modulation and sinusoidal pulse width modulation techniques. Although sinusoidal pulse width modulation reduces the input harmonics to a great extent, its implementation is complex using microcontroller. In the present work equal pulse width modulation technique is employed to control the pulse width modulated converter used as a current source. The input harmonics in this technique is more as compared to sinusoidal pulse width modulation, but its microcontroller implementation is easier.

4.3.1 Development of Power Circuit of the PWM Converter

The power circuit of PWM converter is designed on the basis of maximum d.c.link current requirement for motor and the input supply voltage. Suitable rating all the switching devices are selected. The ratings of all the devices are shown in Appendix B.

It is necessary to connect a snubber circuit across the thyristor and MOSFET to protect the device from supply and load side transients. Snubber circuit reduces the off state and reapplied dv/dt magnitude of peak reverse voltage and device switching loss. Fig 4.4 shows the snubber circuit for the thyristor. The selection of R and C in the snubber circuit ensures that the dv/dt across the capacitor during its charging is less than the specified dv/dt rating of the thyristor and discharge current at the turn off of the thyristor is within reasonable limit. The values of R and C selected for the snubber circuit of the thyristor are given in Appendix B.

Fig. 4.4. Snubber circuit for Thyristor.
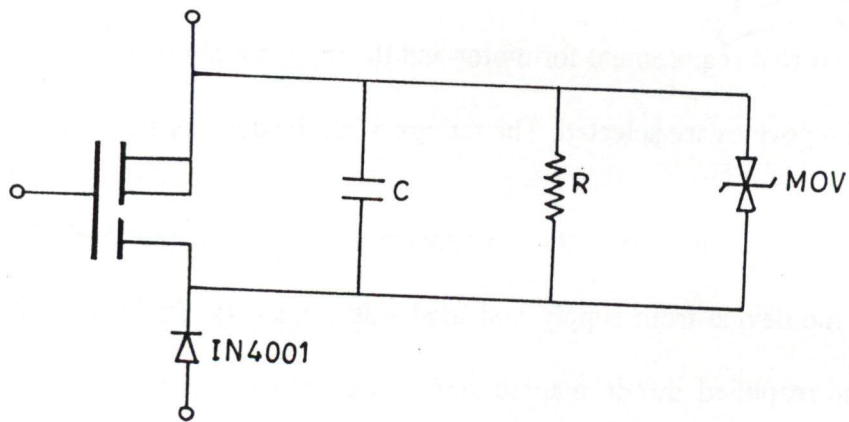
Fig. 4.5. Snubber circuit for MOSFET.

The Fig 4.5 shows the snubber circuit for MOSFET. When the MOSFET is turned on, the energy stored in the capacitor is dissipated in the resistor R. At the turn-on instant, the resistor should limit the peak discharge current through MOSFET to a safe value.

Along with the snubber circuit, an additional device MOV (Metal Oxide Varistor) is also connected across each MOSFET to protect it from the transient over voltage. The selected values of R,C and MOV are given in Appendix B. All devices are mounted on heat sink, to dissipate the internally generated heat of the device.

4.3.2 Development of Microcontroller System

The firing pulses of PWM microcontroller are generated using microcontroller. The use of microcontroller for the control purpose increases the reliability of circuit as hardware requirement is drastically reduced. There is no drift problem and magnetic interference associated with the controller.

The INTEL 8031 based controller has two in built timers, four input and output ports, two external interrupts, and a 128 bytes RAM. An external program memory chip (INTEL 2764 A, 8KB) is interfaced with the microcontroller to store the program. Port 1 of 8031 is used for issuing the firing pulses to the thyristors and MOSFETS of front-end power converter. Timer 0 of 8031 is programmed in (mode1) to generate the interrupts at the firing instants. Timer 1 is used as baud rate generator for serial communication. Zero crossing signals are required by the microcontroller to identify the 60° period. INT0 interrupt is used for zero crossing interrupts and has the highest priority. INT1 is used to stop the drive. Port 0 and 2 provide the multiplexed address bus to the EPROM. Port 3 is used to read the status of the three-quantizer signals. An RxD line of microcontroller is used to receive the information about the pulse widths of the power converter from the

PC- AT. The microcontroller with I/O activities performed by it and its serial communication with the personal computer is shown in the Fig 4.6.

4.3.3   Quantizers and Zero Crossing Interrupts

To synchronize the firing signals of the front- end converter with the input power supply, three quantizers are used along with zero crossing interrupts as shown in Fig 4.7. The three-phase line to line voltage is stepped down and is fed to low offset voltage comparator used as a zero crossing detector. The outputs of comparators are used to trigger the positive edge triggered and negative edge triggered monoshots. Outputs of all the monoshots are combined to achieve zero crossing signals (ZOI) at every $60°$. The zero crossing signals are connected to an interrupt line of the microcontroller (INT0). The comparator outputs are inverted to get quantizer signals (ϕ_R, ϕ_Y, ϕ_B), which are logic 1 during positive half cycle of input voltage and logic 0 in the negative half of the input cycle. The status of the quantizer signals is read via a port. Using the status of these quantizer signals, the controller issues the firing pulses through a port of microcontroller.

4.3.4   Pulse Amplification Circuit for MOSFET

The pulse amplification circuit for MOSFET is shown in Fig 4.8. The pulses issued from the microcontroller port are not strong enough to turn on the MOSFETs. Since MOSFET is a voltage operated device, the voltage level of the pulses are amplified using pulse amplification circuit. The gate to source voltage is clipped to 12 volts by zener diode. To protect the devices used in the microcontroller based system, an isolation between power circuit and control circuit is provided with the help of opto-coupler MCT 2E.

Fig. 4.6. System configuration for front-end converter control.
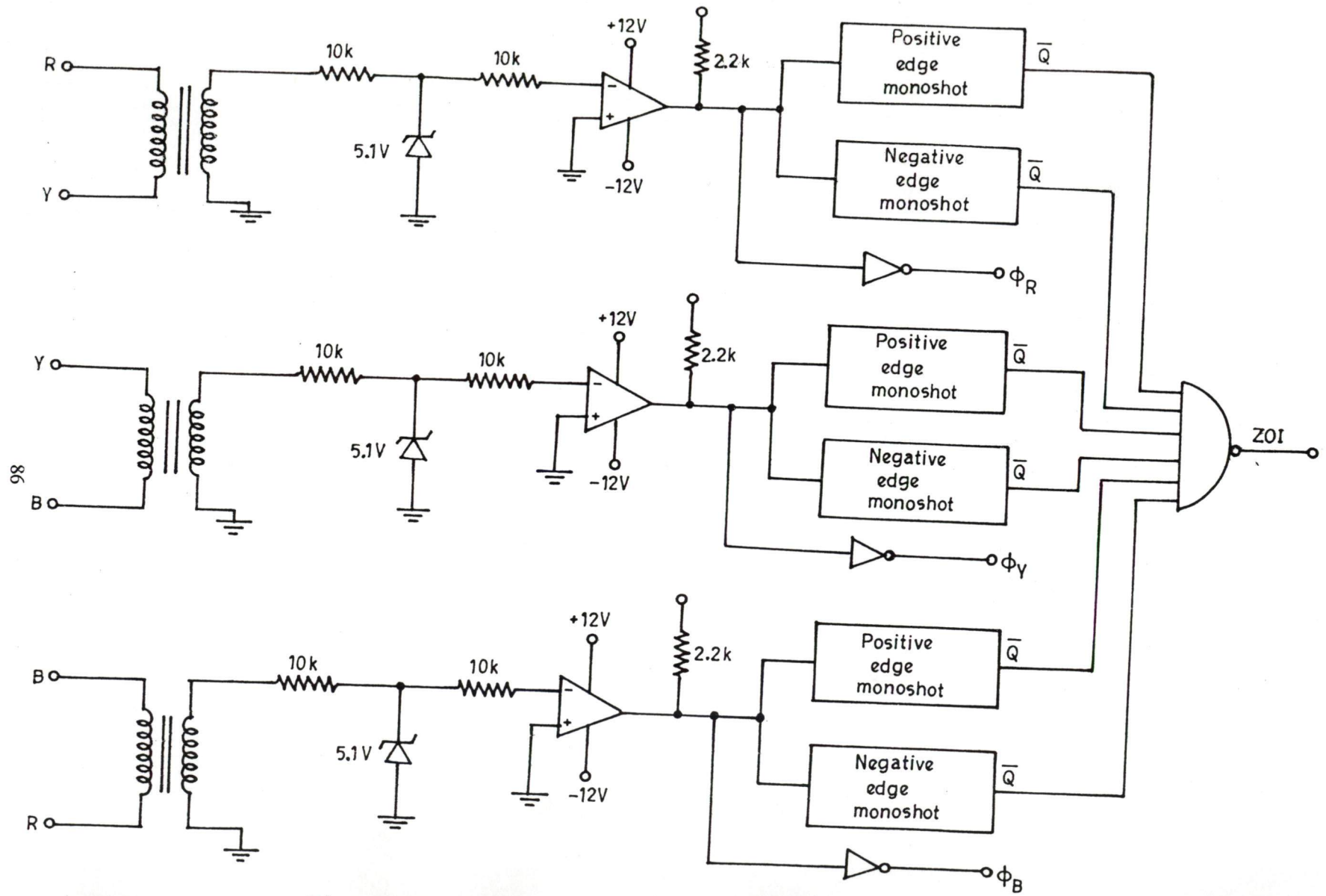
Fig.4.7. Zero crossing detector circuit.

98
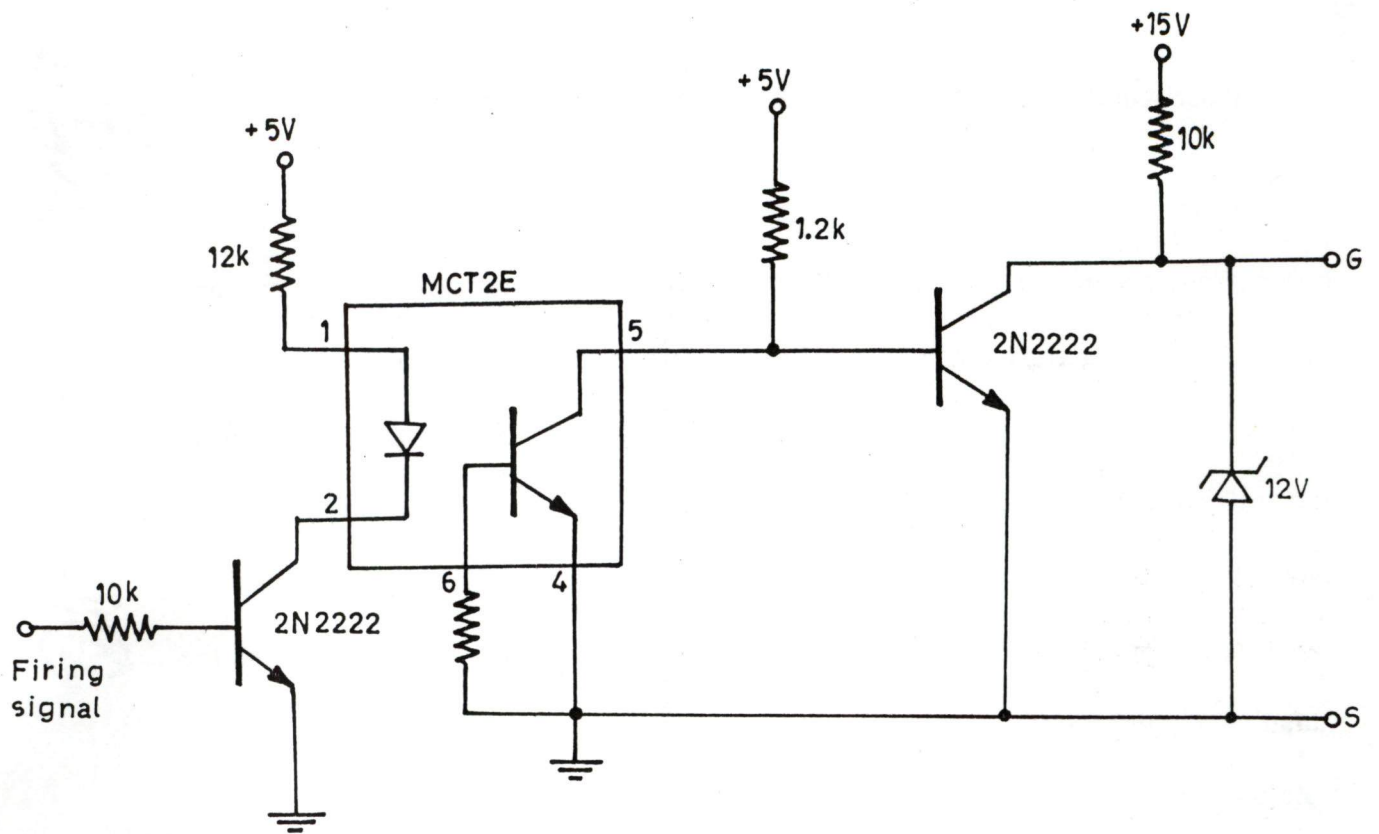
Fig.4.8. Pulse amplification circuit for MOSFET.
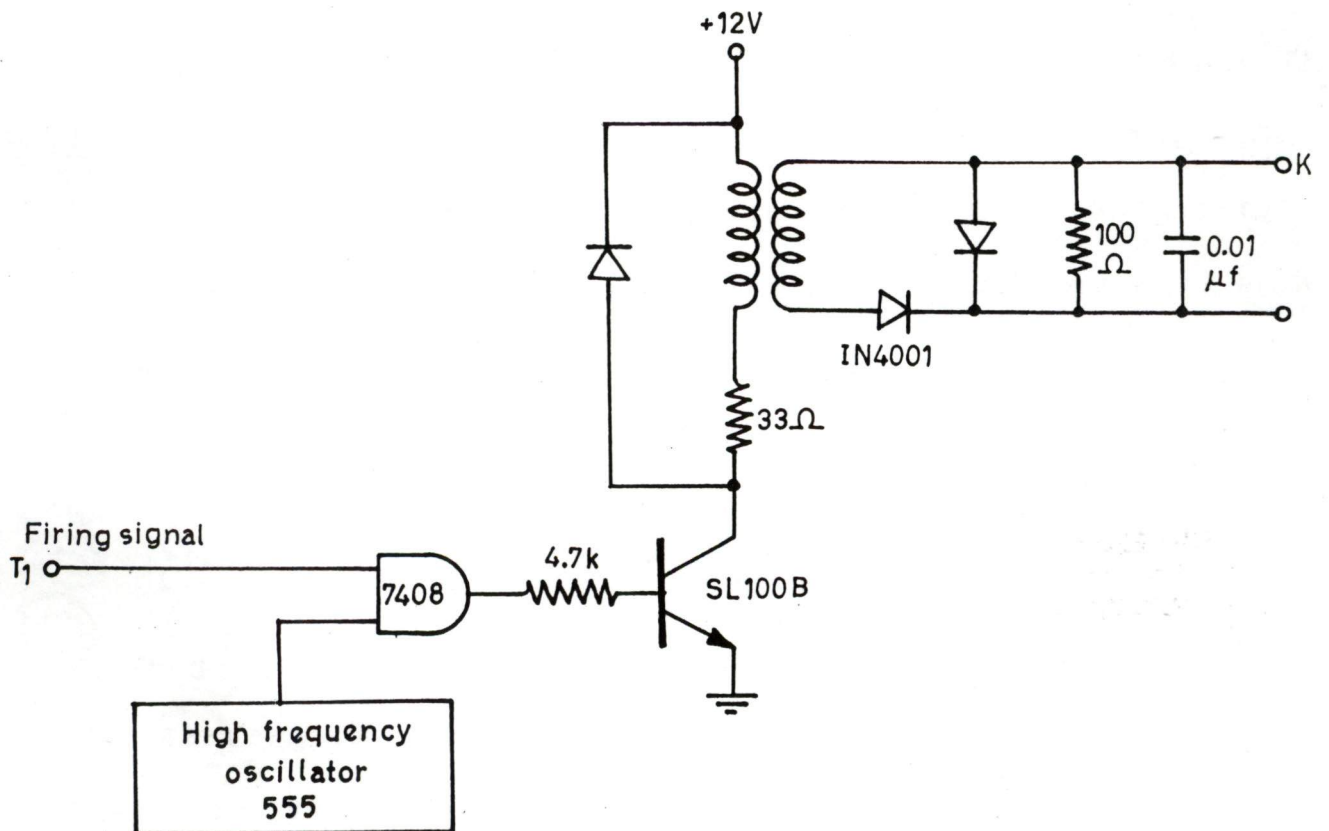
Fig.4.9. Pulse amplification circuit for Thyristor.

4.3.5 Pulse Amplification Circuit for Thyristor

The pulse amplification circuit for thyristor is shown in Fig 4.9. The pulses issued from the microcontroller ports are ANDed with high frequency signals and amplified. The thyristor is a current operated device; therefore to ensure proper triggering of the SCRs, sufficient magnitude gate current pulses are applied to the thyristors. To provide electrical isolation between low potential control circuit and high potential power converter, a pulse transformer is used. A diode is connected across collector resistor and the primary winding of the pulse transformer to protect the transformer and to avoid the saturation of pulse transformer core. Gate- to- cathode junction of thyristor should also be protected for over voltage and over current. A diode is connected in series with secondary winding of the pulse transformer to prevent the reverse current flow through the gate junction. When thyristor is reverse biased, the gate- to- cathode junction may be damaged due to the reverse voltage. Therefore a diode is connected across gate to cathode to limit the reverse voltage. A common problem in SCR circuits is spurious triggering of the thyristor. These spurious pulses may be induced at the gates due to turn on and turn off of neighboring SCR or transients in the power circuit. These undesirable pulses may turn on the SCR, thus causing improper operation of the circuit. Gates are protected against such spurious signals by connecting a capacitor and a resistor across the gate and cathode to bypass the noise pulses.

4.4 DEVELOPMENT OF 3-PHASE PULSE WIDTH MODULATED CURRENT SOURCE INVERTER

The conventional three-phase current source inverter has the short- coming of introducing increased lower order harmonics in the output currents which give rise to losses, noise and torque pulsation in the machine, specially at lower frequency of

operation. To overcome these drawbacks, the drive is fed from the pulse width modulated current source inverter. There are number of pulse width modulation techniques to control the inverter output current. In the present work, space vector technique is employed for the modulation of the pulse widths. This technique is a carrier less method to generate PWM patterns for the entire range of operating frequency. In this technique the synchronization of carrier to signal is not needed, which greatly facilitates the control circuit. The number of output current pulses of the inverter depends upon its frequency of operation. At low operating frequency of the inverter the number of output current pulses of the inverter are more in comparison to its number at high frequency. In the present scheme modulation index continuously changes with the change in the reference frequency as shown below:

$$m = 0.82 + .18 * (ref\_fq / 50)$$

The minimum value of modulation index is 0.82 due to the consideration of the switching loss and if the modulation index exceeds more than 1 it is clamped to 1.0.

To incorporate the PWM operation in a 3-phase current source inverter fast switching devices are needed. Therefore in both the halves (upper and lower) of each leg MOSFETs are used. To increase the reverse voltage blocking capabilities of each self-commutating device, fast recovery diodes are connected in series with each MOSFET. The protection and pulse amplification circuit of each MOSFET is same as in the three phase pulse width modulated converter. The schematic diagram of three phase pulse width modulated inverter is shown in Fig 4.10.

4.4.1 Schematic Diagram of the Inverter and Control

The system configuration is shown in Fig 4.11. The PWM firing pulses of the current source inverter is generated through the personal computer using ADD- ON card.
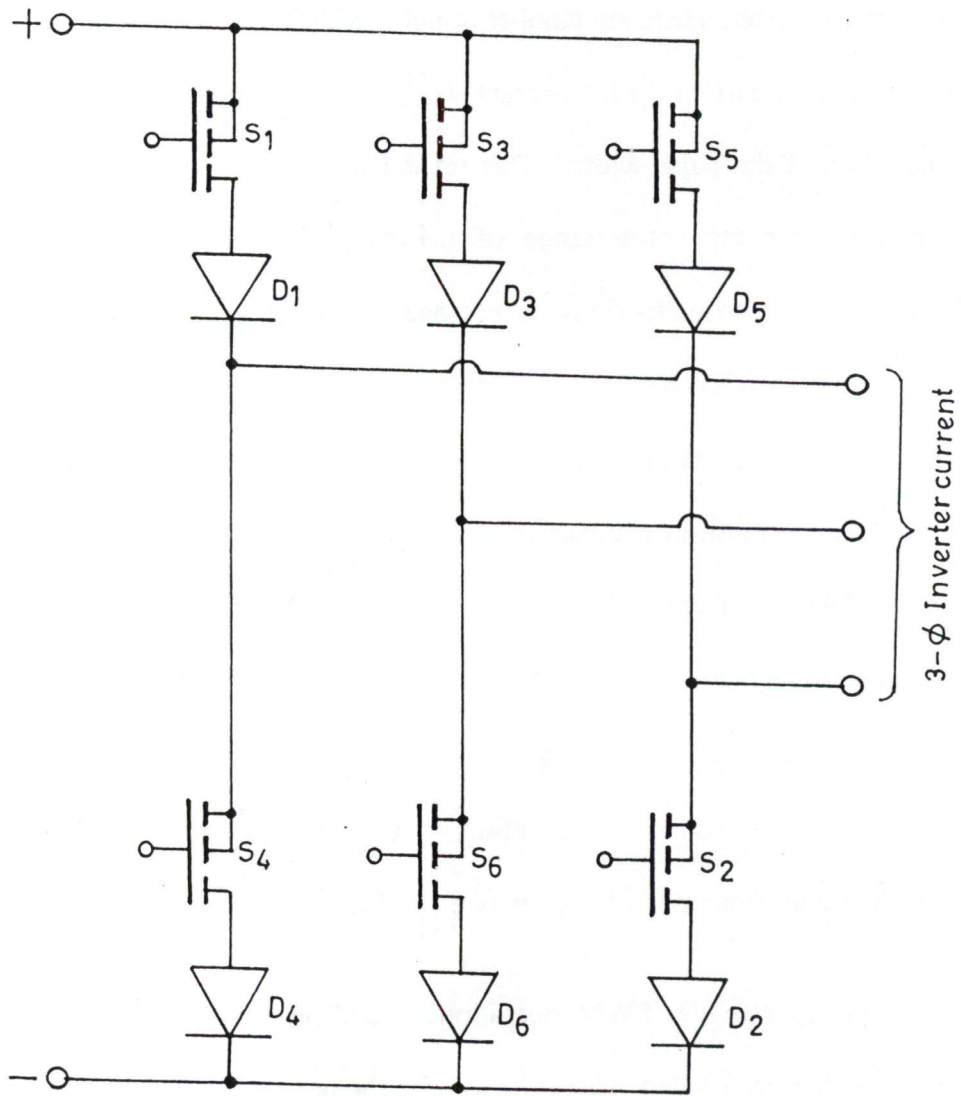
Fig. 4.10. 3-ϕ Current source inverter.

90
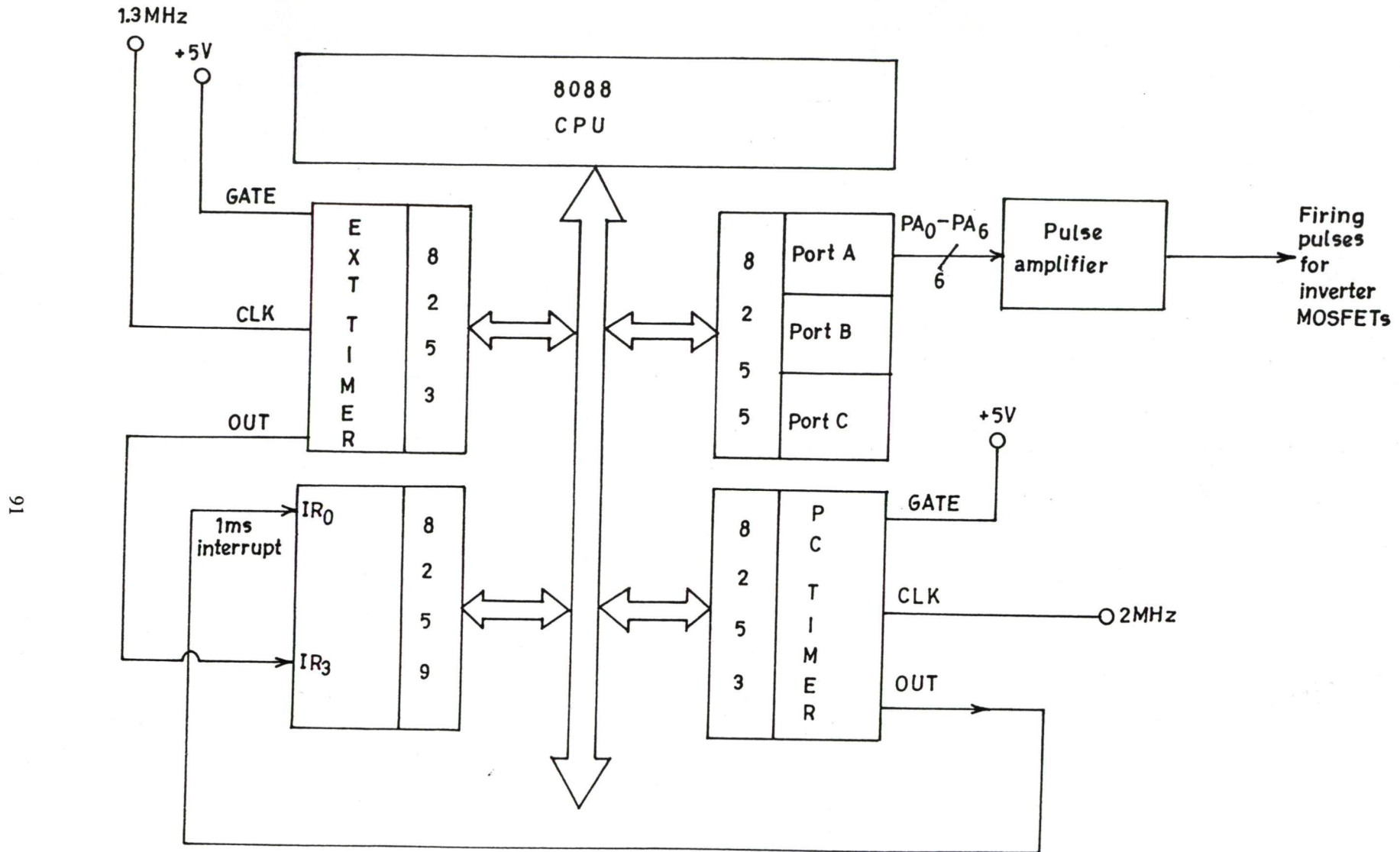
Fig.4.11. System configuration for inverter control.

The PC internal timer TM_0 of 8253, Timer '0' of ADD- ON card , PORT- A of 8255 are used for the firing pulse generation. The gate of the timer is permanently high connecting them to + 5 V supply. PC timer output is connected to an interrupt IR_0 and output of ADD-ON card timer is connected to IR_3 of 8259 respectively. PC timer generates interrupts at every 1 ms. At this instant ADD-ON card timer is loaded by the respective count. The output of the external timer generates the interrupt on the termination of the respective count and the required port bits are made high or low to generate PWM pattern for any number of output pulses at any operating frequency.

4.5   DEVELOPMENT OF POWER CIRCUIT

The ratings of the MOSFETs of the inverter are selected on the basis of induction motor rating. The power circuit of the three phase PWM current source inverter is developed by selecting the proper ratings of the semiconductor devices on the basis of induction motor rating, proper values of snubber circuit component, proper voltage rating of MOV. The ratings of the devices, snubber circuit components and MOV are given in Appendix B.

4.6   MEASUREMENT OF SYSTEM PARAMETERS

The motor speed and d.c.link current is required for feedback purposes in closed loop control of the developed drive. The d.c.link current is measured using the Hall effect current sensor, and rotor speed is measured using rotary pulse tacho generator. The details of speed and current measurement are discussed in the following sections.

4.6.1 Speed Measurement

In the present closed loop control scheme, the synchronous speed of the machine is obtained by adding the reference slip speed with the actual rotor speed.

The operating frequency of the inverter depends upon the synchronous speed of the machine. To operate the machine under rated flux condition, accurate measurement of speed is necessary. A pulse tachogenerator is used for the measurement of the speed of the machine. The pulse tachogenerator is coupled to the shaft of the induction motor. It is supplied with +5 V supply. It generates square wave pulses. Frequency of the square wave pulses generated by the tachogenerator depends upon the speed of the induction motor. The actual speed of the induction motor is measured with the help of two timers, one is internal timer of the PC and other is timer 0 of ACL-8112 DG/HG card. PC internal timer is programmed in mode 3 (square wave mode) while the timer of the ACL-8112 DG/HG card is in mode 0 (Interrupt on terminal count mode).

A computer program in C language is developed to measure the speed. A graph is plotted between the actual speed obtained by tachometer and speed measured by the pulse tacho generator through software. The graph is shown in the Fig 4.12. Both the curves are closely matching and hence accurate measurement of the speed is possible with the pulse encoder.

4.6.2 Current Measurement

The measurement of d.c.link current is needed for the successful operation of inner current loop. Various methods are reported in the literature to measure the current. In the present work Hall effect current sensor is used for the measurement of the current. The main advantage of such a transducer is that it is non-contact device with high
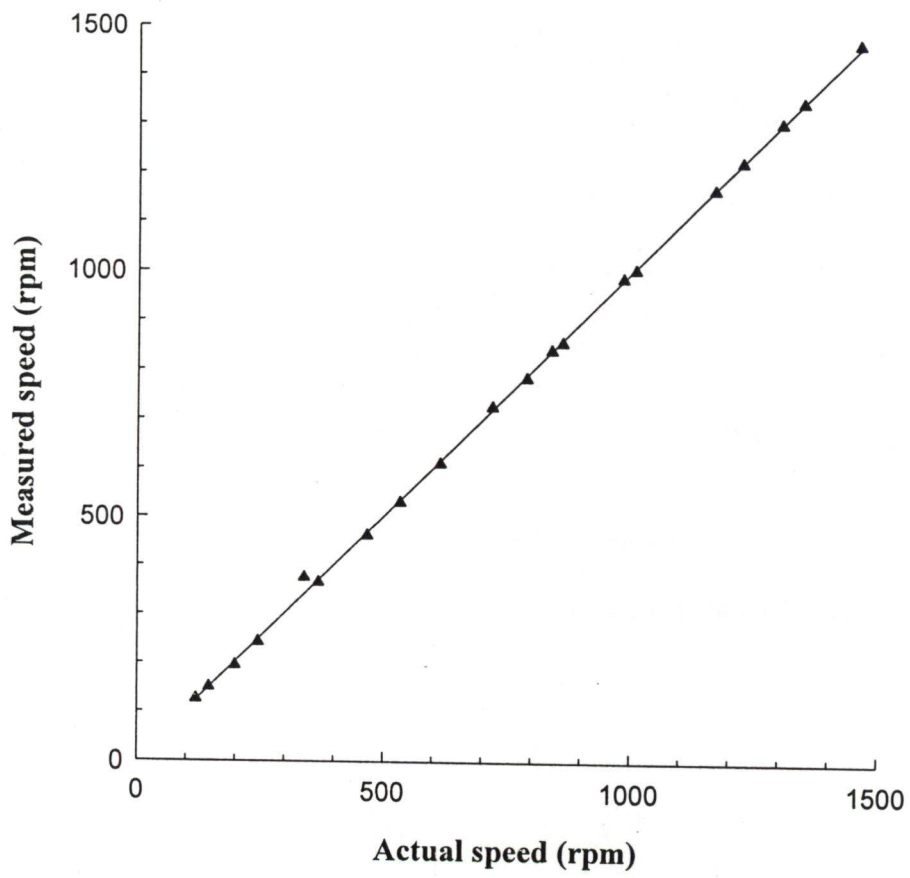
Fig 4.12. Measured speed vs Actual speed

resolution and very small in size. The scheme to measure the current using Hall effect current sensor is shown in the Fig 4.13.

The output of the sensor is current which depends on the number of turns wound on sensor itself and current flowing in the primary circuit. The output current is given by the following equation:

$$I_O = I_L * \left(\frac{N_P}{N_S} \right)$$

where ,

$$N_P \quad = \quad \text{Number of turns in the primary}$$
$$N_S \quad = \quad \text{Number of turns in the secondary}$$
$$I_O \quad = \quad \text{Output current}$$
$$I_L \quad = \quad \text{Load current}$$

Secondary of the sensor is wound for large number of turns, while primary is normally wound for one or two turns. The output current of the sensor is converted to voltage signal by passing it across the 100 KΩ resistor. This output voltage is given to an OP- AMP. To eliminate the ripples in d.c. current, a low pass R- C filter is used. A 10 KΩ trimpot is used in the negative feed back path of the OP- AMP for gain adjustment so as to obtain a maximum voltage of 5 volt corresponding to 10 Amp. Another trimpot is used for the d.c. adjustment. A zener diode is connected across the output to restrict the voltage at +5 volt.

To convert the voltage signal into digital signal ADC of ACL- 8112 HG card is used. ADC is B.B. ADS 774 successive approximation type, having resolution of 12- bit. This ADC can be programmed in both bipolar and unipolar mode. Since the current obtained from 3- phase pulse width modulated converter is unidirectional, so it is
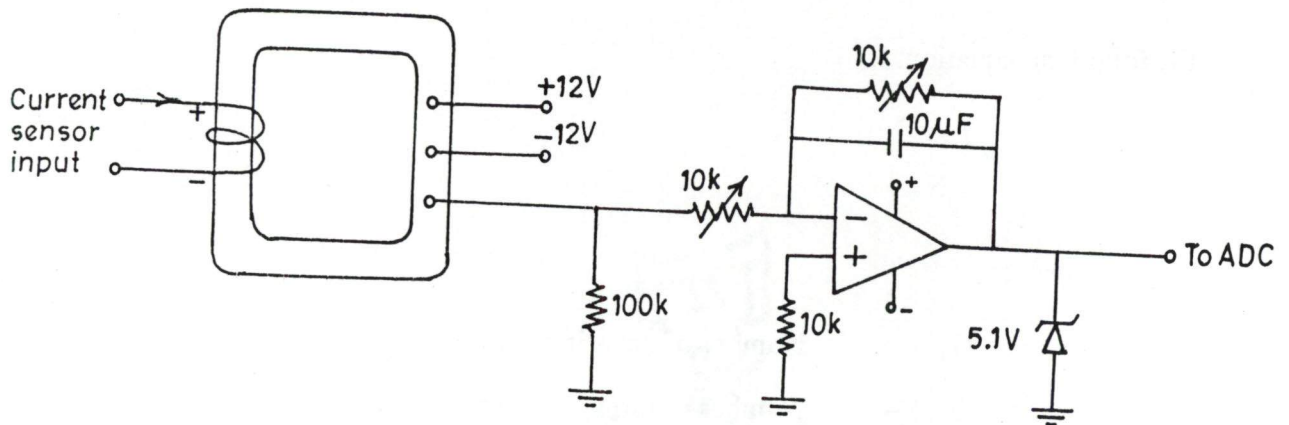
Fig.4.13: Current measurement circuit.
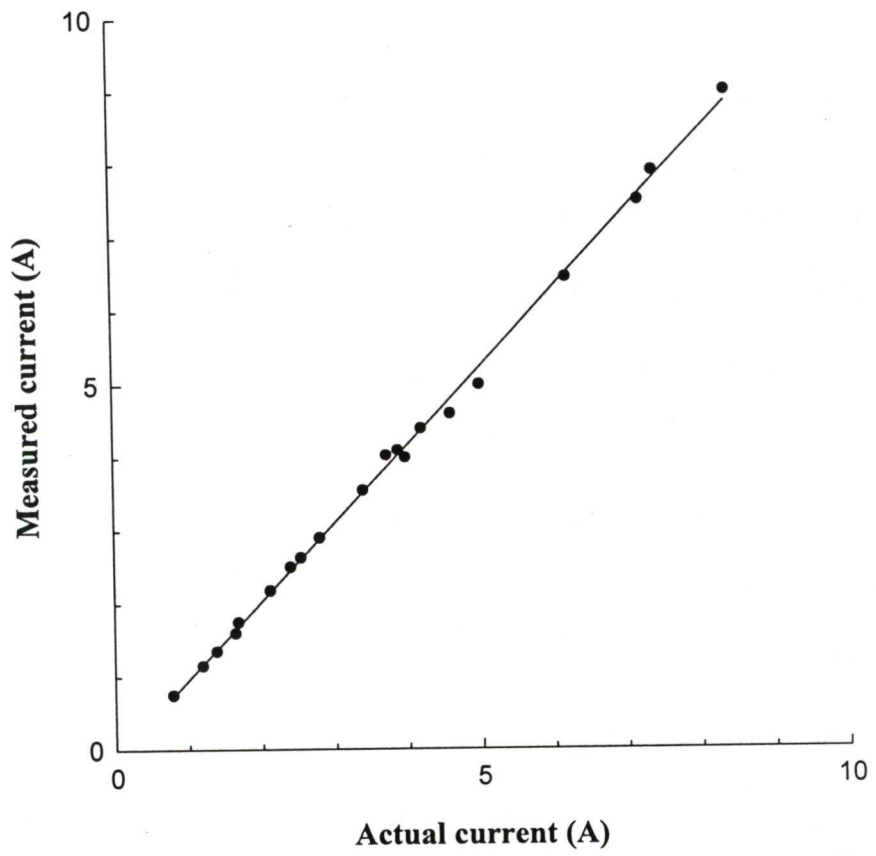
Fig 4.14 Measured current vs Actual current

programmed in unipolar mode. The conversion time is 8μ sec. For checking the performance of the current sensor, the converter is loaded by the resistive load. The actual current flowing in the load is noted by an accurate ammeter, and the current measured by the software using Hall effect current sensor is also determined.

A curve is plotted between the actual current and the measured current as shown in Fig 4.14. The two curves are closely matching and hence accurate measurement of the current is possible using Hall effect current sensor.

4.7   CONCLUSION

The complete detail of the hardware of various components of the electric drive is described, it consists of three phase pulse width current source, three phase PWM inverter circuit, speed and current measurement circuits, microcontroller based system, protection circuits, pulse amplification circuits of MOSFETS and thyristors are discussed. Quantizers and zero crossing detection circuits essential for the generation of the firing pulses for the front- end PWM converter are also discussed. The interfacing of ADD- ON cards with personal computer is discussed. The timers, interrupts, ports, of the personal computer, the serial communication of Rx D lines of microcontroller with PC-AT are discussed. Timer and interrupt details of ADD_ON cards and their interfacing with PC is discussed. The speed is measured by the rotary incremental pulse encoder and current is measured by the Hall effect current sensor. The measured values of speed and current are compared with the actual speed obtained by d.c.tacho generator and actual current obtained by d.c. ammeter. The current and speed measured by the Hall effect current sensor and rotary pulse encoder are quite close to the actual current and speed; therefore the accurate measurements of speed and current are possible.

CONTROL TECHNIQUE AND SOFTWARE
DEVELOPMENT

5.1   INTRODUCTION

The performance of any drive depends on the control technique and its implementation. In the present drive, the control is implemented through 8088 microprocessor and 8031 microcontroller. Microprocessor based control reduces the complexity of the hardware, increases the reliability and makes the control system fast. Equal pulse width technique is used to control the front-end PWM converter and space vector technique is used to control the motor-end PWM CSI.

The system hardware of the induction motor drive has been discussed in chapter 4. The complete drive is controlled using PC-AT. ADD- ON cards is used for speed and current measurement and inverter firing pulse generation. An external microcontroller 8031 based system is used to generate the firing signal for the front-end converter. Microcontroller communicates serially with PC-AT to get the converter command.

For superior performance and fast response of the drive system, suitable software has to be developed. The system software development consists of the main program of the drive system in open and closed loop, current measurement, interrupt service subroutine for converter and inverter firing pulse generation, subroutine for speed measurement, current PI processing and speed PI processing. Only pictorial representation of the various software is given through flow charts.

The software is developed in two parts; one part is developed in assembly language of 8031 for converter control and other part is developed in 'C' language for

inverter control and measurements. The developed software is implemented to control the drive in open and closed loop.

The testing of front-end converter and motor-end converter has been carried out separately. Control and power signals of the front-end and motor-end converters are recorded. For the front-end converter; quantizer signals, zero crossing detection signals, firing pulses, input line current and voltage waveforms, load current and voltage across the load for the different duty cycles are recorded. For the motor-end converter; firing pulses at the different operating frequencies, inverter line current and voltage waveforms, motor line current and voltage waveforms, are recorded with and without capacitance at the machine terminals. The d.c.link current and voltage waveforms are also recorded at the different operating frequencies. All the power and control waveforms are recorded using X- Y recorder.

5.2   CONTROL TECHNIQUE USED IN THE PWM CONVERTER

Equal pulse width modulated scheme [47] used in the front-end pulse width modulated converter is described here. In this control technique a d.c. modulating signal of variable amplitude A and a triangular carrier wave of fixed amplitude A_m are compared to get the switching instants of the upper- leg devices as shown in Fig. 5.1. The frequency of the triangular wave is kept 12 times the input supply frequency, so that 12 output pulses per cycle are obtained. Thyristors TH_2, TH_4 and TH_6 are triggered at the lowest possible angle λ as shown in Fig 5.1; each thyristor conducts for 120° duration. When the two devices (one from upper half and other from lower half) belonging to different legs conduct, then output voltage is equal to the line to line voltage and supply current is equal to the load current. If two devices of the same leg conduct then free
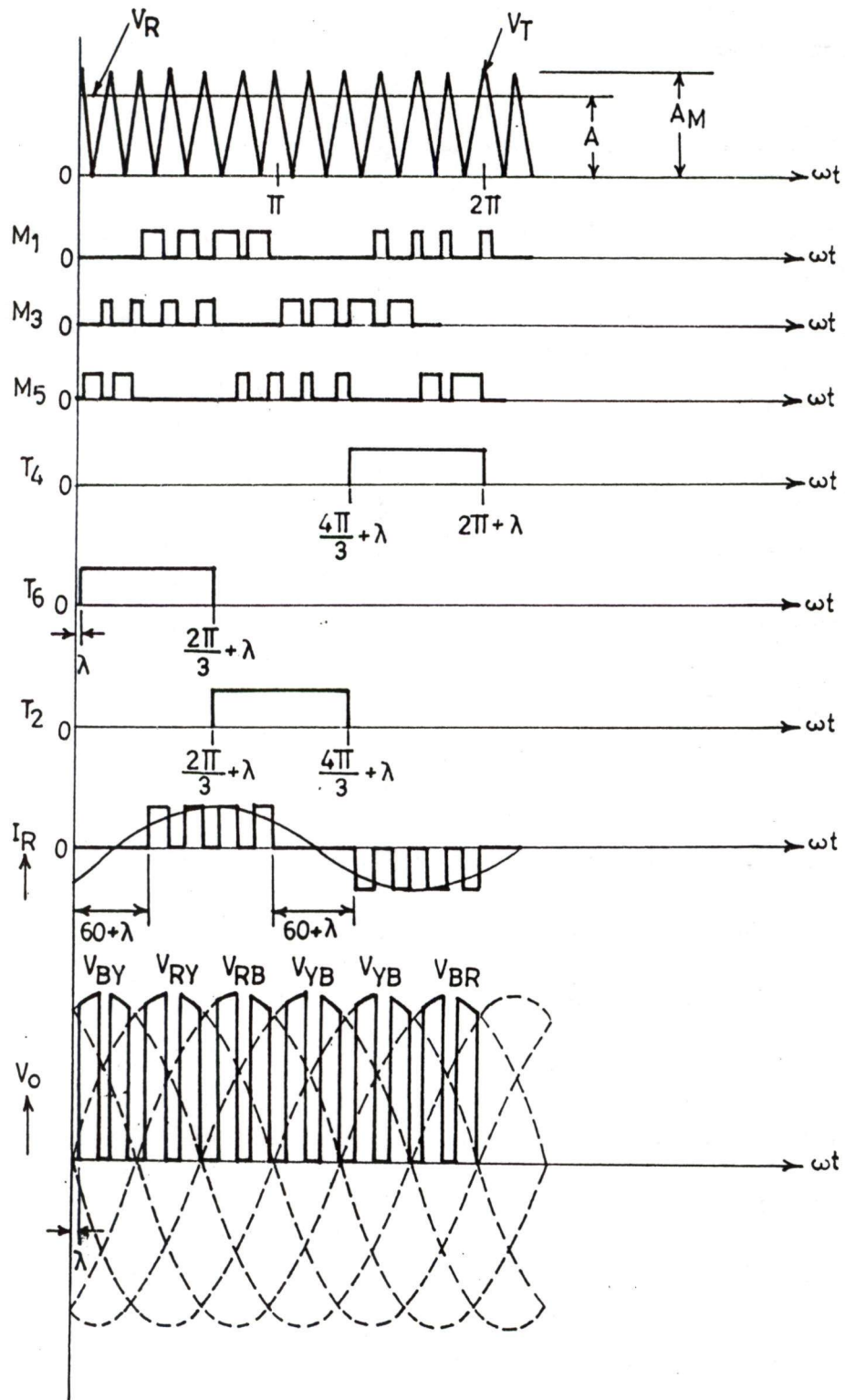
Fig.5.1   Operation of three phase PWM converter
           in rectification mode.

wheeling action takes place, and output voltage and current become zero. Fig 5.1 also shows the firing pulses (M) for MOSFETs and (T) for thyristors, load current (I_R), supply current and output voltage (V_0).

5.3 CONTROL TECHNIQUE USED IN THE PWM CURRENT SOURCE INVERTER

The space vector PWM modulation technique [92] is used for the control of 3-phase PWM current source inverter. It is a carrier less method of generating PWM pattern for the entire range of operating frequency. The space vector technique has the advantage that harmonics from the line currents are drastically reduced. This technique can be employed on-line with a single chip processor. The synchronization of carrier to modulating signal is not needed, which reduces the burden of control and firing circuits. In the present scheme six space vectors are defined, for each sector of $60°$ over a cycle. The zero vector is not considered in the analysis. The current space vector (i_r^-) is obtained by transforming the three line currents of a non PWM current source inverter as

$$i_r^- = \frac{2}{3} (i_R^- + a\, i_Y^- + a^2\, i_B^-) \qquad (5.1)$$

where, $\qquad a = e^{j\frac{2\pi}{3}}$

If the current in d.c.link is a constant (I_{dc}), and inverter frequency is ω_e. Then the three line currents are expressed as:

$$i_R^- = \frac{2\sqrt{3}}{\pi} I_{dc} \left(\cos\omega_e t - \frac{1}{5}\cos 5\omega_e t + \frac{1}{7}\cos 7\omega_e t - \dots\dots \right) \qquad (5.2)$$

$$i_Y^- = \frac{2\sqrt{3}}{\pi} I_{dc} \left(\cos(\omega_e t - \frac{2\pi}{3}) - \frac{1}{5}\cos 5(\omega_e t - \frac{2\pi}{3}) + \frac{1}{7}\cos 7(\omega_e t - \frac{2\pi}{3}) - \dots\dots \right) (5.3)$$

102

$$i_B^- = \frac{2\sqrt{3}}{\pi} I_{dc} \left(\cos(\omega_e t + \frac{2\pi}{3}) - \frac{1}{5}\cos 5(\omega_e t + \frac{2\pi}{3}) + \frac{1}{7}\cos 7(\omega_e t + \frac{2\pi}{3}) - \ldots \ldots \right) (5.4)$$

The switching sequences [6,1], [1,2], [2,3], [3,4], [4,5], [5,6], [6,1] will give six space current vectors $i_{r1}^-, i_{r2}^-, i_{r3}^-, i_{r4}^-, i_{r5}^-, i_{r6}^-$ in sectors 1 to 6 respectively. For designing the PWM switching sequences, the time average of three switching current state vectors, located adjacent to the reference vector ($i_r^- = I_r e^{j\alpha}$) is considered over a sub cycle T_s (half carrier period) .T_s is defined as

$$T_s = \frac{1}{2} * T_c \qquad (5.5)$$

where,

$$T_c = \text{carrier time period}$$

Reference current vector i_r^- is shown in a $60°$ sector (between dotted lines) as shown in Fig 5.2 along with the three current state vectors. Referring to Fig 5.2 the reference current vector i_r^- is defined as:

$$I_r \angle \alpha \ T_s = i_{r1}^- t_1 + i_{r2}^- t_2 + i_{r6}^- t_3 \qquad (5.6)$$

$$= I_{r1} t_1 + I_{r1} \angle 60° t_2 + I_{r1} \angle -60° t_3 \qquad (5.7)$$

Where, I_r is the fundamental peak value of reference current vector, while I_{r1} is the fundamental peak value of line currents shown in the equations 5.2, 5.3, 5.4 and it is defined as:

$$I_{r1} = \frac{2\sqrt{3}}{\pi} I_{dc} \qquad (5.8)$$

103
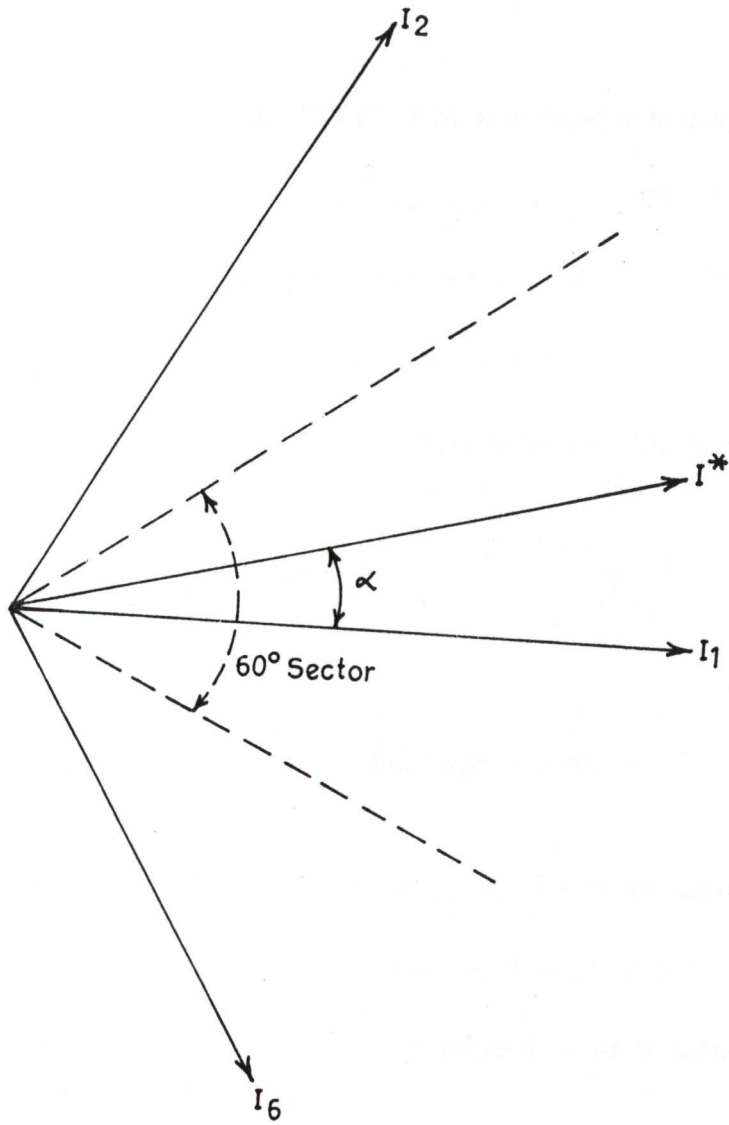
Fig.5.2. Three state current vectors.

$$I_r (\cos \alpha + j \sin \alpha) T_s = I_{rl} [t_1 + 0.5 t_2 + 0.5 t_3] + j I_{rl} [t_2 \sqrt{3}/2 - \sqrt{3}/2\ t_3]$$

$$(5.9)$$

Equating the real and imaginary parts of equation (5.9)

$$t_1 + 0.5 t_2 + 0.5 t_3 = \frac{1}{T_s} \left(\frac{I_r}{I_{rl}} \right) \cos \alpha \qquad (5.10)$$

$$t_2 - t_3 = \frac{1}{T_s} \frac{2}{\sqrt{3}} \frac{I_r}{I_{rl}} \sin \alpha \qquad (5.11)$$

$$t_1 + t_2 + t_3 = T_s \qquad (5.12)$$

Solving equations (5.10), (5.11) and (5.12)

$$\frac{t_1}{T_s} = \left(2 \frac{I_r}{I_{rl}} \cos \alpha - 1 \right) \qquad (5.13)$$

$$\frac{t_2}{T_s} = 1 - \frac{2}{\sqrt{3}} \frac{I_r}{I_{rl}} \sin \left(\frac{\pi}{3} - \alpha \right) \qquad (5.14)$$

$$\frac{t_3}{T_s} = 1 - \frac{2}{\sqrt{3}} \frac{I_r}{I_{rl}} \sin \left(\frac{\pi}{3} + \alpha \right) \qquad (5.15)$$

The above expressions can be represented in terms of modulation index (m) defined as:

$$m = \frac{I_{rl}}{I_{dc}} \qquad (5.16)$$

$$\frac{I_r}{I_{rl\,(Fundamental)}} = \frac{I_r}{\frac{2}{\sqrt{3}} I_{dc}} = \frac{\sqrt{3}}{2} m \qquad (5.17)$$

Substituting equation (5.16) in (5.13), (5.14), (5.15), the value of $\frac{t_1}{T_s}, \frac{t_2}{T_s}, \frac{t_3}{T_s}$ can be expressed as:

$$\frac{t_1}{T_s} = \left(\sqrt{3}\, m \cos\alpha - 1\right) \tag{5.18}$$

$$\frac{t_2}{T_s} = \left(1 - m \sin\left(60 - \alpha\right)\right) \tag{5.19}$$

$$\frac{t_3}{T_s} = \left(1 - m \sin\left(60 + \alpha\right)\right) \tag{5.20}$$

The modulated line currents of the 3- phase current source inverter employing the space vector modulation technique obtained through simulation over a cycle for (N-cmds = 2) in a period of 30°, are shown in the Fig 5.3 (a), 5.3 (b), 5.3(c) for R, Y and B lines respectively.

The above three switching timings of state current vectors are used for the calculation of timer_count for the timer of the ADD-ON card shown in Fig. 4.11. Timer of the ADD- ON card is used for the generation of PWM firing pulses in different sectors 1 to 6. The firing commands generated by the ADD- ON card timer depend upon the timer_ count and it depends upon the number of switching commands (N_cmds) over a period of 30° and the sector numbers. Expressions for the timer_ count of ADD- ON for different sectors are given below.

For sector 6 and 1

$$\text{tmr\_count} = \left(1 - m \sin\left(\frac{\pi}{3} + \alpha\right)\right) * T \_ \Delta\alpha$$

For sector 2 and 5

$$\text{tmr\_count} = \left(-1 + m \sqrt{3} \cos\left(\alpha\right)\right) * T \_ \Delta\alpha$$
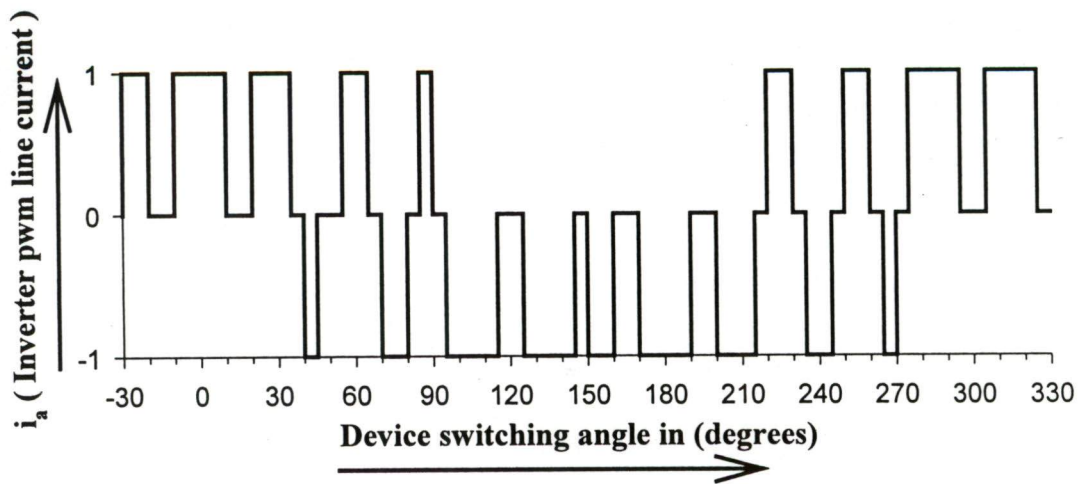
Fig 5.3 (a). Inverter pwm line current (i_a) vs switching angle over a cycle (For 9 number of switching per 90 degree)
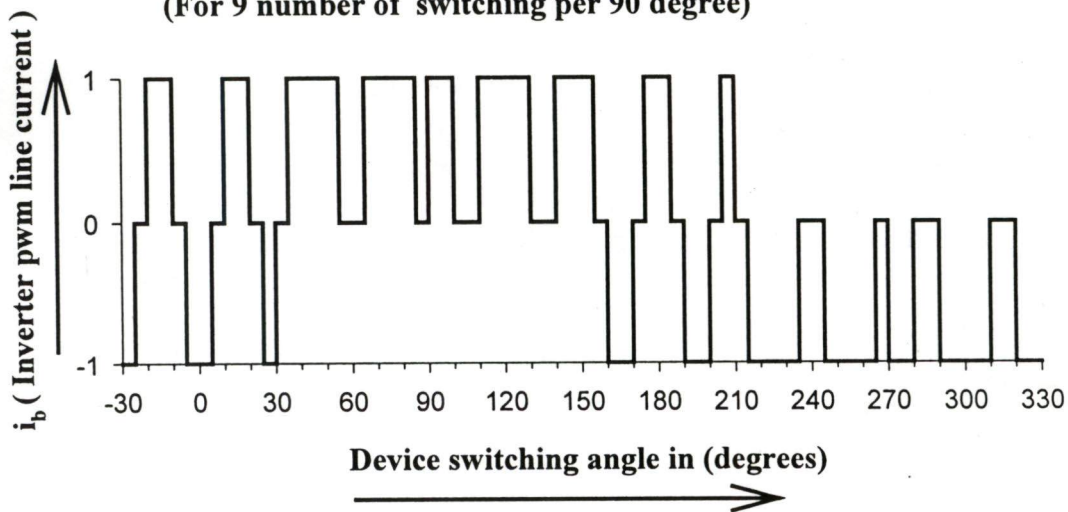
Fig 5.3 (b). Inverter pwm line current (i_b) vs switching angle over a cycle (For 9 number of switching per 90 degree)
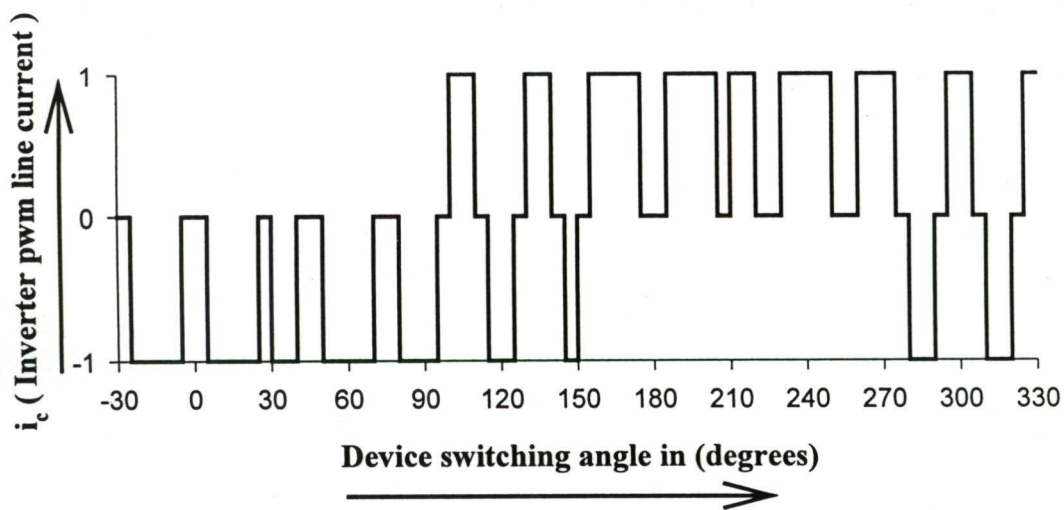
Fig 5.3(c). Inverter pwm line current (i_c) vs switching angle over a cycle (For 9 number of switching per 90 degree)

For sector 3 and 4

$$\text{tmr\_count} = (1 - m \sin(\frac{\pi}{3} - \alpha)) * T\_\Delta\alpha$$

where,

$$\Delta\alpha = (\pi/6)/ \text{N\_cmds}$$

$$\alpha = -(\pi/6) + \delta\alpha/2.0$$

$$T\_\Delta\alpha = (\text{PC\_fq} * \Delta\alpha)/(\text{ref\_freq}. * 2\pi)$$

5.4   OPEN LOOP PROGRAM OF THE CONVERTER

Open loop converter software program consists of main program, interrupt service subroutine for zero crossing interrupt, timer interrupt and serial interrupt. The desired T_{ON} period of firing pulses for the PWM operation of the converter is sent serially from PC-AT to microcontroller.

5.4.1   Main Program for Converter Control

The flow chart for the main program is shown in Fig 5.4. The program starts with the initialization of various input , output ports, timers and serial port etc. After initialization all interrupts have been disabled and only serial interrupt have been enabled. Indices I, J are also initialized. The micro controller continuously monitors the R x D line to check for any character or data received from the personal computer. Index I is made '1' in serial subroutine to indicate that microcontroller has received a character or data.. If the character received is 'G ' then program sets the index J to receive the count for T_{on} period of PWM pulses. The PC-AT sends, the lower and higher byte of T_{on} one by one serially. If the character received is 'R' then processor enables all other interrupts to

108
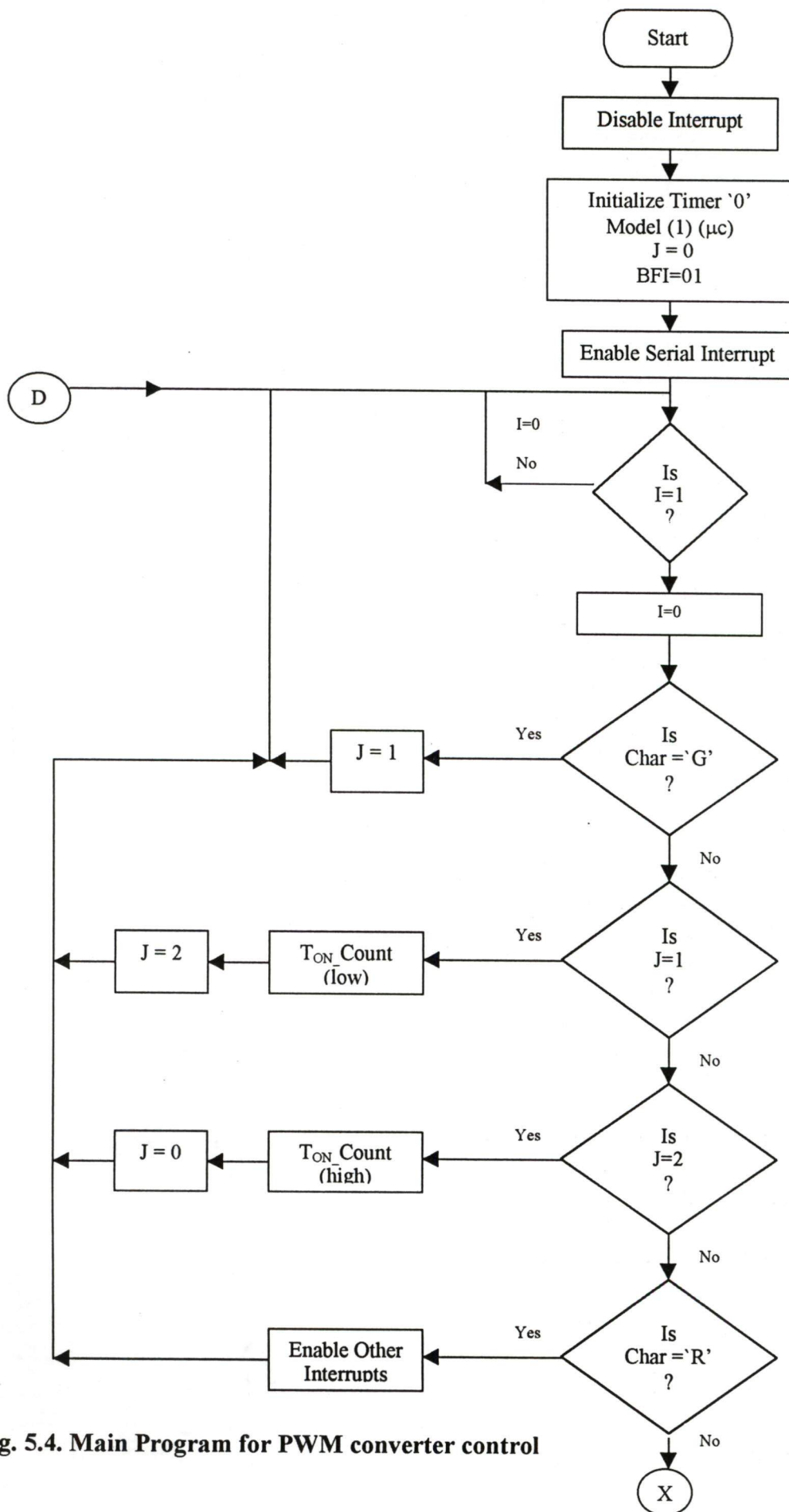
Fig. 5.4. Main Program for PWM converter control

Contd............

109
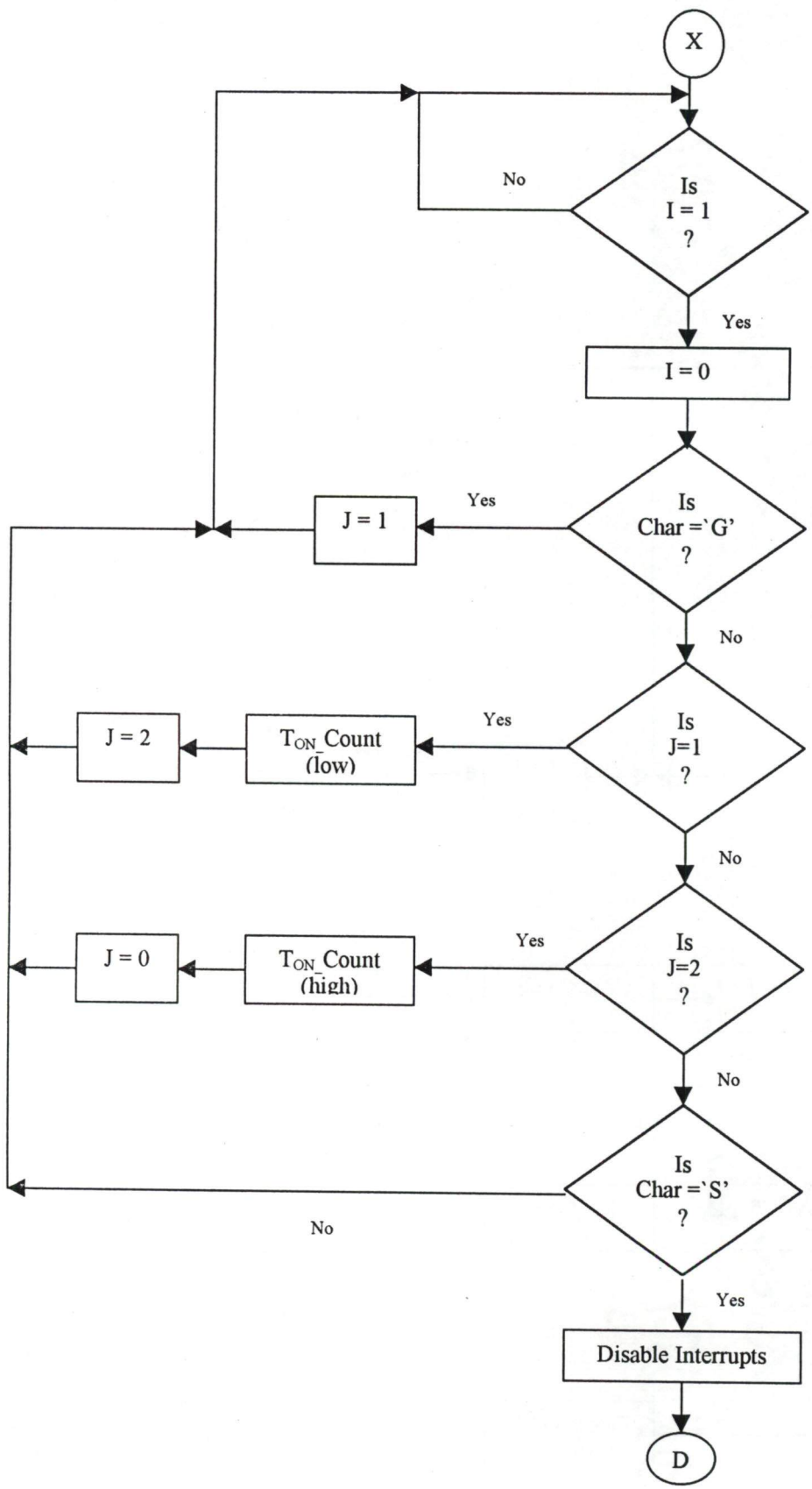
generate the firing pulses. If the character received is 'S' the processor disables the interrupts and stops generating the firing pulses.

5.4.2 Serial Subroutine

The flow chart for the serial subroutine is shown in Fig.5.5. The control is transferred to this ISS, whenever microprocessor receives a character or data serially. The received character or data is read from the serial buffer and stored as 'char'. Before returning to the main program the registers have been retrieved and interrupts are enabled.

5.4.3 Zero Crossing Interrrput Service Subroutine

The flow chart for zero crossing interrupt service subroutine is shown in Fig 5.6. Zero crossing signal goes to INT '0' of the micro controller from the synchronization circuit and it interrupts the processor, at every zero crossing of line to line a.c. supply voltage. The zero crossing occurs at an interval of every 60°. The timer '0' is loaded with half of the off time period (T_{OFF}) and is triggered .The two variable indices I and J are initialized to '1'. The variable index I is used to check whether the timer is to be loaded with T_{ON} or T_{OFF}. The variable index J checks whether the half cycle of the input wave is completed or not. After loading the timer, the quantizer signals are read from port . The memory address is obtained, where the firing commands are stored. The firing command is read from the table and stored, to be issued at appropriate instant.

5.4.4 Timer Interrupt Service Subroutine

The timer interrupts the processor at the end of T_{ON} and T_{OFF}. The flow chart is shown in Fig 5.7. In this service subroutine, the firing command is issued at the port 1 of
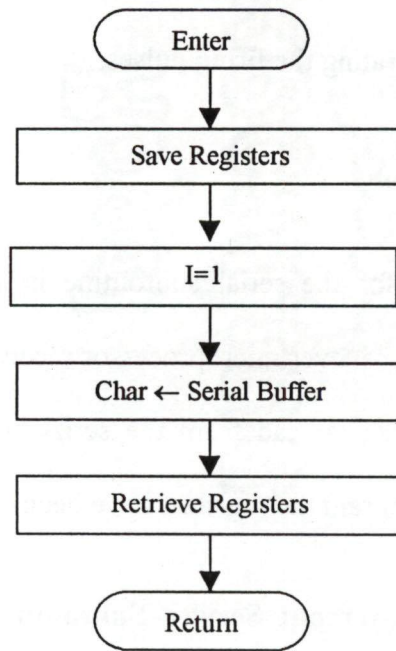
Fig. 5.5. Serial Subroutine
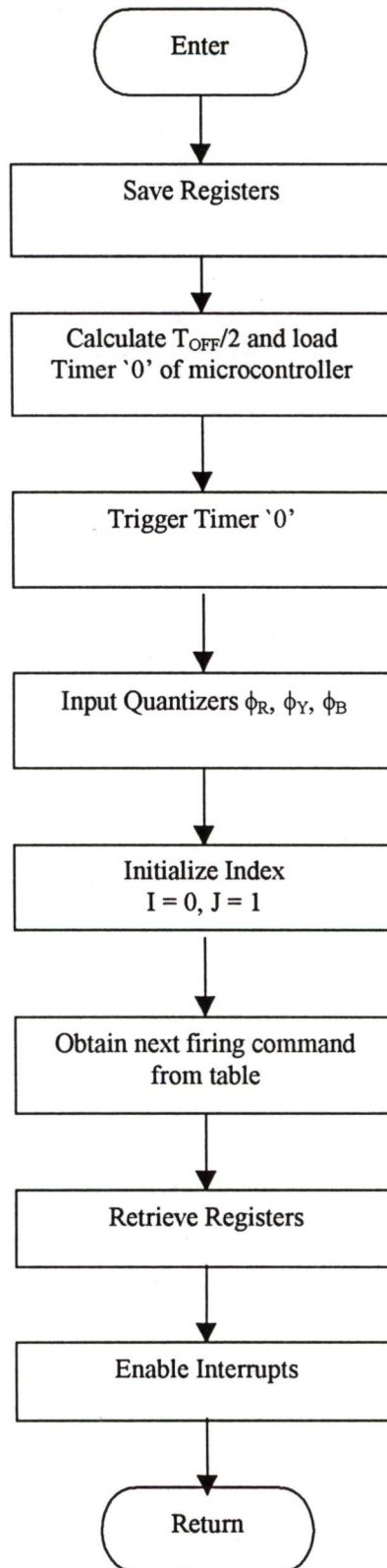
Fig 5.6. ISS for Zero crossing Interrupt

113
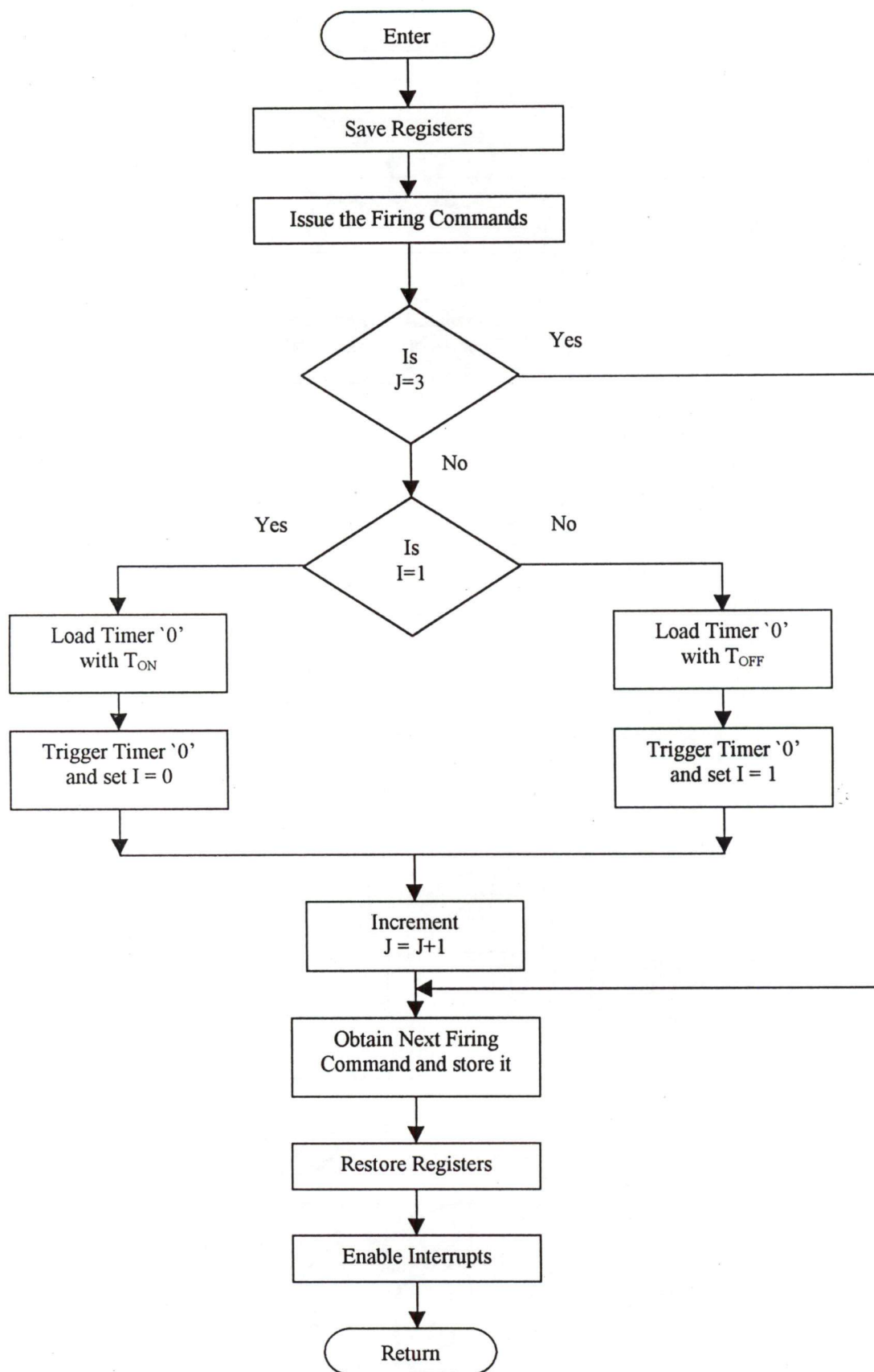
Fig 5.7. Timer Interrupt Service Subroutine

the micro controller. The index I is checked to load timer '0' with T_{ON} or T_{OFF}. If I is 1, timer '0' is loaded with T_{ON} and I is set to zero. If I is 0, then timer '0' is loaded with T_{OFF} and I is set to '1'. The index J is also incremented at every timer interrupt for counting the number of pulses in the output voltage. After restoring the registers, the interrupt structure is enabled.

5.4.5 Main Program for Open Loop Operation of the Converter

The flow chart for open loop control of the PWM converter is shown in Fig 5.8. All the variables are initialized and baud rate is set at 2400. A look up table for control voltage vs T_{ON_count} is prepared. The program checks for any key pressed. If key pressed is 'm' then menu is displayed. If key pressed is 'c' then reference control is read and if it is accepted, T_{ON} value is obtained from look up table. The lower and higher bytes are sent in a sequence to microcontroller after sending a char 'G'. To start the converter operation character 'R' is send. To stop the converter character 'S' is send.

5.4.6. T_{ON_Count} Table for the Converter Firing Pulses

Flow chart for the program is shown in Fig 5.9. This program is used for calculating the T_{ON} period of the firing pulses of the PWM converter. Since the internal clock frequency of the microcontroller is 12 MHz and count corresponding to 1.667 ms is 1667.Therefore to calculate count for any time period control voltage V_c is used. It is assumed that control voltage varies from 167 to 1667.Hence the T_{ON} can be calculated from the following equations:

$$T_{ON}[j] = V_c[j]$$
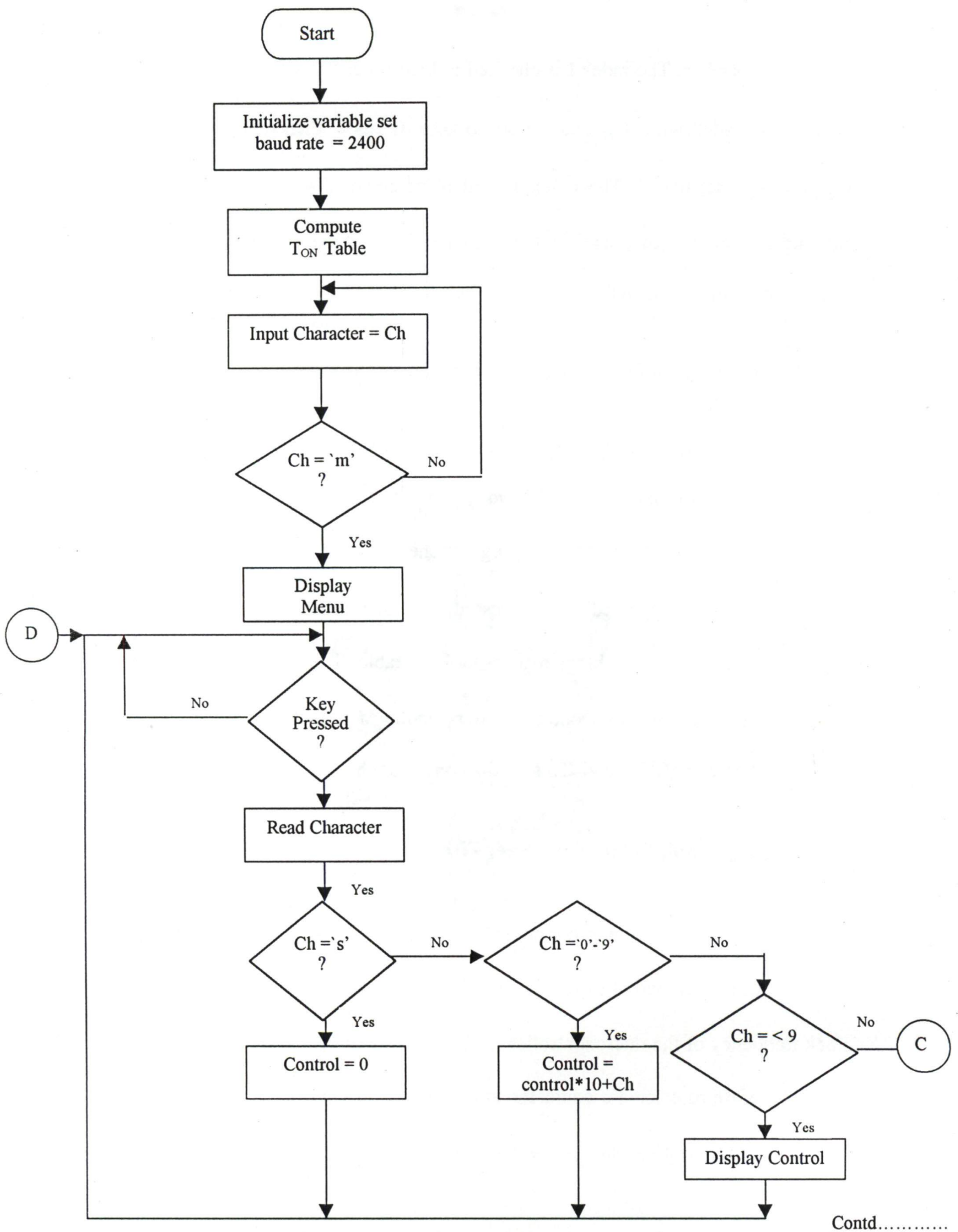
Fig. 5.8. Flow Chart of Main for Open Loop Operation of the Converter

116
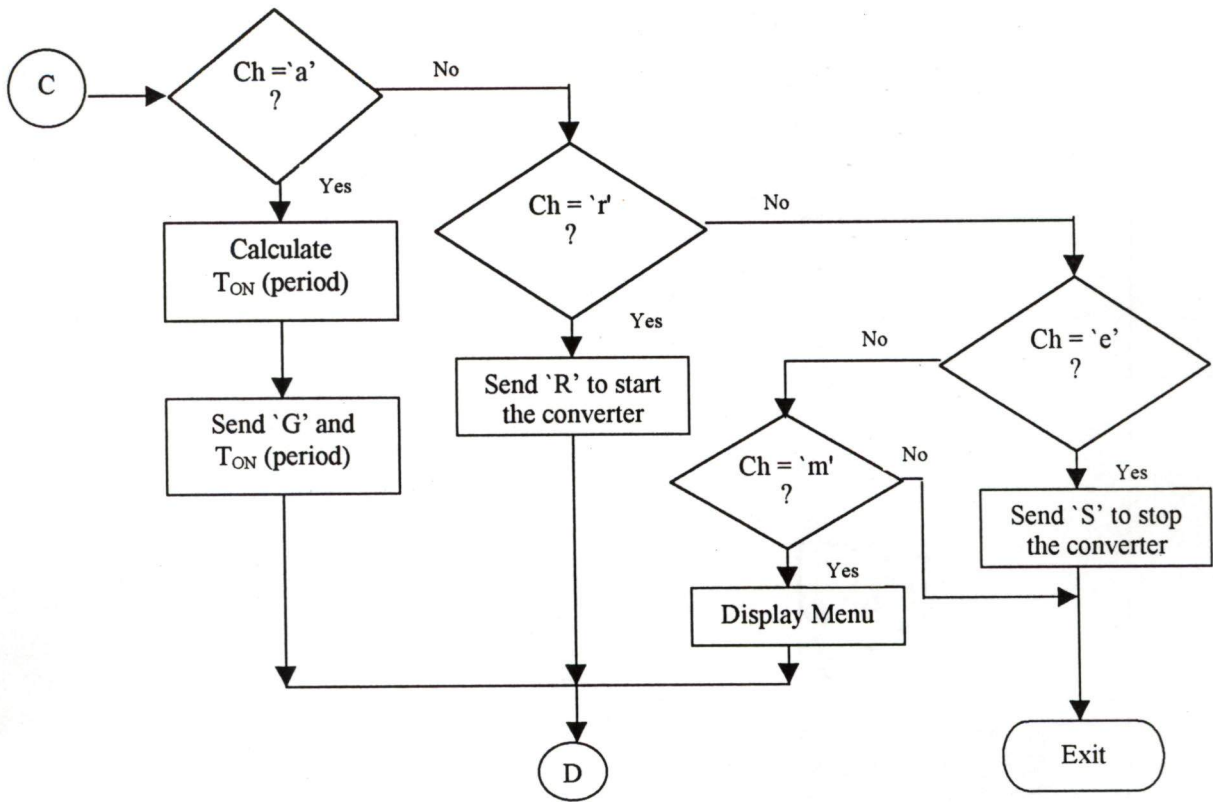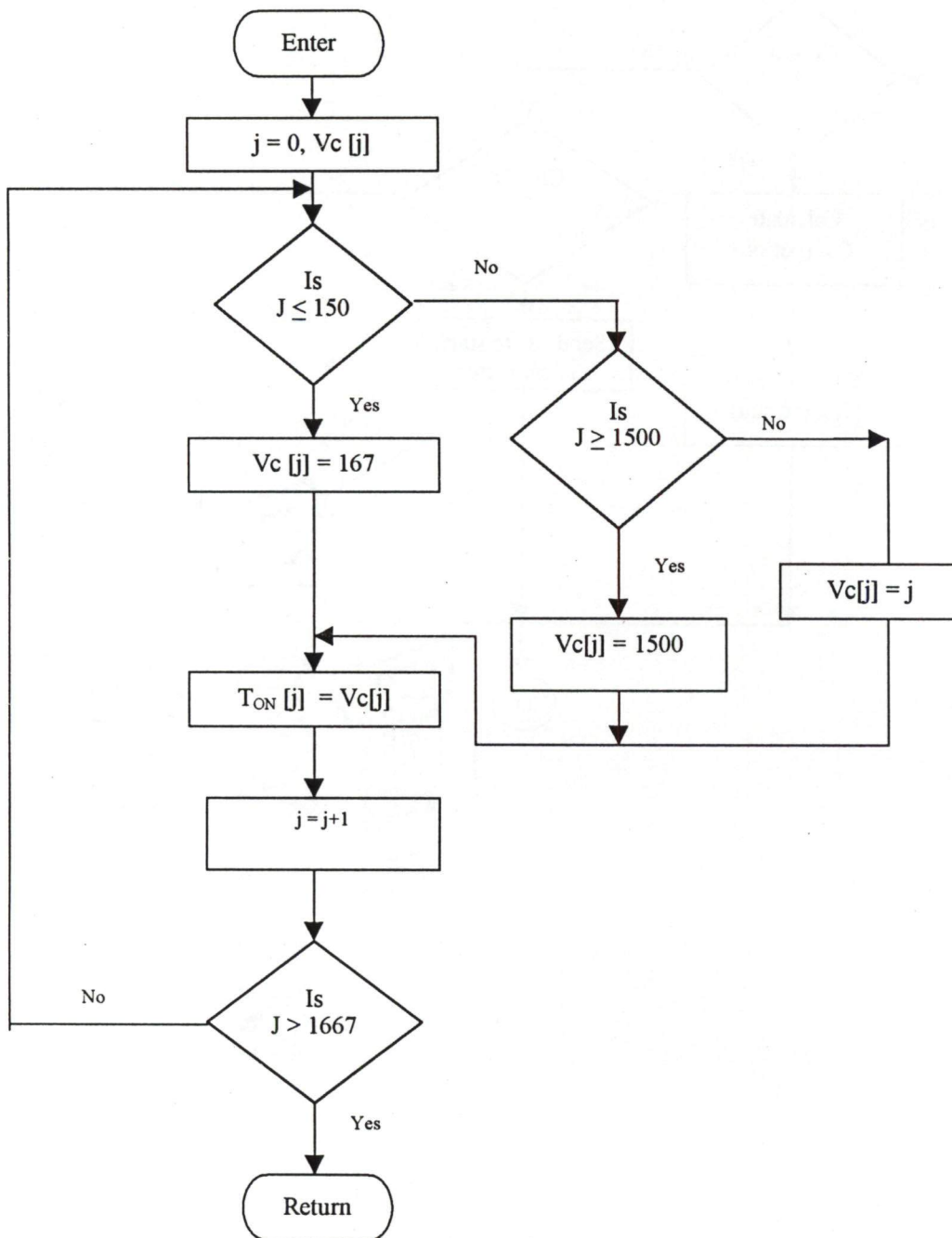
Fig. 5.9. Flow Chart for T_{ON} Table for Firing Pulses

where,

j varies from 0 to 1667.

5.5 OPEN LOOP OPERATION OF CSI-FED INDUCTION MOTOR DRIVE

To investigate the performance of the inverter, the drive is operated in open loop, i.e. without speed feedback .The front-end PWM converter is operated in closed loop with d.c.link current as a feedback so that it acts as a current source, however the inverter is operated in open loop .The software consists of main program for inverter control, interrupt subroutine for PC Timer_0, Ext_Timer, subroutines for current error and current PI processing. The converter is controlled in the same manner as discussed in section 5.4, by sending the T_{on} period serially to the microcontroller-based system.

5.5.1 Main program

The flow chart for the main program is shown in Fig.5.10. Program starts with the initialization of I/O ports, PC_ Timer and Ext_ Timer. After initialization, reference current is inputted through the keyboard. Setting actual current to be zero, the d.c.link current measurement and current PI processing is carried out at 1 ms interval, to calculate T_{ON} period of PWM converter and it is send to micro controller serially. The actual current of the d.c. link is sensed using Hall effect current sensor. Analog voltage obtained from the Hall effect current sensor corresponding to actual current is directly converted into digital value using 12-bit ADC. Starting frequency of the inverter is set at 2.5 Hz and corresponding to this frequency modulation index is set at a minimum value of 0.82 and number of switching commands are set at 4 for 30° of inverter output frequency. Six sectors each of 60° are defined. An index start of sector (Sos) is set at 1, which indicates

```
                    ┌─────────┐
                    │  Start  │
                    └────┬────┘
                         │
                         ▼
              ┌────────────────────────┐
              │  Initialize variables, │
              │  Ports, P.C. timers, Ext-│
              │  timer Interrupts      │
              └───────────┬────────────┘
                          │
                          ▼
              ┌────────────────────────┐
              │   Disable Interrupts   │
              │                        │
              └───────────┬────────────┘
                          │
                          ▼
              ┌────────────────────────┐
              │  Input reference current│
              └───────────┬────────────┘
                          │
                          ▼
              ┌────────────────────────┐
              │ Initialize actual current = 0│
              └───────────┬────────────┘
                          │
                          ▼
              ┌────────────────────────┐
              │ Call current PI and calculate $T_{ON}$│
              └───────────┬────────────┘
                          │
                          ▼
              ┌────────────────────────┐
              │ Send $T_{ON}$ to micro controller│
              └───────────┬────────────┘
                          │
                          ▼
              ┌────────────────────────┐
              │ Set starting frequency = 2.5│
              └───────────┬────────────┘
                          │
                          ▼
              ┌────────────────────────┐
              │ Modulation Index = 0.82│
              └───────────┬────────────┘
                          │
                          ▼
              ┌────────────────────────┐
              │     N_cmds = 4         │
              └───────────┬────────────┘
                          │
                          ▼
              ┌────────────────────────┐
              │ Set sos = 1 (60° sector)│
              │    and new data = 1    │
              └───────────┬────────────┘
                          │
                          ▼
              ┌────────────────────────┐
              │ Load Ext-timer `0' with an│
              │ arbitrary value and trigger to│
              │    get first Interrupt │
              └───────────┬────────────┘
                          │
                          ▼
              ┌────────────────────────┐
              │  Set Char `R' to micro │
              │ controller to start the drive│
              └───────────┬────────────┘
                          │
                          ▼
                        ( + )
```

Fig. 5.10. Main Program in open loop

120

```
                              ( + )
                                │
                                ▼
                    ┌───────────────────────┐
                    │  Reference current if │
                    │  key pressed = `c'    │
                    └───────────────────────┘
                                │
                                ▼
                    ┌───────────────────────┐
                    │  Reference frequency if│
                    │  key pressed = `f'    │
                    └───────────────────────┘
                                │
                                ▼
                            ◇─────────◇
                  No       ╱    Is     ╲
            ◄───────────────   KK = 1    
                            ╲    ?      ╱
                            ◇─────────◇
                                │ Yes
                                ▼
                    ┌───────────────────────┐
                    │   Set index KK = 0    │
                    └───────────────────────┘
                                │
                                ▼
                    ┌───────────────────────┐
                    │ Read reference d.c.link current│
                    └───────────────────────┘
                                │
                                ▼
                    ┌───────────────────────┐
                    │    Call Current PI    │
                    └───────────────────────┘
                                │
                                ▼
                    ┌───────────────────────┐
                    │    Calculate T_ON     │
                    └───────────────────────┘
                                │
                                ▼
                    ┌───────────────────────┐
                    │ Send T_ON to microcontroller│
                    └───────────────────────┘
                                │
                                ▼
                    ┌───────────────────────┐
                    │   Set new_data = 1    │
                    └───────────────────────┘
                                │
                                ▼
            Yes             ◇─────────◇            No
      ┌───────────────────╱     Is     ╲───────────────────┐
      │                   ╲ ref_freq ≤ 40╱                  │
      ▼                   ◇─────────◇                        ▼
┌──────────────────┐                            ┌──────────────────┐
│ No. of commands = 4│                          │ No. of commands = 2│
└──────────────────┘                            └──────────────────┘
      │                                                      │
      └────────────────────┬─────────────────────────────────┘
                           ▼
                 ┌───────────────────────┐
                 │   Set new_data = 1    │
                 └───────────────────────┘
```
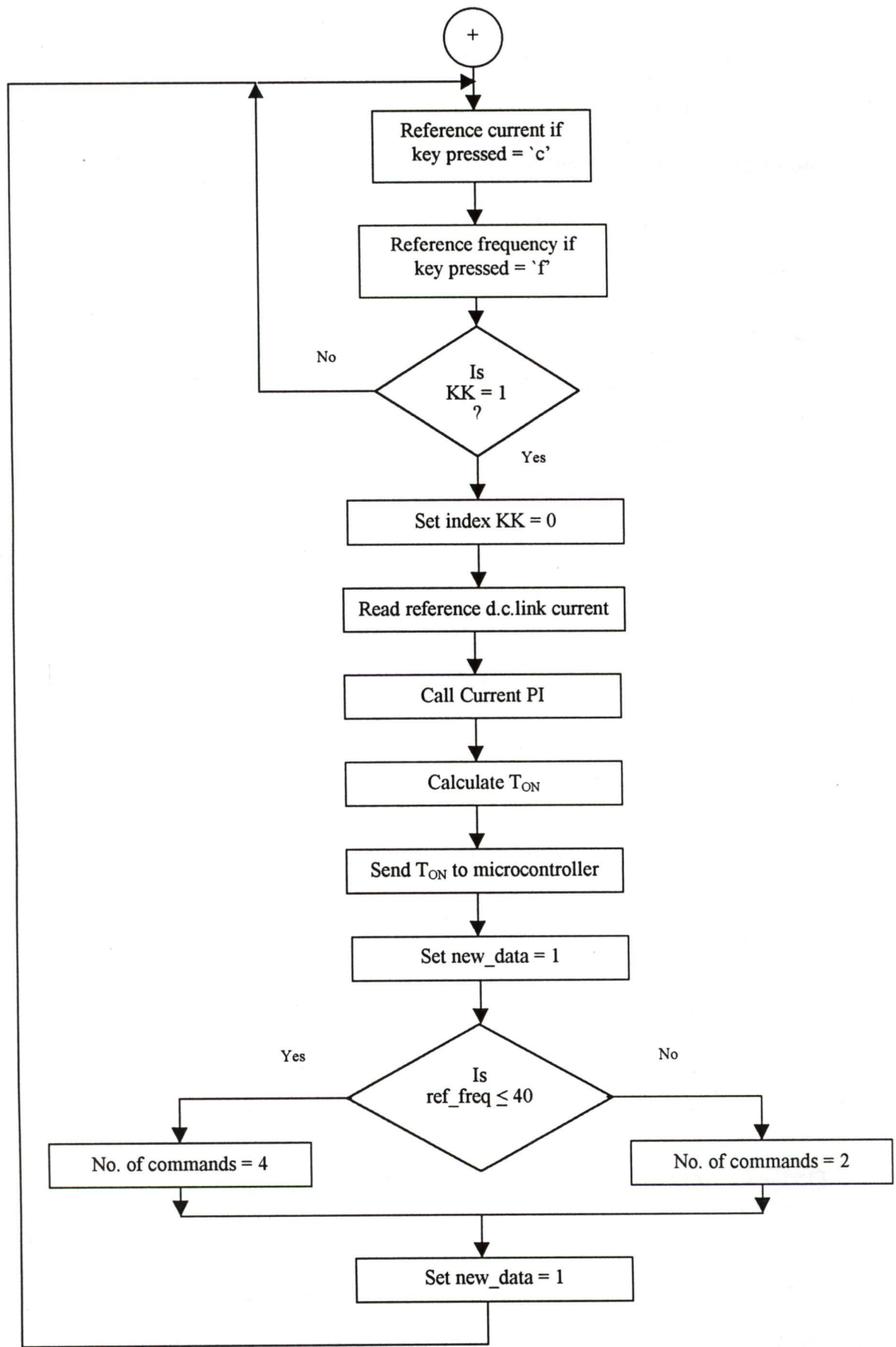
beginning of a 60° sector. To change the operating frequency and modulation index under running condition, an index new_ data is used. It is set to '1' whenever there is a change in operating frequency and after implementing the change it is reset to '0'. Ext_ Timer 0 is used for generating the interrupt at the desired instants for inverter firing pulse generation. Therefore switching command per 30° over a cycle are calculated and new_ data index is set to '1'. Ext_timer 0 is loaded with an arbitrary value and it is triggered to get the first interrupt. Char 'R' is send to microcontroller to start the drive. The current measurement and current PI processing is done at every 1 ms interval. Therefore the internal timer of PC is initialized and triggered to generate interrupt at 1 ms interval. In every sampling interval, actual d.c.link current is read and current PI processing is carried out to calculate T_{ON} of the converter and sent to microcontroller. Reference current and reference frequency are inputted via the keyboard of the computer, if key pressed is 'c' and 'f' respectively.

5.5.2 ISS PC_ Timer '0'

The ISS PC_ Timer '0' subroutine is shown in the Fig 5.11. The PC timer generates interrupts at every 1 ms interval. The index KK is set to 1, to indicate the beginning of 1 ms interval and it is reset to '0' after PI processing in main program.

5.5.3 ISS Ext_ Timer _0

Flow chart for the ISS Ext_Timer 0 is shown in the Fig 5.12. The index Sos is checked first. If it is 1, then program calculates the modulation index M.I. for the operating frequency and if it is more than 1.0, it is clamped to 1.0. The program calculates the switching angles of the inverter and timer_count corresponding to the switching

122

Fig. 5.11. ISS for PC Timer_0

Inside the process box:

$$M.I. = 0.82 + \left(\frac{ref\_freq}{50}\right) * 0.18$$

If (M.I. > 1.0) M.I. = 1.0

$\Delta\alpha = (\pi/6)/$ Number of commands

$\alpha = -(\pi/6) + (\Delta\alpha/2)$

$T\Delta\alpha = (PC\_freq \times \Delta\alpha) / (ref\_freq \times 2 \times \pi)$

Number of commands = switching
commands per 30° over a cycle

mk = 1

New_data = 0

Sos = 0

X

Contd............

Fig. 5.12. ISS for Ext_timer

X

Sector 1
tmr_count =
$(1.0 - M.I.*$
$\sin((\pi/3)+\alpha))*T\Delta\alpha$

Sector 2
tmr_count =
$(-1.0 + 1.732*M.I..*$
$\cos(\alpha)*T\Delta\alpha$

Sector 3
tmr_count =
$(1.0 - M.I.*$
$\sin((\pi/3) - \alpha))*T\Delta\alpha$

Sector 4
tmr_count =
$(1.0 - M.I.*$
$(2.0 \; \sin((\pi/3) - \alpha))*T\Delta\alpha$

Sector 5
tmr_count =
$(-1.0 + 1.732*M.I..*$
$\cos(\alpha)*T\Delta\alpha$

Sector 6
tmr_count =
$(1.0 - M.I.*$
$\sin((\pi/3) + \alpha))*T\Delta\alpha$

$\alpha = \alpha + \Delta\alpha$

mk = mk++

mk = mk++

Is
mk > n_ comds

No

Yes

$\alpha = \alpha + \Delta\alpha$

Sos = 1

Sector++

Sec > 6

No

Yes

Sector 1

Firing commands to the inverter devices

Load Ext_timer with tmr_count & trigger

Return

124

angles for the different sectors in a sequence 1,2,3,6, using the expression given by the equation (5.21 to 5.23) .The firing commands for the different sectors are also obtained from the look up table stored in the memory of the computer. Firing command is issued from port A and Ext_ timer is loaded with timer count and triggered. A sector index is incremented every time, timer interrupt is generated. If sector index is more than 6, it is set to 1. If new data index is '1' then indices Sos and new_data are reset to '0'.

5.5.4 Current Error Subroutine

The flow chart is shown in Fig 5.13. This subroutine calculates the error between reference current obtained from the PI processing of the speed loop and actual d.c.link current. If current error is more than a positive current error then it is clamped to maximum positive current. Similarly if it is more than a maximum negative error, it is clamped to a maximum negative error defined in the program.

5.5.5 Current PI Sub routine

The electrical time constant of the drive is less, than mechanical time constant therefore current PI is done at every 1ms i.e. 20 times in a supply period to regulate the d.c.link current. The current PI processing can be expressed mathematically as:

$$V_r(n) = V_r(n-1) + k_{p_i}(e_i(n) - e_i(n-1)) + k_{i_i}e_i(n)$$

Since the rectifier output voltage is directly related to the T_{on} period of firing pulses, therefore the T_{on} time period of the PWM converter can be obtained directly with the rectifier output voltage as:

$$T_{ON}(n) = V_r(n)$$
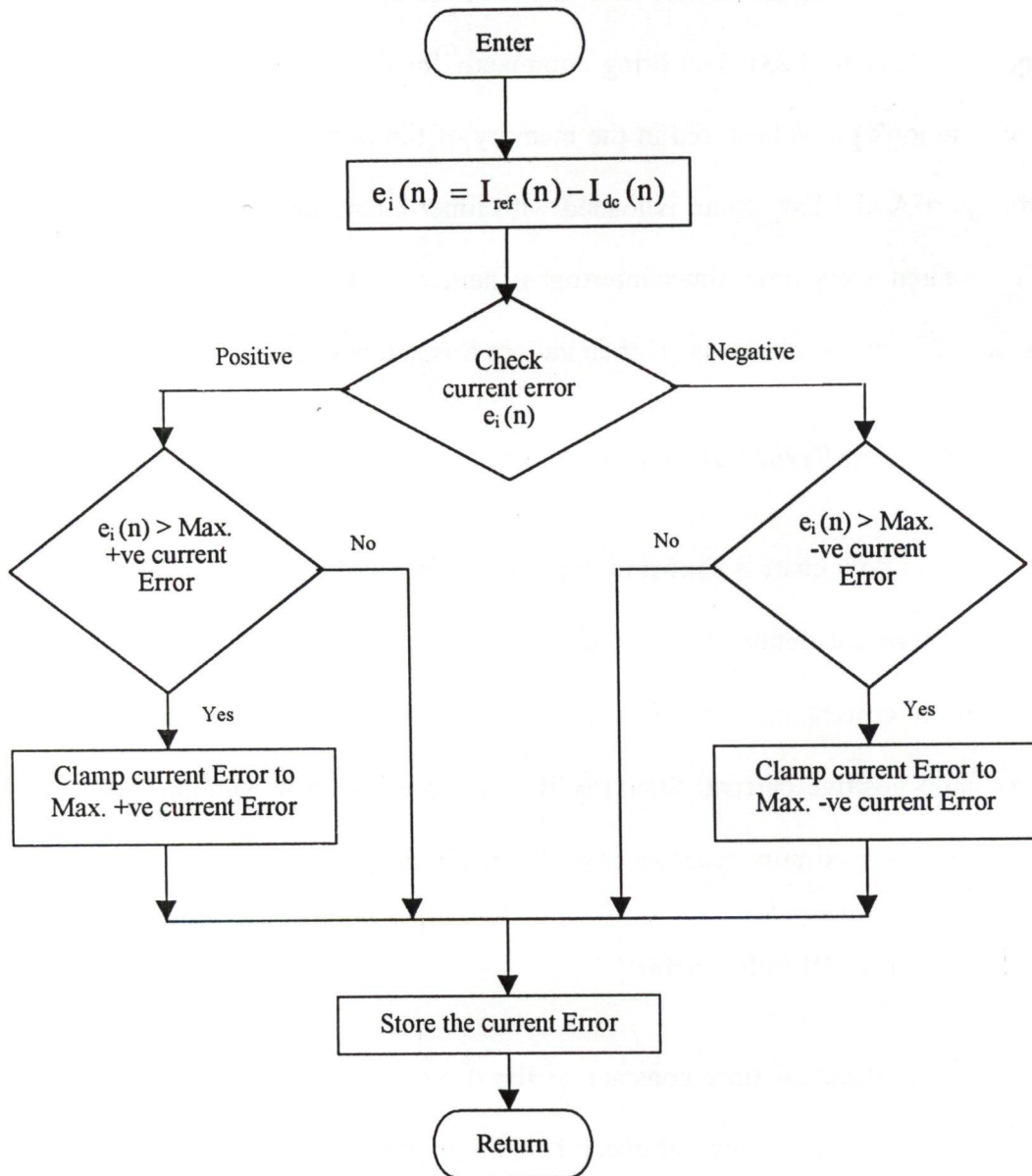
Fig. 5.13. Current Error Processing

$e_i(n)$ = Current error between reference d.c.link current and actual d.c.link

      Current at nth sampling instant

$e_i(n-1)$ = Current error between reference d.c.link current and actual d.c.link

      Current at (n-1) th sampling instant

$V_r(n)$ = Rectifier output voltage at n th sampling instant

$V_r(n-1)$ = Rectifier output voltage at (n-1) th sampling instant

$T_{ON}(n)$ = On time period of firing pulses at n th sampling instant

T_{s_i} = Sampling rate of current loop (1ms)

If the calculated value of T_{ON} time is less than a minimum value defined in the program, it is clamped to a minimum value of T_{ON} defined in the program. If the calculated value of T_{ON} time is more than a maximum value defined in the program, it is clamped to a maximum value of T_{ON} time and stored otherwise calculated T_{ON} is stored as T_{ON} at a particular memory location. Turn off time is calculated by subtracting the T_{ON} time from T_{s_i} (sampling instant). The flow chart of the program is shown in the Fig. 5.14.

5.6 CLOSED LOOP OPERATION OF CSI-FED INDUCTION MOTOR DRIVE

The system software is developed when the inverter is operating in the closed loop. The software consists of main program, current measurement, interrupt service subroutines for converter and inverter control, subroutines for current PI processing, speed measurement, speed error, speed PI processing and slip regulator. The current error and current PI processing is already discussed in the section 5.5.
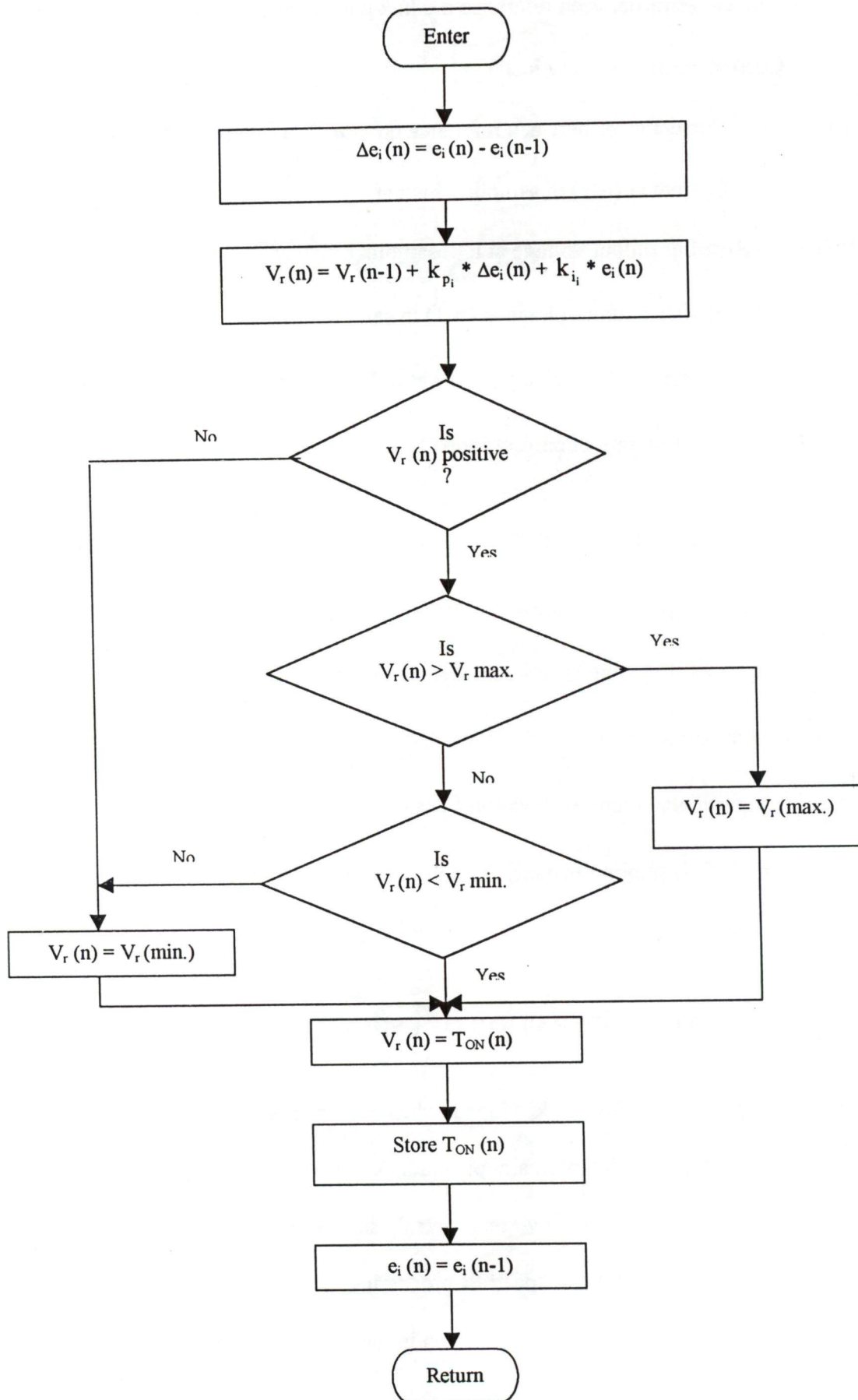
Fig. 5.14. Current PI Processing

128

5.6.1 Main Program

The flow chart for the main program is shown in Fig 5.15. All the variables are initialized and baud rate is set as 2400. Various timers and ports are initialized. (T_{ON} vs V_r) table is prepared and store in the beginning after interrupts are enabled. Software waits for the command input through keyboard. If key pressed is 'm' then menu is displayed. To input the reference speed key 's' is pressed, followed by the reference speed and it is accepted when key 'a' is pressed. If key pressed is 'r', then the actual speed of the machine and actual d.c.link current are set to zero, because machine is at rest. Speed loop and current loop PI processing is done to calculate T_{ON} time of the PWM converter and starting operating frequency of the machine. The T_{on} period is sent serially to microcontroller and char 'R' is send to start the motor. After sending the start command to the motor, PC_ Timer '0' is initialized to generate 1ms interrupt. An index KK is used which is set to '1' in the beginning of 1 ms interrupt. And it is set to 2 at every 10 ms interval. If KK is 2, then the actual speed is measured and speed loop processing is done to obtain the new reference slip speed and hence the reference active and reactive currents of the stator. The capacitor current is calculated. The reference d.c.link current is obtained using stator active reference current, stator reference reactive current and capacitor current. The actual d.c.link current is measured and the current PI processing is done to calculate the control voltage. This control voltage is used to calculate the T_{ON} time of the firing pulses and transmitted to micro controller. If KK = 1 only current loop processing is carried out.

5.6.2 Timer Interrupt Subroutine

The flow chart for this subroutine is shown in Fig. 5.16. The speed measurement of the motor is carried out with the help of PC internal timer '0' and timer of ADD-ON

129
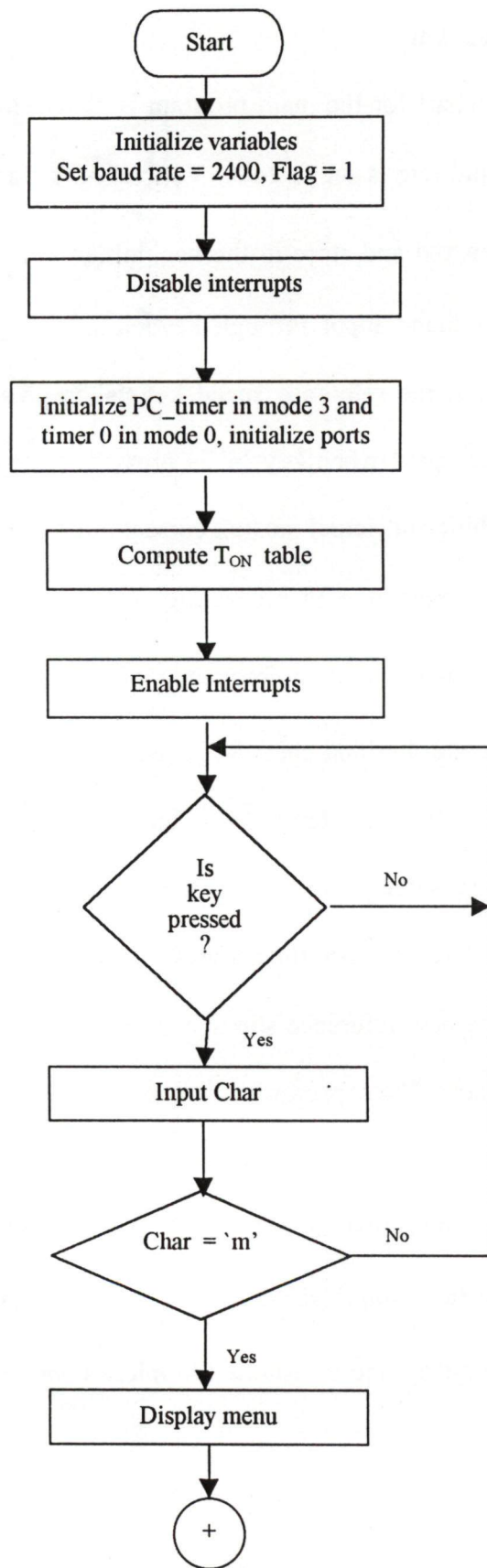
Fig. 5.15. Main Program in close loop

130

A

Reference speed = speed

Actual speed = 0

Speed PI processing

Actual current = 0

Current PI processing

Calculate $V_r(n)$ & obtain T_{ON}

Transmit 'G' and T_{ON} to microcontroller

C

B

Char = 'e'

No

Yes

Send 'S' to stop the motor

Char = 'q'

No

Yes

Stop

Contd............

133

Contd............

```
        ( + )
          │
          ▼
      ╱───────╲        No   (KK = 1)
     ╱  KK = 2  ╲──────────────────────────┐
     ╲         ╱                            │
      ╲───────╱                             │
          │ Yes                             │
          ▼                                 │
   ┌───────────────┐                        │
   │   Spd_meas    │                        │
   └───────────────┘                        │
          │                                 │
          ▼                                 │
   ┌────────────────────────┐               │
   │ Speed PI processing to │               │
   │ calculate slip_speed   │               │
   └────────────────────────┘               │
          │                                 │
          ▼                                 │
   ┌──────────────────────────┐             │
   │ Calculate Capacitor      │◄───────┐    │
   │ current (I_c)            │        │    │
   └──────────────────────────┘        │    │
          │                            │    │
          ▼                            │    │
   ┌──────────────────────────┐        │    │
   │ Calculate Ref_current    │        │    │
   │ = I_ref                  │        │    │
   └──────────────────────────┘        │    │
          │                            │    │
          ▼                            │    │
   ┌──────────────┐                    │    │
   │   KK = 1     │                    │    │
   └──────────────┘                    │    │
          │◄──────────────────────────────────┘
          ▼
   ┌──────────────────────┐
   │  d.c. link cur_meas  │
   └──────────────────────┘
          │
          ▼
   ┌─────────────────────────────┐
   │ Current PI processing to    │
   │ calculate V_r               │
   └─────────────────────────────┘
          │
          ▼
   ┌──────────────────────────┐
   │ Obtain T_ON_count        │
   │ from table               │
   └──────────────────────────┘
          │
          ▼
   ┌──────────────────────────┐
   │ Transmit 'G' and         │
   │ T_ON_count               │
   └──────────────────────────┘
          │
          ▼
   ┌──────────────┐
   │   KK = 0     │
   └──────────────┘
          │
          ▼
        ( D )
```

$$\text{Syn\_speed} = \omega_r + \omega_{sl}^*$$

$$\text{Ref\_freq} = (\text{syn\_speed}) / 30$$

Is $0 \le f \le 50$

No → M.I. = 1

Yes → M.I. = $0.82 + 0.18 * (\text{ref\_freq}) / 50$

Is $2.5 \le f \le 40$

Yes → N_cmd = 4

No → Is $40 \le f \le$

Yes → N_cmd = 2

No

Soc = 1
New Data = 1

Calculate active and reactive currents

Fig. 5.16. PC Internal Timer Interrupt

135

card. The PC internal timer '0' is used for the generation of 1ms interrupt. These interrupts are used to identify the instants of speed and current error processing. An index KK is initialized to one every time, timer interrupt comes. Speed measurement is done at every 10 ms, by down counting the ADD – ON card timer '0' for a period of 8 ms and rest 2 ms time is used for PI processing. If spd_ms index is zero then timer '0' is loaded with FFFF and this index is incremented when first interrupt of PC timer comes on ADD-ON card . Timer '0' starts down counting and at 8th interrupt from PC timer it stops down counting and returns.

5.6.3   Speed Measurement Subroutine

The actual speed of the motor is obtained by down counting the ADD – ON card timer '0'.Lower and higher byte of speed obtained from timer interrupt subroutine is used to calculate the speed in RPM. One bit of speed obtained from measurement corresponds to 1 RPM. SPD_MS_O index is set to zero when speed measurement gets over. The flow chart is shown in Fig. 5.17.

5.6.4   Speed Error Subroutine

This subroutine calculates the difference in reference speed (ω_r^*) and actual speed (ω_r). If the difference in the error is more than a defined positive speed error, then it is clamped to maximum positive speed error (ω_{al}). Similarly if it is more than a maximum negative speed error, it is clamped to a maximum negative speed error defined in the program. The flow chart is shown in the Fig. 5.18. The speed error is stored in the memory of the computer and returns to the calling program.
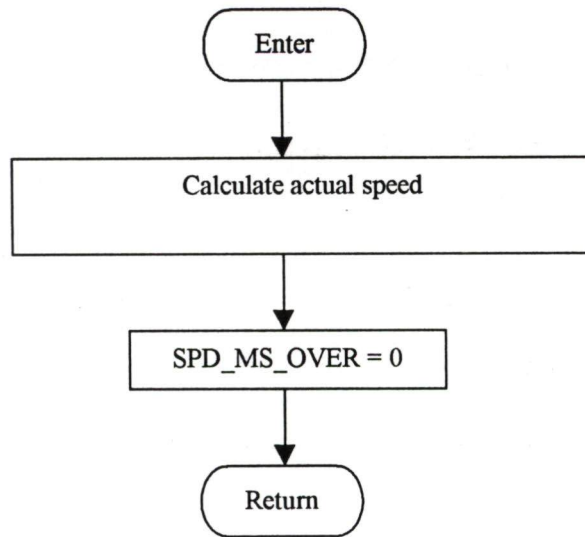
Fig. 5.17. Speed Measurement
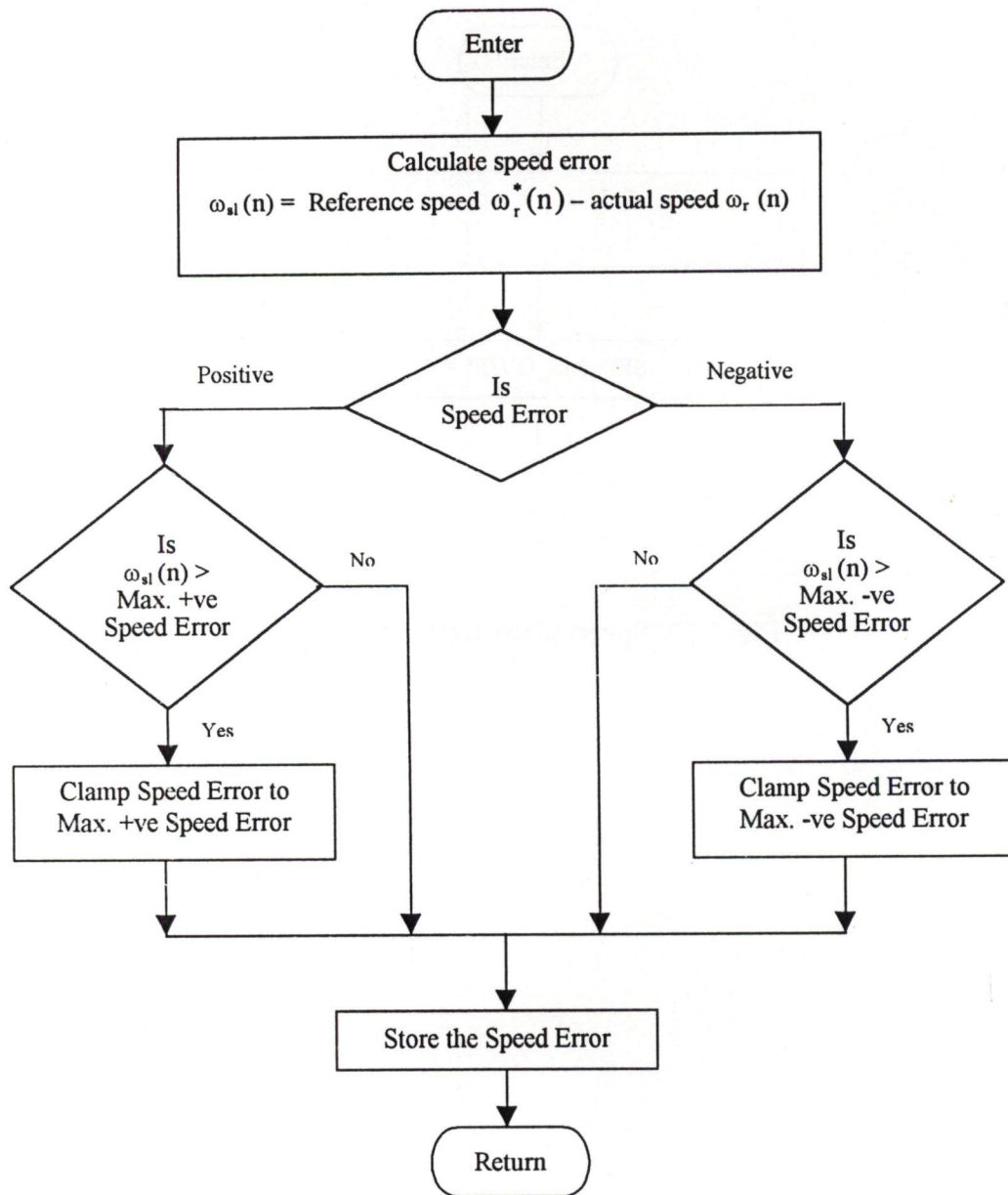
Fig. 5.18. Speed error sub routine

5.6.5 Speed PI Processing

The speed of the motor is measured at every 10 ms, reference speed is inputted to the PC via keyboard. Since the mechanical time constant of the motor is large, therefore the speed is measured only twice in a supply period. The speed PI processing is done to obtain the reference slip speed ω_{sl}^*. It can be expressed as

$$\omega_{sl}^*(n) = \omega_{sl}^*(n-1) + k_{p_s}\left(\omega_{sl}(n) - \omega_{sl}(n-1)\right) + k_{i_s} * T_{s_s} * \omega_{sl}(n)$$

where,

$\omega_{sl}(n)$ = Speed error at nth sampling instant

$\omega_{sl}(n-1)$ = Speed error at (n-1) th sampling instant

T_{s_s} = Sampling rate of the speed loop (10 ms)

$\omega_{sl}^*(n)$ = Reference slip speed at nth sampling instant

$\omega_{sl}^*(n-1)$ = Reference slip speed at (n-1) th sampling instant

The reference slip speed (ω_{sl}^*) after PI processing is limited to a maximum and minimum value. By using reference slip speed (ω_{sl}^*), the stator reference active current (I_{act}^*) and stator reference reactive current (I_{react}^*) are calculated using look up table of I_{act}^* vs. ω_{sl}^* and I_{react}^* vs. ω_{sl}^*. Using I_{act}^*, I_{react}^* and rms current of the capacitor ($I_{c)}$), the d.c.link reference current is calculated as discussed in Chapter 2. The flow chart for speed PI processing is shown in Fig 5.19.

5.6.6 Slip Regulator Subroutine

Slip regulator maintains the rated flux in the machine at each value of the operating frequency. The flow chart for speed regulator subroutine is shown in Fig 5.20.

Enter

$$\omega_{sl}(n) = \omega_r^*(n) - \omega_r(n)$$

Is $\omega_{sl}(n)$ positive

Yes

No

Error flag = 1

Error flag = -1

$$\Delta\omega_{sl}(n) = \omega_{sl}(n) - \omega_{sl}(n-1)$$

$$\omega_{sl}^*(n) = \omega_{sl}^*(n-1) + k_{p_s} * \Delta\omega_{sl}(n) + k_{i_s} * \omega_{sl}(n)$$

Limit $\omega_{sl}^*(n)$ between min.^{m} and max.^{m} values

Return
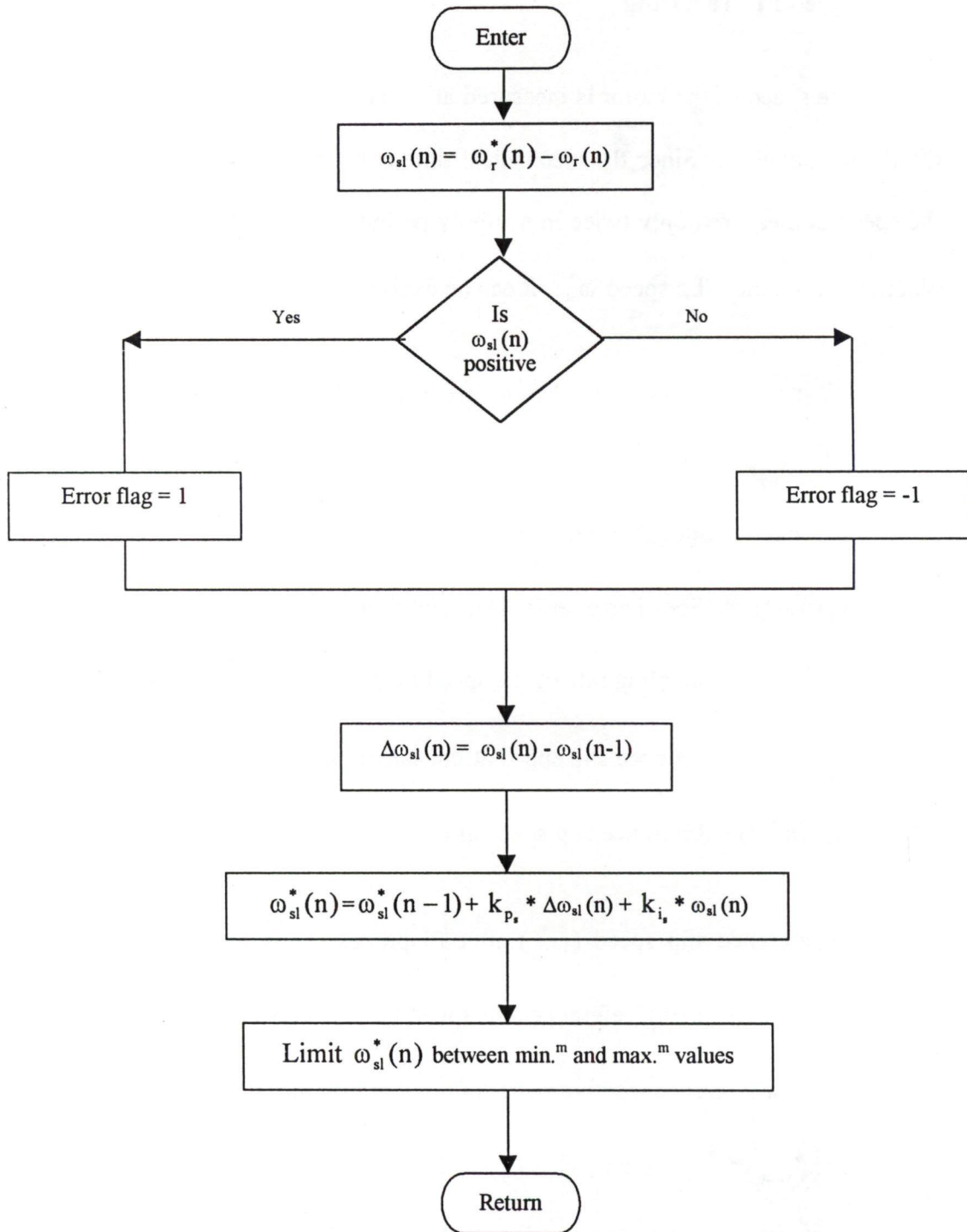
Fig. 5.19. Speed PI Processing
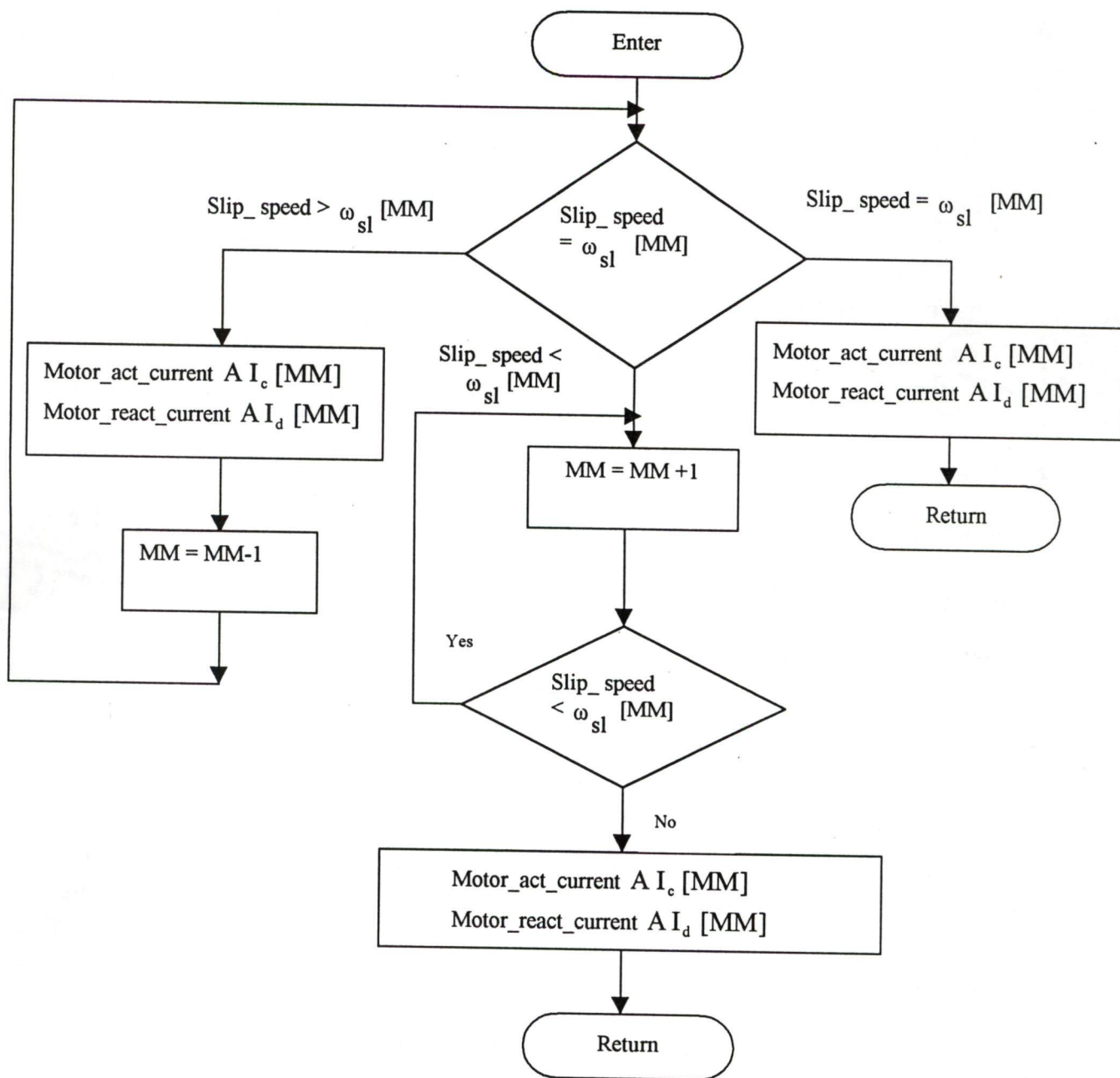
Fig. 5.20. Flow chart for speed regulator

141

A variable MM is initialized in the beginning of the main program, which points to maximum slip speed. This value is modified by comparing the actual speed and reference speed. The stator active and reactive current of the motor is read from the lookup table (I_{act} vs ω_{sl} I_{react} vs ω_{sl}) stored in the memory of the computer.

5.7 TESTING OF THE DEVELOPED DRIVE

Testing of the developed drive is carried out experimentally by recording the current and voltage waveforms of various power and control signals through X- Y recorder. First the testing of front-end converter is carried out. Once it is found to be satisfactory the performance of the load- end converter is carried out in open loop by using the front-end converter as a current source.

5.7.1 Testing of the Front- end Converter.

Testing of the Front- end converter is carried out by recording the line voltage, quantizer signals, zero crossing interrupts, firing signals of the devices, input line currents and voltages, output line currents and voltage at the different duty cycles for low inductance R-L load and high inductance R-L load. Fig 5.21 shows the line voltage waveform of R-Y line, quantizer signal of RY line voltage. As desired zero crossing signals occur at every $60°$ in a cycle, quantizer signal of RY line voltage is synchronized with RY line voltage. Fig 5.22 shows the three quantizer (ϕ_R, ϕ_R, ϕ_B) and zero crossing interrupts signals. The quantizer signals are exactly at a phase difference of $120°$ from each other. Fig 5.23 shows the firing signals for the upper leg device MOSFET (M_1) and the lower leg device (T_4). Fig 5.24 shows the zero crossing signals, firing signals for the upper leg devices, MOSFETs M_1, M_3 and M_5. Twelve numbers of pulses per cycle are
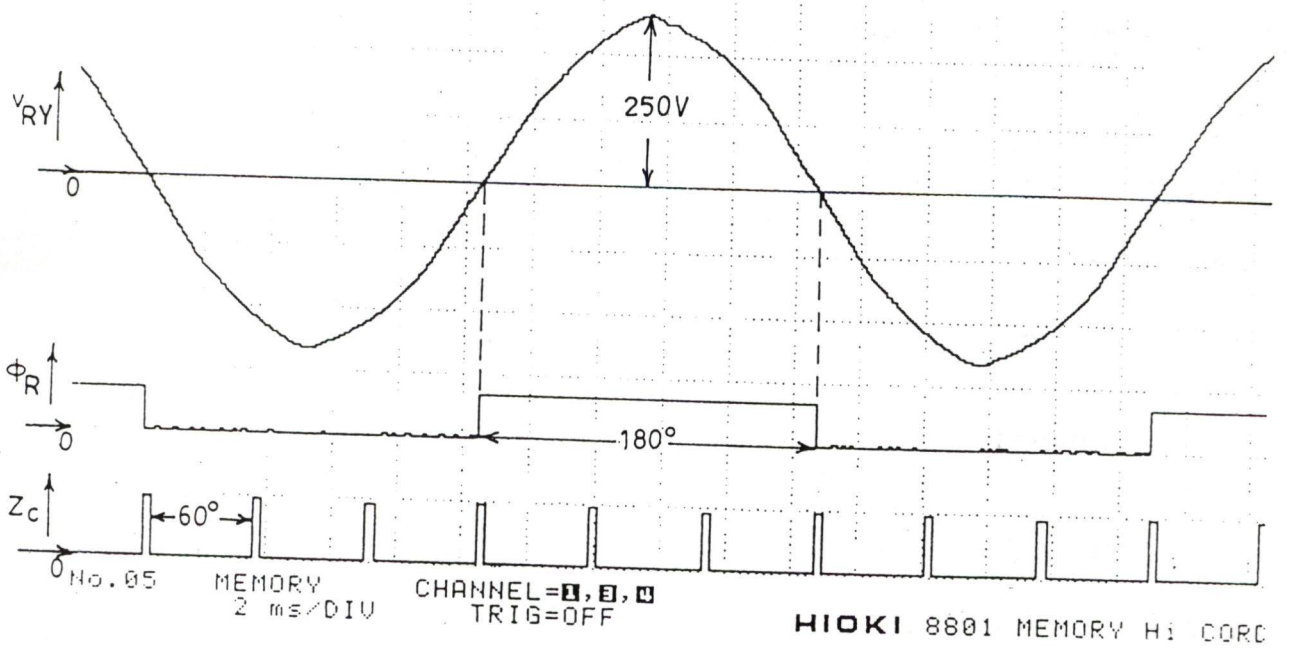
Fig 5.21. Line voltage, quantizers and zero crossing interrupt
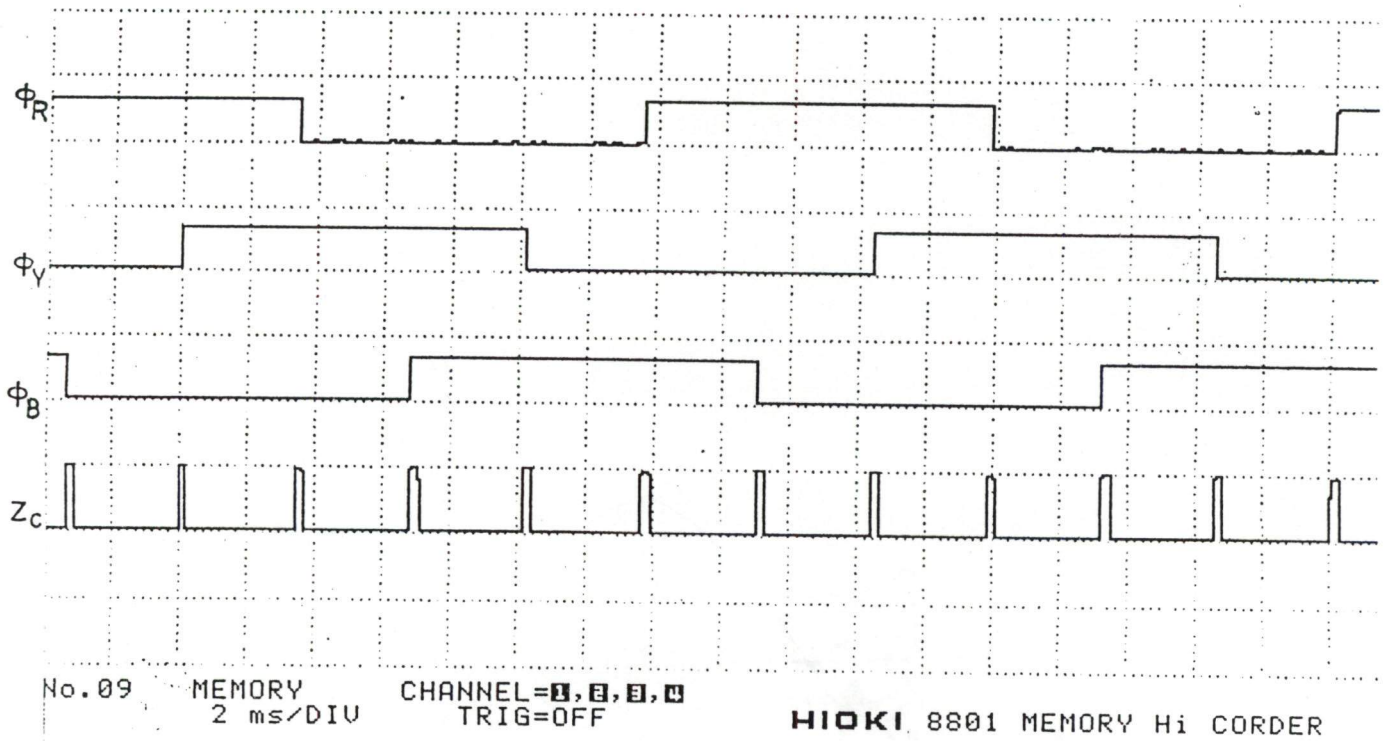
Fig 5.22. Quantizers and zero crossing interrupt
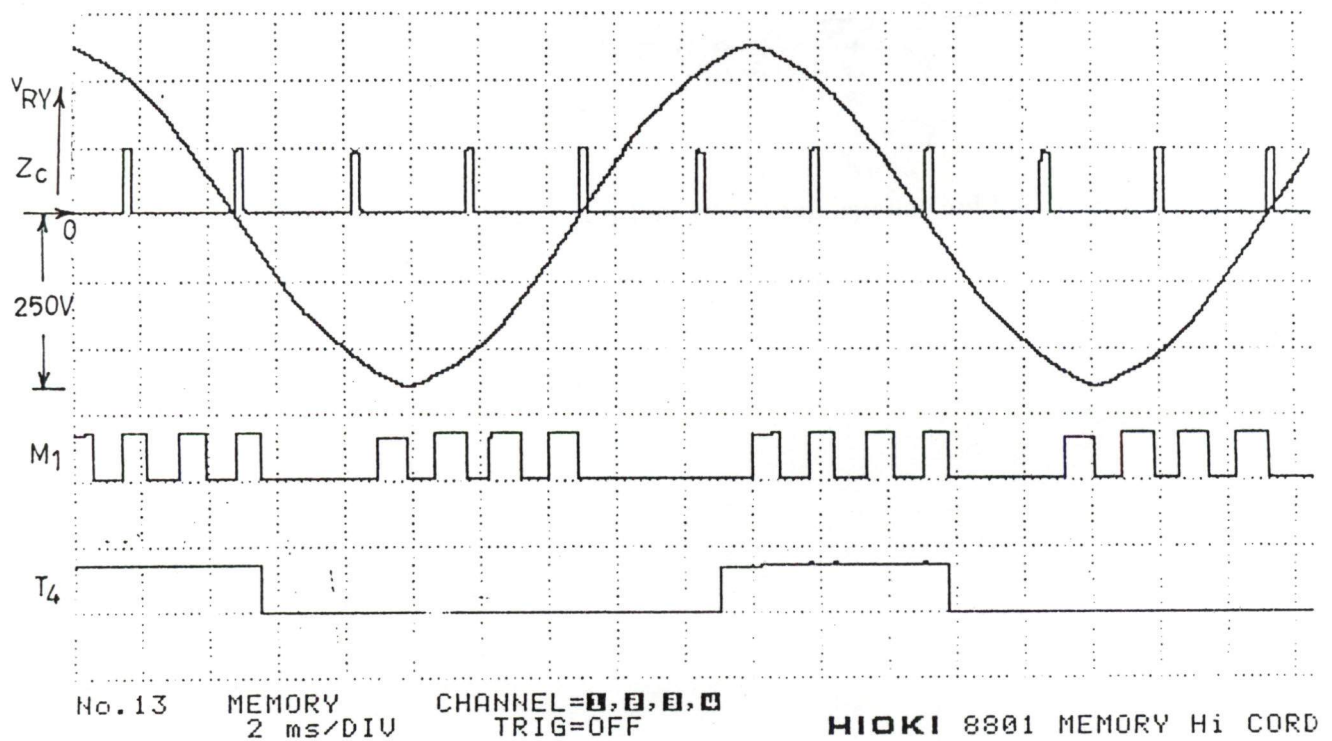
**Fig 5.23. Line voltage, zero crossing interrupt, and firing pulses for
MOSFET and THYRISTOR of PWM converter**
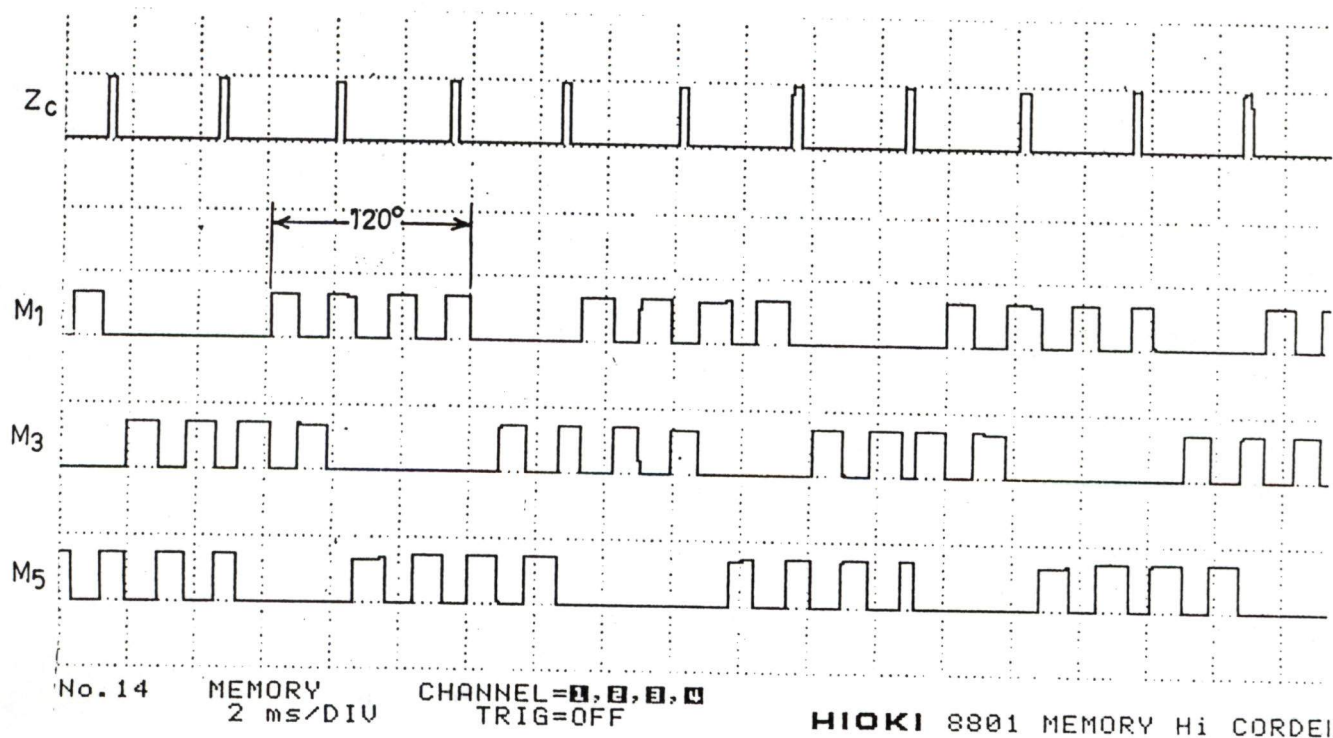
Fig 5.24. Zero crossing interrupt, and firing pulses for MOSFETS of PWM converter
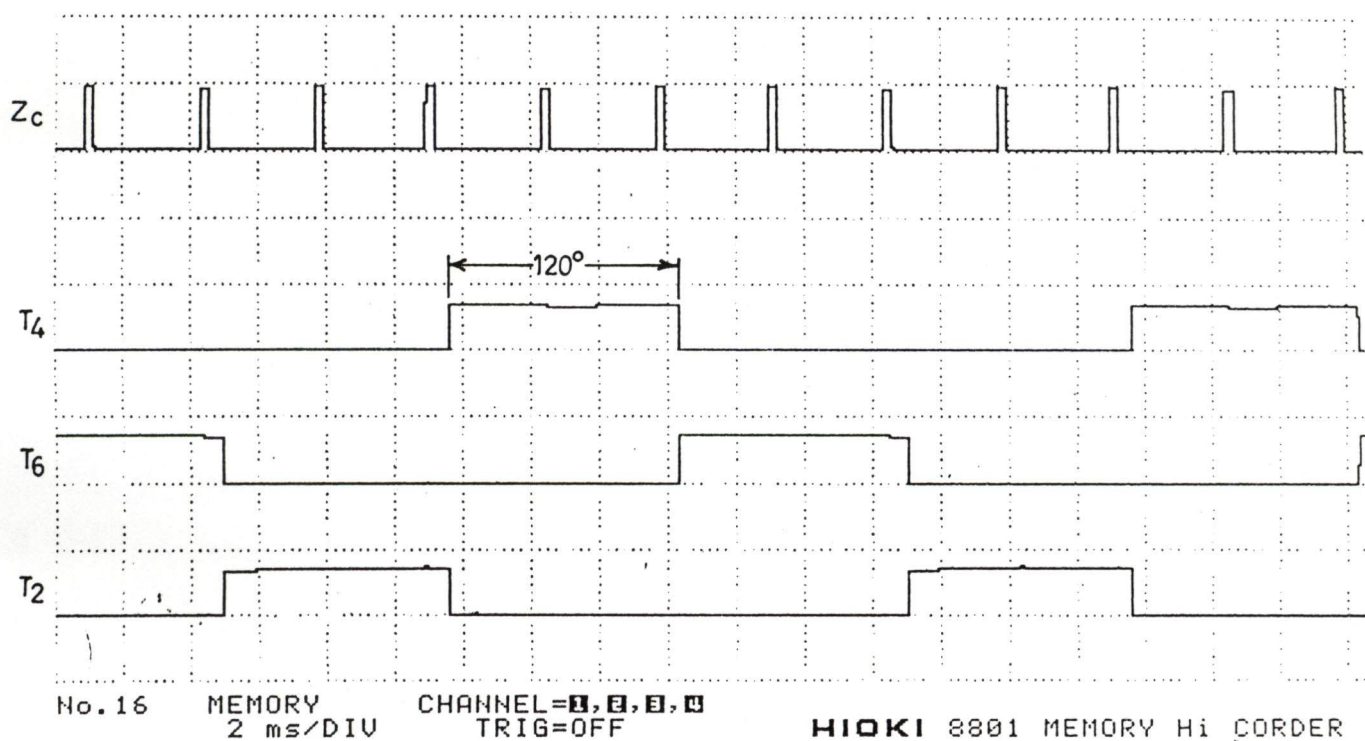
Fig 5.25. Zero crossing interrupt, and firing pulses for THYRISTORS of PWM converter

issued to each MOSFET. Fig 5.25 shows the zero crossing signals, firing signals for the lower leg devices, Thyristors, T_4, T_6 and T_2. Each thyristor is fired for a period of 120°. Firing pulses to all the upper and lower leg switching devices are generated using single chip microcontroller 8031.

Figs 5.26 to 5.28 show the output voltage and current for the (20%, 50%, 80%) duty cycles for R-L load having low value of inductance. The output voltage increases as the duty cycle increases. The output current is discontinuous because of low value of inductance. Figs 5.29 to 5.34 show the output voltage, output current, input voltage, and input current at R-L load having high value of inductance and at a duty cycle of (20%, 50%, and 80%) respectively. At each duty cycles output current is continuous because of high value of inductance. From these Figures it is clear that the fundamental component of the input supply current is approximately in phase with the supply voltage. Thus the fundamental power factor is very close to unity. This is the main feature of the PWM converter that the power factor remains unity irrespective of the load.

5.7.2   Testing of the 3 phase Current Source Inverter in open loop

Testing of the load-end 3 phase current source inverter is carried out by recording the firing pulses at the different operating frequencies, inverter line current and voltage waveforms, motor line current waveforms with capacitor at the machine terminals. The d.c.link current and voltage waveforms are also recorded at the different operating frequencies. All the power and control waveforms are recorded through X- Y recorder. Fig 5.35 shows the firing pulses at an operating frequency of 10 Hz, for two devices of the upper leg and two devices of the lower leg. Fig 5.36 shows the firing pulses at the above operating frequency for all the three devices of the upper legs of the inverter. Firing
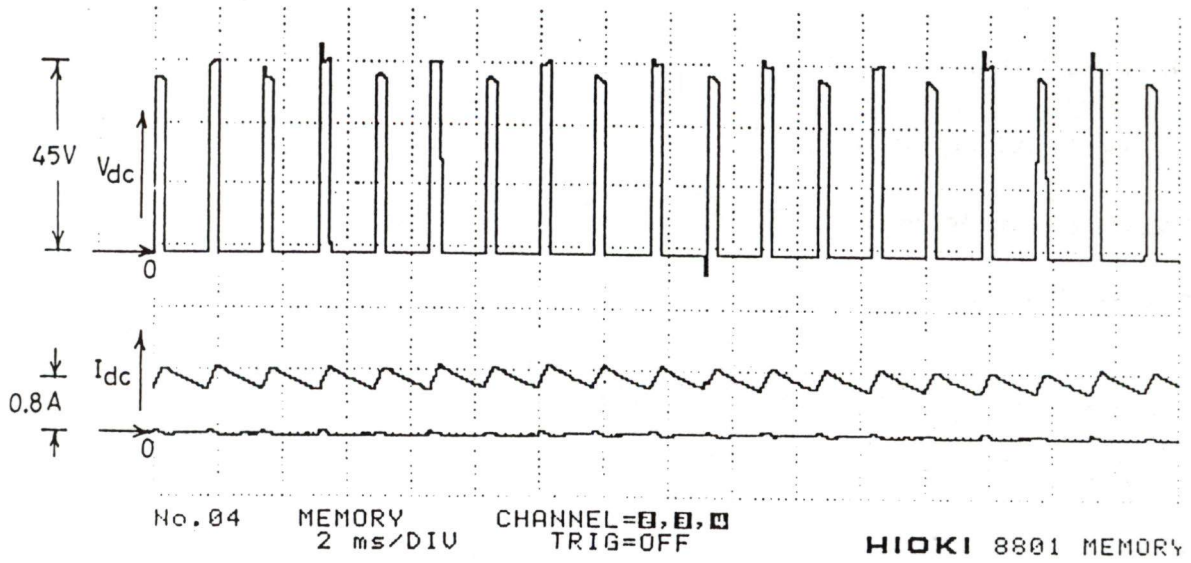
Fig 5.26. Output voltage, output current of PWM converter for R-L load having low inductance (Duty cycle =20%)
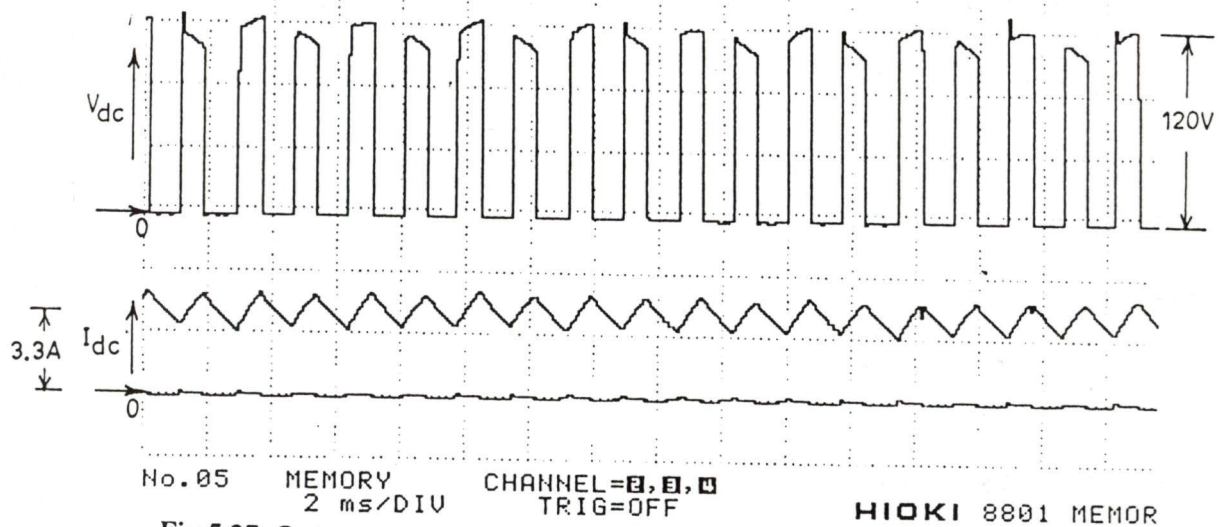
Fig 5.27. Output voltage, output current of PWM converter for R-L load having low inductance (Duty cycle =50%)
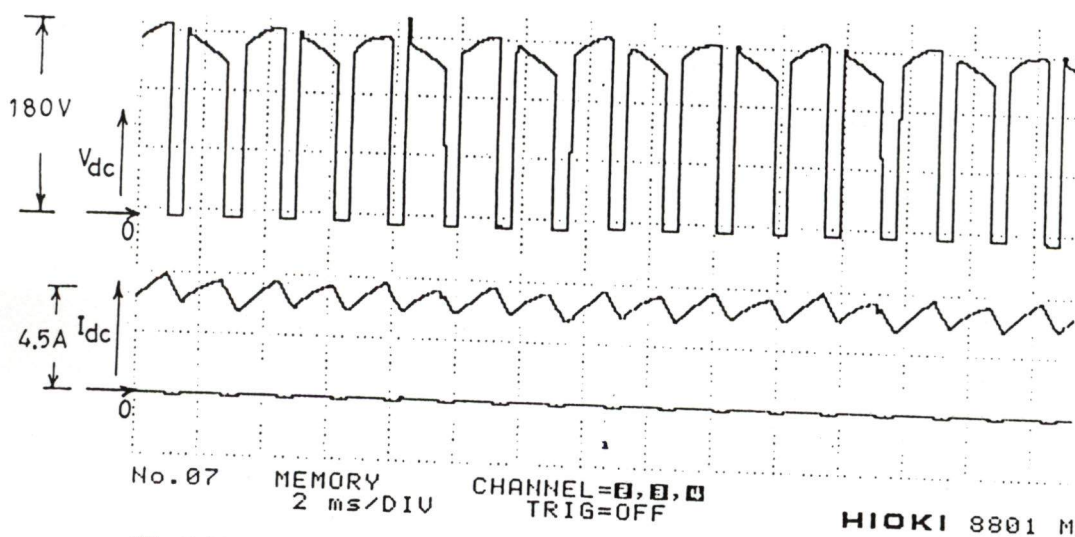
Fig 5.28. Output voltage, output current of PWM converter for R-L load having low inductance (Duty cycle =80%)

147
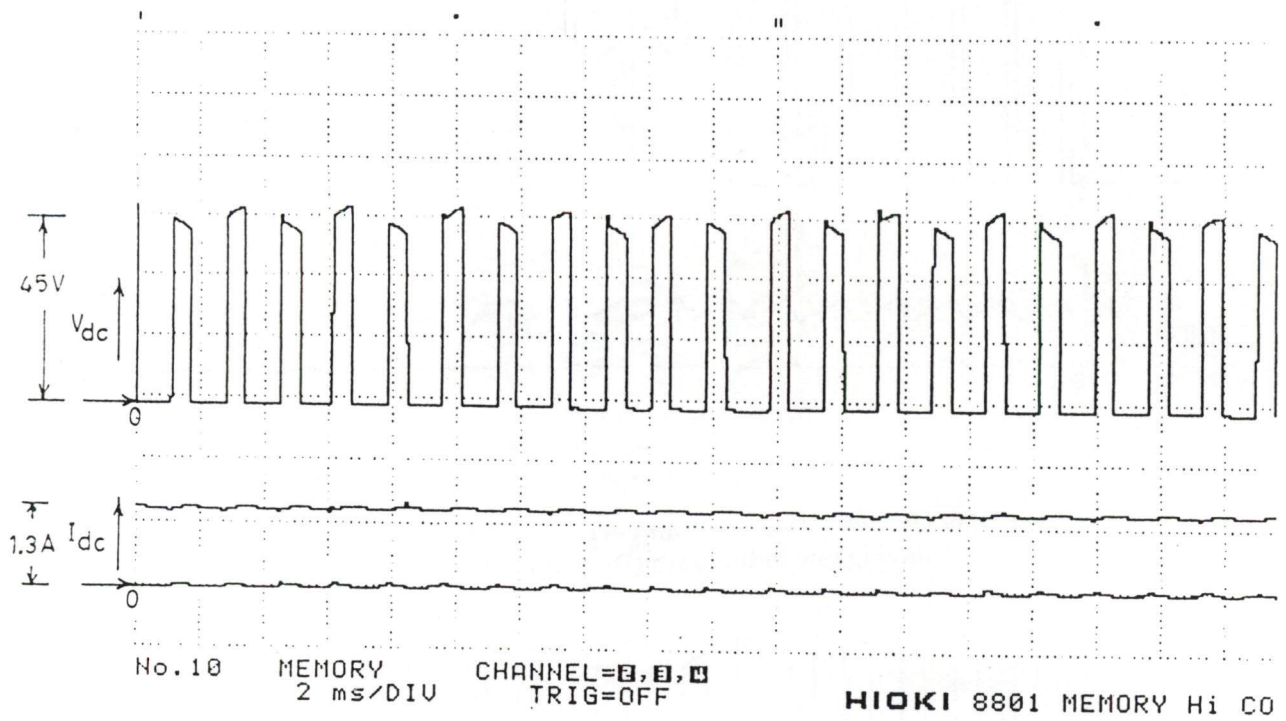
Fig 5.29. Output voltage, output current of PWM converter for R-L load having high inductance (Duty cycle =20%)
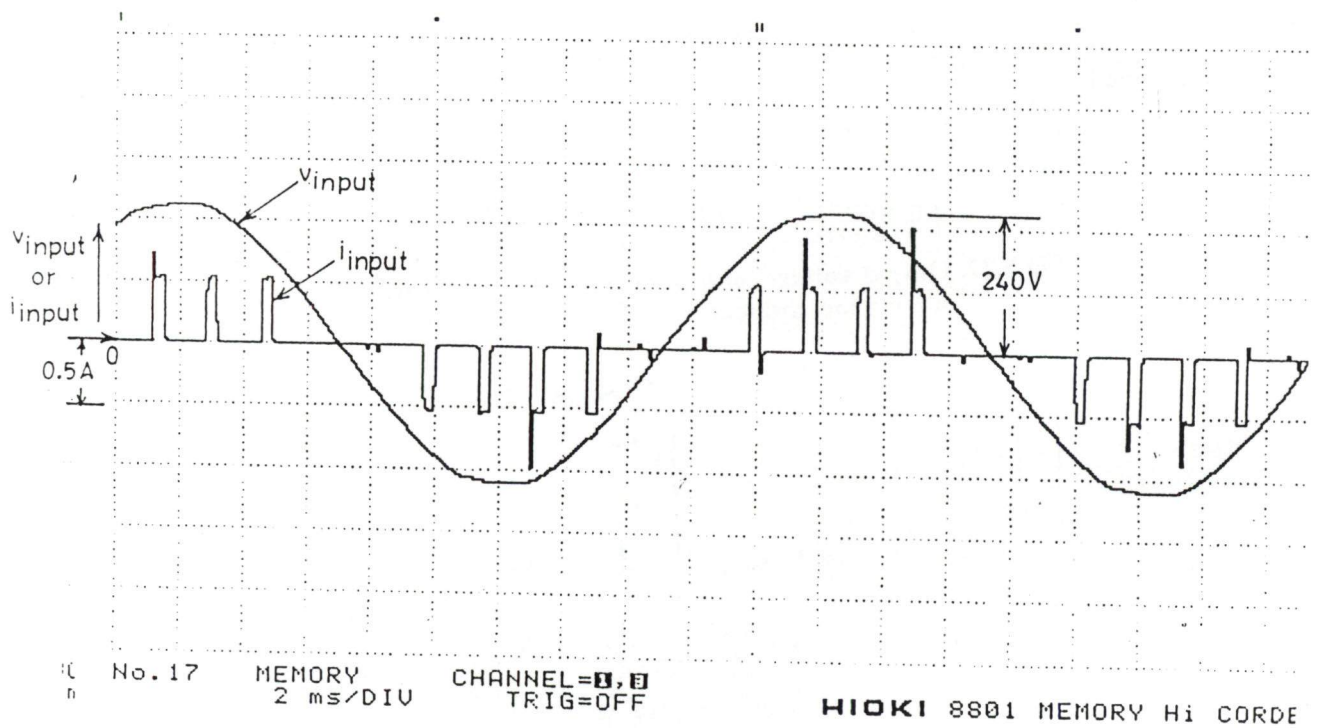
Fig 5.30. Input voltage, input current of PWM converter for R-L load having high inductance (Duty cycle =20%)
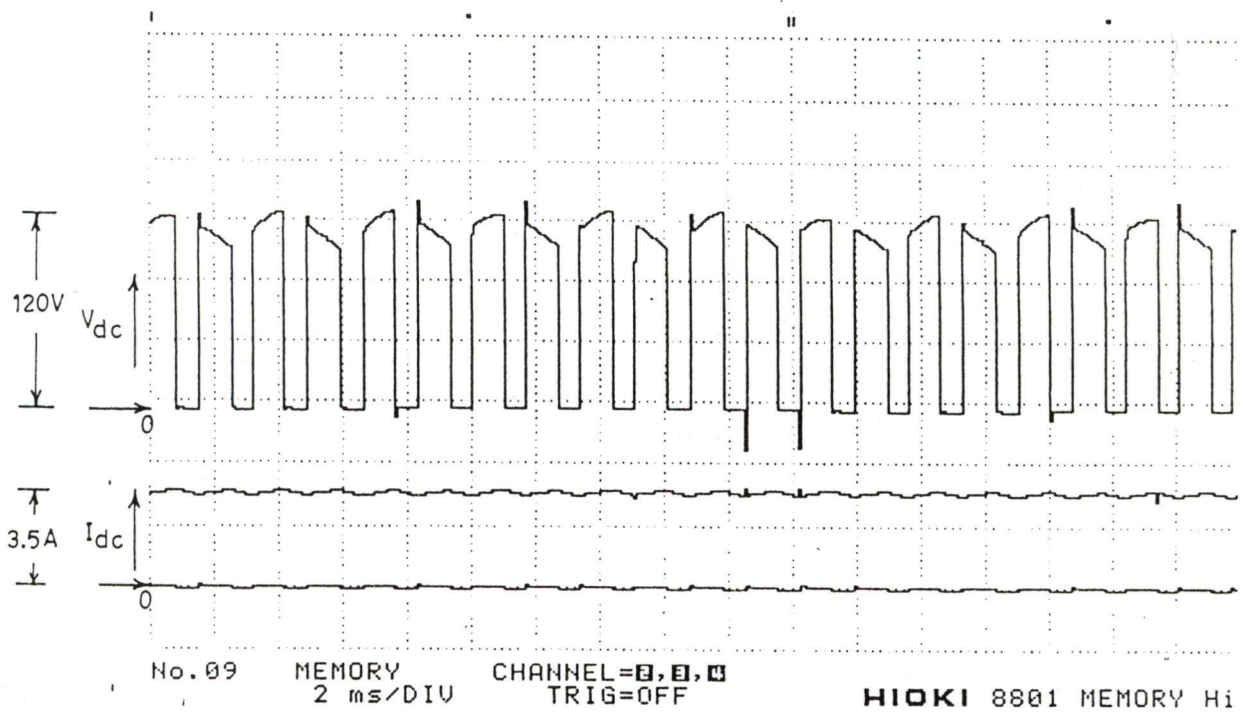
Fig 5.31. Output voltage, output current of PWM converter for R-L load having high inductance (Duty cycle =50%)
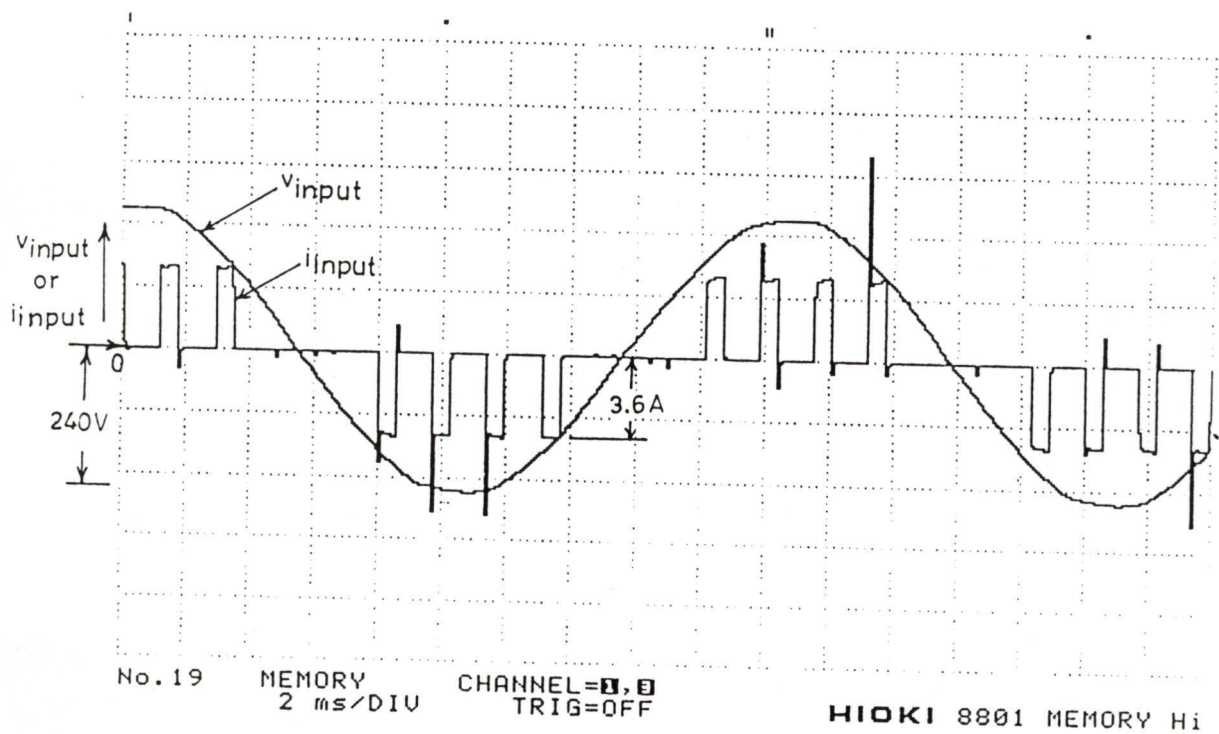
Fig 5.32. Input voltage, input current of PWM converter for R-L load having high inductance (Duty cycle =50%)
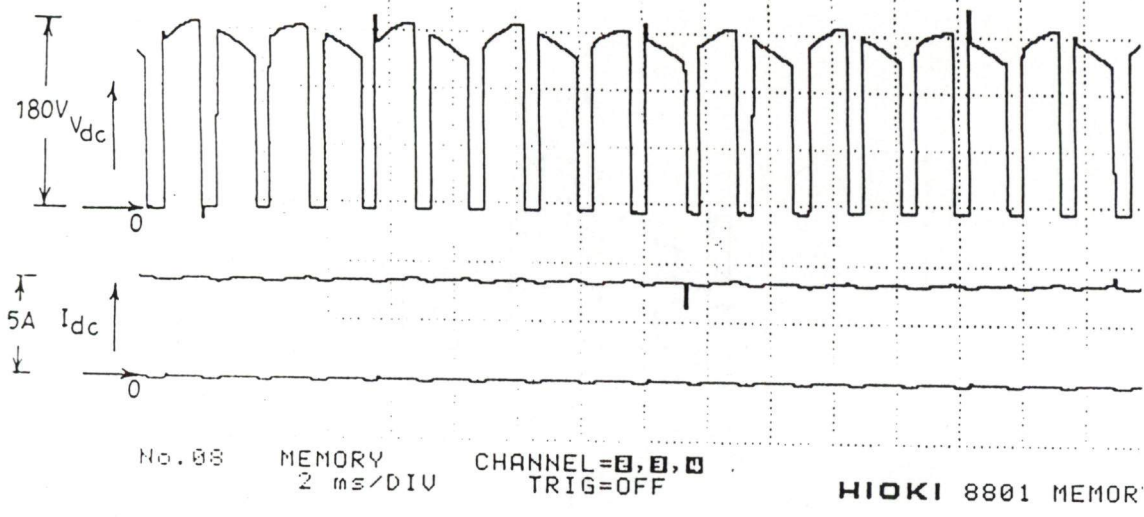
Fig 5.33. Output voltage, output current of PWM converter for R-L load having high inductance (Duty cycle =80%)
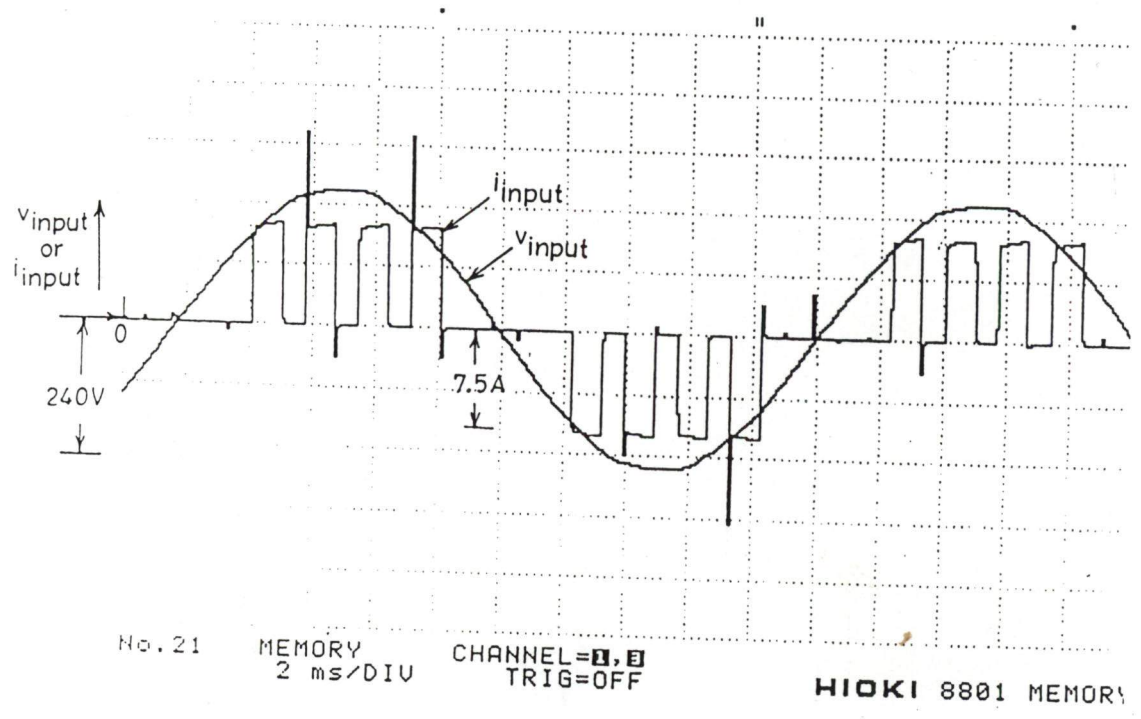
Fig 5.34. Input voltage, input current of PWM converter for R-L load having high inductance (Duty cycle = 80%)

150
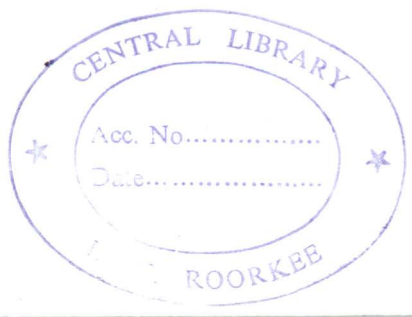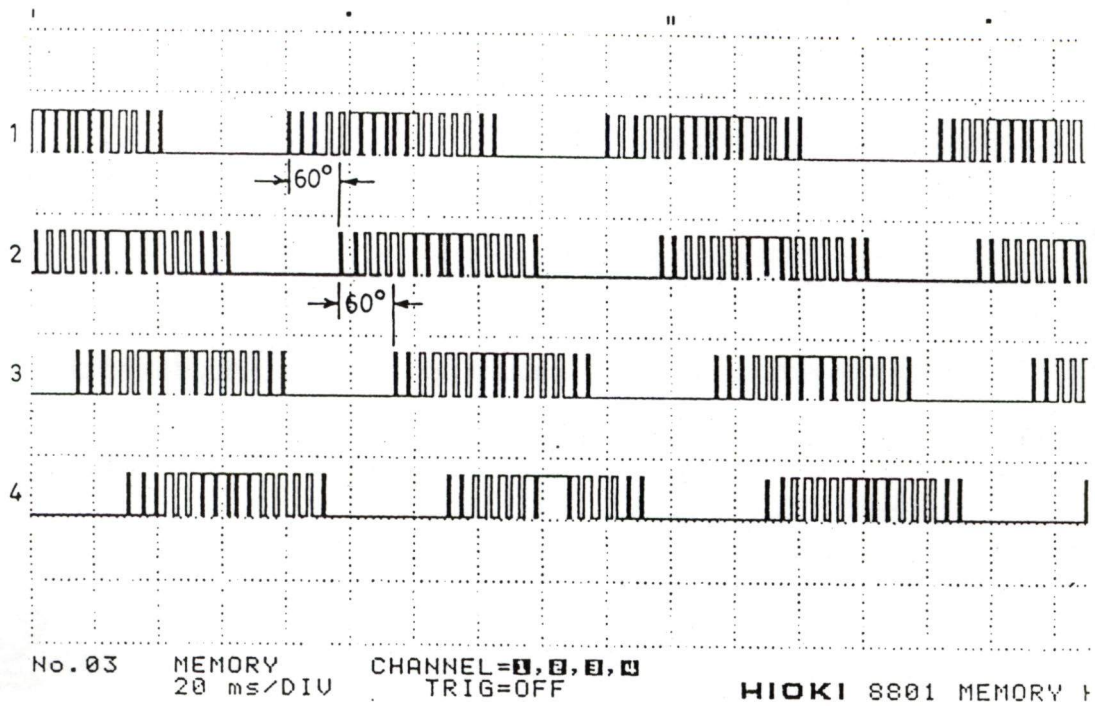
Fig 5.35. Firing pulses of switches of PWM inverter (Frequency = 10 Hz)
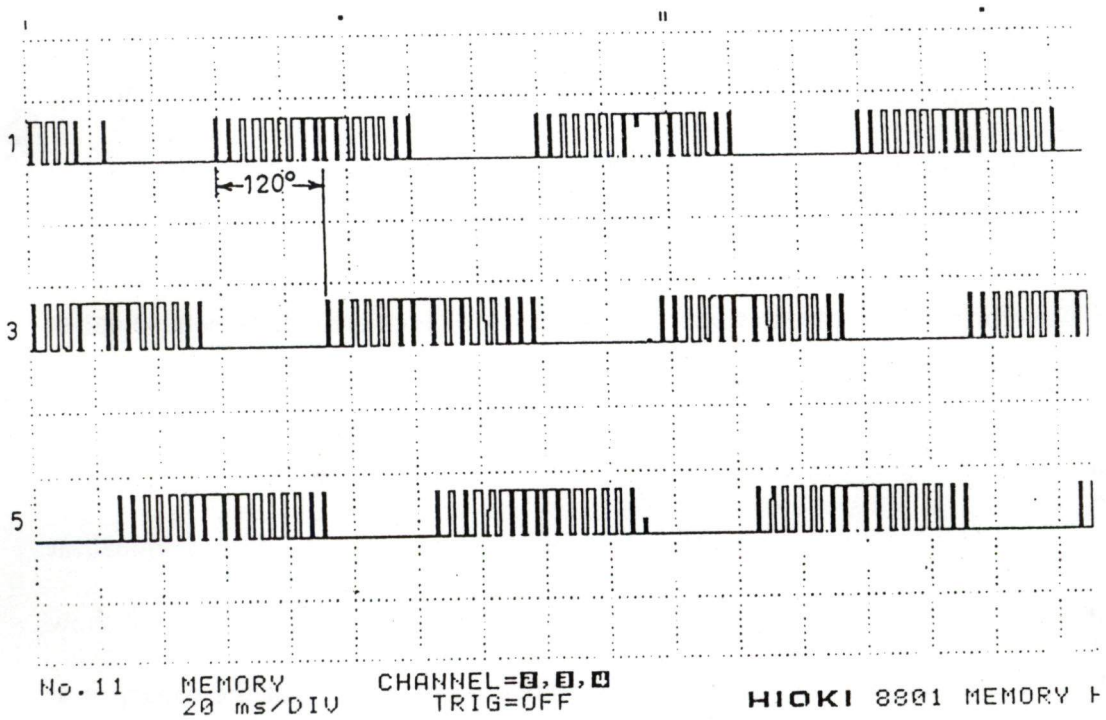
Fig 5.36. Firing pulses of switches of PWM inverter (Frequency = 10 Hz)

151

pulses of any upper two-leg devices are at a phase difference of 120° from each other. The firing pulses of any two successive devices are at a phase difference of 60°. Figs 5.37 shows the firing pulses at the operating frequency of 25 Hz for two devices of the upper leg and two devices of the lower leg. Figs 5.38 shows the firing pulses at the operating frequency of 25 Hz for two devices of the upper leg and two devices of the lower leg. Fig 5.39 shows the firing pulses at the above operating frequency for all the three devices of the upper legs of the inverter. Figs 5.40 shows the firing pulses at the operating frequency of 50 Hz for two devices of the upper leg and two devices of the lower leg. At low (10Hz) and medium (25Hz) operating frequencies the number of firing pulses are more in comparison to the high operating frequency (50Hz), because number of switching commands of the devices are less at high operating frequency than at low and medium operating frequencies. Figs 5.41 to 5.46 show the inverter line currents and the line voltage respectively at an operating frequency of 10Hz, 25 Hz and 50 Hz. From these figures it is observed that the line voltages are almost sinusoidal at each operating frequency, while line currents are not sinusoidal at any of the operating frequency. The motor line current waveforms are recorded with capacitor at the terminals of the motor at the operating frequencies of 10Hz, 25 Hz, 50Hz and shown in the Figs. 5.47 to 5.49. Recorded waveforms show that the line currents and voltages are almost sinusoidal at each operating frequency at the selected value of capacitance at motor terminals. To observe the effect of capacitor on the line currents and the line voltage of the machine, the line currents and voltage are also recorded without capacitor at the machine terminal, at an operating frequency 10 Hz. The recorded waveforms shown in Fig 5.51 and 5.52 show that neither the line currents nor the line voltage are sinusoidal without the capacitor at the machine terminals. Recorded waveforms in Figs 5.52 to 5.54 show the d.c. link
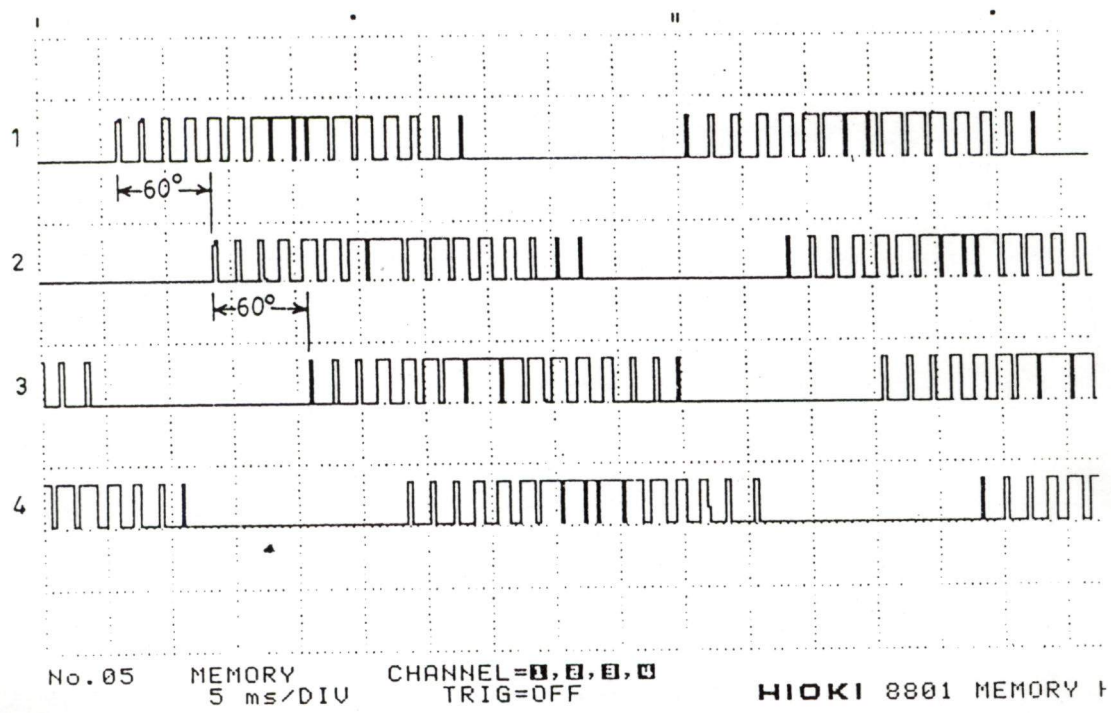
Fig 5.37. Firing pulses of switches of PWM inverter (Frequency = 25 Hz)
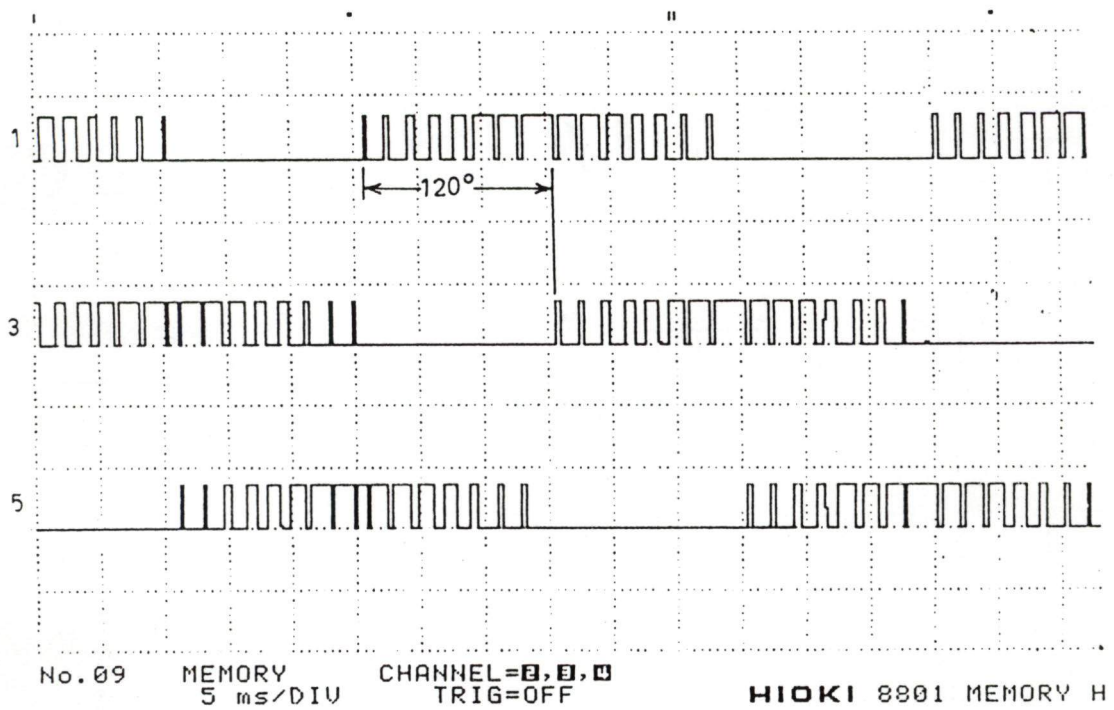
Fig 5.38. Firing pulses of switches of PWM inverter (Frequency = 25 Hz)

153

No.07   MEMORY   CHANNEL=1,2,3,4
         5 ms/DIV   TRIG=OFF
                                        HIOKI 8801 MEMORY H
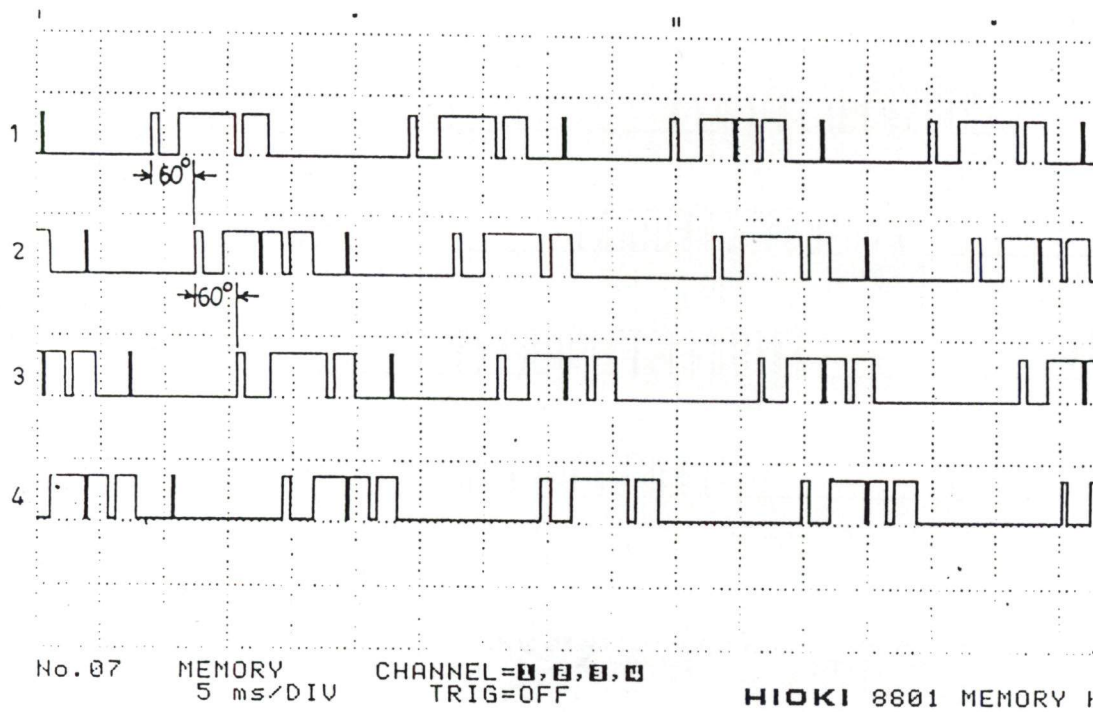
Fig 5.39. Firing pulses of switches of PWM inverter (Frequency = 50 Hz)

No.08   MEMORY   CHANNEL=3,3,4
         5 ms/DIV   TRIG=OFF
                                        HIOKI 8801 MEMORY I
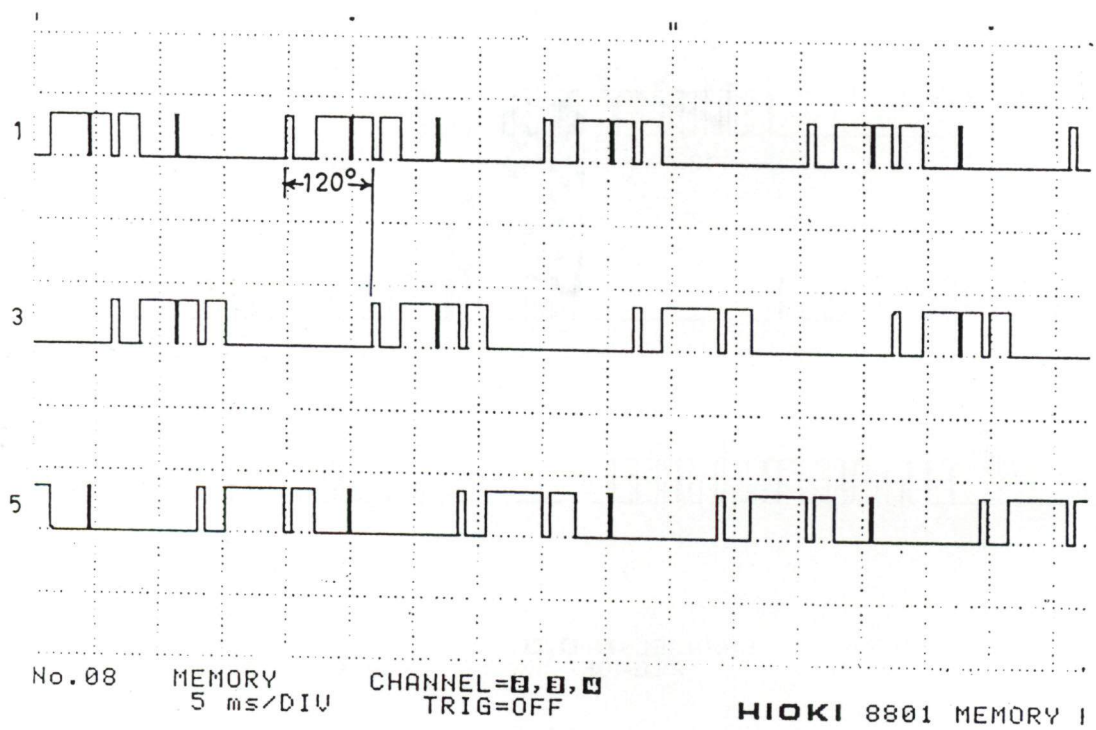
Fig 5.40. Firing pulses of switches of PWM inverter (Frequency = 50 Hz)

154
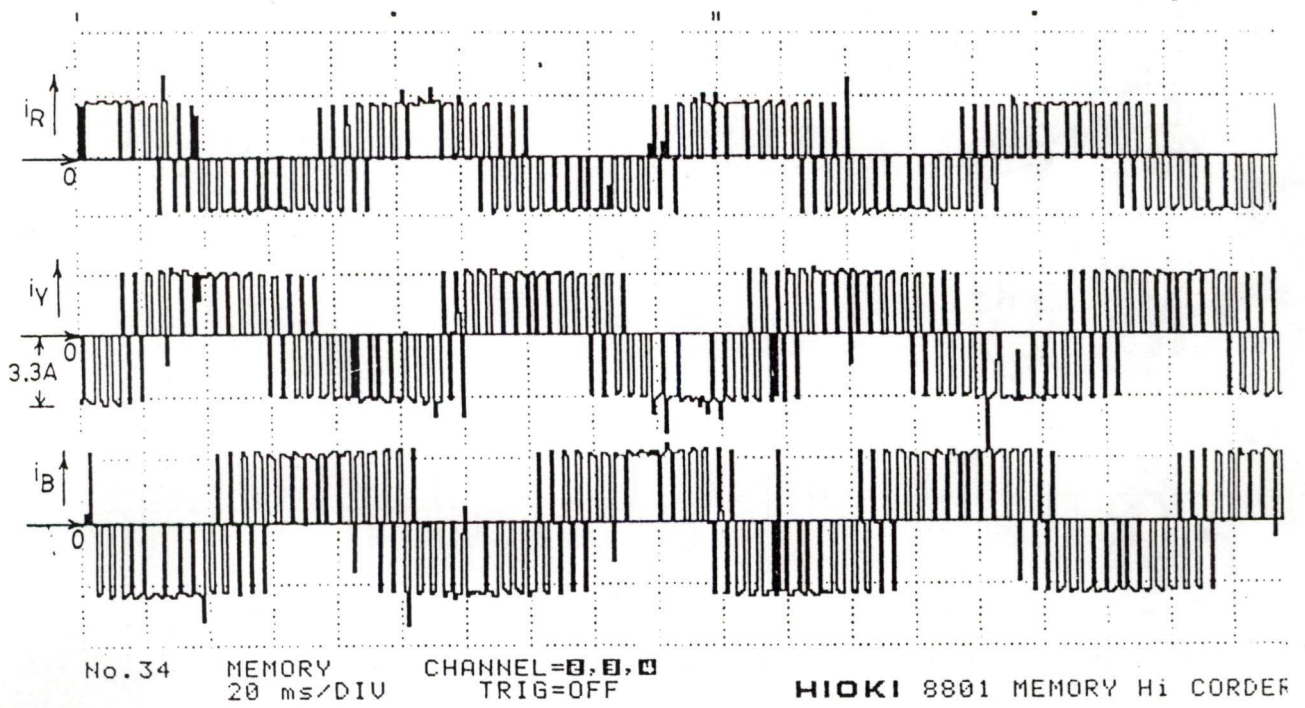
Fig 5.41. Inverter line currents with capacitor at the motor terminals
(Frequency = 10Hz)
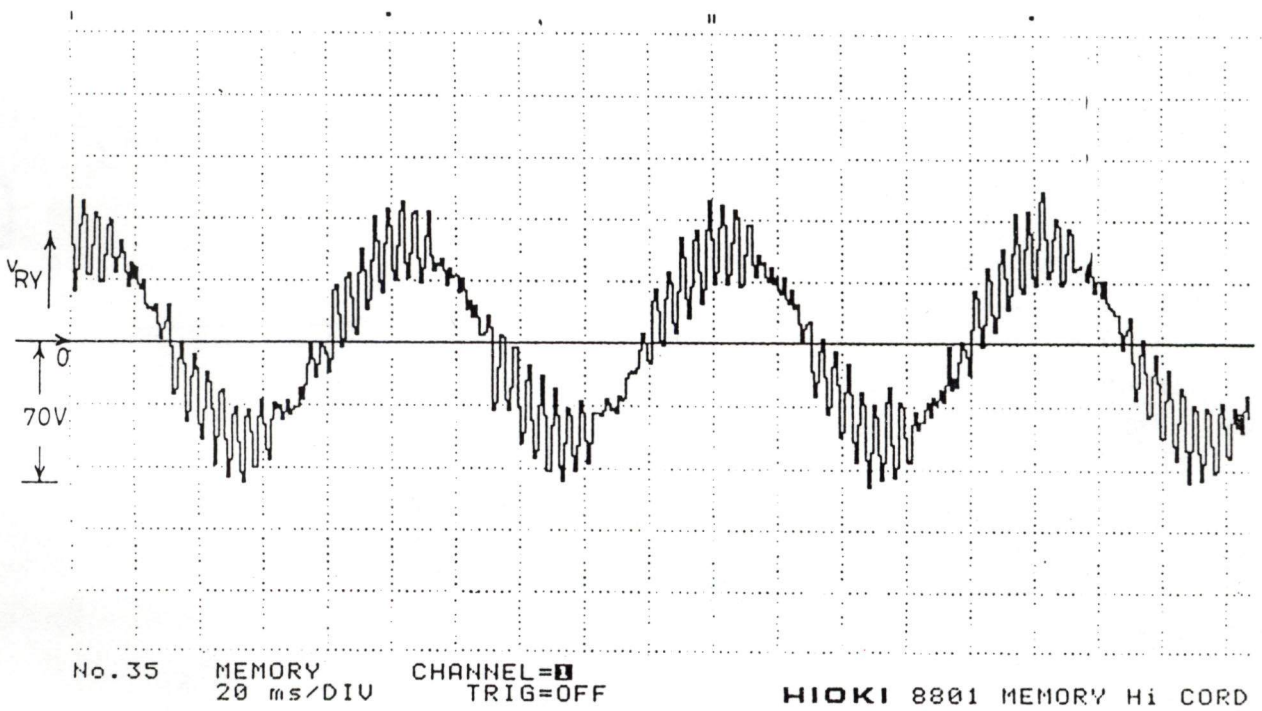
Fig 5.42. Inverter line voltage with capacitor at the motor terminals
(Frequency = 10Hz)
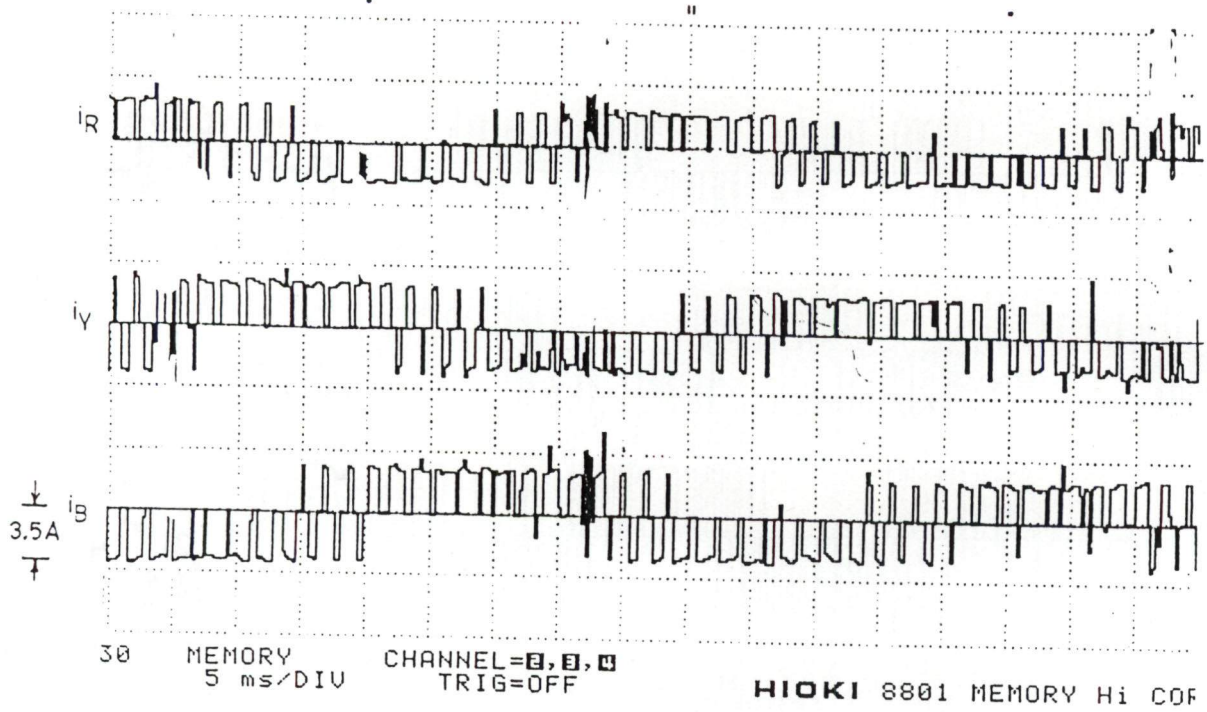
Fig 5.43. Inverter line currents with capacitor at the motor terminals
(Frequency = 25Hz)
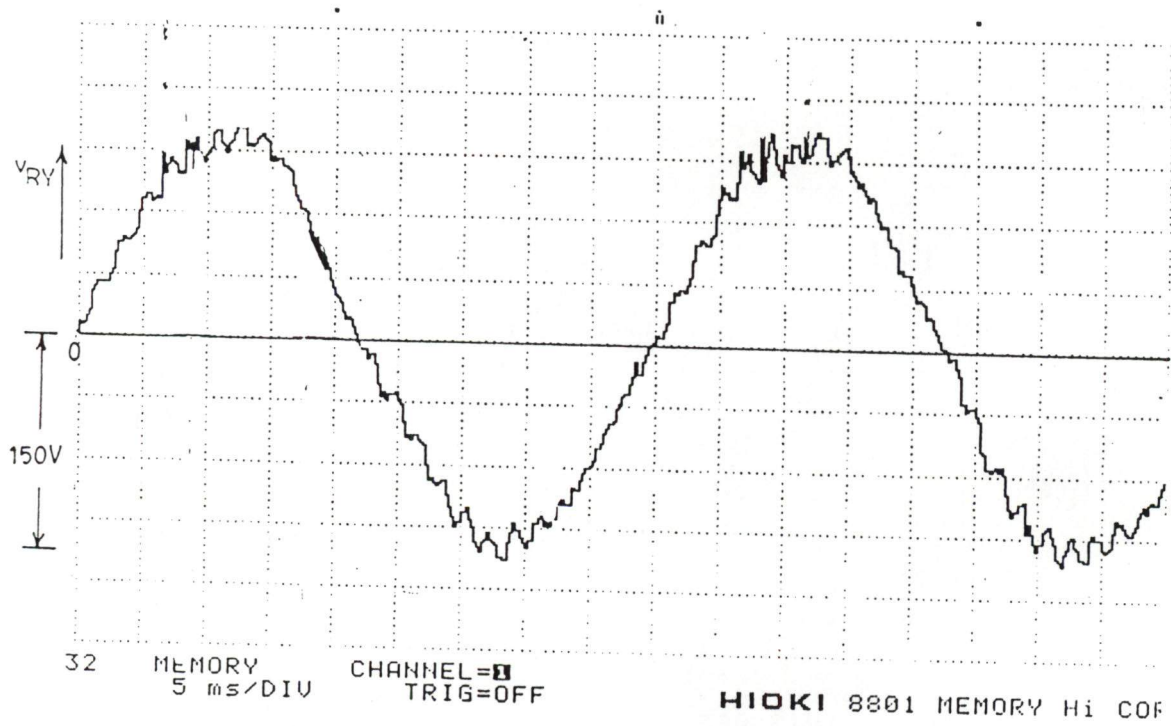
Fig 5.44. Inverter line voltages with capacitor at the motor terminals
(Frequency = 25Hz)
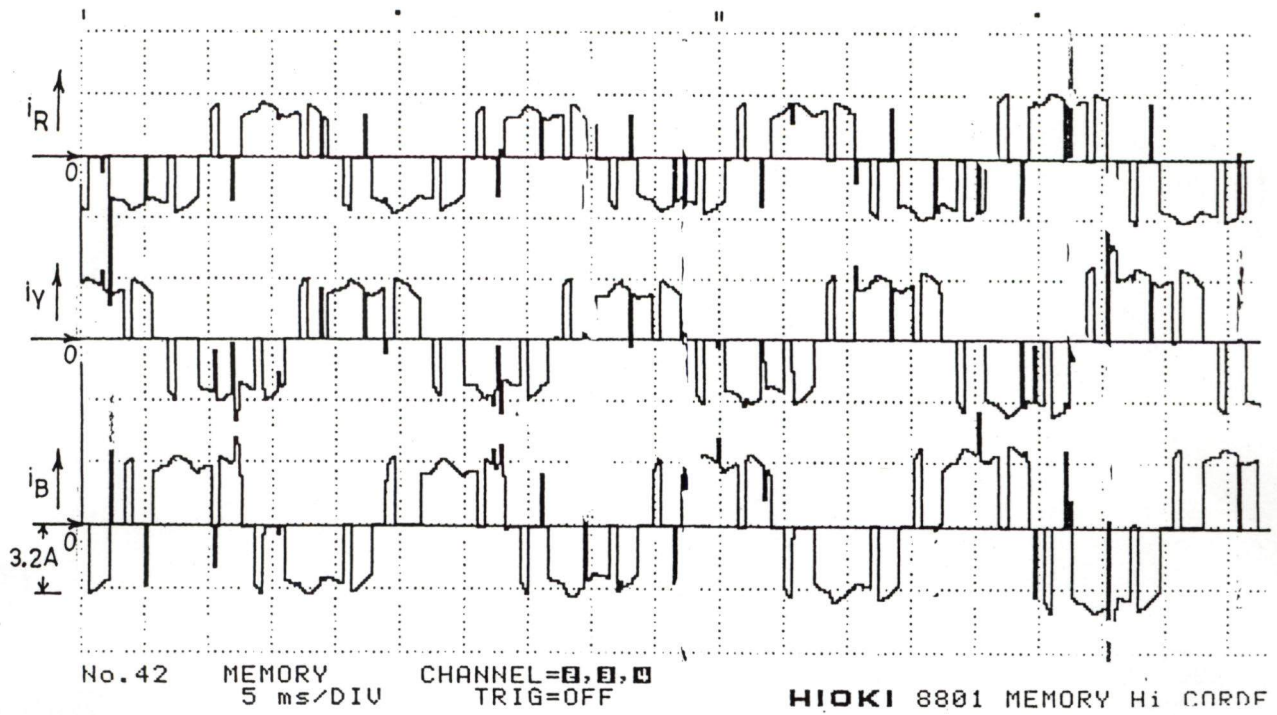
Fig 5.45. Inverter line currents with capacitor at the motor terminals
(Frequency = 50Hz)
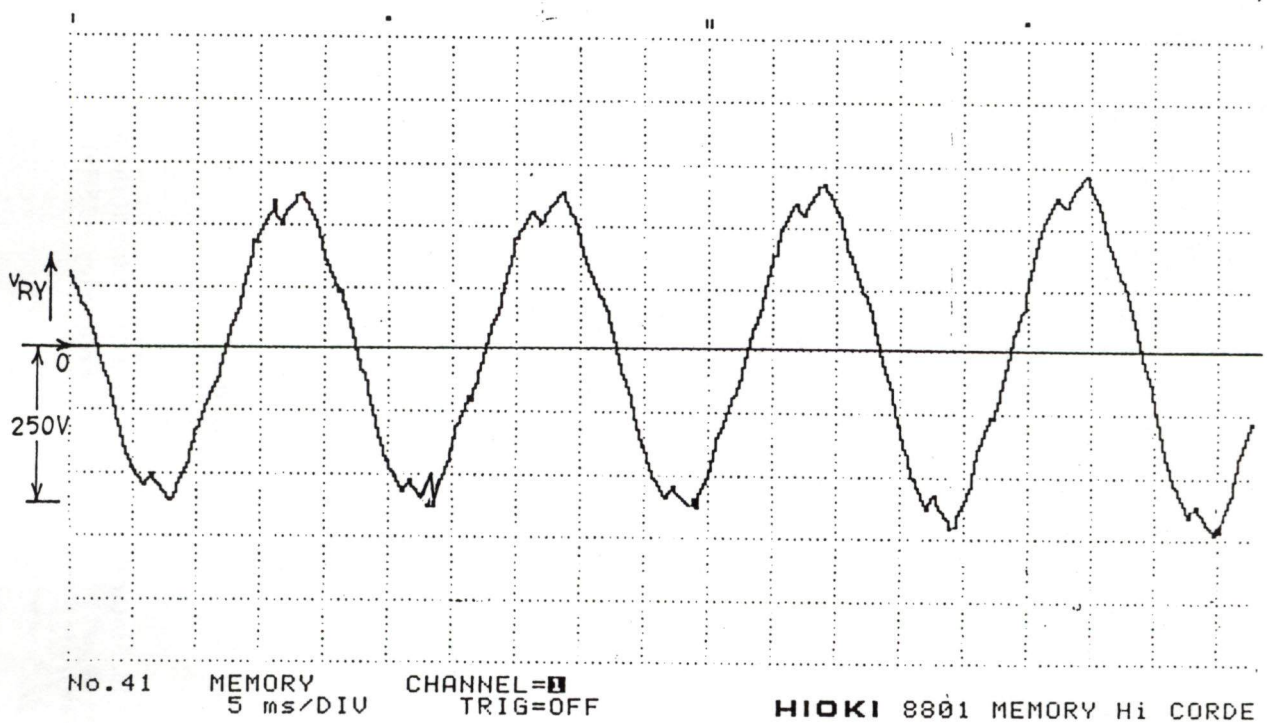
Fig 5.46. Inverter line voltage with capacitor at the motor terminals
(Frequency = 50Hz)
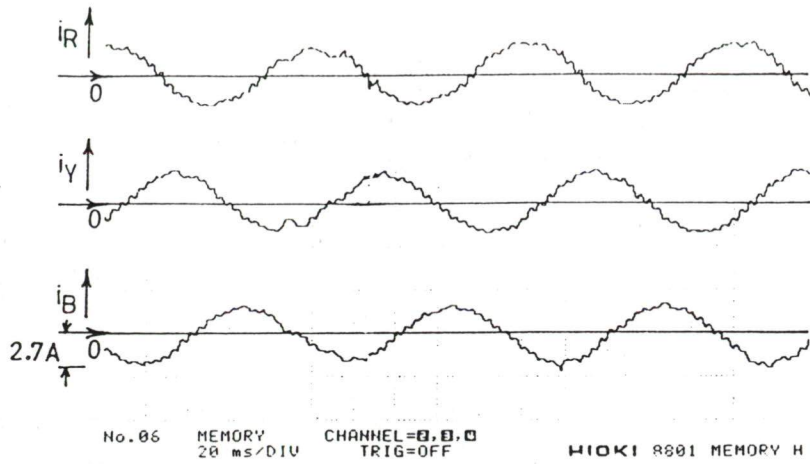
Fig 5.47. Motor line currents with capacitor at the motor terminals
(Frequency = 10 Hz)
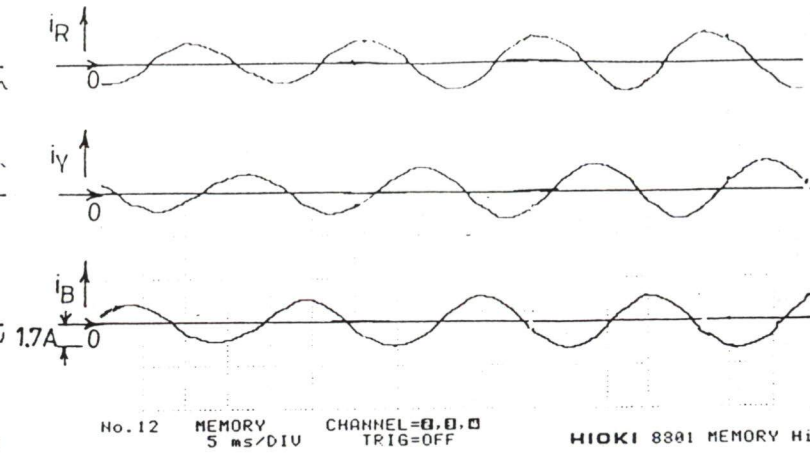
Fig 5.49. Motor line currents with capacitor at the motor terminals
(Frequency = 50Hz)

158
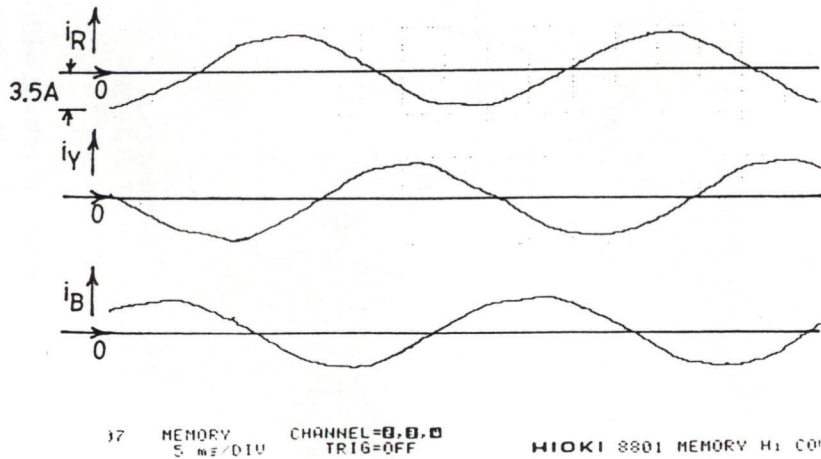
Fig 5.48. Motor line currents with capacitor at the motor terminals
(Frequency = 25Hz)
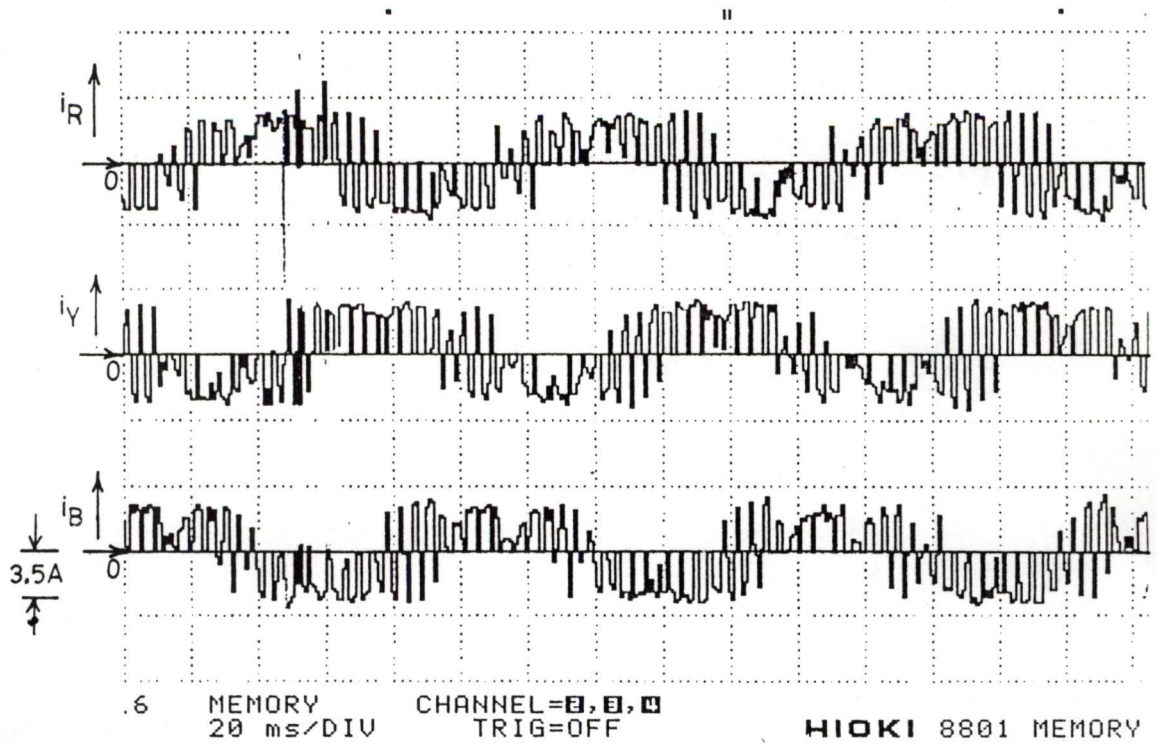
Fig 5.50. Motor line currents without capacitor at the motor terminals
(Frequency = 10 Hz)
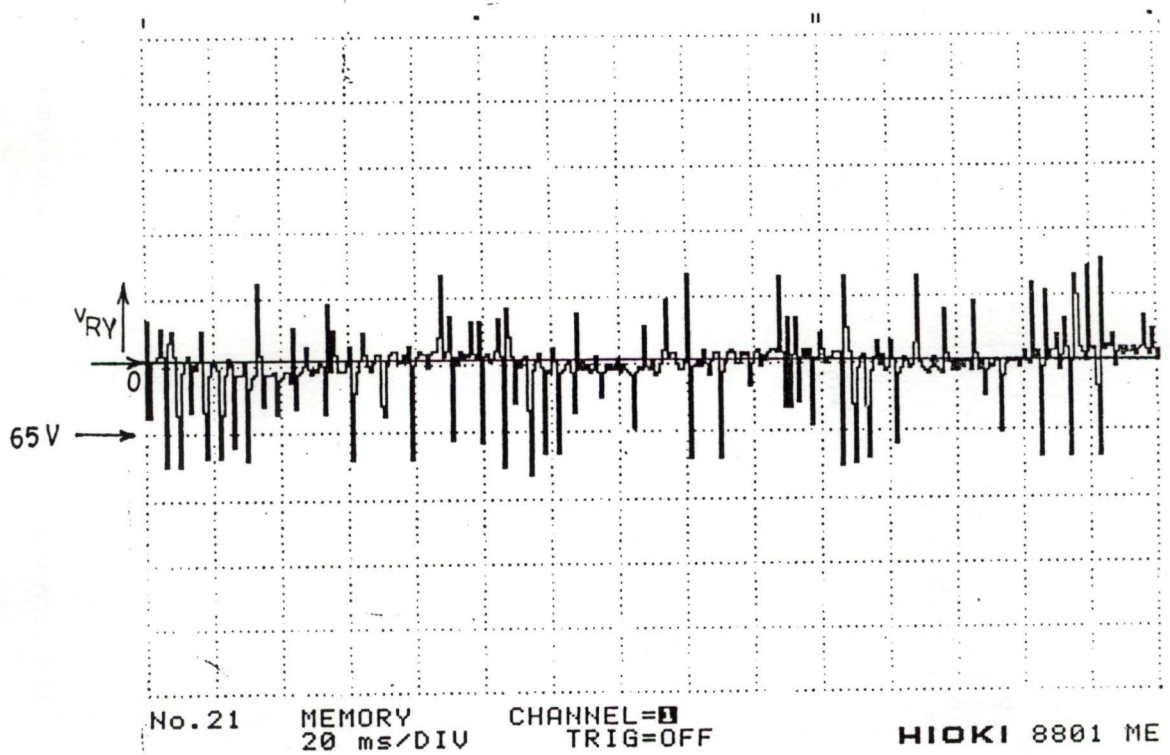
Fig 5.51. Inverter line voltage without capacitor at the motor terminals
(Frequency = 10 Hz)
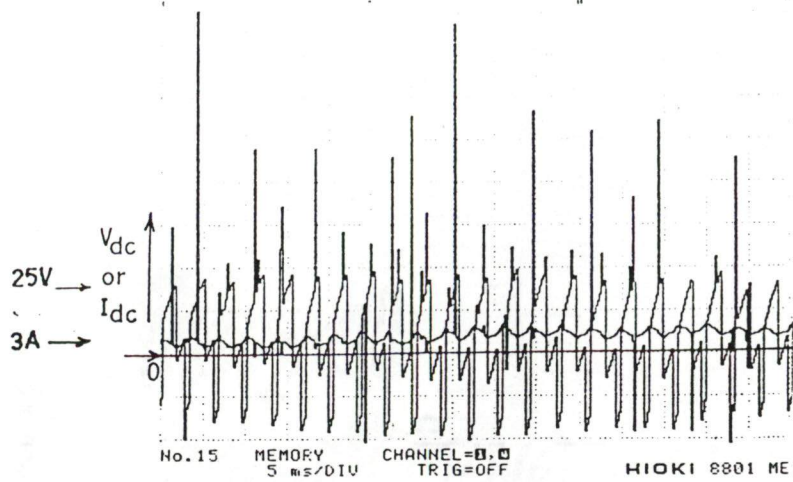
Fig 5.52. D.C. Link current and voltage with capacitor at the motor terminals
(Frequency = 10 Hz)
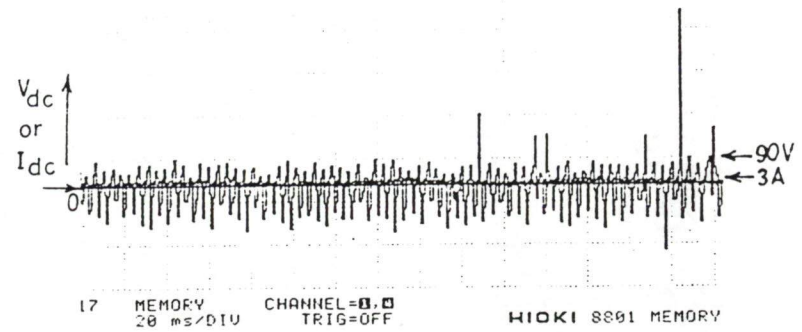
Fig 5.54. D.C. Link current and voltage with capacitor at the motor terminals
(Frequency = 50Hz)
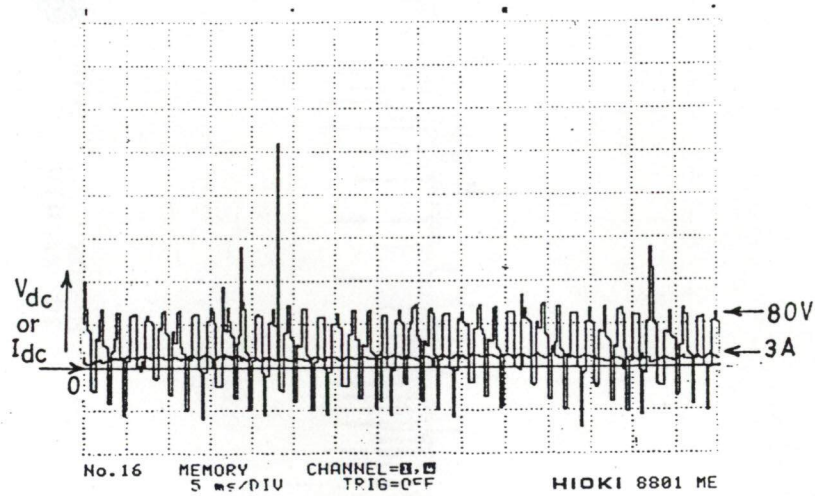
Fig 5.53. D.C. Link current and voltage with capacitor at the motor terminals
(Frequency = 25 Hz)

voltage and the d.c. link currents at the operating frequencies 10Hz, 25 Hz and 50Hz respectively with the capacitor across the machine terminals.

5.8 CONCLUSION

The PWM techniques used in the front-end converter and motor-end inverter are described. The flowcharts for the open and closed loop operation of converter and inverter are discussed in detail along with interrupt service subroutine. Other subroutines such as: speed measurement, speed PI processing, current PI processing, firing pulse generation of front- end converter using microcontroller and its serial communication through PC are also discussed.

For smooth operation of the induction motor, it is fed from the PWM current source inverter, which gives the better quality of the input line currents to the induction motor. The number of firing pulses issued to the switching devices are more at low and medium value of the operating frequencies for PWM operation of the inverter, while it is less at high value of the operating frequencies. This is due to the consideration of the switching frequency limitation of the devices.

The speed of the induction motor is controlled by controlling the operating frequency of the current source inverter, by maintaining the rated air gap flux through the slip regulator, stored in the memory of the computer. The operating frequency of the inverter is obtained by adding the reference slip speed with the actual speed of the motor .

The testing of the PWM rectifier alone and PWM rectifier as a current source and the inverter in the open loop has been done experimentally. The various power and control signals are recorded. The experimentally recorded waveforms show that the input

power factor of the front-end converter is almost unity at any value of the duty cycle. The input line currents and voltages of the motor are near sinusoidal at each value of the operating frequency. The recorded waveforms show that the developed hardware is working satisfactorily.

DESIGN OF CONTROLLER PARAMETERS

6.1   INTRODUCTION

The performance of a closed loop drive depends upon its controller parameters. The present drive, modified self-commutating CSI-fed induction motor drive consists of speed and current controllers for smooth speed control. Slip regulator is also incorporated in the drive to operate the induction machine at rated value of flux under variable frequency conditions. The transient and dynamic stability of the drive is analyzed for variation in controller parameters.

In the present chapter, a parametric plane synthesis method (D- partition technique) is used for finding the stable region in a plane of controller parameters for a drive modeled as a continuous data system. Both the parameters of speed and current controls obtained by this method decide the steady state and transient response of the drive.

For the determination of regulator parameters by the D-partition technique, the mathematical model of the drive developed in chapter 2 is considered. The small perturbations about steady state operating points are considered to develop the characteristic equation of speed and current loop. The controllers are designed on the basis of system relative stability and response of the drive. The probable stable region obtained is checked by frequency-scanning technique to confirm stability. Using controller parameters obtained by this method, the speed and current response of the drive

is determined for step variation in reference speed and current, and best set of parameters are selected.

6.2 TECHNIQUE FOR DESIGN OF CONTROLLER PARAMETERS

With small perturbation in machine operating variables about a steady state operating point, a linear relation in drive variables could be obtained. The steady state operating point is rated operating condition as shown below:

$$V_{s(L-L)} = 400V, i_s = 3.27A, t_e = 3.93N\_m, I_{dc} = 5.5A, \omega_e = 314 \, rad/sec, I_c = 6.0A$$

This approach is called the small displacement theory. The stability of the system with the help of D- partition technique [121,122] can be obtained with the help of this linear model of the drive. The controllers of present drive are designed by neglecting the effect of harmonics, i.e., the effect of only fundamental components are considered for applying small displacement. The mathematical equations of machine stator voltages in ($q^e - d^e$) reference frame are given below.

$$v_{ds}^e = -\omega_e l_{ss} i_{qs}^e + (r_s + pl_{ss}) i_{ds}^e - \omega_e \, lm \, i_{qr}^e + pl_m i_{dr}^e \qquad (6.1)$$

$$v_{qs}^e = (r_s + pl_{ss}) i_{qs}^e + \omega_e l_{ss} i_{ds}^e + pl_m i_{qr}^e + \omega_e l_m i_{dr}^e \qquad (6.2)$$

Combining both these equations, the machine stator phase voltage v_s^- can be expressed as shown below:

$$v_s^- = v_{ds}^e + j \, v_{qs}^e \qquad (6.3)$$

Hence,

$$v_s^- = z_s(p) i_s^e + j\omega_e l_{ss} i_s^- + l_m (p + j\omega_e) i_r^- \qquad (6.4)$$

where,

164

$$z_s(p) = r_s + pl_{ss}$$

Perturbing both sides of the equation (6.4) the following equation is obtained

$$\Delta v_s^- = [\, z_s(p) + j\omega_e\, l_{ss}\,]\, \Delta i_s^- + l_m\,(p + j\omega_e)\,\Delta i_r^- + j\psi_s^-\, \Delta\omega_e \tag{6.5}$$

where,

$$\Psi_s^- = l_{ss}\, i_s^- + l_m\, i_r^-$$

Considering the rotor voltage in $(q^e - d^e)$ reference frame, as described in chapter 2,

$$v_{qr}^e = p\, l_m\, i_{qs}^e + \omega_{sl}\, l_m\, i_{ds}^e + (r_r + pl_{rr})\, i_{qr}^e + \omega_{sl}\, l_r\, i_{dr}^e \tag{6.6}$$

$$v_{dr}^e = -\omega_{sl}\, l_m\, i_{qs}^e + p\, l_m\, i_{ds}^e - \omega_{sl}\, l_{rr}\, i_{qr}^e + (r_r + pl_{rr})\, i_{dr}^e \tag{6.7}$$

Combining above equations, the rotor phase voltage is obtained as given below:

$$v_r^- = z_r(p)\, i_r^- + l_m\,(p + j\omega_{sl})\, i_s^- + j\omega_{sl}\, l_{rr}\, i_r^- \tag{6.8}$$

where,

$$v_r^- = 0$$

Perturbing equation (6.8), following perturbed rotor voltage equation is obtained

$$\Delta v_r^- = [\, z_r(p) + j\omega_{sl}\, l_{rr}\,]\, \Delta i_r^- + l_m\,(p + j\omega_{sl})\,\Delta i_s^- + j\psi_r^-\, \Delta\omega_{sl} = 0 \tag{6.9}$$

where, $\quad z_r(p) = r_r + pl_{rr}$

$$\Psi_r^- = l_{rr}\, i_r^- + l_m\, i_s^-$$

From equation (6.9), the value of Δi_r^- is obtained as

$$\Delta i_r^- = -\frac{[\, l_m \,(\, p + j\,\omega_{sl}\,)\,\Delta i_s^- + j\,\psi_r^-\,\Delta\omega_{sl}\,]}{(\, z_r\,(p) + j\,\omega_{sl}\,l_{rr}\,)} \tag{6.10}$$

Separating the real and imaginary part of Δi_r^-

$$\Delta i_r^- = -\, l_m\,[\, F_3\,(p) + j\,F_4\,(p)\,]\,\Delta i_s^- + [\, F_2\,(p) - j\,F_1\,(p)\,]\,\psi_r^-\,\Delta\omega_{sl} \tag{6.11}$$

where,

$$F_1\,(p) = \frac{z_r\,(p)}{[\,(z_r\,(p)\,)^2 + \omega_{sl}^2\,l_{rr}^2\,]} \tag{6.12}$$

$$F_2\,(p) = \frac{-\,\omega_{sl}\,l_{rr}}{[\,(z_r\,(p)\,)^2 + \omega_{sl}^2\,l_{rrr}^2\,]} \tag{6.13}$$

$$F_3\,(p) = p\,F_1\,(p) - \omega_{sl}\,F_2\,(p) \tag{6.14}$$

$$F_4\,(p) = \omega_{sl}\,F_1\,(p) + p\,F_2\,(p) \tag{6.15}$$

Substituting the value of Δi_r^- from equation (6.11) in equation (6.5), following perturbed stator voltage (Δv_s^-) is obtained

$$\Delta v_s^- = [\, F_5\,(p) + j\,F_6\,(p)\,]\,\Delta i_s^- + [\, F_7\,(p) + j\,F_8\,(p)\,]\,\psi_r^-\,\Delta\omega_{sl} + j\,\psi_s^-\,\Delta\omega_e \tag{6.16}$$

where,

$$F_5\,(p) = z_s\,(p) - p\,l_m^2\,F_3\,(p) + l_m^2\,F_4\,(p)\,\omega_e \tag{6.17}$$

$$F_6\,(p) = \omega_e\,l_s - \omega_e\,l_m^2\,F_3\,(p) - p\,l_m^2\,F_4\,(p) \tag{6.18}$$

$$F_7\,(p) = l_m\,[\, p\,F_2\,(p) + \omega_e\,F_1\,(p)\,] \tag{6.19}$$

$$F_8\,(p) = l_m\,[\, -\,p\,F_1\,(p) + \omega_e\,F_2\,(p)\,] \tag{6.20}$$

Consider the capacitor current equation in ($q^e - d^e$) reference frame

$$i_{dc}^e = c\,(\, -\,v_{qs}^e\,\omega_e + p\,v_{ds}^e\,) \tag{6.21}$$

$$i_{qc}^e = c \left(v_{ds}^e \, \omega_e + p \, v_{qs}^e \right) \tag{6.22}$$

where, c = capacitance/phase. The capacitor banks are connected in star across the motor terminals. Combining equation (6.21) and (6.22), capacitor phase current is given as:

$$i_c^- = i_{dc}^e + j \, i_{qc}^e \tag{6.23}$$

Hence,

$$i_c^- = c \, p \, v_s^- + j \, c \, \omega_e \, v_s^- \tag{6.24}$$

The inverter, machine and capacitor currents are related to each other according to the following equations in $(q^e - d^e)$ reference frame.

$$i_{d(inv)}^e = i_{ds}^e + i_{dc}^e \tag{6.25}$$

$$i_{q(inv)}^e = i_{qs}^e + i_{qc}^e \tag{6.26}$$

Since the inverter output fundamental current peak is taken along the q- axis of reference frame, hence

$$i_{d(inv)}^e = 0 \tag{6.27}$$

$$i_{q(inv)}^e = k \, I_{dc} \tag{6.28}$$

Combining the equation (6.25) and (6.26), following equation is achieved.

$$(i_{d(inv)}^e + j \, i_{q(inv)}^e) = (i_{ds}^e + j \, i_{qs}^e) + (i_{dc}^e + j \, i_{qc}^e) \tag{6.29}$$

Substituting equations (6.27), (6.28) and (6.24) in equation (6.29), i_s^- is given below:

$$i_s^- = j \, k \, I_{dc} - c \, (p + j \, \omega_e) \, v_s^- \tag{6.30}$$

167

Perturbing both sides of the equation (6.30)

$$\Delta i_s^- = j k \, \Delta I_{dc} - c \, (p + j \, \omega_e \,) \, \Delta v_s^- - j \, c \, v_s^- \, \Delta \omega_e \tag{6.31}$$

Substituting the value of Δi_s^-, obtained from equation (6.31) in equation (6.16), following equation is achieved.

$$
\begin{aligned}
[\, 1 + c \, (p + j \, \omega_e \,) \, (\, F_5 \, (p) + j \, F_6 \, (p)\,)\,] \, \Delta v_s^- = \; & j \, k \, [\, F_5 \, (\, p) + j \, F_6 \, (\, p \,) \,] \, \Delta I_{dc} \\
& + j \, [\, \psi_s^- - c \, v_s^- \, (\, F_5 \, (p) + j \, F_6 \, (p)\,] \, \Delta \omega_e \\
& + [\, F_7 \, (p) + j \, F_8 \, (p) \,] \, \psi_r^- \, \Delta \omega_{sl}
\end{aligned}
\tag{6.32}
$$

Consider the torque balance equation of the motor

$$J \, \frac{2}{P} \, (p \, \omega_r \,) = t_e - t_l \tag{6.33}$$

where,

$\qquad$ J $=$ Moment of inertia

$\qquad$ P $=$ Number of poles

and,

$$t_e \; = \frac{3}{2} \cdot \frac{P}{2} \cdot l_m \, (\, i_{dr}^e \, i_{qs}^e - i_{qr}^e \, i_{ds}^e \,) \tag{6.34}$$

Substituting equation (6.34) in (6.33) yields

$$J \frac{2}{P} \, (p \, \omega_r \,) \; = \frac{3}{2} \cdot \frac{P}{2} \cdot l_m \, (\, i_{dr}^e \, i_{qs}^e - i_{qr}^e \, i_{ds}^e \,) - t_l \tag{6.35}$$

Separating the real and imaginary parts of the perturbed rotor current (Δi_r^-) equation (6.10), the following expressions of Δi_{dr}^e, Δi_{qr}^e are achieved.

$$\Delta i_{dr}^e = F_9 \, (\, p) \, \Delta i_{ds}^e + F_{11} \, (p) \, \Delta i_{qs}^e + F_{13} \, (\, p) \, \Delta \omega_{sl} \tag{6.36}$$

168

$$\Delta i_{qr}^{e} = F_{10}\ (p)\ \Delta i_{ds}^{e} + F_{12}\ (p)\ \Delta i_{qs}^{e} + F_{14}\ (p)\ \Delta \omega_{sl} \qquad (6.37)$$

where,

$$F_{9}\ (p) = -\,l_{m}\,F_{3}\ (p)$$

$$F_{10}\ (p) = -\,l_{m}\,F_{4}\ (p)$$

$$F_{11}\ (p) = \,l_{m}\,F_{4}\ (p) \qquad (6.38)$$

$$F_{12}\ (p) = -\,l_{m}\,F_{3}\ (p)$$

$$F_{13}\ (p) = [\ F_{2}\ (p)\ \psi_{dr}^{e} + F_{1}\ (p)\ \psi_{qr}^{e}\ ]$$

$$F_{14}\ (p) = [\ -\,F_{1}\ (p)\ \psi_{dr}^{e} + F_{2}\ (p)\ \psi_{qr}^{e}\ ]$$

Perturbing both sides of equation (6.35) and neglecting the variation in load torque,

$$\Delta t_{1} = 0 \qquad (6.39)$$

and substituting the value of Δi_{dr}^{e}, Δi_{qr}^{e} obtained from equation (6.36) and (6.37) in equation (6.35), following equation is achieved.

$$J\frac{2}{P}\ (p\ \Delta \omega_{r}\ ) = F_{15(P)}\ \Delta i_{qs}^{e} + F_{16(P)}\ \Delta i_{ds}^{e} + F_{17(p)}\ \Delta \omega_{sl} \qquad (6.40)$$

where,

$$F_{15}\ (p) = \frac{3}{2} \cdot \frac{P}{2} \cdot l_{m}\ [\ i_{dr}^{e} + F_{11}\ (p)\ i_{qs}^{e} - F_{12}\ (p)\ i_{ds}^{e}\ ]$$

$$F_{16}\ (p) = \frac{3}{2} \cdot \frac{P}{2} \cdot l_{m}\ [\ -\,i_{qr}^{e} + F_{9}\ (p)\ i_{qs}^{e} - F_{10}\ (p)\ i_{ds}^{e}\ ] \qquad (6.41)$$

$$F_{17}\ (p) = \frac{3}{2} \cdot \frac{P}{2} \cdot l_{m}\ [\ F_{13}\ (p)\ i_{qs}^{e} - F_{14}\ (p)\ i_{ds}^{e}\ ]$$

Separating the real and imaginary parts of equation (6.30)

$$\Delta i_{ds}^{e} = - c \, (\, p \, \Delta v_{ds}^{e} - \omega_{e} \, \Delta v_{qs}^{e} \,) + c \, v_{qs}^{e} \, \Delta \omega_{e} \qquad (6.42)$$

$$\Delta i_{qs}^{e} = k \, \Delta I_{dc} - c \, (\, p \, \Delta v_{qs}^{e} + \omega_{e} \, \Delta v_{ds}^{e} \,) \qquad (6.43)$$

Substituting the value of Δi_{ds}^{e}, Δi_{qs}^{e} and $\Delta \omega_{e} = \Delta \omega_{sl} + \Delta \omega_{r}$, in equation (6.40), following equation is obtained.

$$\begin{aligned} F_{21} \, (p) \Delta \omega_{r} = {} & F_{18} \, (p) \, \Delta v_{ds}^{e} + F_{19} \, (p) \, \Delta v_{qs}^{e} \\ & + [\, F_{20} \, (p) + F_{17} (p) \,] \, \Delta \omega_{e} + k \, F_{15} \, (p) \, \Delta I_{dc} \end{aligned} \qquad (6.44)$$

where,

$$\left. \begin{aligned} F_{18} \, (p) &= - c \, [\, F_{15} \, (p) \, \omega_{e} + p \, F_{16}(p) \,] \\[2mm] F_{19} \, (p) &= - c \, [\, p \, F_{15} \, (p) - \omega_{e} \, F_{16}(p) \,] \\[2mm] F_{20} \, (p) &= - c \, [\, F_{15} \, (p) \, v_{ds}^{e} - F_{16} (p) \, v_{qs}^{e} \,] \\[2mm] F_{21} \, (p) &= F_{17} \, (p) + J \frac{2}{P} \cdot p \end{aligned} \right\} \qquad (6.45)$$

Separating the real and imaginary parts of equation (6.32), following equations are achieved.

$$\begin{aligned} [F_{24} \, (p) \Delta v_{ds}^{e} - F_{25} \, (p) \, \Delta v_{qs}^{e}] = {} & - [\, F_{7} \, (p) \, \psi_{dr}^{e} - F_{8}(p) \, \psi_{qr}^{e} - F_{22}(p) \,] \, \Delta \omega_{r} \\ & - k \, F_{6}(p) \, \Delta I_{dc} + F_{22} \, (p) \, \Delta \omega_{sl} \end{aligned} \qquad (6.46)$$

$$\begin{aligned} [F_{25} \, (p) \, \Delta v_{ds}^{e} + F_{24} \, (p) \, \Delta v_{qs}^{e}] = {} & - [\, F_{8} \, (p) \, \psi_{dr}^{e} + F_{7} \, (p) \, \psi_{qr}^{e} - F_{23} \, (p) \,] \, \Delta \omega_{r} \\ & + F_{23} \, (p) \, \Delta \omega_{sl} + k F_{5} \, (p) \, \Delta I_{dc} \end{aligned} \qquad (6.47)$$

where,

$$F_{22}(p) = [-\psi_{qs}^e + cF_5(p)v_{qs}^e + cF_6(p)v_{ds}^e + F_7(p)\psi_{dr}^e - F_8(p)\psi_{qr}^e]$$

$$F_{23}(p) = [\psi_{ds}^e - cF_5(p)v_{ds}^e + cF_6(p)v_{qs}^e + F_8(p)\psi_{dr}^e + F_7(p)\psi_{qr}^e] \qquad (6.48)$$

$$F_{24}(p) = 1 + c[pF_5(p) - \omega_e F_6(p)]$$

$$F_{25}(p) = c[\omega_e F_5(p) + pF_6(p)]$$

The parameters of speed PI controller are k_{p_s} and k_{i_s}, while the parameters of current PI controller are k_{p_i} and k_{i_i}. The rectifier output voltage V_r and inverter input voltage (V_{inv}) are related according to the following equation.

$$V_r = (r_f + pl_f)I_{dc} + V_{inv} \qquad (6.49)$$

where,

$$V_{inv} = \frac{3}{2}.k.v_{qs}^e \qquad (6.50)$$

V_{inv} is obtained by the power invariance theorem, as discussed in chapter 2

Substituting equation (6.50) in equation (6.49) the following equation is obtained.

$$V_r = (r_f + pl_f)I_{dc} + \frac{3}{2}kv_{qs}^e \qquad (6.51)$$

V_r may be expressed in terms of current controller parameters as shown below:

$$V_r = (k_{p_i} + \frac{k_{i_i}}{p})(I_{ref} - I_{dc}) \qquad (6.52)$$

From equations (6.51) and (6.52)

$$(k_{p_i} + \frac{k_{i_i}}{p})(I_{ref} - I_{dc}) = (r_f + pl_f)I_{dc} + \frac{3}{2}kv_{qs}^e \qquad (6.53)$$

Perturbing equation (6.53)

$$(k_{p_i} + \frac{k_{i_i}}{p})(\Delta I_{ref} - \Delta I_{dc}) = (r_f + pl_f)\Delta I_{dc} + \frac{3}{2}k\Delta v_{qs}^e \qquad (6.54)$$

where,

$$I_{ref}^2 = [(I_{act}^*)^2 + (I_{react}^* - I_c)^2] \times (\frac{\sqrt{2}}{k})^2 \qquad (6.55)$$

Perturbing equation (6.55) following equation is obtained.

$$\Delta I_{ref} = [\frac{\{I_{act}^* \Delta I_{act}^* + (I_{react}^* - I_c).(\Delta I_{react}^* - \Delta I_c)\}}{I_{ref}}] \times (\frac{\sqrt{2}}{k})^2 \qquad (6.56)$$

where,

$$I_{act}^* = k_1 \omega_{sl}^* + constant \qquad (6.57)$$

Perturbing the equation (6.57) following equation is obtained.

$$\Delta I_{act}^* = k_1 \Delta \omega_{sl}^* \qquad (6.58)$$

Since I_{react} is almost constant, hence $\Delta I_{react}^* = 0$ $\qquad (6.59)$

Capacitor r.m.s. phase current is related to the machine voltage and frequency according to the following equation:

$$I_c = c \omega_e V_s \qquad (6.60)$$

where, V_s = r.m.s. value of stator voltage/phase.

For the $\left(\dfrac{V}{f_e}\right)$ control operation of the drive the equation (6.60) may be expressed as

$$I_c = k_{11} \, \omega_e{}^2 \qquad (6.61)$$

where,

$$k_{11} = \frac{I_{c\,(rated)}}{(\omega_{e\,(rated)})^2}$$

Perturbing equation (6.61) following equation is obtained.

$$\Delta I_c = 2 k_{11} \, \omega_e \, \Delta \omega_e \qquad (6.62)$$

Substituting $k_{12} = 2 k_{11} \, \omega_e \qquad (6.63)$

Equation (6.61) may be expressed as

$$\Delta I_c = k_{12} \, \Delta \omega_e \qquad (6.64)$$

From the proposed control structure as shown in Fig. 2.1

$$\omega_e = \omega_r + \omega_{sl}^* \qquad (6.65)$$

where,

$$\omega_{sl}^* = (k_{p_s} + \frac{k_{i_s}}{p})\,(\omega_{ref} - \omega_r) \qquad (6.66)$$

Perturbing equation (6.66) following equation is obtained.

$$\Delta \omega_{sl}^* = -(k_{p_s} + \frac{k_{i_s}}{p})\,\Delta \omega_r \qquad (6.67)$$

Perturbing equation (6.65) following equation is obtained.

$$\Delta \omega_e = \Delta \omega_r + \Delta \omega_{sl}^* \qquad (6.68)$$

173

Substituting the value of $\Delta\omega^*_{sl}$ from equation (6.67) in equation (6.68) following equation is obtained.

$$\Delta\omega_e = (1 - k_{p_s} - \frac{k_{i_s}}{p})\,\Delta\omega_r \tag{6.69}$$

Substituting the value of $\Delta\omega_e$, equation (6.64) may be expressed as

$$\Delta I_c = k_{12}\,(1 - k_{p_s} - \frac{k_{i_s}}{p})\,\Delta\omega_r \tag{6.70}$$

Substituting the value of $\Delta I_{act}, \Delta I_{react}$ and ΔI_c in equation (6.56), following equation is obtained.

$$\Delta I_{ref} = \frac{[-I^*_{act}\,k_1\,(k_{p_s} + \frac{k_{i_s}}{p})\,\Delta\omega_r - (I^*_{react} - I_c)\times k_{12}\,(1 - k_{p_s} - \frac{k_{i_s}}{p})\,\Delta\omega_r]}{I_{ref}} \times (\frac{\sqrt{2}}{k})^2 \tag{6.71}$$

Defining,

$$A_1 = \frac{I^*_{act} \times k_1 \times 2}{k^2\,I_{ref}} \tag{6.72}$$

$$A_2 = \frac{-(I^*_{react} - I_c)\times k_{12} \times 2}{k^2\,I_{ref}} \tag{6.73}$$

Hence,

$$\Delta I_{ref} = -A_1\,(k_{p_s} + \frac{k_{i_s}}{p})\,\Delta\omega_r + A_2\,(1 - k_{p_s} - \frac{k_{i_s}}{p})\,\Delta\omega_r$$

$$= -(A_1 + A_2\,)(k_{p_s} + \frac{k_{i_s}}{p})\,\Delta\omega_r + A_2\,\Delta\omega_r \tag{6.74}$$

Substituting the value of ΔI_{ref} from equation (6.74), in the equation (6.54)

174

$$(k_{p_i} + \frac{k_{i_i}}{p}) \, [\{(k_{p_i} + \frac{k_{i_i}}{p})(-A_1 - A_2)\} \, \Delta\omega_r + A_2 \, \Delta\omega_r - \Delta I_{dc}] = (r_f + pl_f) \Delta I_{dc} + \frac{3}{2} k \Delta v_{qs}^e$$

.... (6.75)

Rearranging the equation (6.75) following equation is achieved.

$$(k_{p_i} + \frac{k_{i_i}}{p}) \, [\{(k_{p_i} + \frac{k_{i_i}}{p})(-A_1 - A_2)\} + A_2] \Delta\omega_r - (k_{p_i} + \frac{k_{i_i}}{p} + r_f + pl_f) \Delta I_{dc} - \frac{3}{2} k \Delta v_{qs}^e = 0$$

.... (6.76)

Equation (6.44), (6.46), (6.47) and (6.76) are used for the design of speed controller parameters and equations (6.46); (6.47) and (6.76) are used for the design of current controller parameters. First the inner current loop is considered for the design of current controller parameters and then outer speed loop is considered for the design of speed controller parameters.

6.2.1   Design of Current Controller

The PI speed controller sets the reference slip speed (ω_{sl}^*) which in turn sets the reference d.c. link current (I_{ref}). The current error between I_{ref} and I_{dc} is processed in the current PI controller. The current controller controls the pulse widths of PWM pulses, hence the output voltages of PWM rectifier. For the design of current controller parameters (k_{p_i} and k_{i_i}), the speed of the motor is assumed constant, as mechanical time constants of motor is much higher than the electrical time constants, and hence reference slip speed (ω_{sl}^*) and (ω_e) are also considered as constants for the design of current controller parameters.

Since,

$$\Delta\omega_e = \Delta\omega_{sl} = \Delta\omega_r = 0$$

175

Hence equations (6.46), (6.47) and (6.76) may be expressed as.

$$F_{24}(p)\Delta v_{ds}^e - F_{25}(p)\Delta v_{qs}^e + kF_6(p)\Delta I_{dc} = 0 \qquad (6.77)$$

$$F_{25}(p)\Delta v_{ds}^e + F_{24}(p)\Delta v_{qs}^e - kF_5(p)\Delta I_{dc} = 0 \qquad (6.78)$$

$$(k_{P_i} + \frac{k_{i_i}}{p} + r_f + pl_f)\Delta I_{dc} + \frac{3}{2}k\Delta v_{qs}^e = 0 \qquad (6.79)$$

The above equations are expressed in matrix form to obtain the characteristic equation of current regulator.

$$\begin{bmatrix} 0 & 1.5k & (k_{P_i} + \frac{k_{i_i}}{p} + r_f + pl_f) \\ F_{24}(p) & -F_{25}(p) & kF_6(p) \\ F_{25}(p) & F_{24}(p) & -kF_5(p) \end{bmatrix} \begin{bmatrix} \Delta v_{ds}^e \\ \Delta v_{qs}^e \\ \Delta I_{dc} \end{bmatrix} = 0 \qquad (6.80)$$

The characteristic equation of above matrix is given by.

$$D(p) = 0$$

where D (p) is the characteristic polynomial, stated below in matrix form :

$$D(p) = \begin{vmatrix} 0 & 1.5k & (k_{P_i} + \frac{k_{i_i}}{p} + r_f + pl_f) \\ F_{24}(p) & -F_{25}(p) & kF_6(p) \\ F_{25}(p) & F_{24}(p) & -kF_5(p) \end{vmatrix} \qquad (6.81)$$

Substituting (6.81) in (6.80) and expanding it, following equation is obtained.

$$1.5k^2[F_{24}(p)F_5(p) + F_6(p)F_{25}(p)] + (k_{P_i} + \frac{k_{i_i}}{p} + r_f + pl_f)[\{(F_{24}(p))^2 + (F_{25}(p)\}^2] = 0$$

$$.....(6.82)$$

The equation (6.82) is used to obtain the D-partition boundary of current controller parameters.

Define,

$$c_1 = [F_{24}(p) F_5(p) + F_6(p)F_{25}(p)]$$

$$c_2 = r_f + pl_f$$

$$c_3 = [(F_{24}(p))^2 + (F_{25}(p))^2]$$

Substituting c_1, c_2, and c_3 in equation (6.82) following equation is obtained.

$$(k_{p_i} + \frac{k_{i_i}}{p} + c_2)\, c_3 + 1.5\,k^2 c_1 = 0 \qquad (6.83)$$

Rearranging the equation (6.83), the final characteristic equation of current regulator matrix is available for the designing of controller parameters

$$p\,k_{p_i} c_3 + k_{i_i} c_3 + p c_2 c_3 + 1.5 p k^2 c_1 = 0 \qquad (6.84)$$

Define,

$$c_4 = p\, c_3$$

$$c_5 = p(c_2 c_3 + 1.5\,k^2 c_1)$$

Substituting the value of c_4 and c_5 in equation (6.84) following equation is obtained.

$$k_{p_i} c_4 + k_{i_i} c_3 + c_5 = 0 \qquad (6.85)$$

Upon substituting $p = (\sigma + j\omega)$ or $p = (-\xi\omega + j\omega\sqrt{1 - \xi^2})$ in equation (6.85), c_3, c_4 and c_5 assume complex values and can be written as

$$c_3 = c_{3r} + j c_{3i}$$

$$c_4 = c_{4r} + j c_{4i}$$

$$c_5 = c_{5r} + j c_{5i}$$

Separating the real and imaginary parts of the equation (6.85) yields following two equations:

$$k_{p_i} c_{4r} + k_{i_i} c_{3r} + c_{5r} = 0 \tag{6.86}$$

$$k_{p_i} c_{4i} + k_{i_i} c_{3i} + c_{5i} = 0 \tag{6.87}$$

Solving equation (6.86) and (6.87) for k_{p_i} and k_{i_i}

$$k_{p_i} = \frac{\begin{vmatrix} -c_{5r} & c_{3r} \\ -c_{5i} & c_{3i} \end{vmatrix}}{\Delta} \tag{6.88}$$

$$k_{i_i} = \frac{\begin{vmatrix} c_{4r} & -c_{5r} \\ c_{4i} & -c_{5i} \end{vmatrix}}{\Delta} \tag{6.89}$$

where,

$$\Delta = c_{4r} c_{3i} - c_{4i} c_{3r} \tag{6.90}$$

Substituting $p = (-\sigma + j\omega)$ in the equations (6.88), (6.89) and (6.90) and varying ω from $-\infty$ to $+\infty$, for a constant σ, the D-partition boundary is plotted in (k_{p_i}, k_{i_i}) plane. For $\sigma = 0.0$, the D-partition boundary is shown in Fig.6.1. For obtaining the region having maximum number of roots in the left half of p-plane, the D-partition boundary is shaded according to the sign of the denominator term Δ, as given by the equation (6.90). Facing the direction in which ω is increasing, the boundary curve in (k_{p_i}, k_{i_i}) plane is shaded twice on the left hand side if $\Delta > 0$ and right hand side if $\Delta < 0$. Spatial line is plotted for $\omega = 0.0$, using equation (6.86) and shaded in the matching manner as shown in Fig 6.1;the spatial line is along the real axis. The inner most region in the sense of shading is the probable stable region. It is the region having maximum number of roots in
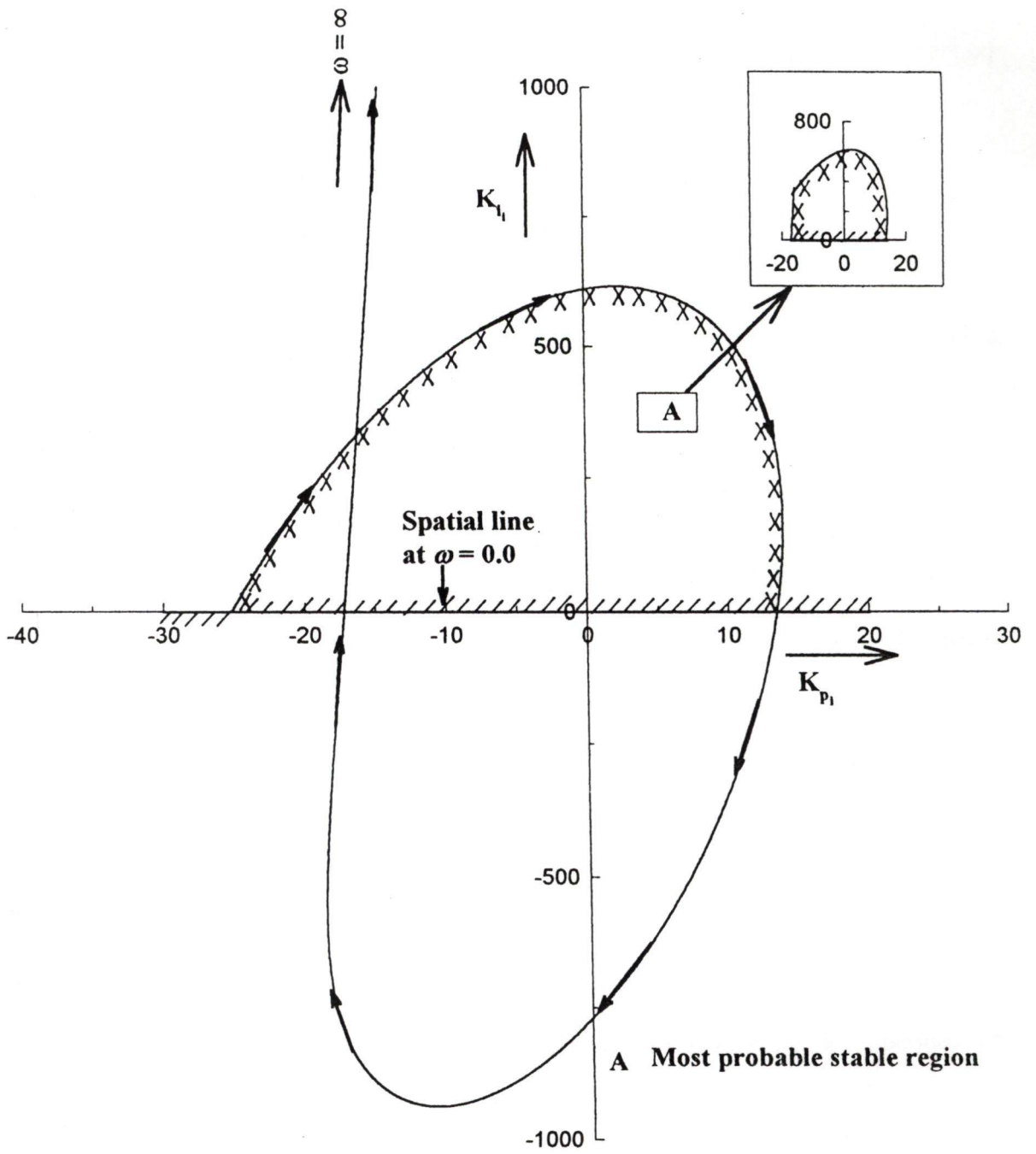
Fig. 6.1. **D-partition boundary for current controller design for absolute stability**

the left half of p-plane. The stability of this region having maximum number of roots in the left half of p-plane is checked by frequency scanning technique. In the Fig.6.1 all the points in the hatched region A are the stable points.

Relative stability boundaries curves are also plotted, to get the stability region in parametric plane for better performance. Using equations (6.88) and (6.89), for the different values of σ and varying ω from $-\infty$ to $+\infty$, the D- partition curves are obtained as shown in Fig 6.2.

Another set of relative stability boundaries curves are also plotted by substituting $p = (-\xi\omega + j\omega \sqrt{1-\xi^2})$ with different values of damping ratio (ξ) and are shown in Fig 6.3. The probable stable region in the parametric plane is identified and point check for stability is done by frequency scanning technique.

From the Figs.6.2 and 6.3, it is clear that as the σ and ξ are increased from their minimum value of zero, smaller regions in parametric plane are achieved.

For checking the stability using frequency-scanning technique, a point $X(k_{p_i} = 1.0, k_{i_i} = 300.0)$ is considered in the probable stable region (k_{p_i}, k_{i_i}), and corresponding k_{p_i}, k_{i_i} values are substituted in the left hand side of equation (6.85). This yields.

$$D(p) = k_{p_i} c_4 + k_{i_i} c_3 + c_5$$

For fixed σ, the locus of the vector D $(-\sigma + j\omega)$ is plotted in the real and imaginary plane with the variation in ω. The characteristic curve is shaded once on its left hand side as ω increases from $-\infty$ to $+\infty$. The system is stable at the chosen
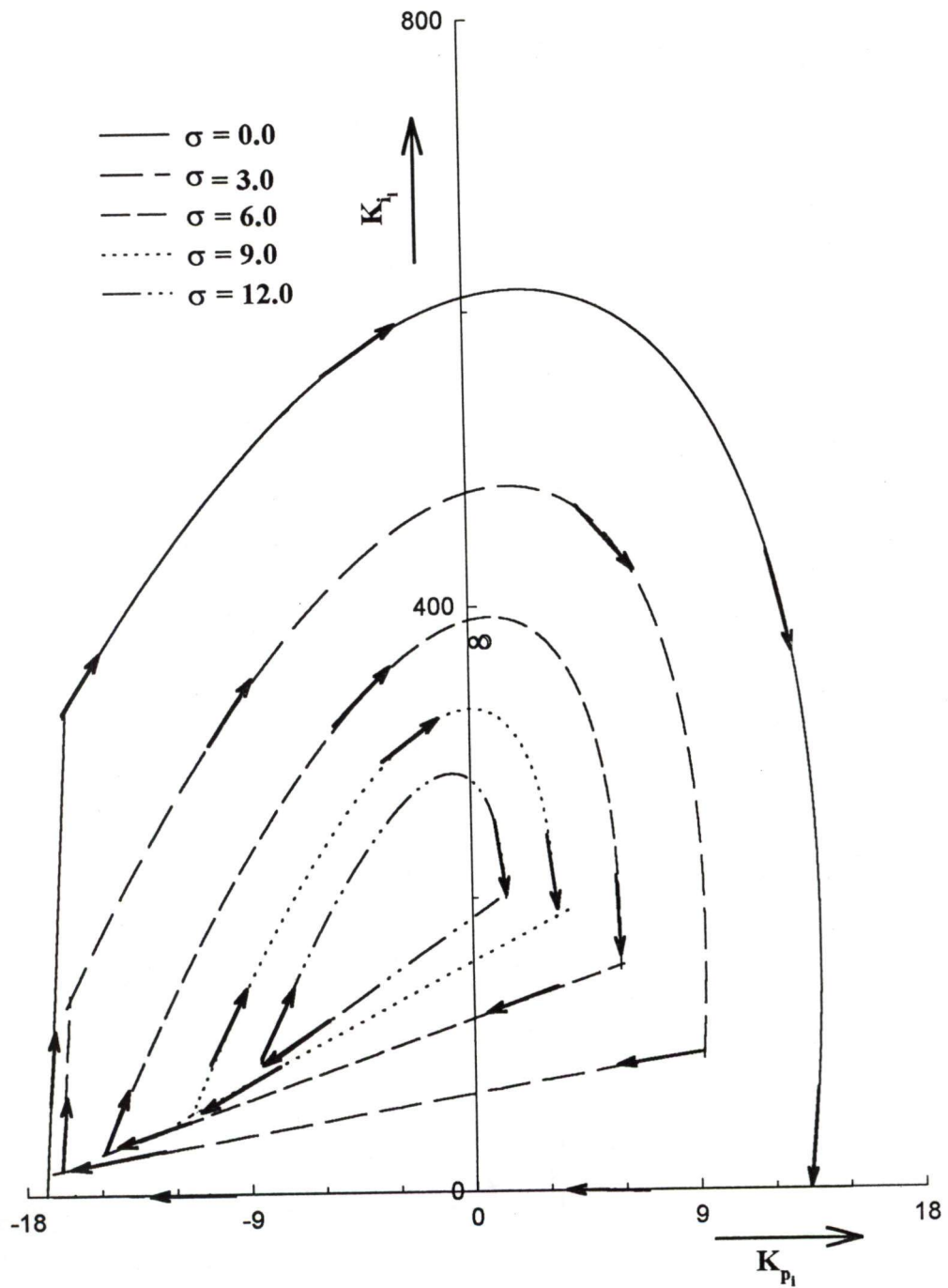
Fig 6.2. Relative stability boundries for current controller design for different values of σ
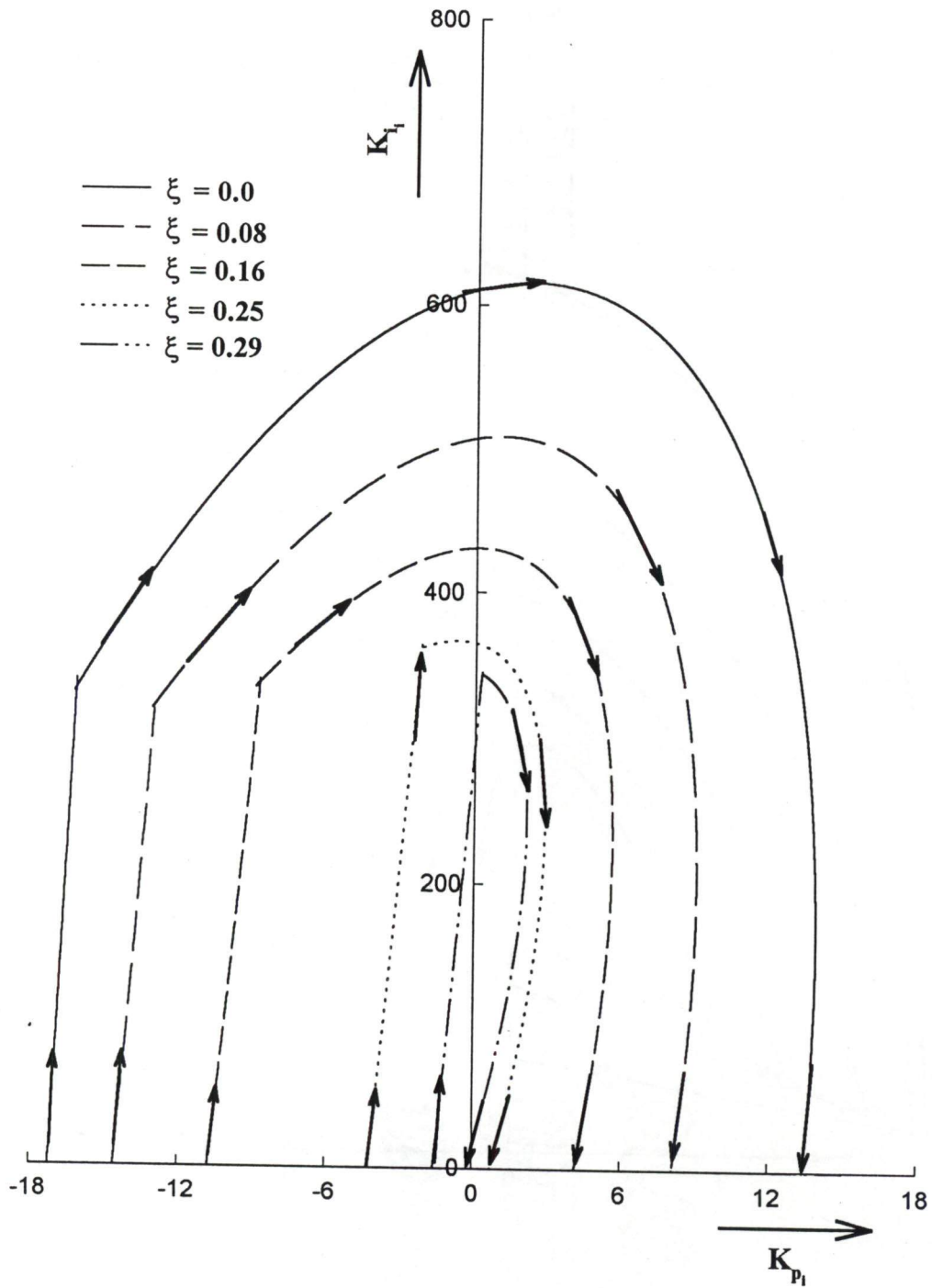
Fig 6.3. Relative stability boundries for current controller design for different values of ξ

operating point, if the origin lies in the inner most shaded region. If so then the entire probable stable region (A), determined earlier is the stable region. The locus of D $(-\sigma + j\omega)$ for $\sigma = 0.0$ is shown in Fig (6.4). The curve of characteristic vector encloses the origin. Hence, the operating point X is a stable point and the entire region A is the stable region. To further confirm the stability of this region, another point Y $(k_{p_i} = 20.0, k_{i_i} = 800.0)$ is considered out side this region and the characteristic vector D (p) is plotted. As shown in Fig. 6.5, the curve does not enclose the origin; hence Y is an unstable operating point and the region outside A is unstable.

For checking the stability of a point for variation in ξ, the relative stability boundary curve shown in Fig 6.3 is selected. To check the better relative stability in a region two points are considered, one U ($k_{p_i} = 6.0, k_{i_i} = 400.0$) at $\xi \geq 0.08$ and other V $(k_{p_i} = 9.0, k_{i_i} = 550.0)$ at $\xi < 0.08$. Substitute the value of k_{p_i} and k_{i_i} in the equation D (p) $= k_{p_i} c_4 + k_{i_i} c_3 + c_5$. Corresponding to both these points D (p) variation is plotted with $p = (-\xi\omega + j\omega \sqrt{1 - \xi^2})$ and $\xi = 0.08$ by varying ω from $-\infty$ to $+\infty$, as shown in Figs 6.6,6.7 respectively. The curve, Fig 6.6 corresponding to the point U, in the region $(\xi \geq 0.08)$ includes the origin in the sense of shading, while the curve, Fig 6.7 corresponding to the point V, in the region $(\xi < 0.08)$, does not include the origin in the sense of shading. This confirms that the point U in the region $(\xi \geq 0.08)$ is having better relative stability than the point V in the region $(\xi < 0.08)$. Exact decision of controller parameters is taken by determining the transient response of current loop for step variation in reference current from 1.0 to 1.05 of rated current, using the following machine dynamics and regulator equations.
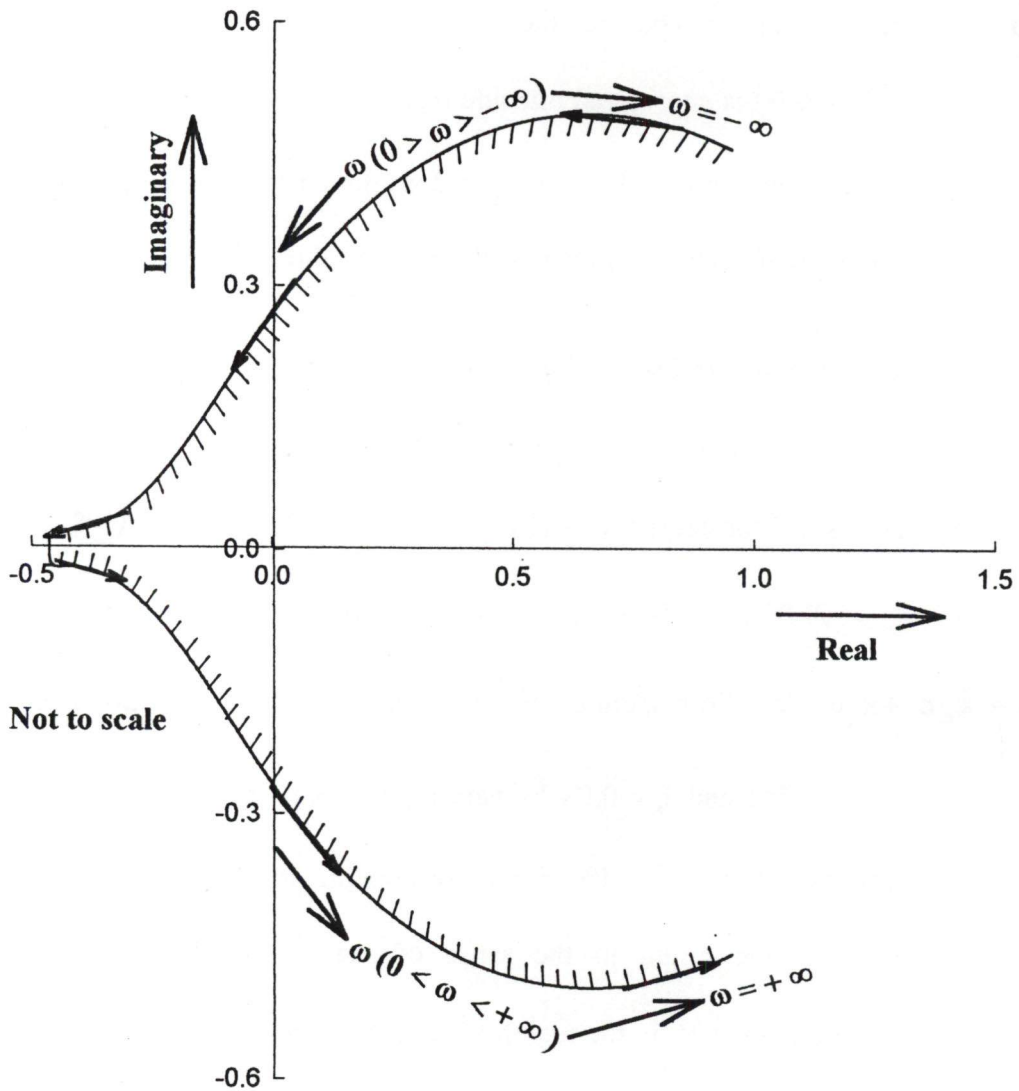
$\sigma = 0.0, K_{p_1} = 1.0, K_{i_1} = 300.0$

Fig 6.4. Frequency scanning for current controller parameters $\sigma = 0.0$
(Stable)
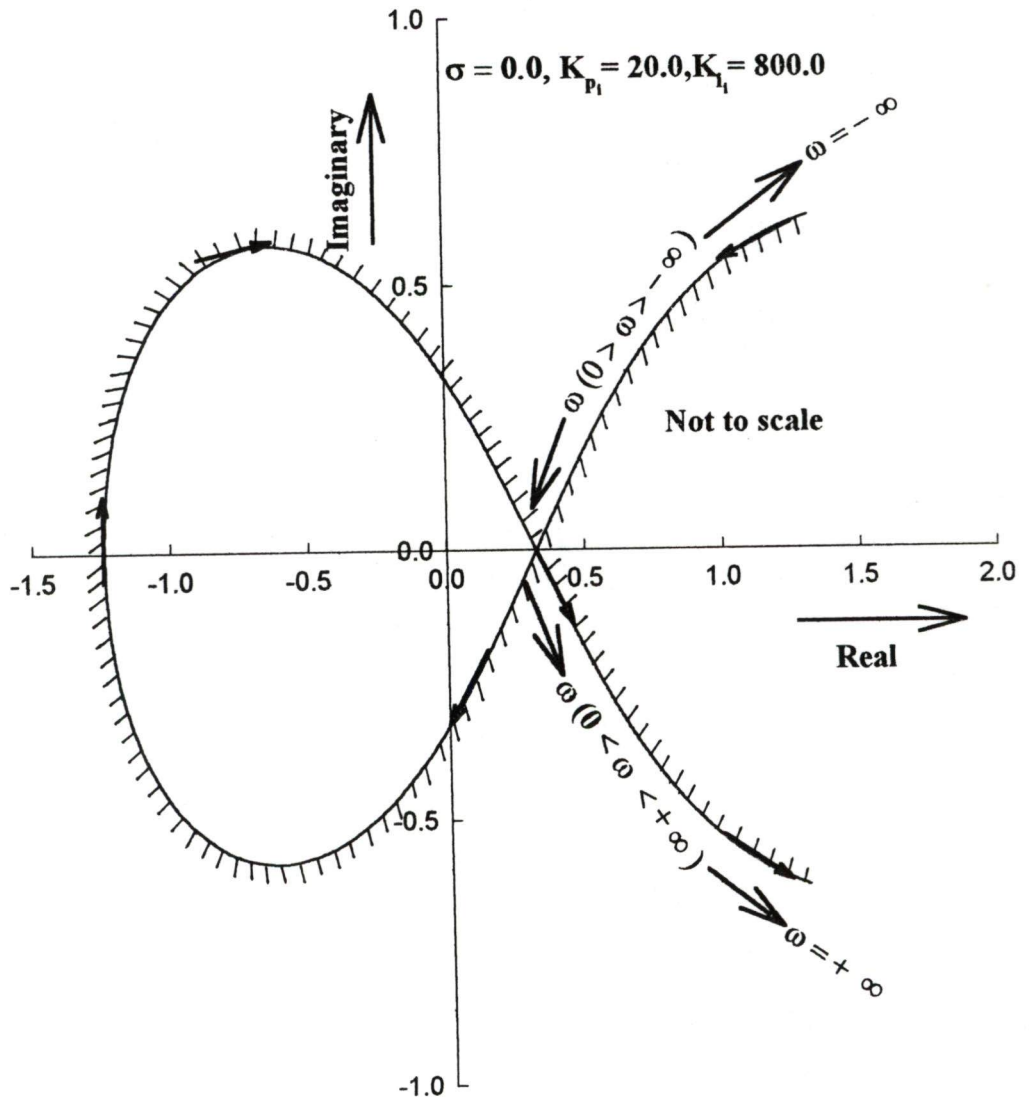
Fig 6.5. Frequency scanning for current controller parameters at σ = 0.0 (Unstable)
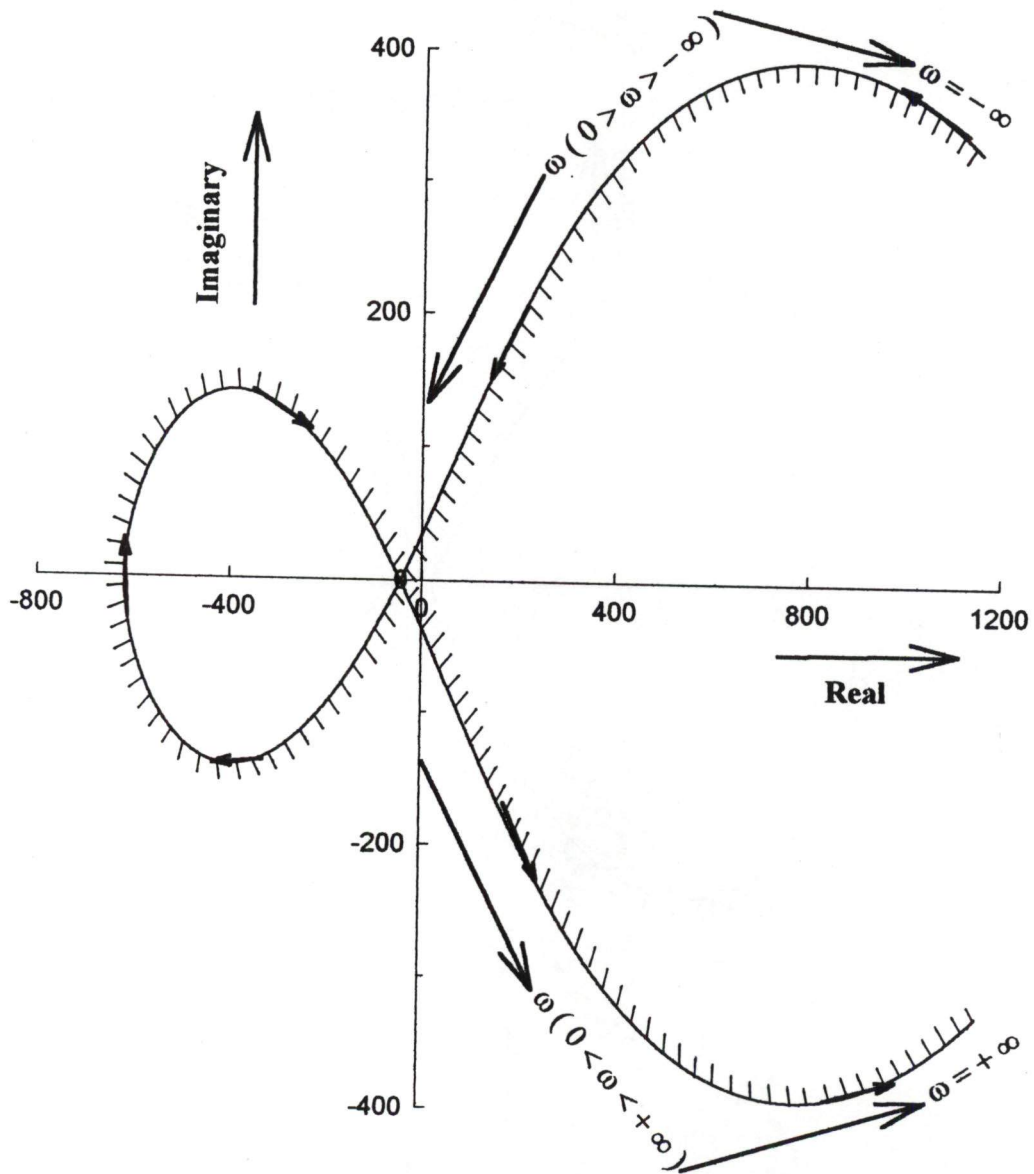
$\xi \geq 0.08, K_{p_i} = 6.0, K_{I_i} = 400.0$

Fig 6.6. Frequency scanning for current controller parameters having $\xi \geq 0.08$
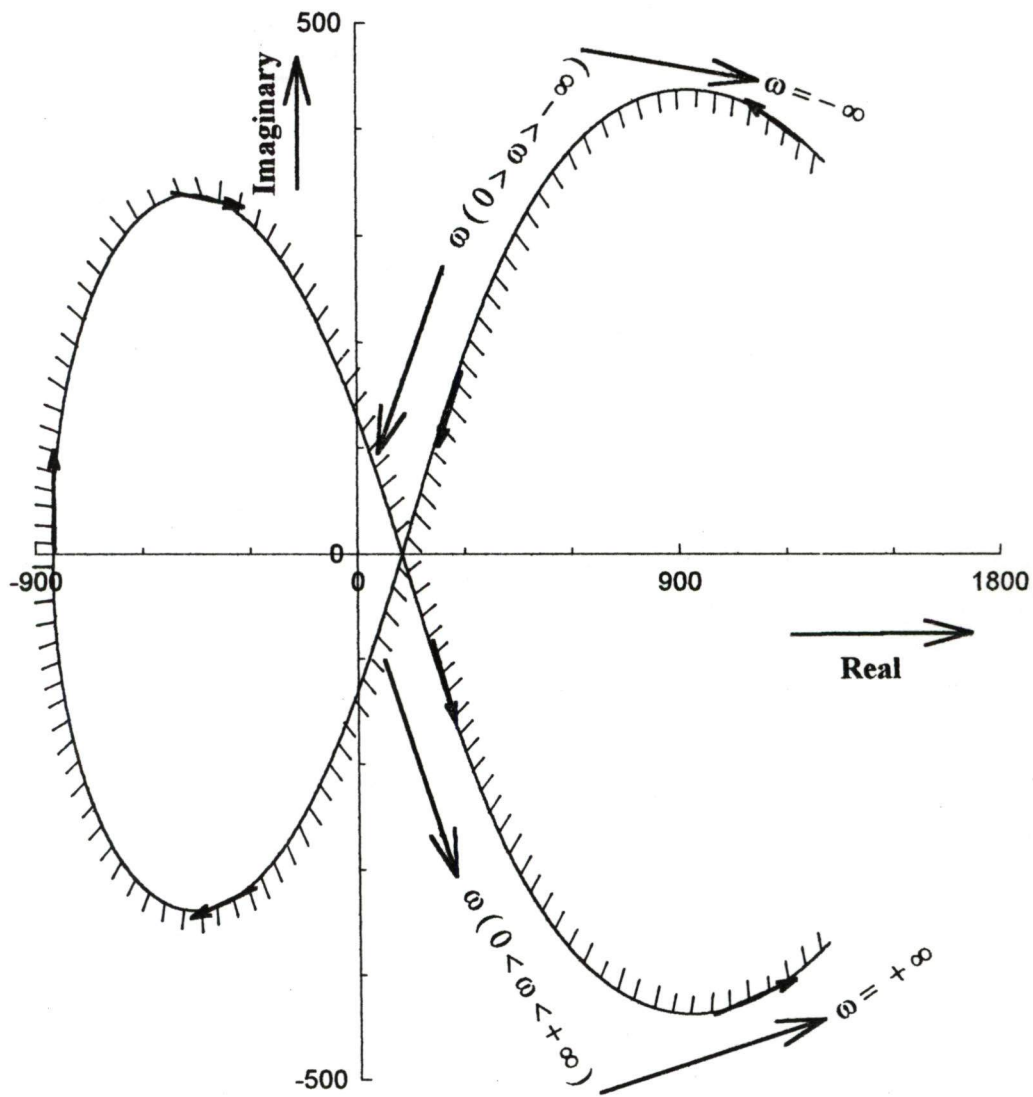
$\xi < 0.08,\ K_{P_1} = 9.0,\ K_{I_1} = 550.0$

Fig 6.7. Frequency scanning for current controller parameters having $\xi < 0.08$

$$pi_{ds}^e = \frac{[(\omega_e l_1 + \omega_r l_m^2) i_{qs}^e - (r_s l_{rr}) i_{ds}^e + (\omega_r l_m l_{rr}) i_{qr}^e + (l_m r_r) i_{dr}^e + l_{rr} v_{ds}^e]}{l_1} \qquad (6.91)$$

$$pi_{qs}^e = \frac{[(-r_s l_{rr}) i_{qs}^e - (\omega_e l_1 + \omega_r l_m^2) i_{ds}^e + (r_r l_m) i_{qr}^e - (\omega_r l_m l_{rr}) i_{dr}^e + l_{rr} v_{qs}^e]}{l_1} \qquad (6.92)$$

$$pi_{dr}^e = \frac{[(-\omega_r l_m l_{ss}) i_{qs}^e + (r_s l_m) i_{ds}^e + (\omega_e l_1 - \omega_r l_{ss} l_{rr}) i_{qr}^e - (l_{ss} r_r) i_{dr}^e - l_m v_{ds}^e]}{l_1} \qquad (6.93)$$

$$pi_{qr}^e = \frac{((l_m r_s) i_{qs}^e + (\omega_r l_{ss} l_m) i_{ds}^e - (l_{ss} r_r) i_{qr}^e - (\omega_e l_1 - \omega_r l_{ss} l_{rr}) i_{dr}^e + l_m v_{qs}^e)}{l_1} \qquad (6.94)$$

$$pv_{ds}^e = \frac{1}{c} (c \omega_e v_{qs}^e - i_{ds}^e) \qquad (6.95)$$

$$pv_{qs}^e = \frac{1}{c} (k I_{dc} - c \omega_e v_{ds}^e - i_{qs}^e) \qquad (6.96)$$

$$pI_{dc} = \frac{1}{l_f} (V_r - r_f I_{dc} - kv_{qs}^e) \qquad (6.97)$$

$$V_r = k_{p_i} (I_{ref} - I_{dc}) + \frac{k_{i_i}}{T_i} \int_0^\infty (I_{ref} - I_{dc}) \qquad (6.98)$$

where,

$$l_1 = l_{ss} l_{rr} - l_m^2$$

To determine the region in the parametric plane ensuring minimum over shoot and minimum settling time, relative stability curves are drawn for different values of σ and ξ in the (k_{p_i}, k_{i_i}) plane by varying ω from $-\infty$ to $+\infty$, as shown in Fig 6.8. A high value of σ and ξ gives the most probable stable region of better performance. A common region B, having high value of σ and ξ is selected; it is shown as hatched region in Fig 6.8.
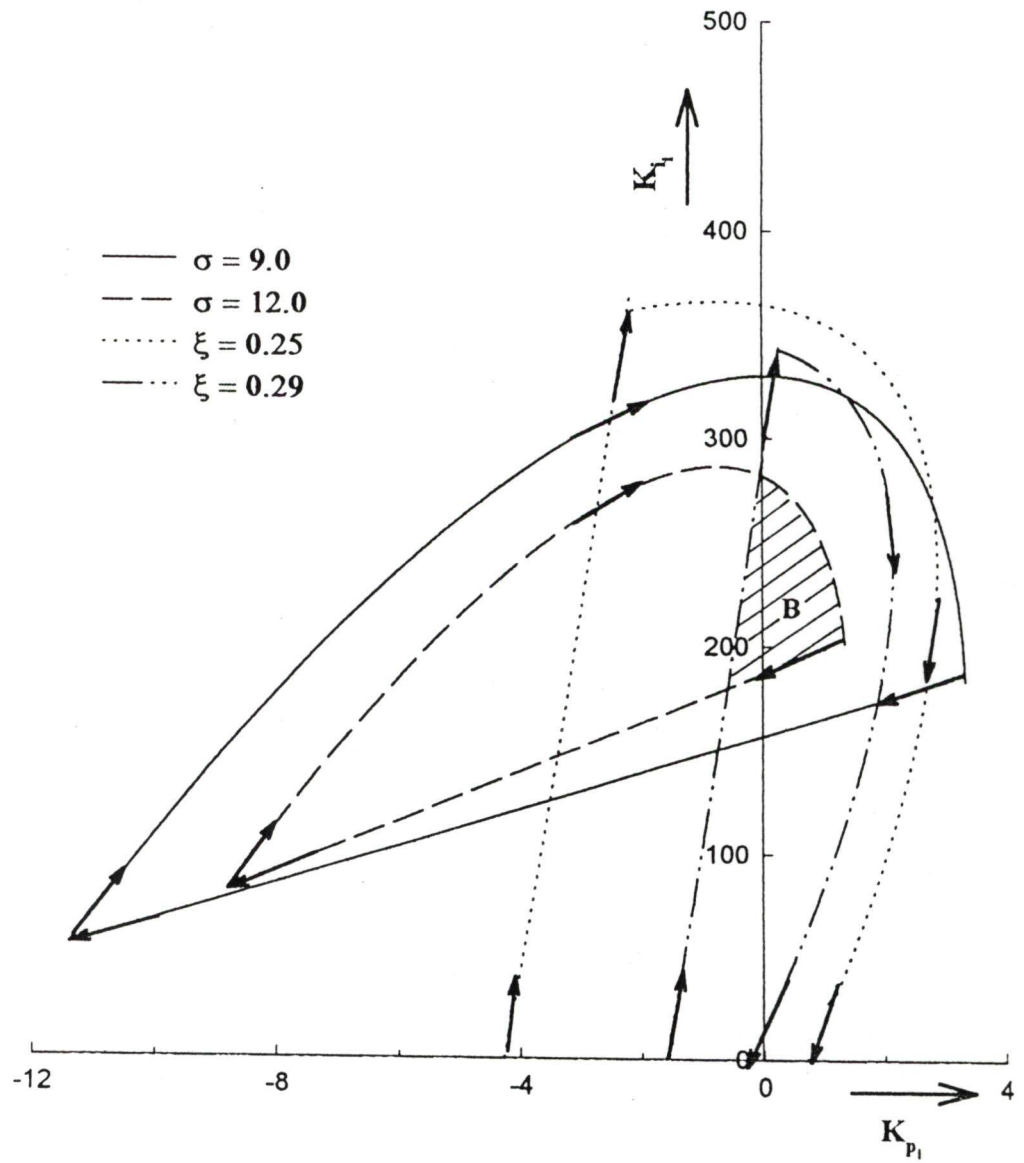
B (Most probable stable region)

Fig. 6.8. Relative stability boundaries for speed controller parameters

for different values of σ and ξ

Fig. 6.8 shows that in the shaded region B, current loop controller has $\sigma \geq 12.0$ and $\xi \geq 0.29$.

The transient response of the current loop are plotted for different sets of k_{p_i} and k_{i_i} values chosen from the region B of Fig 6.8. ($\sigma > 12.0$ and $\xi > 0.29$), using Runga Kutta fourth order integration method. The transient response curves are shown in Fig 6.9, correspond to some values of k_{p_i} and k_{i_i}. Percentage over shoot and settling time corresponding to these chosen values of k_{p_i} and k_{i_i} are shown in the Table 6.1.

Table 6.1

Case	k_{p_i}	k_{i_i}	% over shoot	Settling time (ms)
1	0.9	264	0.68	143
2	1.0	275	3.33	137
3	0.7	272	3.21	139
4	0.1	255	0.27	150

The comparison of various transient response curves, drawn in Fig 6.9, shows that for ($k_{p_i} = 1.0$ and $k_{i_i} = 275.0$), the response is fastest and overshoot within the limit of $\pm 5\%$ tolerance. Hence the selected transfer function of current controller is given by $(1.0 + \dfrac{275}{p})$.

6.2.2 Design of Speed Controller

The speed controller sets the reference active and reactive currents of stator current (i_s) and hence reference current (I_{ref}). The parameters of speed controllers are
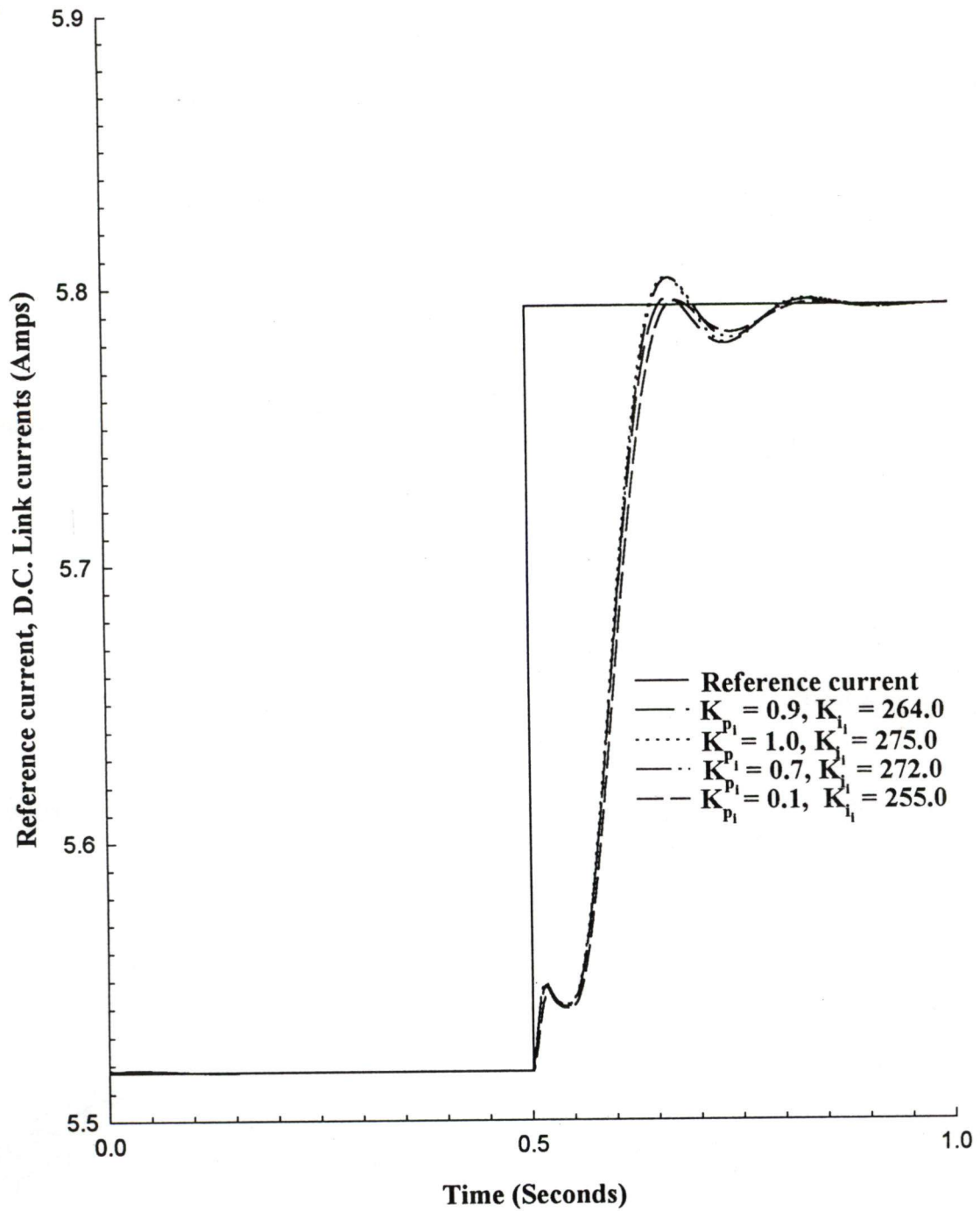
Fig 6.9. Transient response of current loop

191

also selected with the help of D-partitioning technique, followed by frequency scanning. For the design of speed controller parameters, current controller parameters are pre selected and assumed to be constant. For the design of speed controller parameters, perturbed equation (6.44) is considered.

$$F_{21} (p)\Delta\omega_r = F_{18} (p) \Delta v^e_{ds} + F_{19} (p) \Delta v^e_{qs} + [F_{20} (p) + F_{17}(p)]\Delta\omega_e + k F_{15} (p) \Delta I_{dc}$$

$$............ \quad (6.44)$$

Substituting $\Delta\omega_e$ from equation (6.69) in equation (6.44), following equation is obtained.

$$F_{18} (p)\Delta v^e_{ds} + F_{19} (p) \Delta v^e_{qs} + k F_{15}(p) \Delta I_{dc} + [-F_{26(p)}(k_{p_s} +\frac{k_{i_s}}{p}) - F_{27(p)}]\Delta\omega_r = 0$$

$$............(6.99)$$

where,

$$F_{26(p)} = F_{17(p)} + F_{20(p)}$$

$$F_{27(p)} = F_{21(p)} - F_{26(p)}$$

$$\left.\begin{array}{c} \\ \\ \end{array}\right\} \qquad ....(6.100)$$

Considering small perturbation in equation (6.99), together with perturbed equations for machine stator voltage equations (6.46) and (6.47) and perturbed regulators equation (6.76), following equations in matrix form are obtained.

$$\begin{bmatrix} F_{18(p)} & F_{19(p)} & (-F_{26(p)}(k_{p_s} +\frac{k_{i_s}}{p})-F_{27(p)}) & kF_{15(p)} \\ F_{24(p)} & -F_{25(p)} & (F_{7(p)} \psi^e_{dr} - F_{8(p)} \psi^e_{qr} + (k_{p_s} +\frac{k_{i_s}}{p} -1)F_{22(p)}) & kF_{6(p)} \\ F_{25(p)} & F_{24(p)} & (F_{8(p)} \psi^e_{dr} + F_{7(p)} \psi^e_{qr} + (k_{p_s} +\frac{k_{i_s}}{p} -1)F_{23(p)}) & -kF_{5(p)} \\ 0 & -1.5k & (k_{p_i} +\frac{k_{i_i}}{p})[\{(k_{p_s} +\frac{k_{i_s}}{p}) (-A_1 -A_2)\}+A_2] & -(k_{p_i} +\frac{k_{i_i}}{p} +r_f +pl_f) \end{bmatrix} \begin{bmatrix} \Delta v^e_{ds} \\ \Delta v^e_{qs} \\ \Delta\omega_r \\ \Delta I_{dc} \end{bmatrix} = 0$$

$$..........(6.101)$$

192

Accordingly the characteristic equation is given by

$$D(p) = 0 \qquad\qquad (6.102)$$

where D (p) is the characteristic polynomial stated below in matrix form:

$$D(P)=\begin{vmatrix} F_{18(p)} & F_{19(p)} & (-F_{26(p)}(k_{p_s}+\dfrac{k_{i_s}}{p})-F_{27(p)}) & kF_{15(p)} \\[2ex] F_{24(p)} & -F_{25(p)} & (F_{7(p)}\,\psi_{dr}^e - F_{8(p)}\,\psi_{qr}^e + (k_{p_s}+\dfrac{k_{i_s}}{p}-1)F_{22(p)}) & kF_{6(p)} \\[2ex] F_{25(p)} & F_{24(p)} & (F_{8(p)}\,\psi_{dr}^e + F_{7(p)}\,\psi_{qr}^e + (k_{p_s}+\dfrac{k_{i_s}}{p}-1)F_{23(p)}) & -kF_{5(p)} \\[2ex] 0 & -1.5k & (k_{p_i}+\dfrac{k_{i_i}}{p})[\{(k_{p_s}+\dfrac{k_{i_s}}{p})(-A_1-A_2)\}+A_2] & -(k_{p_i}+\dfrac{k_{i_i}}{p}+r_f+pl_f) \end{vmatrix}$$

$$\ldots\ldots(6.103)$$

Interchanging the 1st and 3rd column of D (p)

$$D(p)=\begin{vmatrix} (-F_{26(p)}(k_{p_s}+\dfrac{k_{i_s}}{p})-F_{27(p)}) & F_{19(p)} & F_{18(p)} & kF_{15(p)} \\[2ex] (F_{7(p)}\,\psi_{dr}^e - F_{8(p)}\,\psi_{qr}^e + (k_{p_s}+\dfrac{k_{i_s}}{p}-1)F_{22(p)}) & -F_{25(p)} & F_{24(p)} & kF_{6(p)} \\[2ex] (F_{8(p)}\,\psi_{dr}^e + F_{7(p)}\,\psi_{qr}^e + (k_{p_s}+\dfrac{k_{i_s}}{p}-1)F_{23(p)}) & F_{24(p)} & F_{25(p)} & -kF_{5(p)} \\[2ex] (k_{p_i}+\dfrac{k_{i_i}}{p})[\{(k_{p_s}+\dfrac{k_{i_s}}{p})(-A_1-A_2)\}+A_2] & -1.5k & 0 & -(k_{p_i}+\dfrac{k_{i_i}}{p}+r_f+pl_f) \end{vmatrix}$$

$$\ldots\ldots(6.104)$$

The characteristic equation can be written in the following form

193

$$D(p) = \begin{vmatrix} C_3 \left(k_{P_s} + \dfrac{k_{i_s}}{p} \right) + C_4 & C_2 & C_1 & C_5 \\ C_9 \left(k_{P_s} + \dfrac{k_{i_s}}{p} - 1 \right) + C_8 & C_7 & C_6 & C_{10} \\ C_{14} \left(k_{P_s} + \dfrac{k_{i_s}}{p} - 1 \right) + C_{13} & C_{12} & C_{11} & C_{15} \\ C_{18} \left(k_{P_s} + \dfrac{k_{i_s}}{p} \right) + C_{19} & C_{17} & C_{16} & C_{20} \end{vmatrix} = 0 \qquad (6.105)$$

where,

$$C_1 = F_{18(p)}$$

$$C_2 = F_{19(p)}$$

$$C_3 = -F_{26(p)}$$

$$C_4 = -F_{27(p)}$$

$$C_5 = k\,F_{15(p)}$$

$$C_6 = F_{24(p)}$$

$$C_7 = F_{25(p)}$$

$$C_8 = F_{22(p)}$$

$$C_9 = F_{7(p)}\,\psi_{dr}^e - F_{8(p)}\,\psi_{qr}^e$$

$$C_{10} = k\,F_{6(p)}$$

$$C_{11} = F_{25(p)}$$

$$C_{12} = F_{24(p)}$$

$$C_{13} = F_{23(p)}$$

$$C_{14} = F_{8(p)}\,\psi_{dr}^e + F_{7(p)}\,\psi_{qr}^e$$

$$C_{15} = -k\,F_{5(p)}$$

194

$$C_{16} = 0$$

$$C_{17} = -1.5k$$

$$C_{18} = -(k_{p_i} + \frac{k_{i_i}}{p})(A_1 + A_2)$$

$$C_{19} = (k_{p_i} + \frac{k_{i_i}}{p}) A_2$$

$$C_{20} = -(k_{p_i} + \frac{k_{i_i}}{p} + r_f + pl_f)$$

After expanding equation (6.105), following equation is achieved.

$$k_{p_i} C_{33} + k_{i_i} C_{31} + C_{34} = 0 \tag{6.106}$$

where,

$$C_{34} = pC_{32}$$

$$C_{33} = pC_{31}$$

$$C_{32} = C_{24} + C_{25} + C_{27} + C_{29}$$

$$C_{31} = C_{23} + C_{26} + C_{28} + C_{30}$$

$$C_{30} = -C_5 \left(C_9 \left(C_{12} C_{16} - C_{11} C_{17} \right) - C_7 \left(C_{14} C_{16} - C_{11} C_{18} \right) + C_6 \left(C_{14} C_{17} - C_{12} C_{18} \right) \right)$$

$$C_{29} = -C_5 \left(C_{21} \left(C_{12} C_{16} - C_{11} C_{17} \right) - C_7 \left(C_{22} C_{16} - C_{11} C_{19} \right) + C_6 \left(C_{22} C_{17} - C_{12} C_{19} \right) \right)$$

$$C_{28} = C_1 \left(C_9 \left(C_{12} C_{20} - C_{15} C_{17} \right) - C_7 \left(C_{14} C_{20} - C_{15} C_{18} \right) + C_{10} \left(C_{14} C_{17} - C_{12} C_{18} \right) \right)$$

$$C_{27} = C_1 \left(C_{21} \left(C_{12} C_{20} - C_{15} C_{17} \right) - C_7 \left(C_{22} C_{20} - C_{15} C_{19} \right) + C_{10} \left(C_{22} C_{17} - C_{12} C_{19} \right) \right)$$

$$C_{26} = -C_2 \left(C_9 \left(C_{11} C_{20} - C_{15} C_{16} \right) - C_6 \left(C_{14} C_{20} - C_{15} C_{18} \right) + C_{10} \left(C_{14} C_{16} - C_{11} C_{18} \right) + C_{10} \left(C_{22} C_{16} - C_{11} C_{19} \right) \right)$$

$$C_{25} = -C_2 \left(C_{21} \left(C_{11} C_{20} - C_{15} C_{16} \right) - C_6 \left(C_{22} C_{20} - C_{15} C_{19} \right) \right.$$
$$\left. + C_{10} \left(C_{22} C_{16} - C_{11} C_{19} \right) \right)$$

$$C_{24} = C_4 \left(C_7 \left(C_{11} C_{22} - C_{15} C_{16} \right) - C_6 \left(C_{12} C_{20} - C_{15} C_{17} \right) \right.$$
$$\left. + C_{10} \left(C_{12} C_{16} - C_{11} C_{17} \right) \right)$$

$$C_{23} = C_3 \left(C_7 \left(C_{11} C_{20} - C_{15} C_{16} \right) - C_6 \left(C_{12} C_{20} - C_{15} C_{17} \right) \right.$$
$$\left. + C_{10} \left(C_{12} C_{16} - C_{11} C_{17} \right) \right)$$

$$C_{22} = C_{13} - C_{14}$$

$$C_{21} = C_8 - C_9$$

Separating equation (6.106) in real and imaginary parts for any complex value of the p operator.

$$k_{p.} C_{33r} + k_{i.} C_{31r} + C_{34r} = 0 \tag{6.107}$$

$$k_{p.} C_{33i} + k_{i.} C_{31i} + C_{34i} = 0 \tag{6.108}$$

where, real and imaginary values for complex terms c_{31}, c_{33} and c_{34} are written with a further suffix r and i respectively.

Solving equations (6.107) and (6.108), $k_{p.}$ and $k_{i.}$ are obtained as shown below:

$$k_{p.} = \frac{\begin{vmatrix} -C_{34r} & C_{31r} \\ -C_{34i} & C_{31i} \end{vmatrix}}{\Delta} \tag{6.109}$$

$$k_{i.} = \frac{\begin{vmatrix} C_{33r} & -C_{34r} \\ C_{33i} & -C_{34i} \end{vmatrix}}{\Delta} \tag{6.110}$$

196

where,

$$\Delta = C_{33r} C_{31i} - C_{31r} C_{33i} \tag{6.111}$$

As earlier, substituting $p = (-\sigma + j\omega)$, and varying ω from $-\infty$ to $+\infty$, for a fixed value of $\sigma = 0.0$, the D- partition boundary is obtained in (k_{p_s}, k_{i_s}) plane using equations (6.109) and (6.110), as shown in Fig. 6.10. There is a spatial line along real axis for $\omega = 0$. It is obtained using equation (6.107) for $\omega = 0.0$ and it is shaded as shown in Fig. 6.10.

By substituting $p = (-\sigma + j\omega)$ and $p = (-\xi\omega + j\omega\sqrt{(1-\xi^2)})$, two sets of relative stability boundaries curves are obtained by varying σ and ξ over a wide range and regions of better stability are obtained in both the case; regions are shown in Figs. 6.11 and 6.12. For checking the stability of region for ($\sigma = 0.0$) in the D-partition plane, the frequency scanning method is applied by considering a point ($k_{p_s} = 0.5, k_{i_s} = 1.0$) inside the probable stable region and a point outside ($k_{p_s} = 2.0, k_{i_s} = 3.0$) this region. Corresponding to these points, the curves for characteristic vectors are plotted in the complex plane by varying ω from $-\infty$ to $+\infty$ as shown in Figs. 6.13 and 6.14 respectively. The curves show that for the first case, the origin lies in the inner most region, and in the second case, origin lies out side the inner most region. This confirms that the operating point ($k_{p_s} = 0.5, k_{i_s} = 1.0$) is stable, while the point ($k_{p_s} = 2.0, k_{i_s} = 3.0$) is unstable.
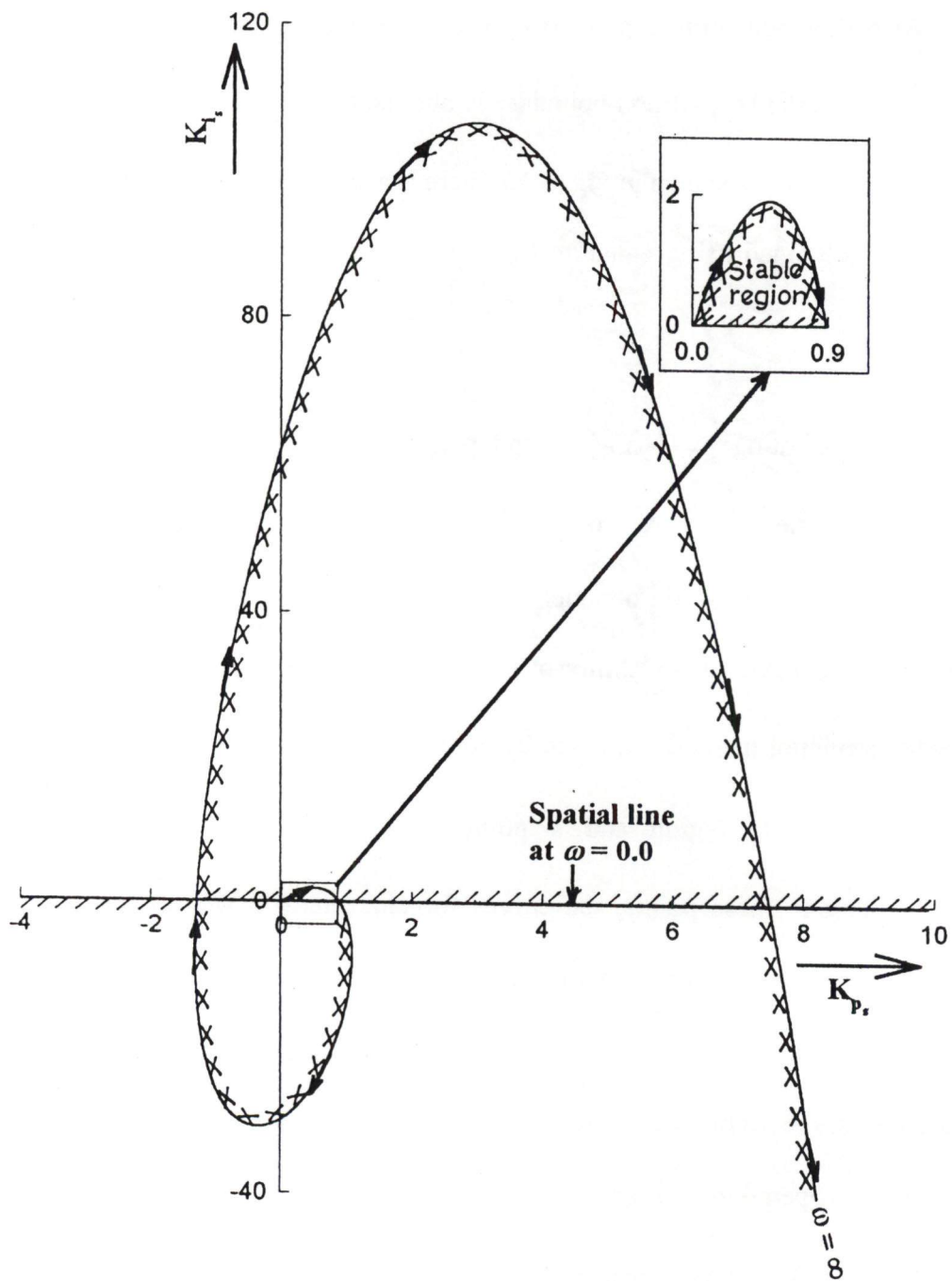
Fig. 6.10. D-partition boundary for speed controller design for absolute stability

198
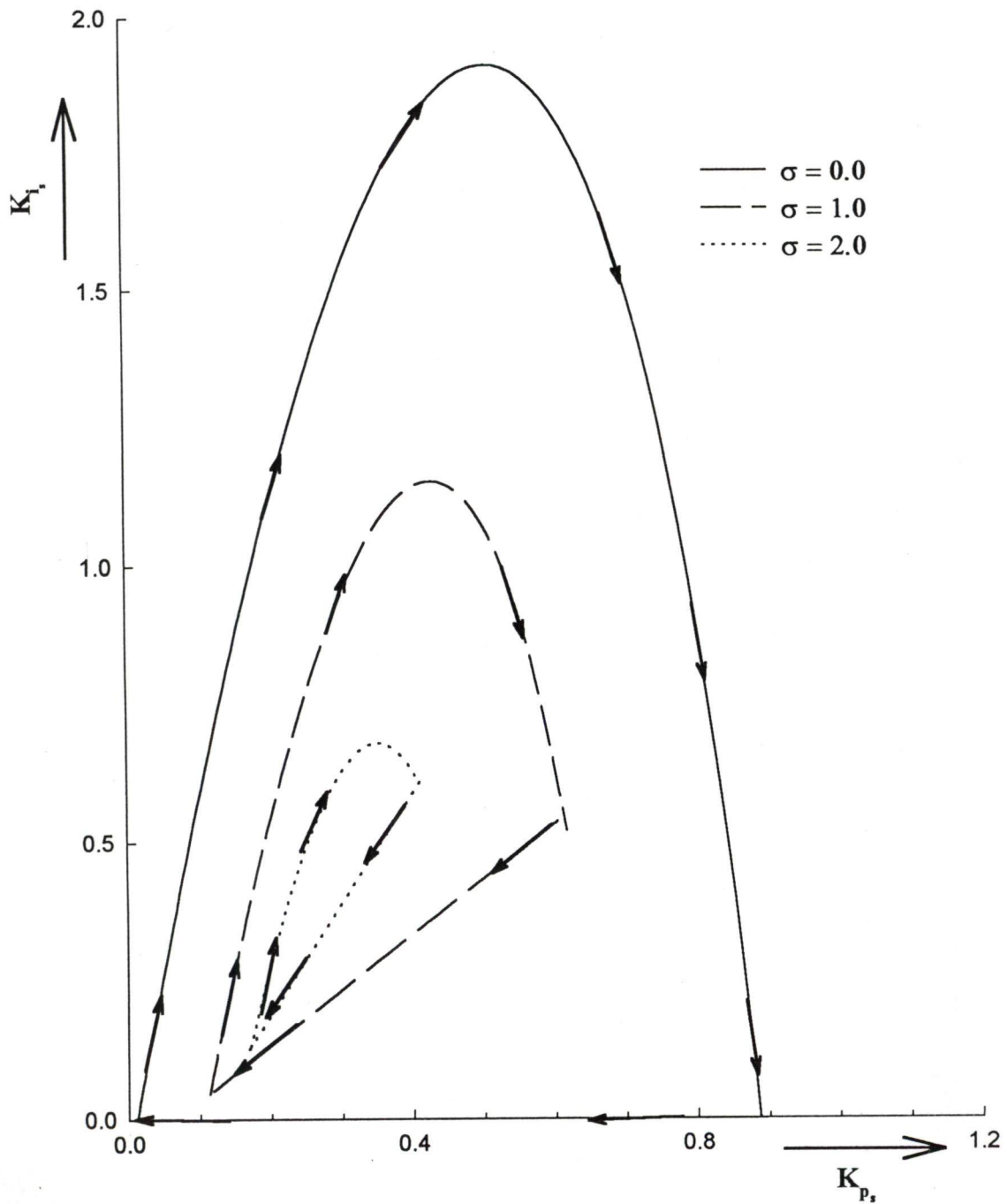
Fig 6.11. Relative stability boundries for speed controller parameters for different values of σ
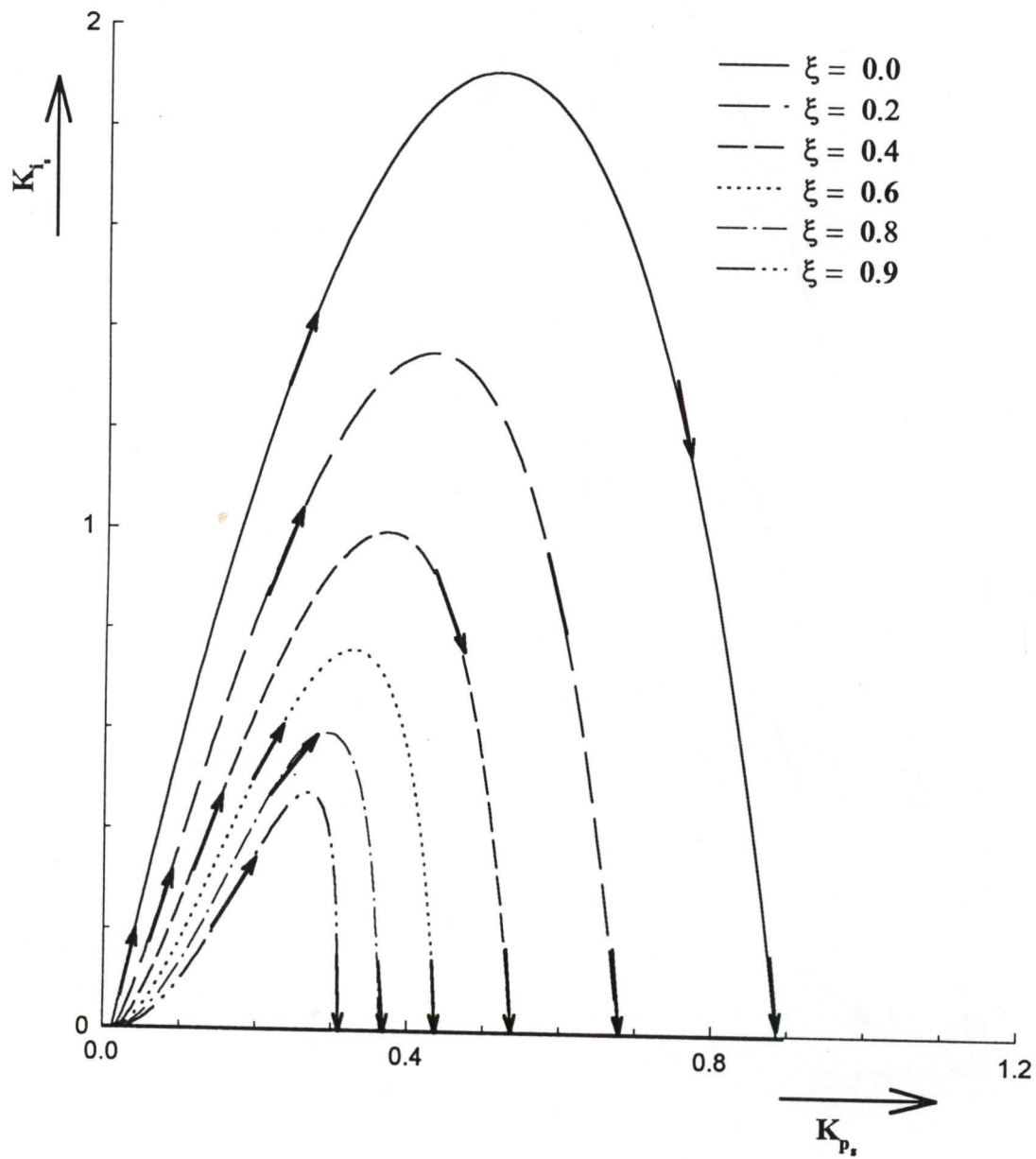
Fig 6.12. Relative stability boundries for speed controller parameters
for different values of ξ

Not to scale
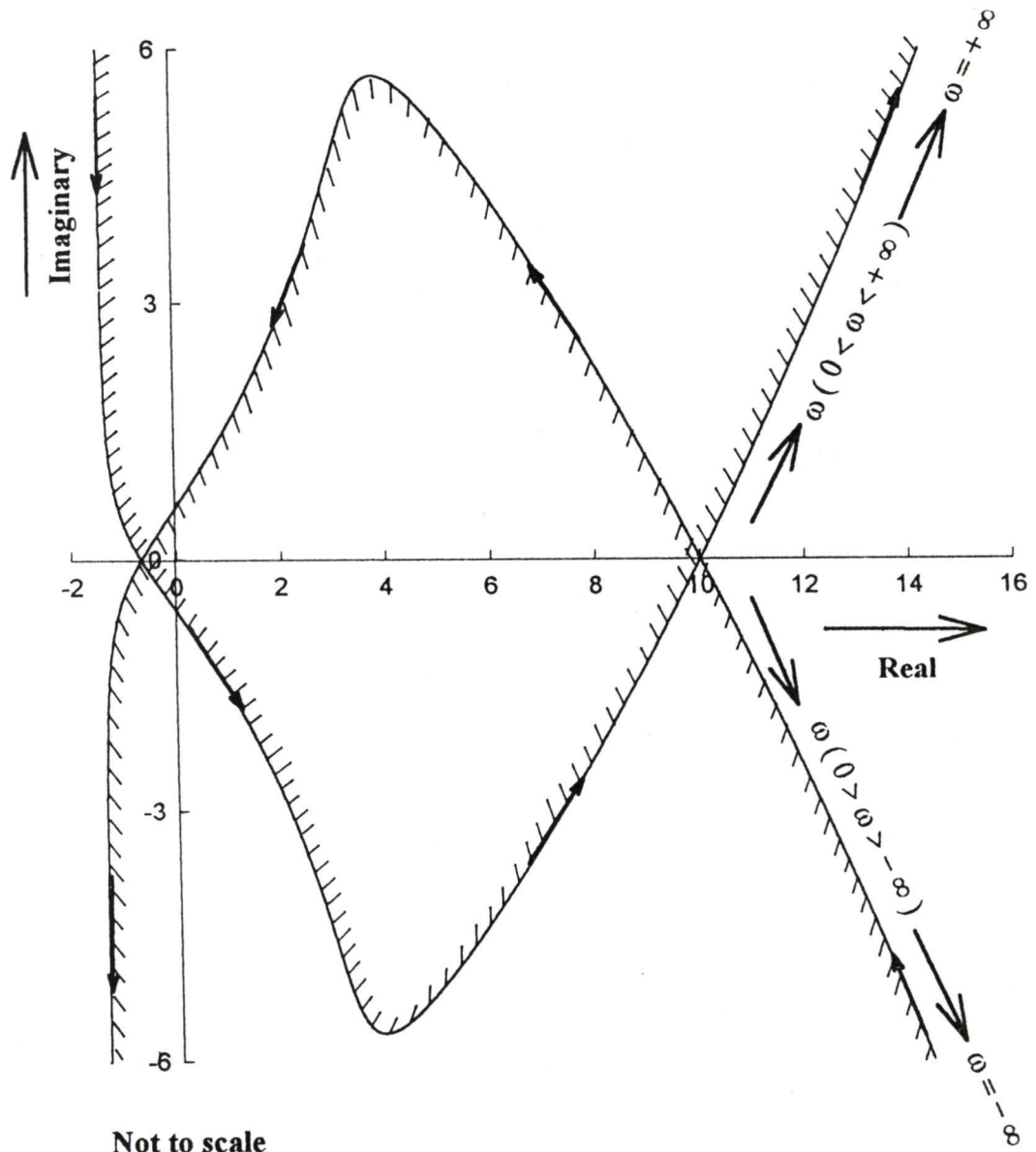
$\sigma = 0.0, \ K_{p.} = 0.5, \ K_{I.} = 1.0$

Fig. 6.13. Frequency for speed controller parameters at $\sigma = 0.0$ (Stable)
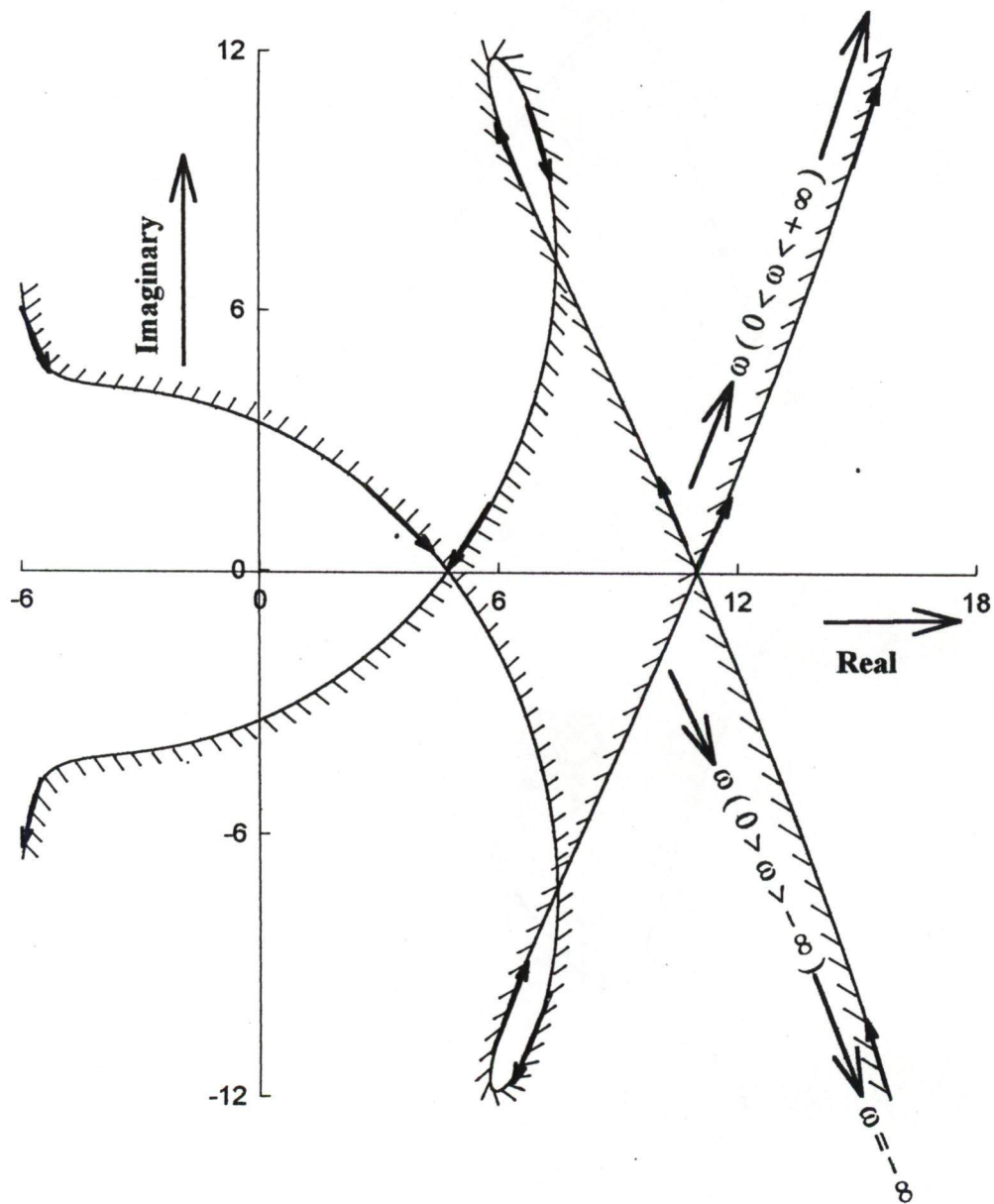
$\sigma = 0.0, \ K_{P_s} = 2.0, \ K_{I_s} = 3.0$

Fig 6.14. Frequency scanning curve for speedcontroller parameters at $\sigma = 0.0$ (Unstable)

For the relative stability curves of (ξ), two points are considered, one ($k_{p_s} = 0.4, k_{i_s} = .8$) at $\xi \geq 0.2$, other ($k_{p_s} = 0.8, k_{i_s} = 1.6$) at $\xi < 0.2$. The frequency scanning is applied to these points, by varying ω from $-\infty$ to $+\infty$. The frequency scanning curves corresponding to these points are shown in Fig. 6.15 and 6.16 respectively. The curve shown in Fig. 6.15 includes the origin in the sense of shading of the curve, while the curve shown in Fig. 6.16 does not include the origin. This confirms that the point in the region $\xi \geq 0.2$ is having better relative stability than the point in the region $\xi < 0.2$.

Relative stability boundary curves plotted for different values of σ and ξ, show that the stability regions keep on shrinking, for higher values of σ and ξ. The stability regions almost vanish for ($\sigma > 2.0$ and $\xi > 0.9$).

The final selection of speed controller parameters (k_{p_s} and k_{i_s}) is made by comparing the transient response of the speed loop for step variation in reference speed from 1.0 to 1.05 of rated speed, using equations (6.91 to 6.98) and following equations.

$$p\,\omega_r = (\frac{P}{2J})\,(t_e - t_l) \tag{6.112}$$

$$t_e = \frac{3}{2}\frac{P}{2}l_m\,(i_{qs}^e\,i_{dr}^e - i_{ds}^e\,i_{qr}^e) \tag{6.113}$$

$$t_l = t_L\,(\frac{\omega_r}{\omega_{base}}) \tag{6.114}$$

where,

$$\omega_{base} = 314\,\text{rad/sec}$$

$$\omega_{sl}^* = k_{p_s}\,(\omega_{ref} - \omega_r) + \frac{k_{i_s}}{T_s}\int_0^\infty (\omega_{ref} - \omega_r)\,dt \tag{6.115}$$
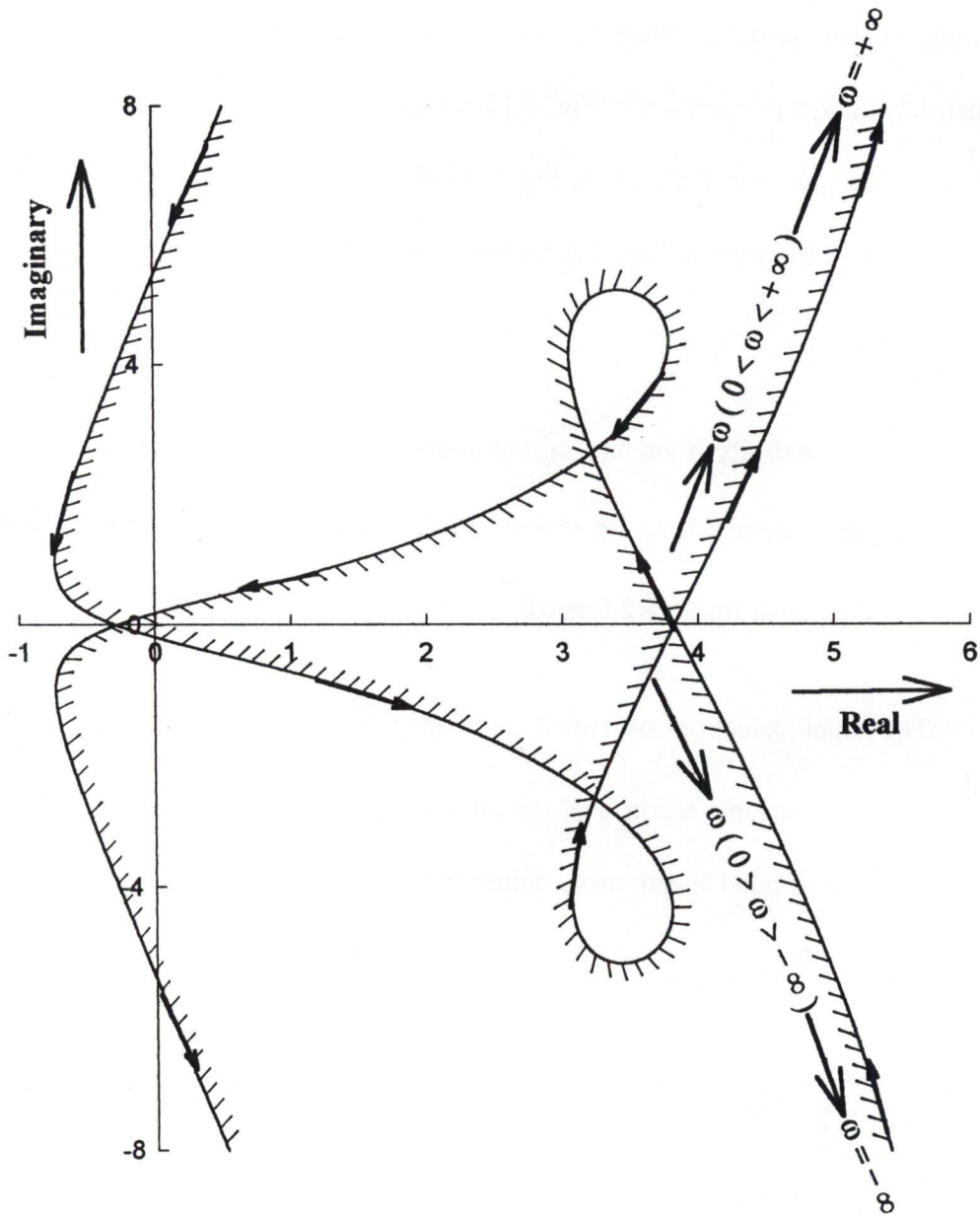
$\xi > = 0.2, K_{P_s} = 0.4, K_{I_s} = 0.8$

Fig 6.15. Frequency scanning curve for speed controller parameters having $\xi > = 0.2$
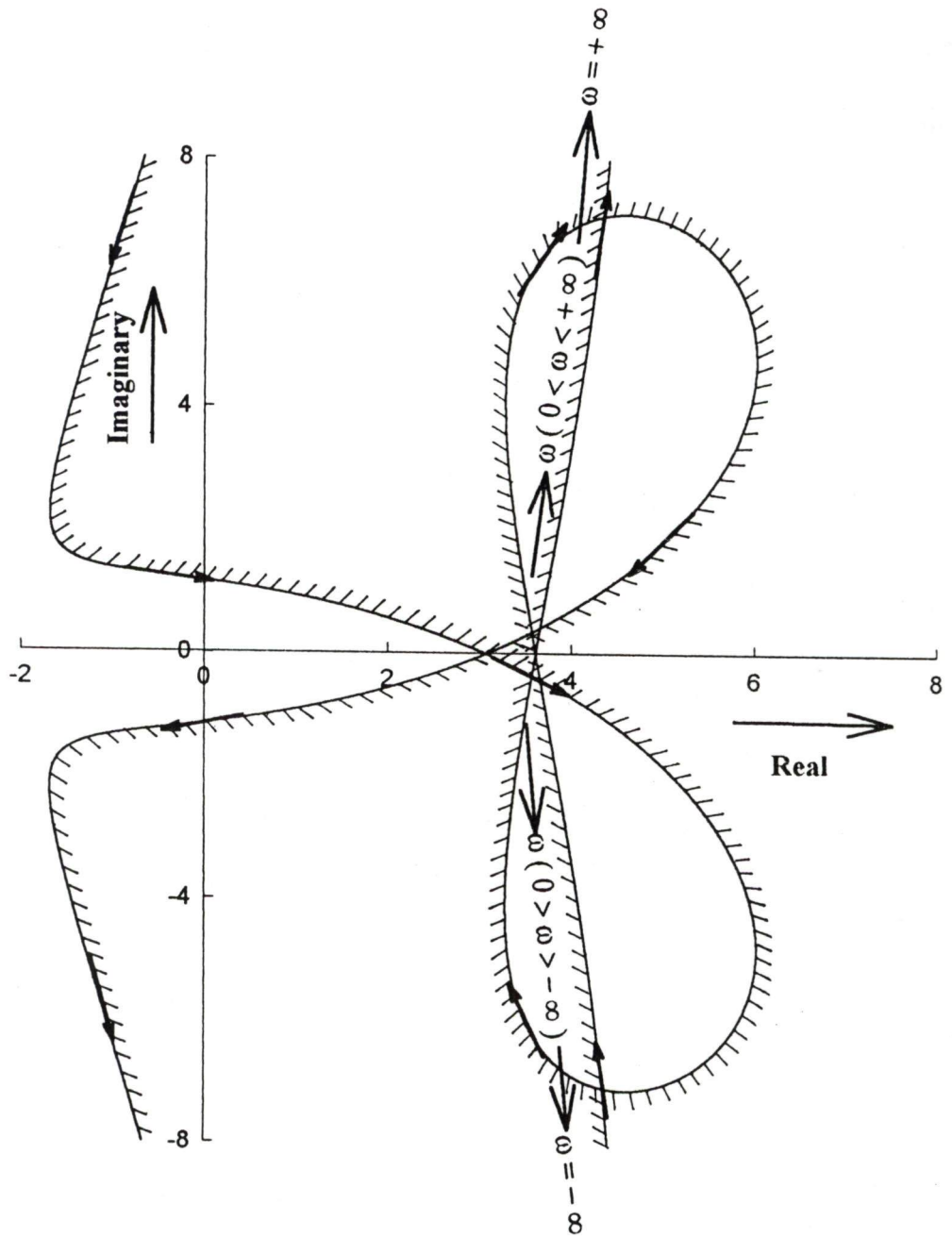
$\xi < 0.2, \ K_{P_s} = 0.8, \ K_{I_s} = 1.6$

Fig 6.16. Frequency scanning curve for speed controller parameters having $\xi < 0.2$

$$\omega_e = \omega_r + \omega_{sl}^*$$

<div align="right">(6.116)</div>

To get the parametric region of minimum over shoot and minimum settling time, relative stability curves are drawn for different values of σ and ξ in the (k_{p_s}, k_{i_s}) plane by varying ω from $-\infty$ to $+\infty$, as shown in Fig 6.17. A high values of σ and ξ gives the stable region of better performance. A common region C, having high value of σ and ξ is selected; it is shown as shaded region in Fig 6.17. Fig 6.17 shows that in the shaded region C, speed loop controller has $\sigma \geq 2.0$ and $\xi \geq 0.9$.

The transient response of the speed loop are plotted for different sets of $(k_{p_s}$ and $k_{i_s})$ values chosen from the region C of Fig 6.17. The transient response curve shown in Fig 6.18, correspond to some values of $(k_{p_s}$ and $k_{i_s})$. Percentage over shoot and settling time corresponding to these chosen values of $(k_{p_s}$ and $k_{i_s})$ are shown in Table 6.2.

<div align="center">Table 6.2</div>

Case	k_{p_s}	k_{i_s}	% over shoot	Settling time (Seconds)
1.	0.18	0.25	3.28	0.437
2.	0.18	0.27	4.14	0.406
3.	0.15	0.29	3.19	0.391
4.	0.16	0.29	4.01	0.387
5.	0.17	0.29	4.76	0.383
6.	0.19	0.25	4.08	0.432
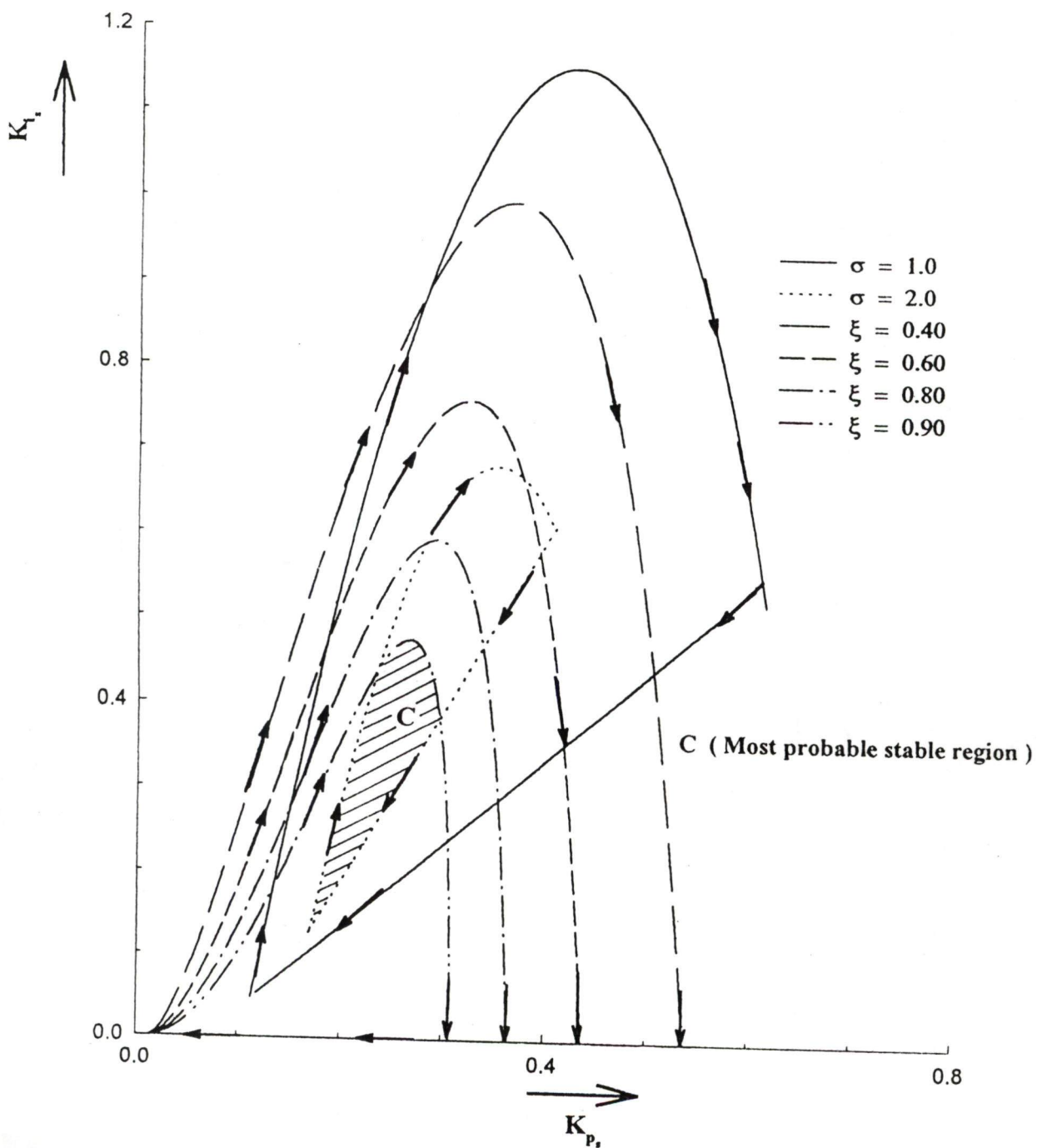
Fig. 6.17. Relative stability boundaries for speed controller parameters for different values of σ and ξ
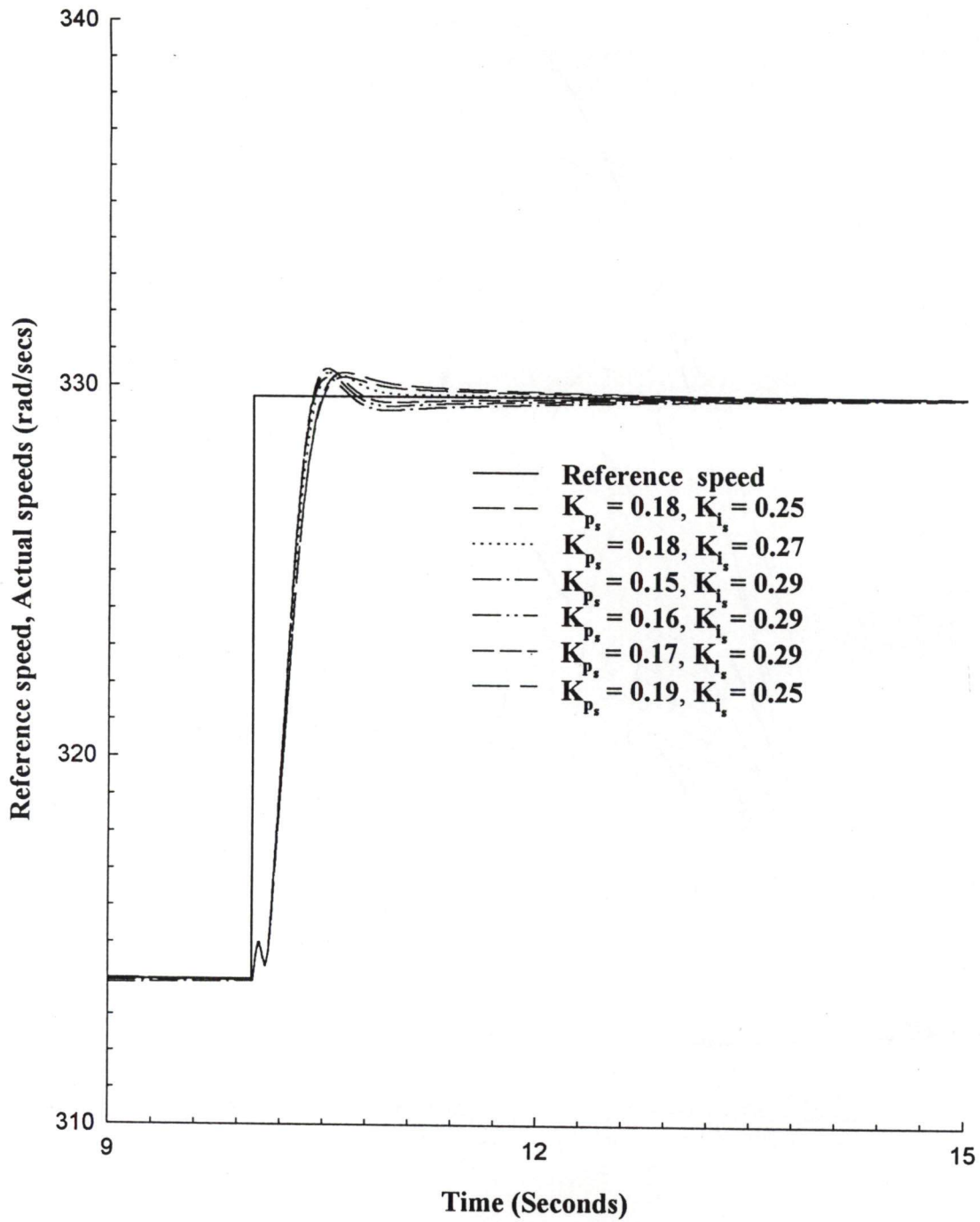
Fig 6.18. Transient response of speed loop

The transient response curves, drawn in Fig. 6.18 show that for ($k_{p_s} = 0.16$ and $k_{i_s} = 0.29$), the overshoot is within the permissible tolerance limit of 5%, and the settling time is near fastest. Hence, the transfer function of the speed controller is

$$(0.16 + \frac{0.29}{p})$$

6.3 CONCLUSION

The modified current source inverter fed induction motor drive has two proportional and integral type controllers, one in current feedback loop, and another in speed feedback loop. These controllers are used to realize the variable speed operation with zero steady state error.

The speed PI controller in the outer loop processes the speed error and hence sets the reference slip speed (ω_{sl}^*) which is required to calculate the reference active (I_{act}^*) and reference reactive (I_{react}^*) currents of the machine and hence reference d.c. link current (I_{ref}). The inner PI current regulator sets the pulse widths of firing pulses of the pulse width modulated rectifier and hence the output voltage of the rectifier.

The transient response of the drive depends upon the choice of speed and current controller parameters. The determination of speed and current controller parameters is done by the D-partition technique. The non - linear equations of the system are linearized by the method of small perturbation about the steady state operating point and the characteristic equations are developed in terms of controller, both for current and speed controller loops. D-partition boundaries are plotted in the parametric plane and stable

regions are identified in the plane of proportional and integral gain parameters of both the controllers. The stability of the identified region is confirmed by the frequency scanning technique for a point inside and outside this region.

For better performance of the drive, constraints of less settling time and good damping are incorporated in the design and the controller parameters are selected from the stable region of high degree of relative stability and good damping ratio.

The final selection of controller parameters is done by comparing the transient response of the drive at different points in the stable region.

To study the transient behaviour of the system, state equations of current loop, speed loop are considered. The selected controller parameters ensure that the response of the system is fast and overshoot within the permissible limit.

EXPERIMENTAL INVESTIGATION OF THE DRIVE

7.1 INTRODUCTION

The current source inverters are more popular as compared to voltage source inverters for the speed control over a wide range, because of controlled current operation. The current control loop does not allow the machine current to exceed the rated value, thus provide inherent over current protection. The pulse width modulated firing pulses of the converters are controlled in closed loop manner to regulate the d.c.link current. The inverter is also operated in PWM mode for reduction of harmonics in the output voltage and current.

This chapter deals with the experimental performance investigation of the drive and its comparison with the analytical steady state performance for both open and closed loop operations. The experimental performance of the drive is investigated based on slip, power output, stator voltage, stator current, efficiency, inverter output power factor, d.c.link voltage, rectifier power factor vs. torque developed by the motor. These characteristics are drawn for both open and closed loop operation and are compared with the analytical results. The transient performance of the drive is determined experimentally.

7.2 OPEN LOOP PERFORMANCE OF MODIFIED CSI-FED INDUCTION MOTOR DRIVE

As discussed in chapter 2, the CSI – fed induction motor should be operated in unstable region of the natural torque-speed characteristic to avoid saturation and to reduce

losses. This needs closed loop operation of the drive. The closed loop operation of the drive is expected to give better performance of the drive; however the drive performance is first investigated in open loop at fixed d.c.link current and different operating frequencies to ensure the proper operation of the drive in closed loop.

The machine is made to run in open loop by neglecting the speed PI processing. However the reference d.c.link current is fixed at a desired value in the software. The current PI processing is carried out at every 1ms to maintain the d.c.link current by adjusting the firing pulses of the pulse width modulated converter. The operating frequency is inputted through keyboard of personal computer to operate the machine at the desired frequency.

To investigate the performance of the drive in open loop the machine is run at variable operating frequencies and fixed d.c.link current and load test is performed. The various performance characteristics such as slip, power output, stator voltage, stator current, efficiency, inverter output power factor, d.c.link voltage, rectifier power factor are determined and plotted against developed torque at different operating frequencies. The performance curves for operating frequencies 62.8 rad/sec, 125.6 rad/sec, 188.4 rad/sec, 314 rad/sec at fixed d.c.link current of 3.0 Amp are shown in Figs 7.1 to 7.32.To confirm the validity of the mathematical model of the drive, the performance characteristics of the drive at the above operating frequencies and above d.c. link current are compared with the computed performance. The computed performance curves are also shown in Figs 7.1 to 7.32. The analytical performance curves are drawn by considering the following assumptions such as no core loss, ripple free d.c.link current, no switching transients, loss- less inverter. The various performance curves are discussed below. The performance curves obtained experimentally and analytically are almost

identical at each operating frequency except at the operating frequency 188.4 rad/sec, due to resonance effect.

(i) Slip vs Torque

The experimental and analytical slip vs torque performance curves are shown in Figs 7.1,7.2,7.3,7.4 at different operating frequencies and at a fixed value of d.c.link current. The experimental and analytical curves are quite close to each other. Slight deviation in the two curves is because of various assumptions taken in the determination of analytical curves. For the same value of torque, slip obtained experimentally is more in comparison to the slip obtained analytically, since due to various power losses motor is not able to generate the same amount of torque at any speed as determined analytically. The difference in slip at low operating frequency is high, because at low value of operating frequency the exact estimation of speed is difficult. In both the cases slip increases with the increase in torque.

(ii) Power output vs Torque

Power output vs torque curves obtained experimentally and computed analytically are shown in Figs 7.5 7.6,7.7,7.8 at different operating frequencies and at a fixed value of d.c.link current. Both the curves are almost identical at each operating frequency. For any value of torque, power output obtained experimentally is less in comparison to the power output obtained analytically because the slip corresponding to any value of torque obtained practically is more than the analytically obtained slip. The power output increases with the increase in torque in both the cases.

213
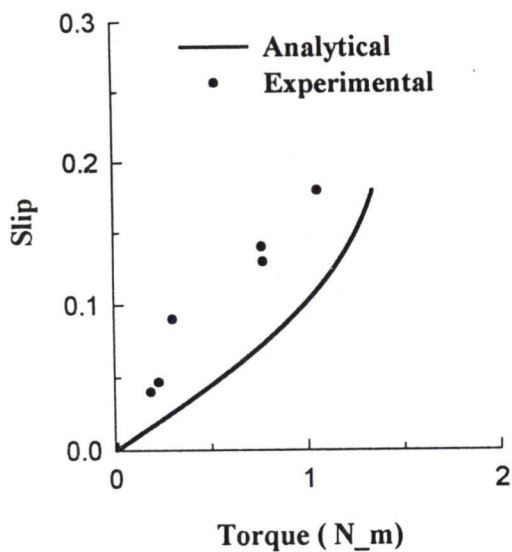
Fig 7.1. Slip vs. torque characteristics
(I_{dc} = 3.0 A,ω_e = 62.8 rad/sec,c = 150μF/phase)
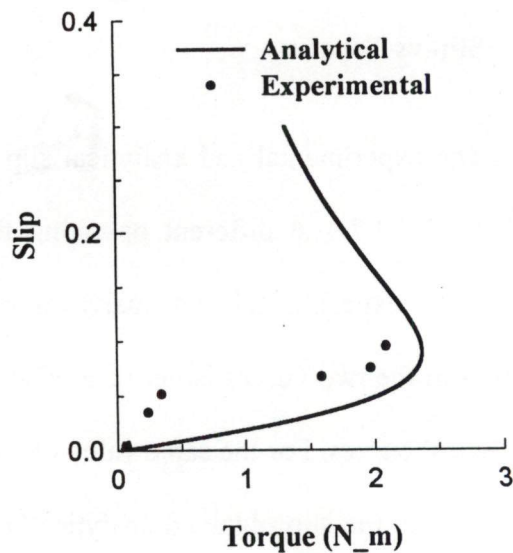
Fig 7.2. Slip vs. torque characteristics
(I_{dc} = 3.0 A,ω_e = 125.6 rad/sec,c = 150 μF/phase)
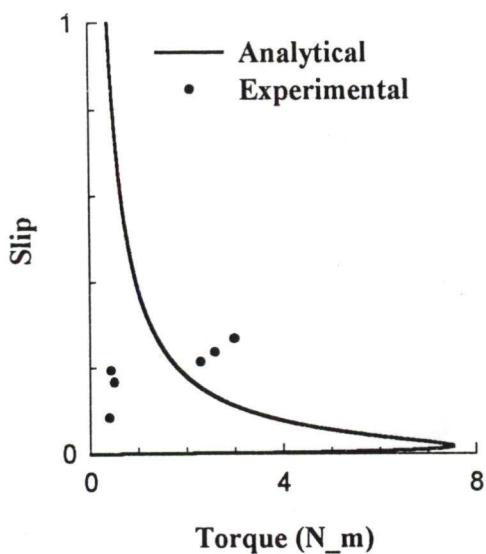
Fig 7.3. Slip vs. torque characteristics
(I_{dc} = 3.0 A,ω_e = 188.4 rad/sec,c = 150 μF/phase)
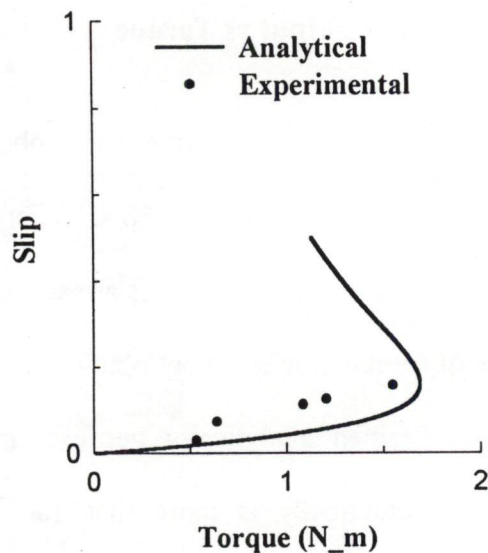
Fig 7.4. Slip vs. torque characteristics
(I_{dc} = 3.0 A,ω_e = 314 rad/sec,c = 150 μF/phase)
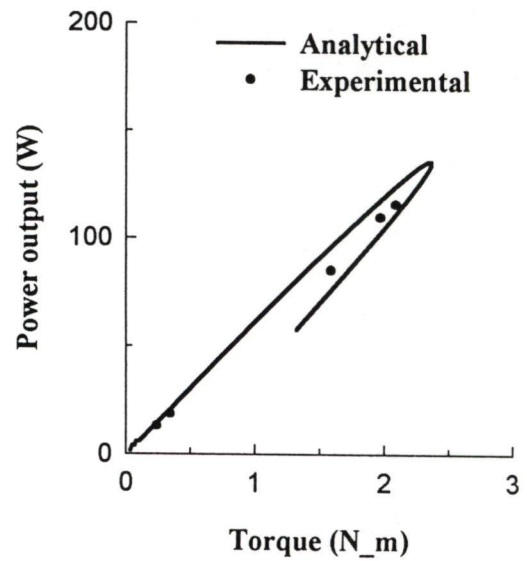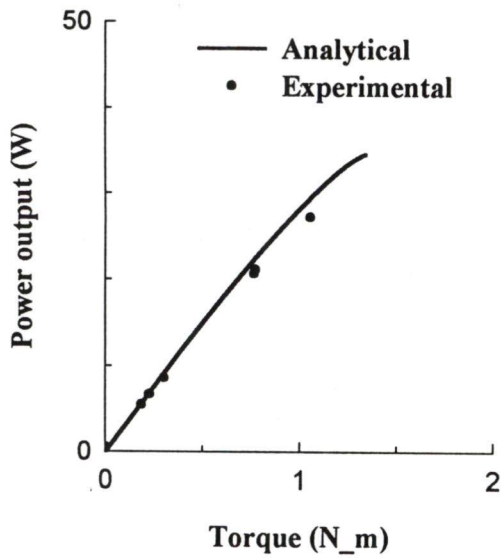
Fig 7.5. Power output vs. torque characteristics
$(I_{dc} = 3.0$ A, $\omega_e = 62.8$ rad/sec, $c = 150$ μF/phase)

Fig 7.6. Power output vs. torque characteristics
$(I_{dc} = 3.0$ A, $\omega_e = 125.6$ rad/sec, $c = 150$ μF/phase)
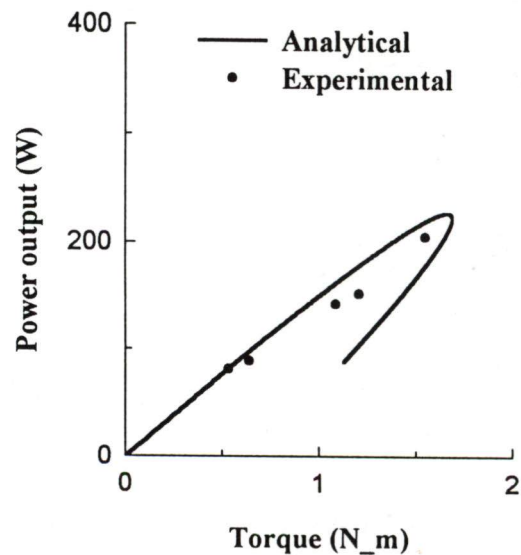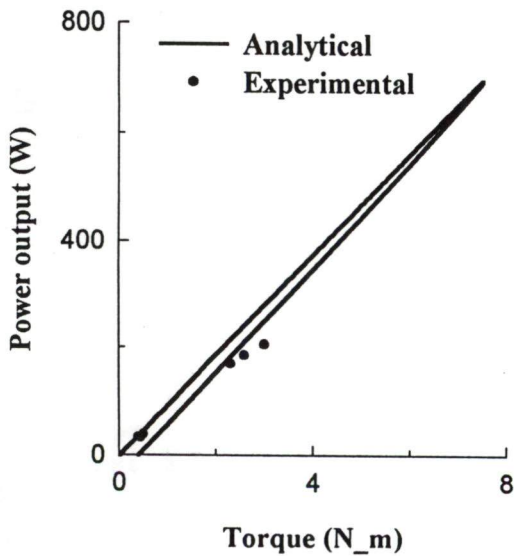
Fig 7.7. Power output vs. torque characteristics
$(I_{dc} = 3.0$ A, $\omega_e = 188.4$ rad/sec, $c = 150$ μF/phase)

Fig 7.8. Power output vs. torque characteristics
$(I_{dc} = 3.0$ A, $\omega_e = 314$ rad/sec, $c = 150$ μF/phase)

215

(iii)   Stator current per phase vs Torque

The experimentally obtained stator current variation with respect to torque and analytically obtained stator current vs torque curves are shown in Figs. 7.9, 7.10, 7.11,7.12. The stator current in both the cases are almost identical and very near to each other at each operating frequency. At each operating frequency, the stator current variation with respect to torque is very small. As discussed already in chapter 3, with capacitance at the machine terminals the magnetization and rotor currents are adjusted in such a manner that their phasor sum i.e. stator current varies very slowly with the torque at each operating frequency.

(iv)   Stator voltage per phase vs Torque

Stator voltages per phase vs torque curves obtained analytically and determined experimentally at the different operating frequencies are shown in Figs. 7.13,7.14,7.15,7.16. Both the curves are almost matching at each operating frequency. The variation of stator voltage with respect to torque is very less in each case because of slow variation of stator current and net impedance (including stator leakage impedance, magnetizing impedance and rotor leakage impedance) with the torque developed.

(v)   Efficiency vs Torque

Percentage efficiency vs torque curves obtained experimentally and analytically are shown in Figs. 7.17,7.18,7.19,7.20. At each operating frequency the analytical and experimental curves are quite close to each other except at low operating frequency $\omega_e =$ 62.8 rad/sec. At low value of operating frequency, the effect of losses not considered in analytical estimation is more prominent in comparison to high value of operating
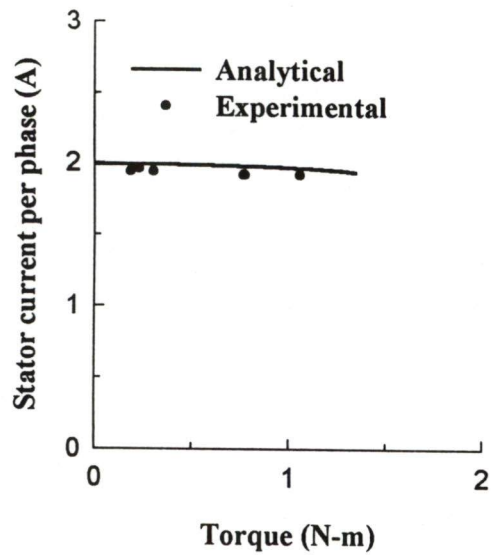
Fig 7.9. Stator current vs. torque characteristics (I_{dc} = 3.0 A, ω_e = 62.8 rad/sec, c = 150 μF/phase)
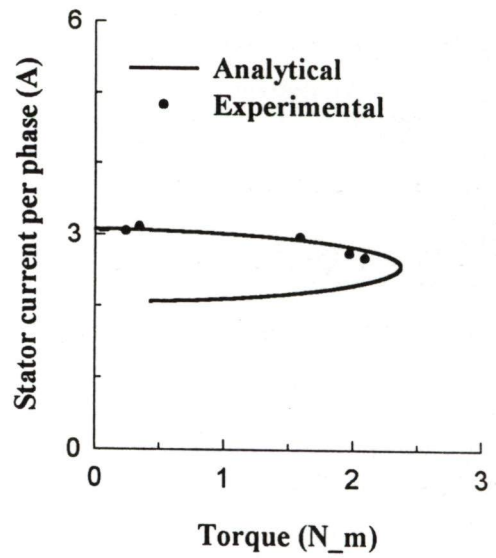
Fig 7.10. Stator current vs. torque characteristics (I_{dc} = 3.0 A, ω_e = 125.6 rad/sec, c = 150 μF/phase)

Fig 7.11. Stator current vs. torque characteristics (I_{dc} = 3.0 A, ω_e = 188.4 rad/sec, c = 150 μF/phase)

Fig 7.12. Stator current vs. torque characteristics (I_{dc} = 3.0 A, ω_e = 314 rad/sec, c = 150 μF/phase)

217

Fig 7.13. Stator voltage vs. torque characteristics (I_{dc}= 3.0 A,ω_e = 62.8 rad/sec,c = 150 μF/phase)

Fig 7.14. Stator voltage vs. torque characteristics (I_{dc}= 3.0 A,ω_e = 125.6 rad/sec,c = 150 μF/phase)

Fig 7.15. Stator voltage vs. torque characteristics (I_{dc}= 3.0 A,ω_e = 188.4 rad/sec,c = 150 μF/phase)

Fig 7.16. Stator voltage vs. torque characteristics (I_{dc}= 3.0 A,ω_e = 314 rad/sec,c = 150 μF/phase)
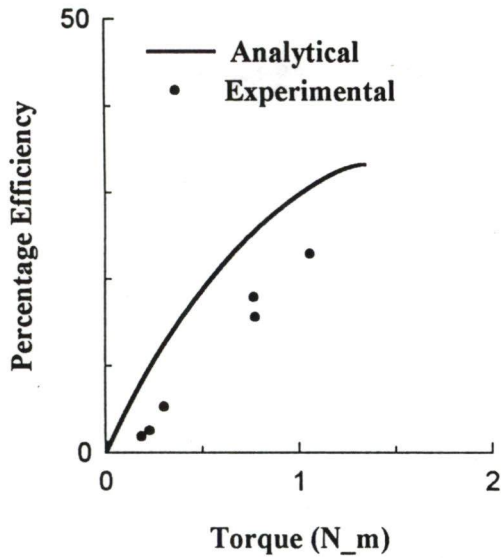
Fig 7.17. Efficiency vs. torque characteristics
(I_{dc} = 3.0 A, ω_e = 62.8 rad/sec, c = 150 μF/phase)
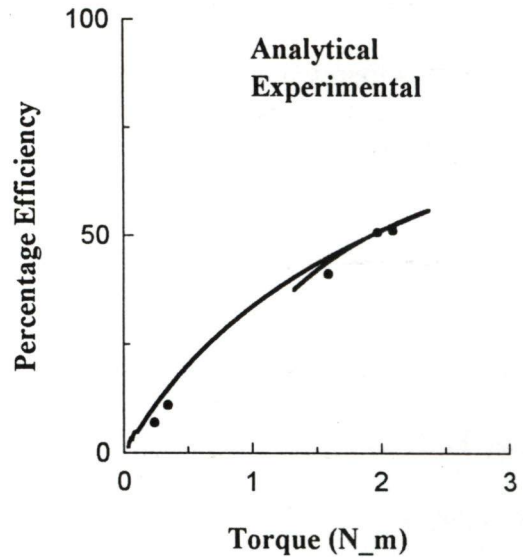
Fig 7.18. Efficiency vs. torque characteristics
(I_{dc} = 3.0 A, ω_e = 125.6 rad/sec, c = 150 μF/phase)
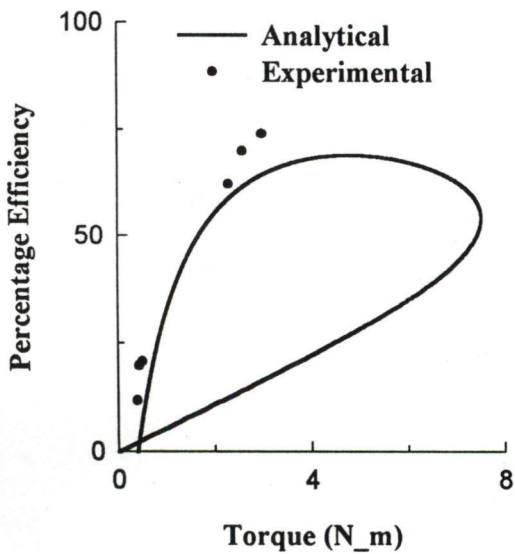
Fig 7.19. Efficiency vs. torque characteristics
(I_{dc} = 3.0 A, ω_e = 188.4 rad/sec, c = 150 μF/phase)
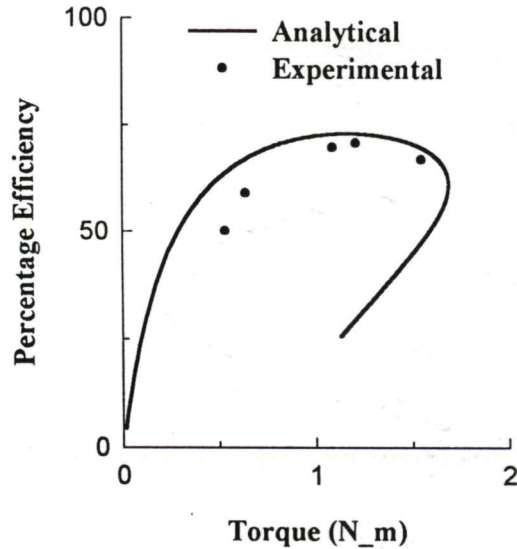
Fig 7.20. Efficiency vs. torque characteristics
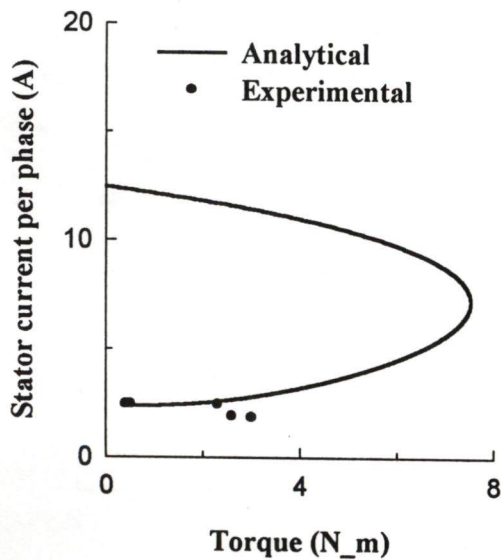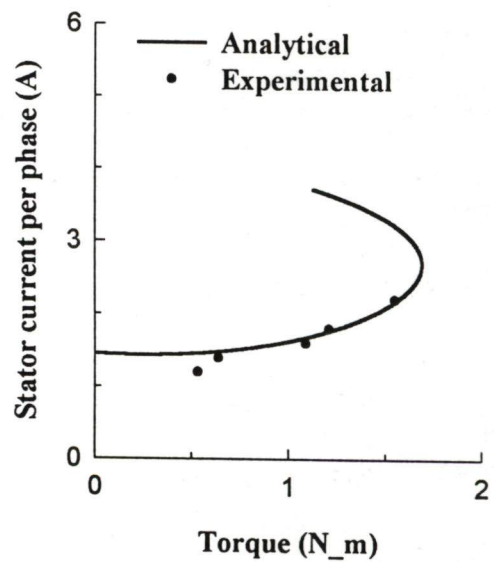(I_{dc} = 3.0 A, ω_e = 314 rad/sec, c = 150 μF/phase)

219

frequency, hence efficiency obtained practically is quite less than analytical value. In both the cases at each operating frequency the efficiency increases with the increase in torque till maximum efficiency is achieved. At any value of torque experimentally obtained efficiency is less than the analytically obtained efficiency because of negligence of core, friction and windage losses.

(vi) Inverter output power factor vs Torque

The analytical and experimental inverter output power factor vs torque curves are shown in Figs 7.21,7.22,7.23,7.24. Both the curves are quite close to each other at different operating frequency. In both the cases as usual the power factor of the machine increases with the torque. Hence power factor of the inverter also increases with the increase in torque at each operating frequency.

(vii) D.C. Link voltage vs Torque

The analytical and experimental d.c.link voltage vs torque curves are shown in Figs 7.25, 7.26, 7.27, 7.28. Both the curves are quite close to each other. The d.c.link voltage increases with the increase in torque at each operating frequency. For fixed value of d.c.link current the d.c link voltage depends upon the input power demand of the machine. As the torque increases the power demand of the drive increases; hence d.c.link voltage increases with the torque at each operating frequency.

(viii) Rectifier power factor vs Torque

The rectifier power factor obtained analytically and experimentally and their variation with respect to torque are shown in Figs 7.29,7.30,7.31,7.32. Both the power factors are quite close to each other at each value of operating frequency and torque. The
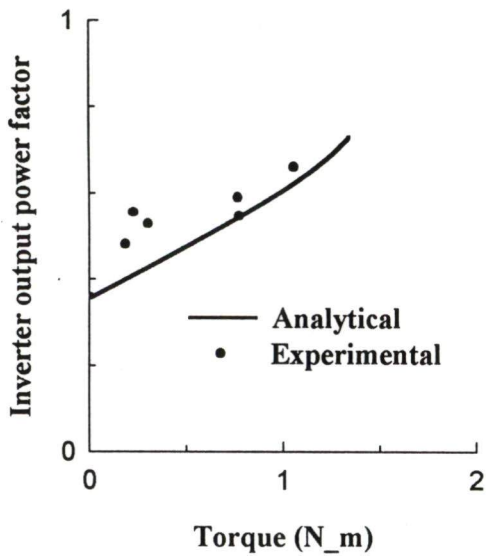
Fig 7.21. Inverter pf vs. torque characteristics
$(I_{dc} = 3.0 \text{ A}, \omega_e = 62.8 \text{ rad/sec}, c = 150 \text{ μF/phase})$
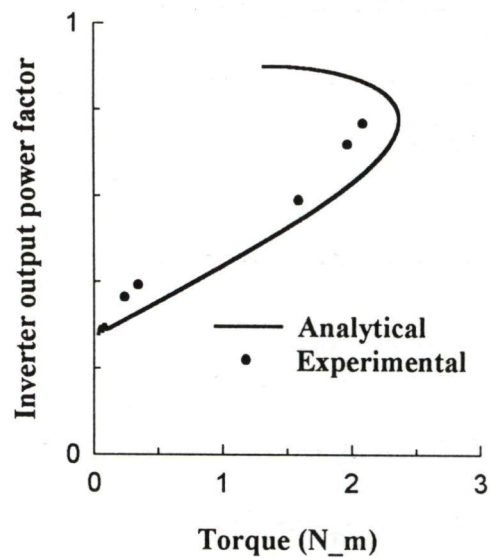
Fig 7.22. Inverter pf vs. torque characteristics
$(I_{dc} = 3.0 \text{ A}, \omega_e = 125.6 \text{ rad/sec}, c = 150 \text{ μF/phase})$
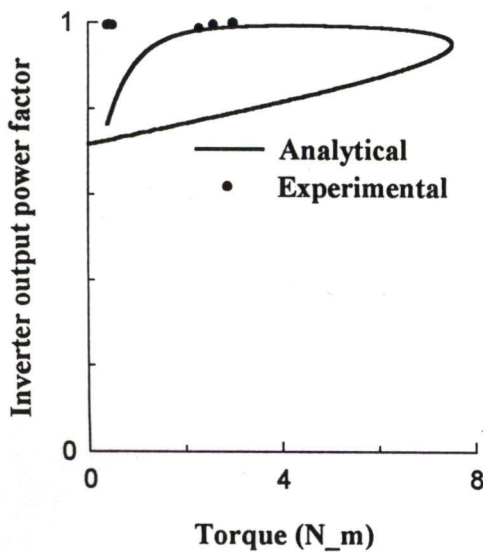
Fig 7.23. Inveter pf vs.torque characteristics
$(I_{dc} = 3.0 \text{ A}, \omega_e = 188.4 \text{ rad/sec}, c = 150 \text{ μF/phase})$
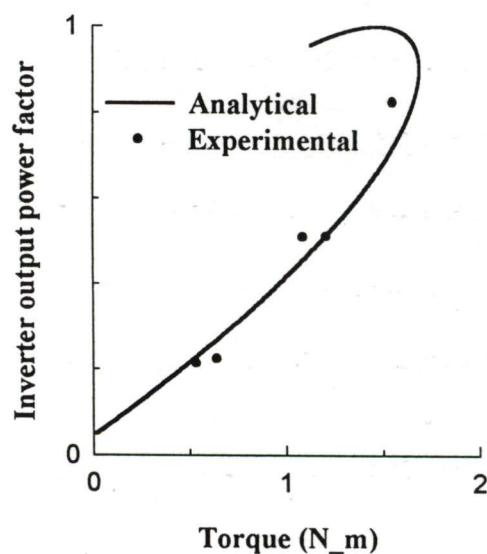
Fig 7.24. Inverter pf vs. torque characteristics
$(I_{dc} = 3.0 \text{ A}, \omega_e = 314 \text{ rad/sec}, c = 150 \text{ μF/phase})$
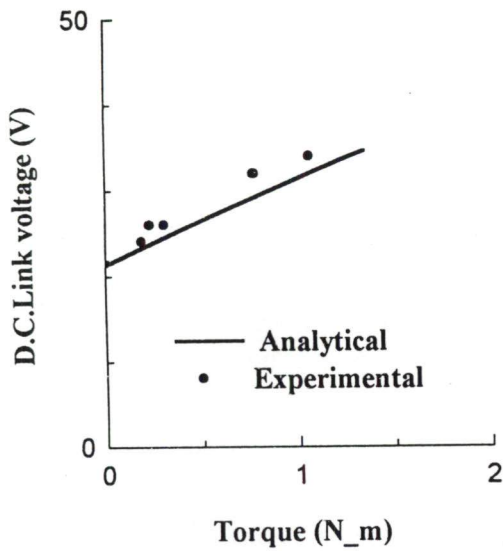
Fig 7.25. D.C.Link voltage vs.torque characteristics $(I_{dc} = 3.0$ A,$\omega_e = 62.8$ rad/sec,$c = 150$ µF/phase)
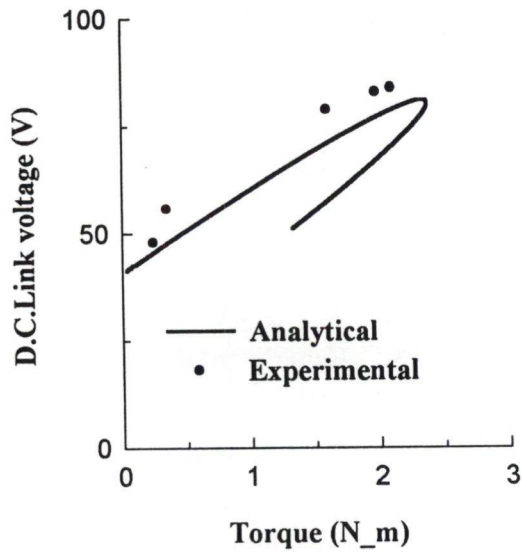
Fig 7.26. D.C.Link voltage vs.torque characteristics $(I_{dc} = 3.0$ A,$\omega_e = 125.6$ rad/sec,$c = 150$ µF/phase)
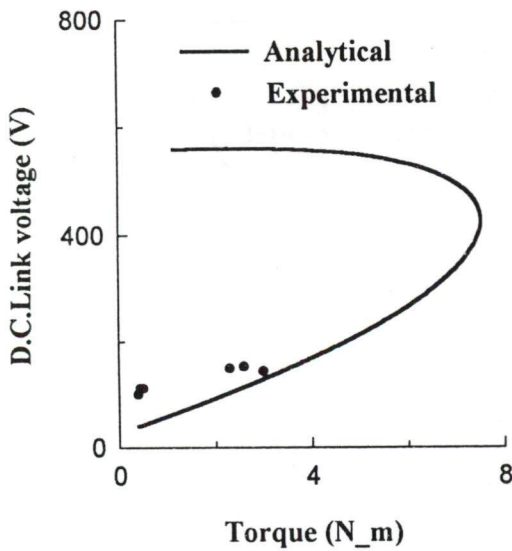
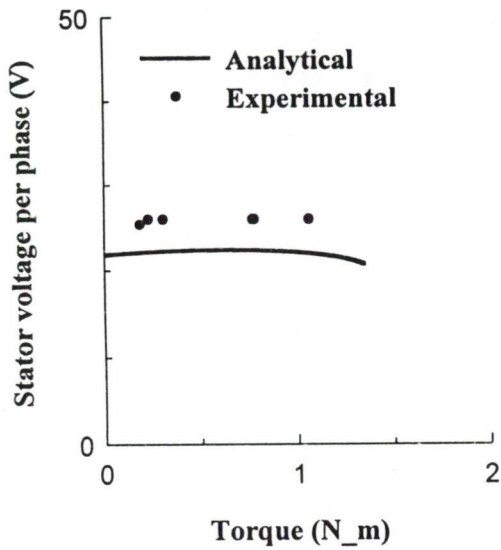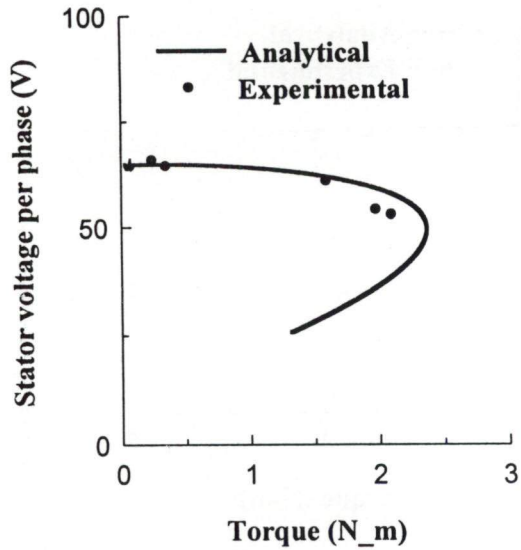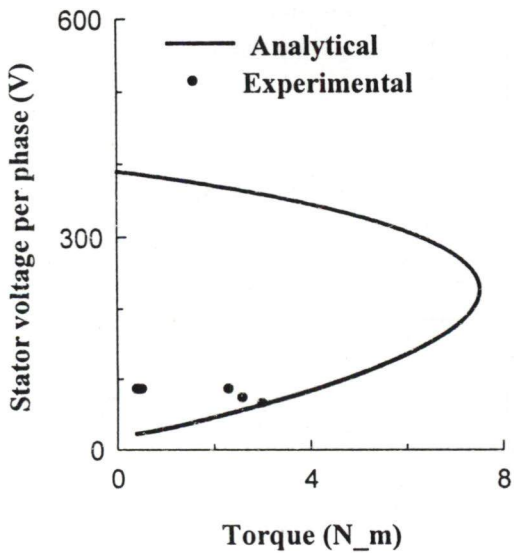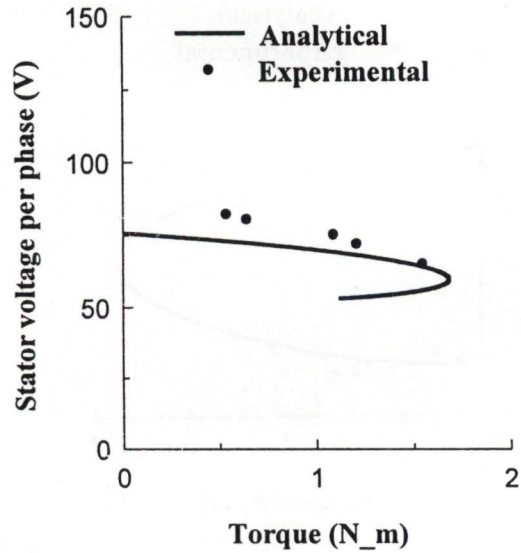Fig 7.27. D.C.Link voltage vs.torque characteristics $(I_{dc} = 3.0$ A,$\omega_e = 188.4$ rad/sec,$c = 150$ µF/phase)
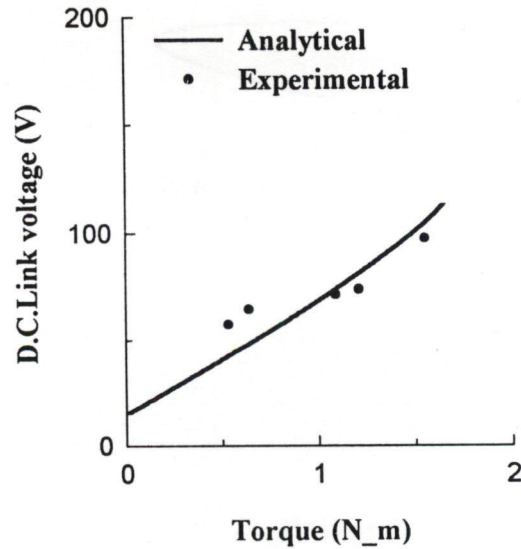
Fig 7.28. D.C.Link voltage vs.torque characteristics $(I_{dc} = 3.0$ A,$\omega_e = 314$ rad/sec,$c = 150$ µF/phase)
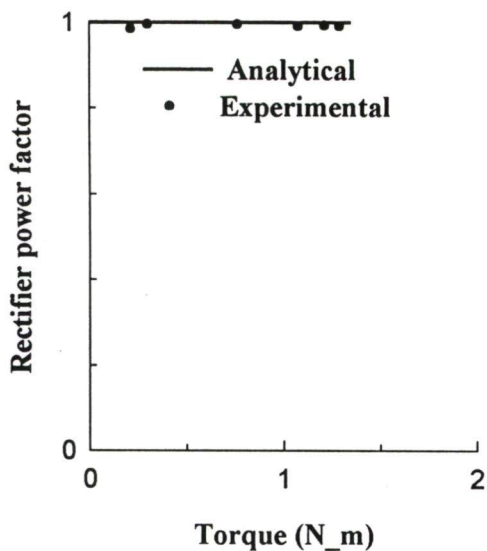
Fig 7.29. Rectifier pf vs. torque characteristics
(I_{dc} = 3.0 A, ω_e = 62.8 rad/sec, c = 150 μF/phase)
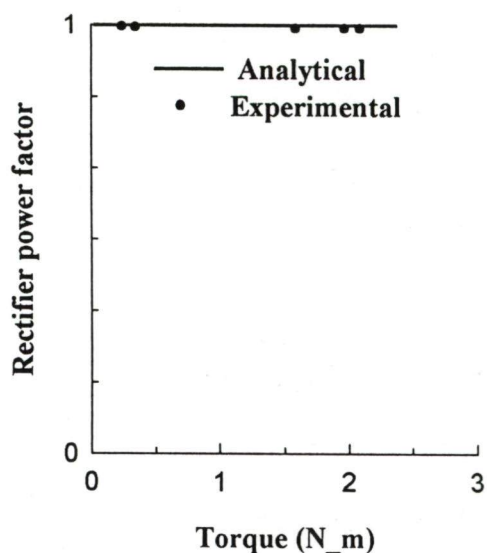
Fig 7.30. Rectifier pf vs. torque characteristics
(I_{dc} = 3.0 A, ω_e = 125.6 rad/sec, c = 150 μF/phase)
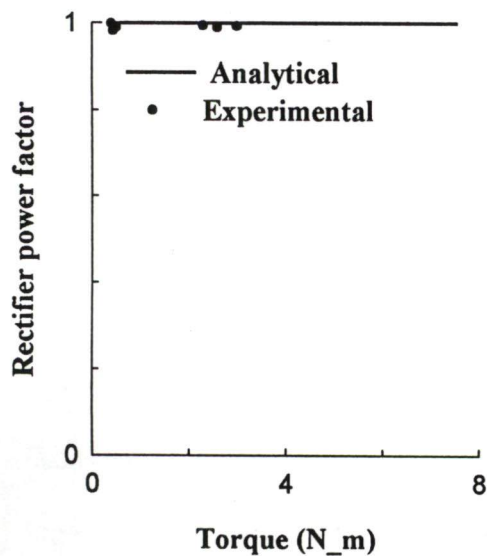
Fig 7.31. Rectifier pf vs. torque characteristics
(I_{dc} = 3.0 A, ω_e = 188.4 rad/sec, c = 150 μF/phase)
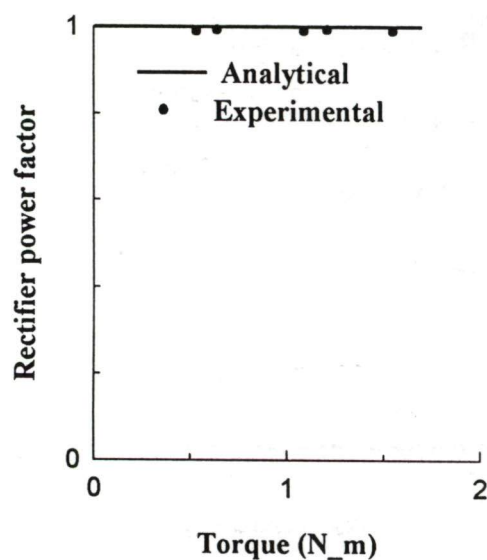

Fig 7.32. Rectifier pf vs. torque characteristics
(I_{dc} = 3.0 A, ω_e = 314 rad/sec, c = 150 μF/phase)

223

analytically obtained power factor of pulse width modulated rectifier is always unity, while the experimentally obtained power factor is found to be very close to unity.

A good co-relation is found between analytical and experimental performance curves. The slight difference in some of the performance curves is found due to certain assumptions and difficulty in speed measurement because the operating slip is very small over the entire operating region. The good agreement between the analytical and experimental performance curves in open loop confirms the validity of the developed model considering various assumptions.

7.3 TRANSIENT PERFORMANCE OF MODIFIED CSI-FED INDUCTION MOTOR DRIVE

The transient performance of the drive is investigated experimentally by implementing the designed value of controller parameters obtained by continuous data approach. To obtain the transient performance of the drive the induction motor is loaded by connecting a fixed resistance across the separately excited d.c.shunt generator coupled to the induction machine .The fixed resistance is selected for full loading of the induction machine at rated speed when operated from rated voltage and rated supply frequency. Therefore the load torque on the machine increases linearly with the speed. The transient performance is obtained by implementing the software through personal computer.

In order to show the validity of the designed controller parameters obtained by the continuous data approach, the transient response of the drive for steps change in reference speed are recorded experimentally by a X-Y recorder as shown in Fig 7.33.The change in reference speed is made via the keyboard of the personal computer. The experimental X-Y recording is carried out by coupling a 3- phase a.c. tacho generator to the induction
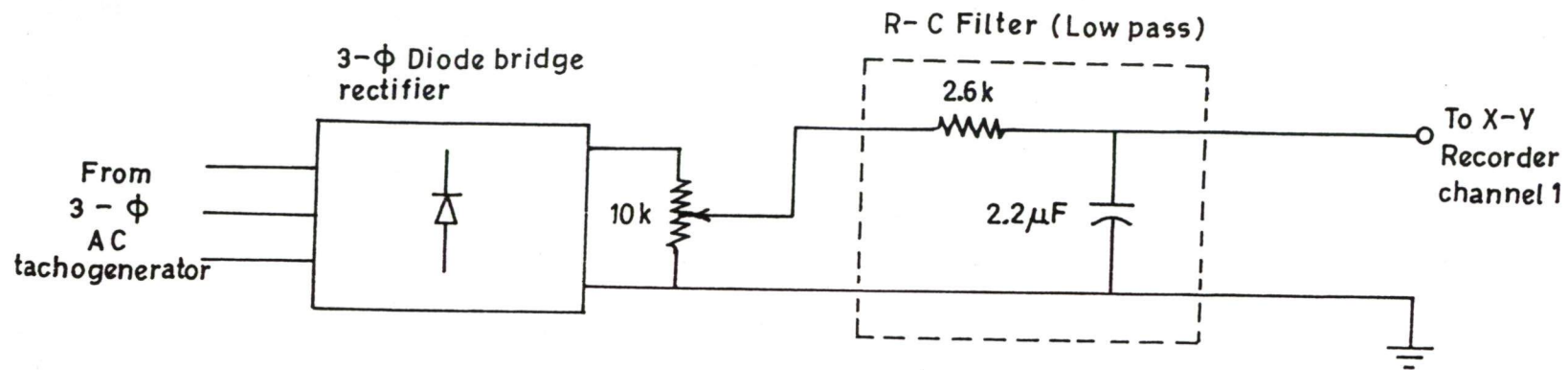
Fig.7.33. Transient speed recording.

motor. The output voltage of tacho generator is rectified in a three-phase diode bridge rectifier. The output voltage ripples are filtered out in a low pass R-C filter, to get the better quality of d.c. output voltage. The R-C filter is selected such that it should filter out the ripples from the output voltage at the same time it should not delay the transient response of the system. The selected value of R-C component of the filter is shown in the Fig 7.33. The maximum value of filtered output voltage is adjusted to 10 volts for rated speed and connected to channel 1 of X-Y recorder. The transient responses for changes in reference speed are shown in Figs 7.34 to 7.39. The Fig 7.34 shows the transient response of the drive for change in reference speed from 0 to 400 rpm. The Fig 7.35 shows the transient response of the drive for change in reference speed from 600 to 1500 rpm. Figure 7.36 and 7.37 show the transient response of the drive for change in reference speed from 400 rpm to 600 rpm and 600 rpm to 400 rpm respectively. Figs 7.38 and 7.39 show the transient response of the drive for change in reference speed from 600 rpm to 800 rpm and 800 rpm to 600 rpm respectively. The recording of the speed transient of the drive is carried out with the help of X - Y recorder, using 3 - phase a.c. tachogenerator. Due to that there are ripples in the recorded speed, an attempt has been made to dies out the ripples with the help of conventional R-C filter, but it is not much effective to filter out ripples from the output voltage. To verify the experimentally recorded transient response, it is compared with the analytically obtained transient response of the drive. The analytical response of the drive is obtained through software program developed for the transient simulation of the drive. To get the analytical transient response of the drive the same load- torque is applied as in experimental recording and the same change in reference speed is applied as in the experimental recording through the software program. When the drive settles in the $\pm 5\%$ of speed tolerance limit, the settling time is noted. The transient responses for changes in reference speed obtained analytically are

226
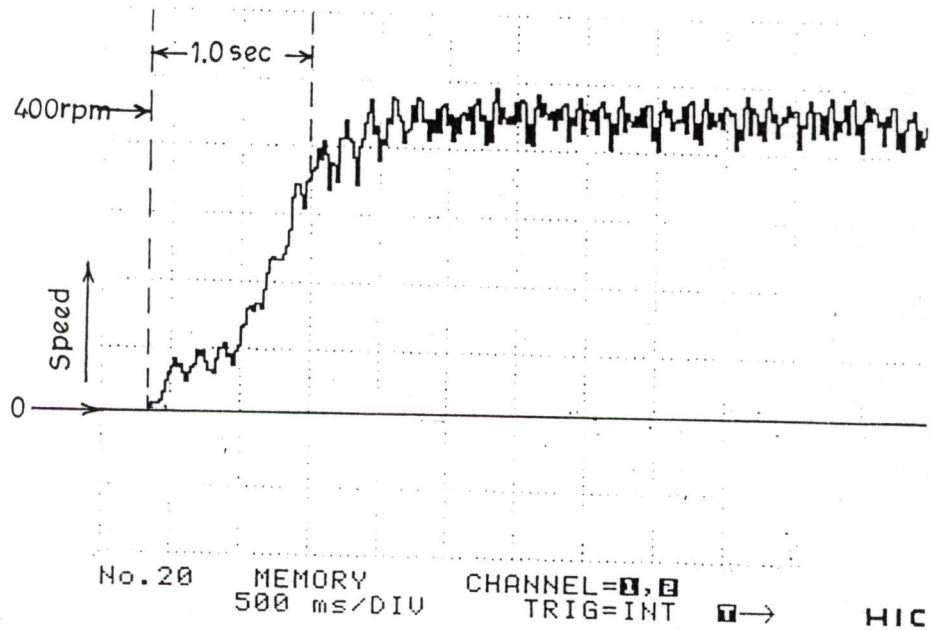
Fig 7.34. Transient response of drive for step change in reference speed from 0 to 400 rpm
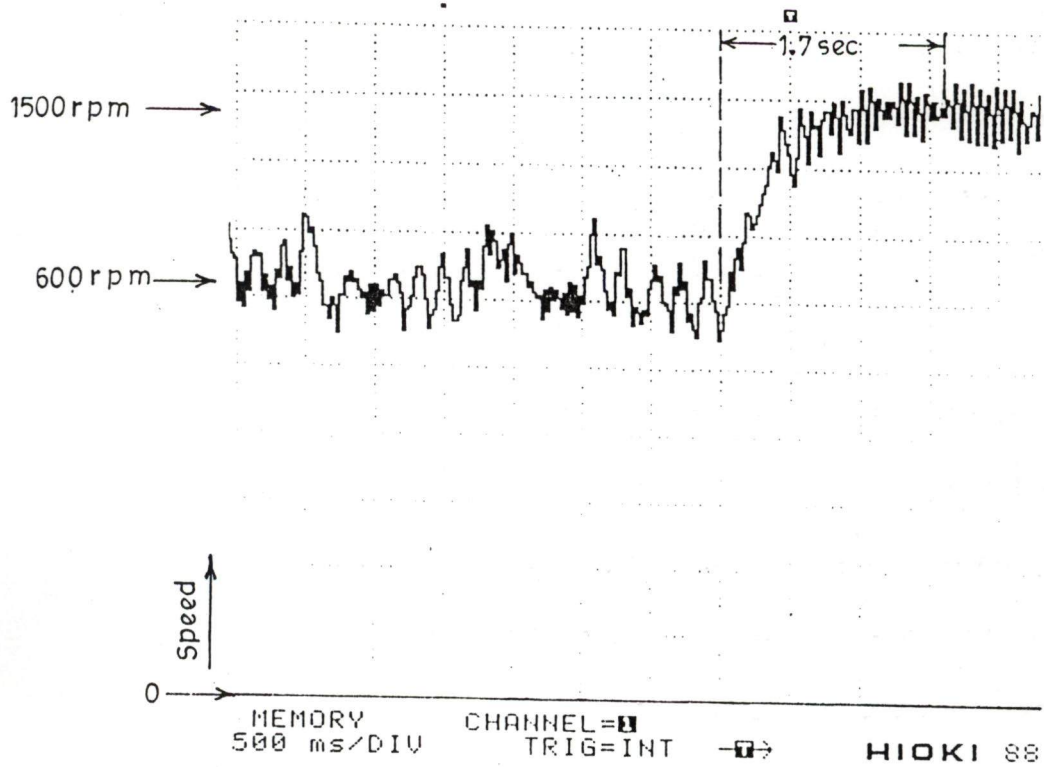
Fig 7.35. Transient response of drive for step change in reference speed from 600 to 1500 rpm
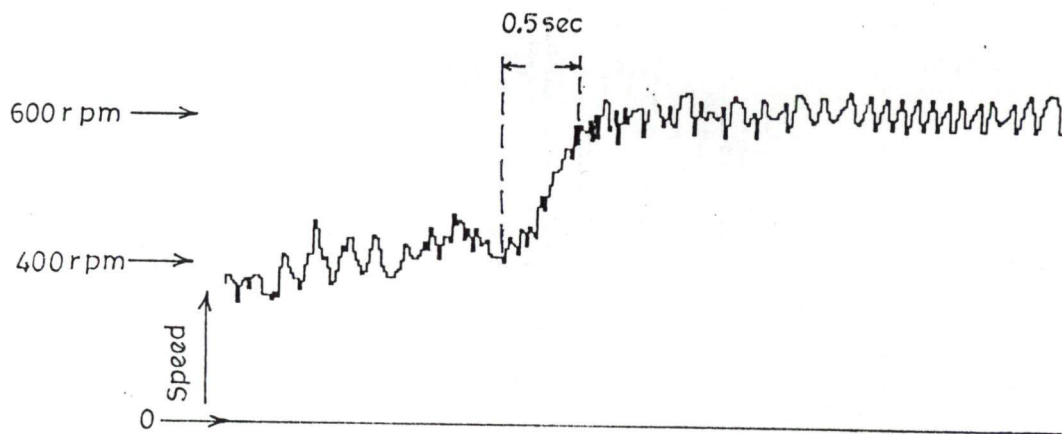
Fig 7.36. Transient response of drive for step change in reference speed from 400 to 600 rpm
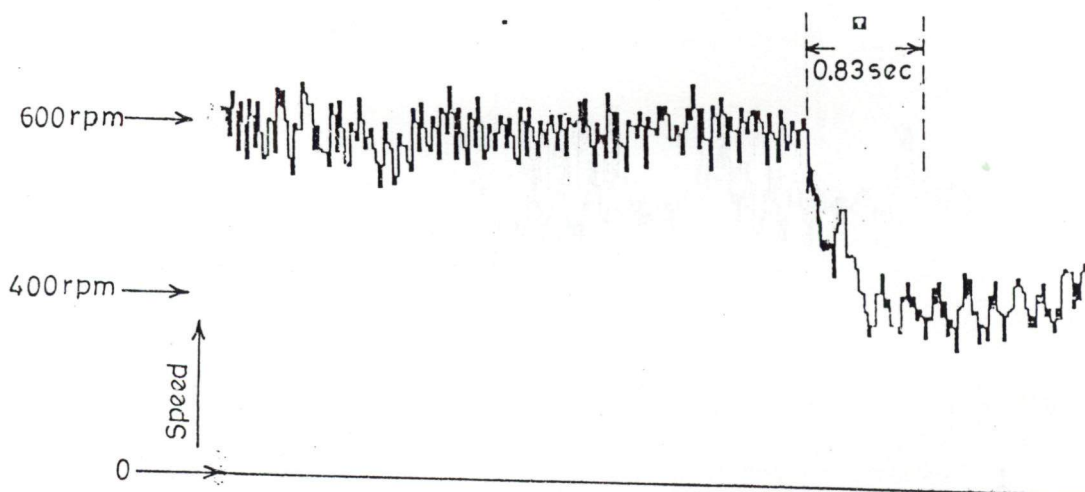
Fig 7.37. Transient response of drive for step change in reference speed from 600 to 400 rpm

800rpm
600rpm

Speed

0
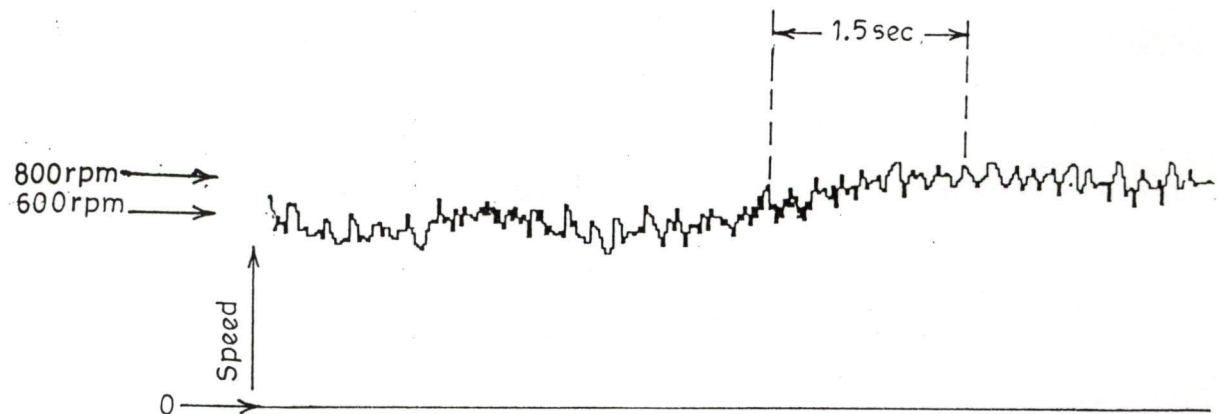
MEMORY   CHANNEL=⬛,⬛
500 ms/DIV   TRIG=INT   ⬛→   HIOKI 8801 MEMC

Fig 7.38. Transient response of drive for step change in reference speed from 600 to 800 rpm

800rpm
600rpm

Speed

0
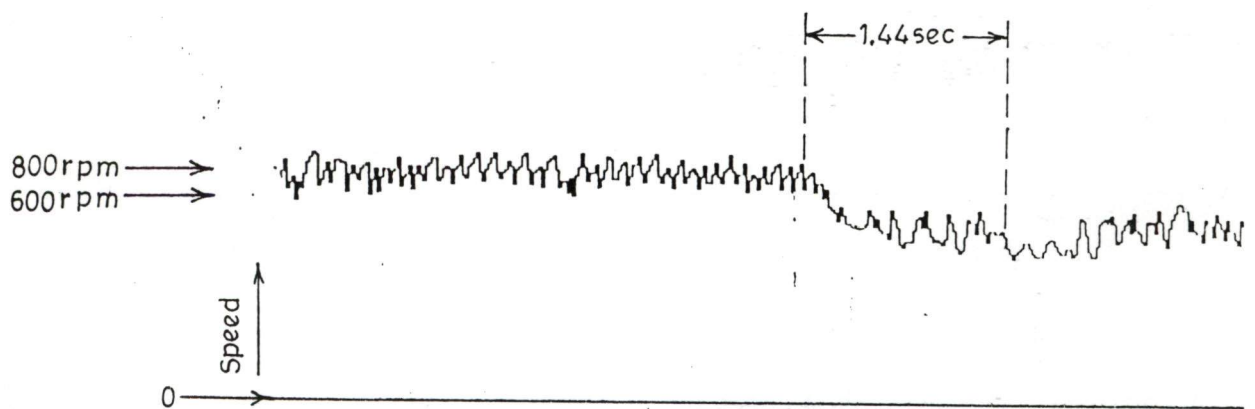
MEMORY   CHANNEL=⬛,⬛
500 ms/DIV   TRIG=INT   ⬛→   HIOKI 8801 MEMOR

Fig 7.39. Transient response of drive for step change in reference speed from 800 to 600 rpm

229

shown in Figs 7.40 to 7.45.The Fig 7.40 shows the transient response of the drive for change in reference speed from 0 to 400 rpm. The Fig 7.41 shows the transient response of the drive for change in reference speed from 600 to 1500 rpm. Figs 7.42 and 7.43 show the transient response of the drive for change in reference speed from 400 rpm to 600 rpm and 600 rpm to 400 rpm respectively. Figs 7.44 and 7.45 show the transient response of the drive for change in reference speed from 600 rpm to 800 rpm and 800 rpm to 600 rpm respectively.

The settling times obtained for step change in reference speeds recorded experimentally and obtained analytically are shown in Table 7.1

Table 7.1

Change in Reference speed (rpm)	Experimentally recorded settling time (sec)	Analytically obtained settling time (sec)
0 to 400	1.00	0.692
600 to 1500	1.75	2.27
400 to 600	0.50	0.38
600 to 400	0.83	0.765
600 to 800	1.50	1.227
800 to 600	1.44	1.31

The settling time of the transient response of the drive recorded experimentally and determined analytically for the step change in reference speeds at the selected value of controller parameters, shows that the settling times in both the cases are almost matching at most of the reference change in speed. This confirms the validity of the design approach of the drive. The settling time in all the cases are very small; this shows the effectiveness of the closed loop operation at the selected value of controller parameters and it is found to be satisfactory.
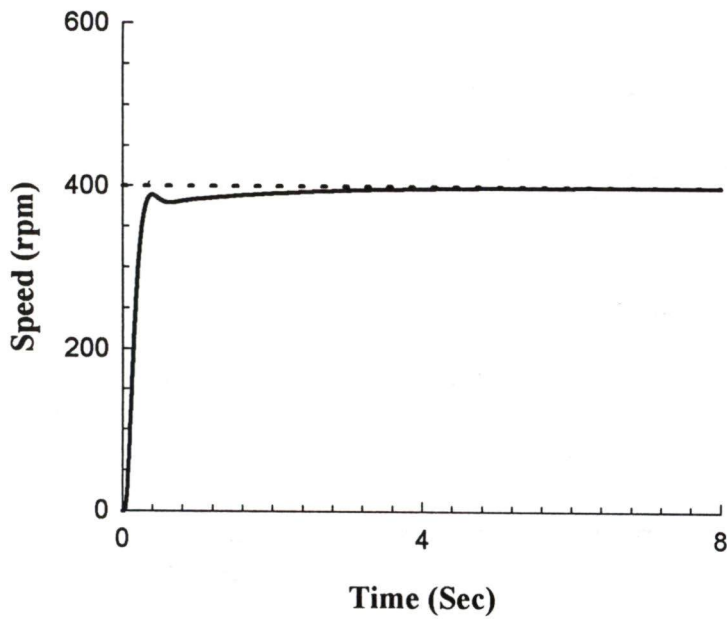
Fig 7.40. Transient response of the drive for step change in reference speed from 0 rpm to 400 rpm
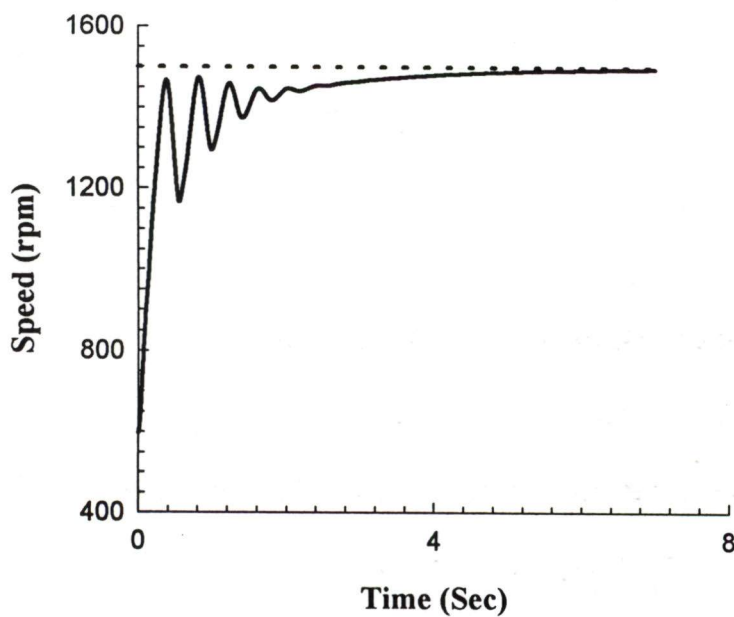
Fig 7.41. Transient response of the drive for step change in reference speed from 600 rpm to 1500 rpm
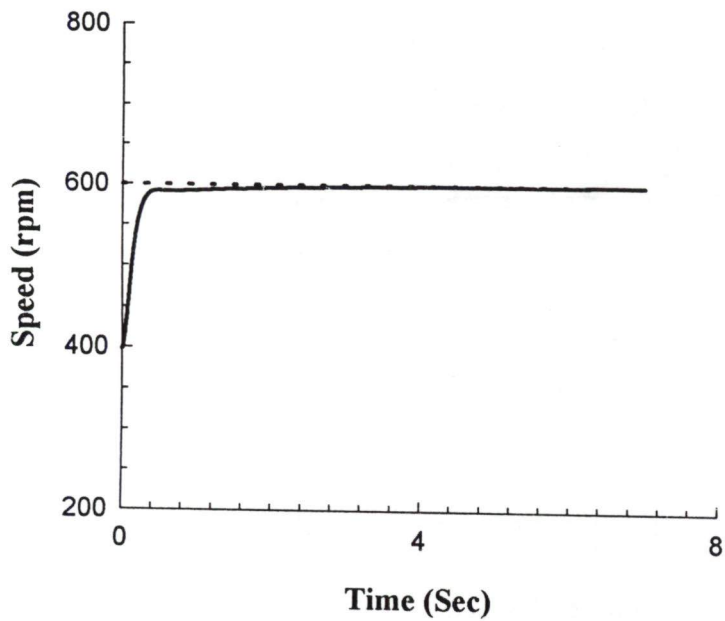
Fig 7.42. Transient response of the drive for step change in reference speed from 400 rpm to 600rpm
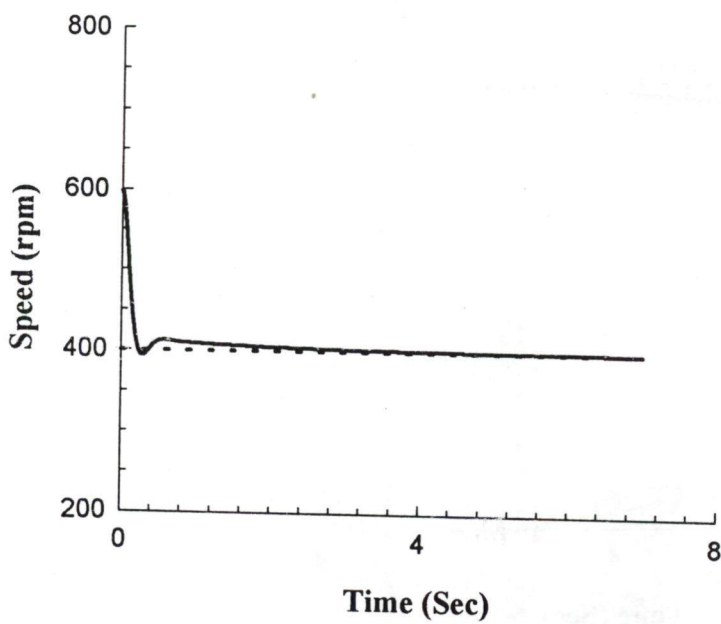
Fig 7.43. Transient response of the drive for step change in reference speed from 600 rpm to 400rpm
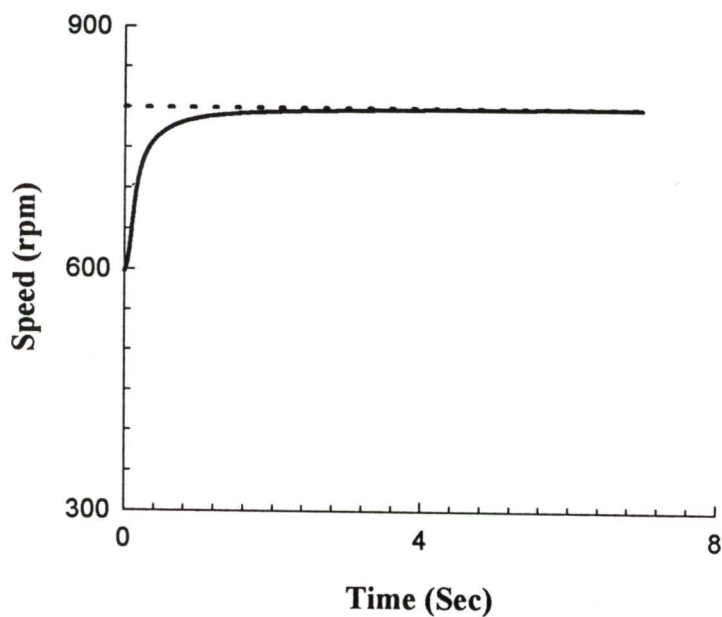
Fig 7.44. Transient response of the drive for step change in reference speed from 600 rpm to 800 rpm
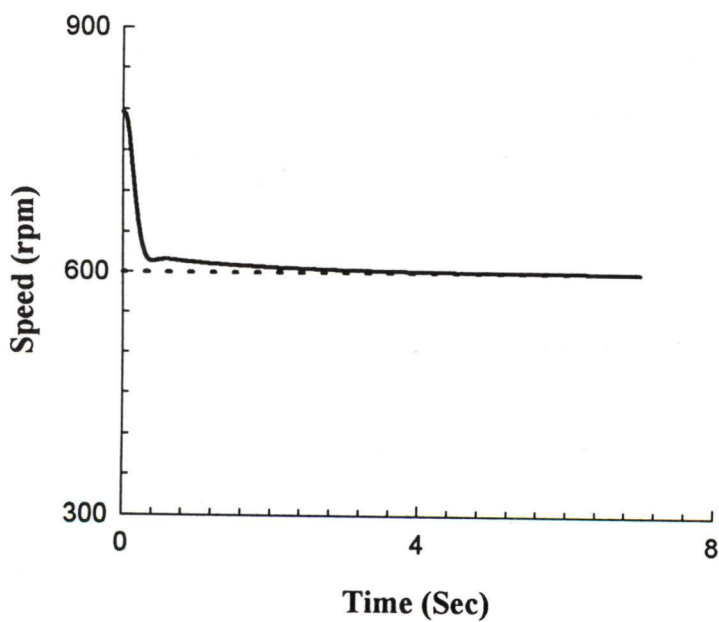
Fig 7.45. Transient response of the drive for stepchange in reference speed from 800 rpm to 600 rpm

The transient response of d.c. link current is also recorded at the selected controller parameters experimentally for the step change in speeds with the help of X- Y recorder. The experimentally recorded transient response of d.c.link current is shown in Fig 7.46 to 7.49. Figs 7.46 and 7.47 show transient response of the d.c.link current of the drive for change in reference speed from 400 rpm to 600 rpm and 600 rpm to 400 rpm respectively. Figs 7.48 and 7.49 show the transient response of the d.c.link current of the drive for change in reference speed from 600 rpm to 800 rpm and 800 rpm to 600 rpm respectively. The analytically determined current transient responses of the drive for the step change in reference speeds are also obtained through computer simulation. . The analytically determined transient responses of d.c.link current are shown in Fig 7.50 to 7.53. Figs 7.50 and 7.51 show transient response of the d.c.link current of the drive for change in reference speed from 400 rpm to 600 rpm and 600 rpm to 400 rpm respectively. Figs 7.52 and 7.53 show the transient response of the d.c.link current of the drive for change in reference speed from 600 rpm to 800 rpm and 800 rpm to 600 rpm respectively. The change in d.c.link currents for the step change in reference speeds for both the cases are shown in Table 7.2

Table 7.2

Change in Reference speed (rpm)	Experimentally determined change in d.c.link current (Amp)	Analytically obtained change in d.c.link current (Amp)
400 to 600	2.81 to 2.39	2.84 to 2.58
600 to 400	2.81 to 3.4	2.91 to 3.245
600 to 800	2.25 to 1.9	2.21 to 1.76
800 to 600	2.1 to 2.27	2.560 to 2.5025
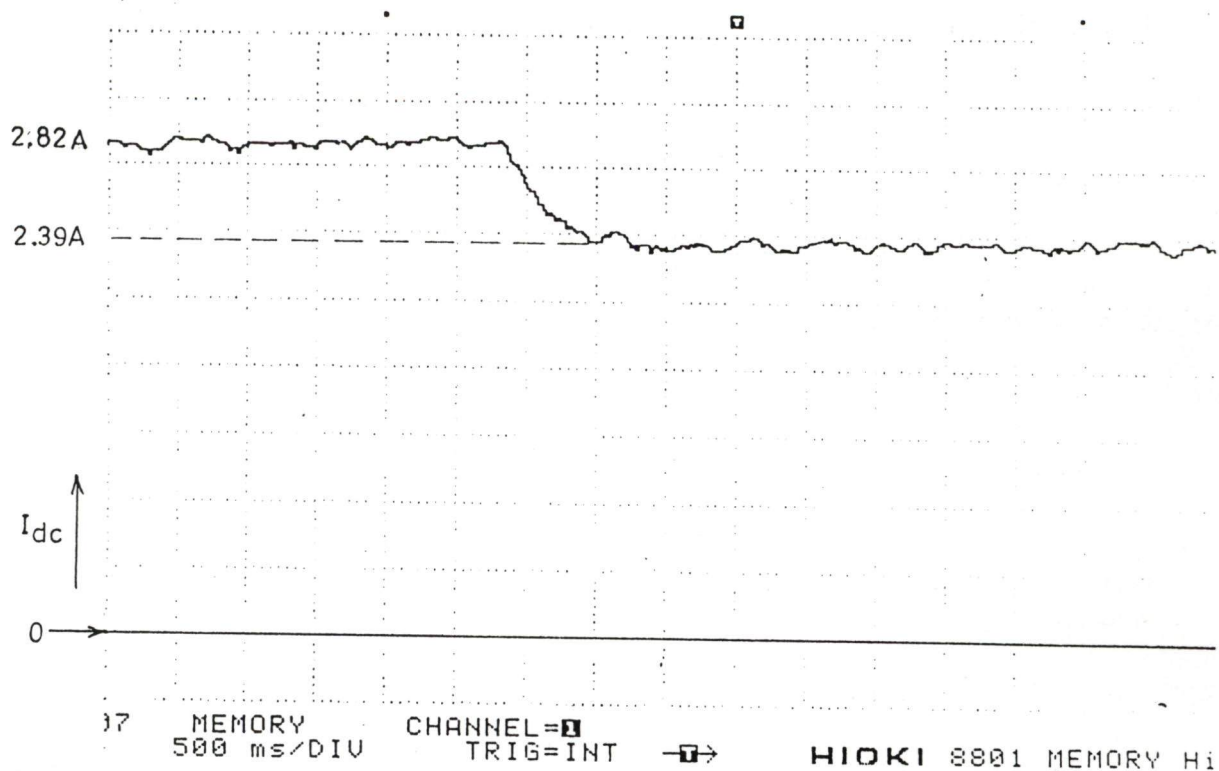
Fig 7.46. Change in d.c.link current for step change in reference speed from 400 to 600 rpm

3.4A

2.81A

I_{dc}

0

18   MEMORY   CHANNEL=1
        500 ms/DIV   TRIG=INT   →1→   HIOKI 8801 MEMORY Hi
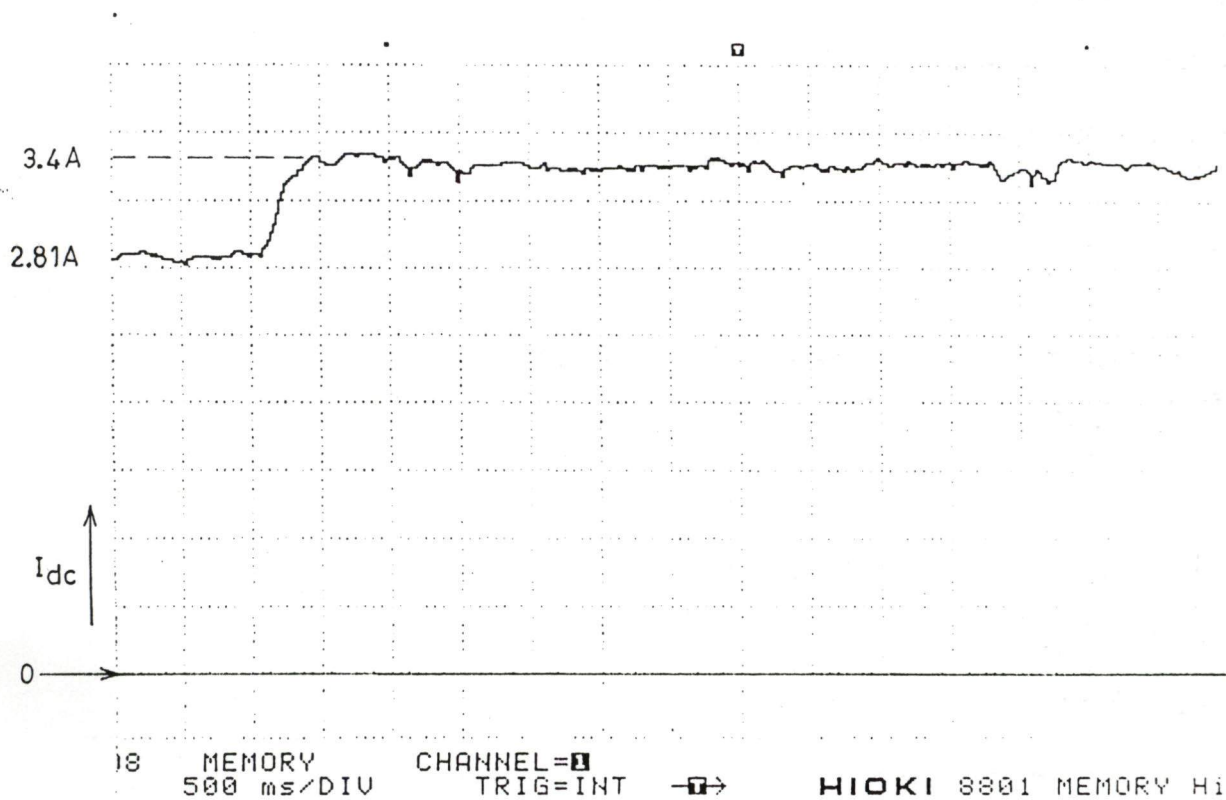
Fig 7.47. Change in d.c.link current for step change in reference speed from 600 to 400 rpm
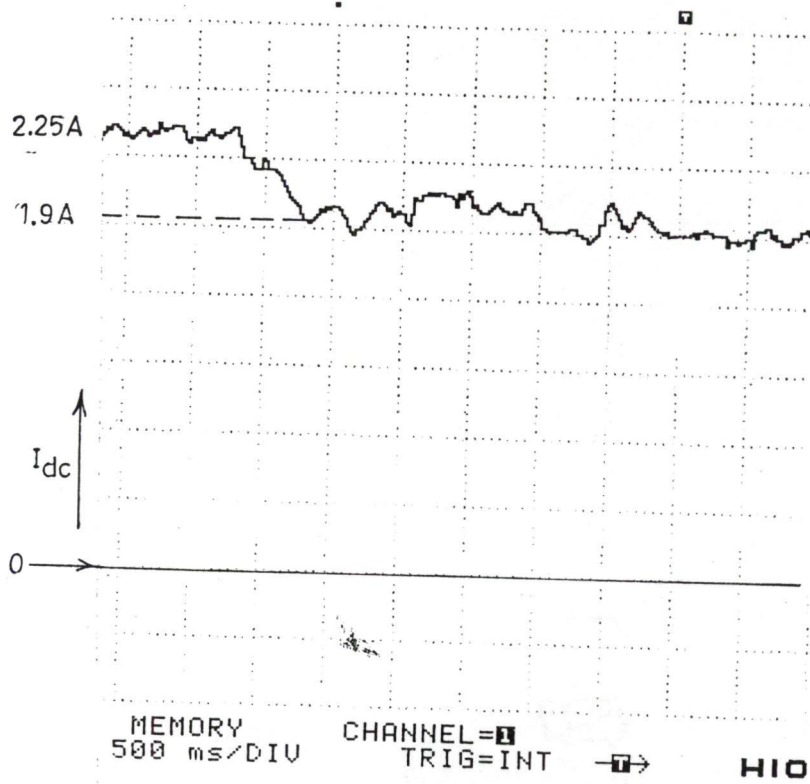
Fig 7.48. Change in d.c.link current for step change in reference speed from 600 to 800 rpm
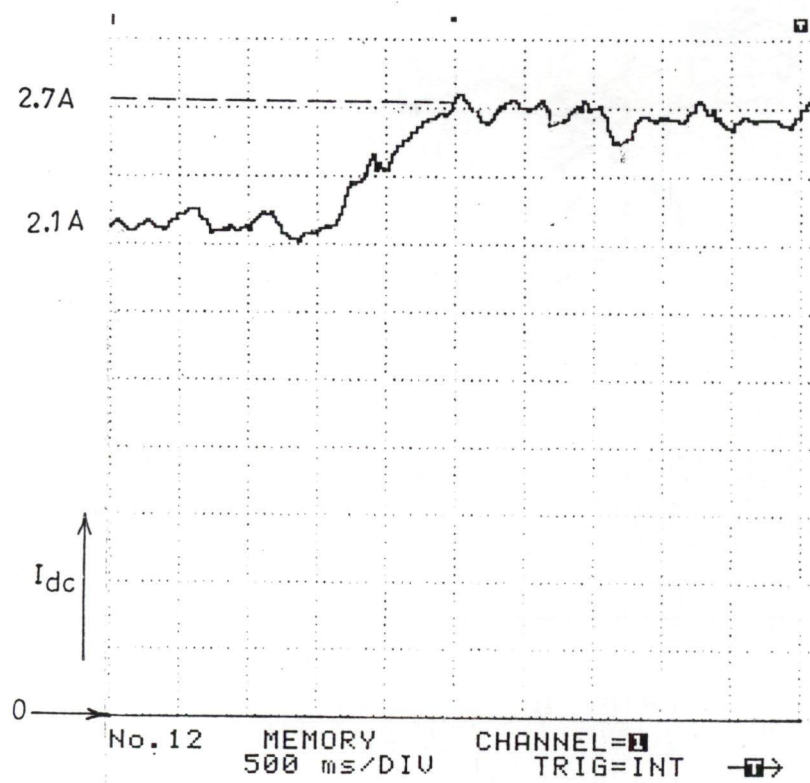
Fig 7.49. Change in d.c.link current for step change in reference speed from 800 to 600 rpm
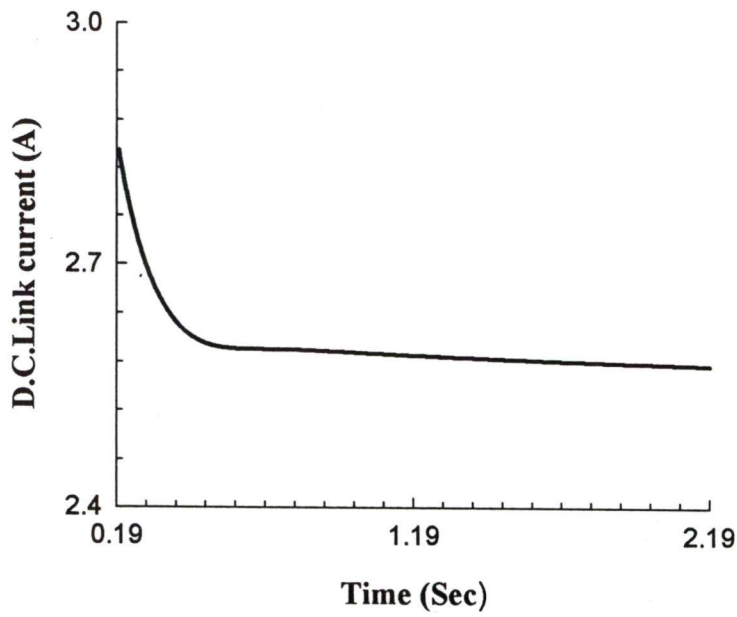
Fig 7.50. Change in d.c.link current for step change in reference speed from 400 rpm to 600 rpm
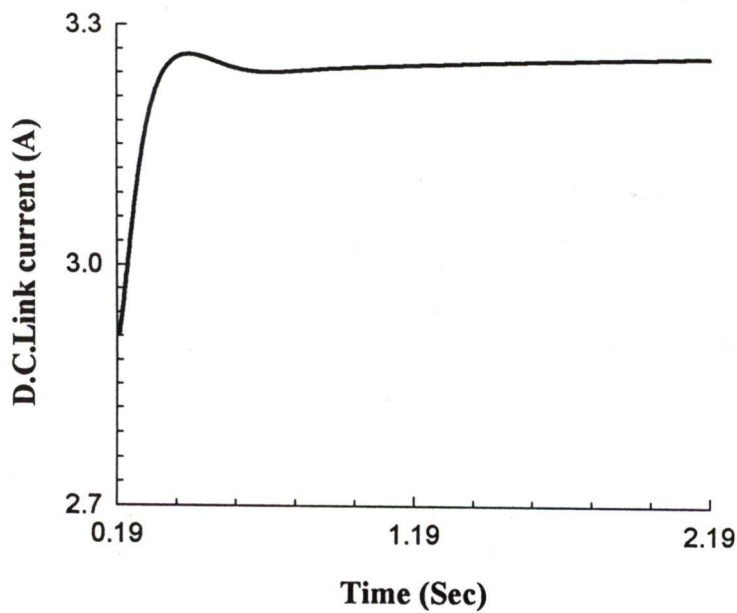
Fig 7.51. Change in d.c.link current for step change in reference speed from 600 rpm to 400 rpm
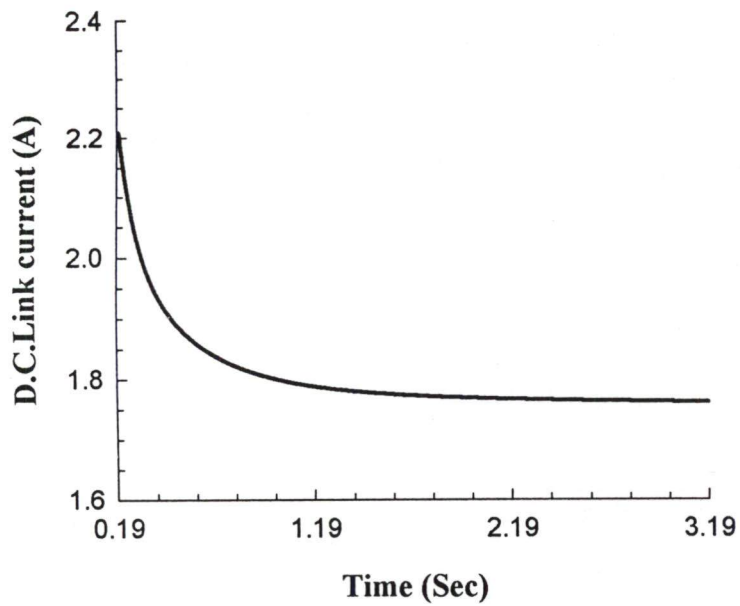
Fig 7.52. **Change in d.c.link current for step change in reference speed from 600 rpm to 800 rpm**
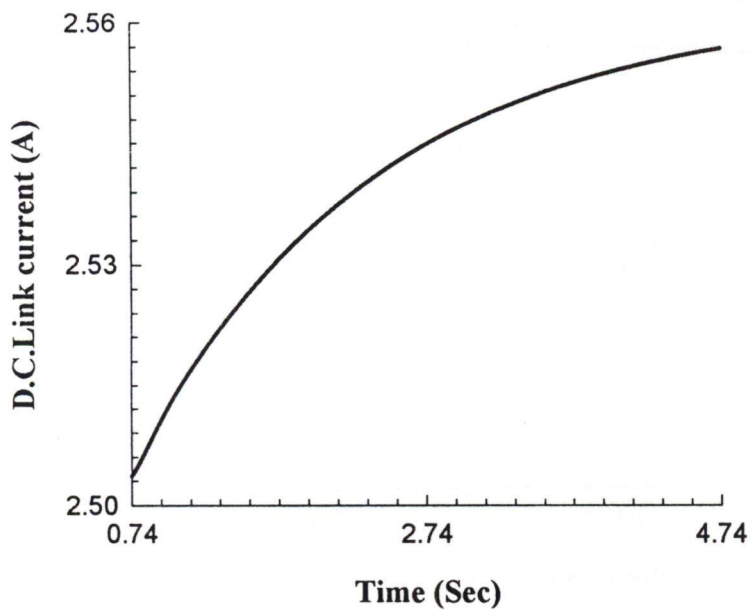
Fig 7.53. **Change in d.c.link current for step change in reference speed from 800 rpm to 600 rpm**

The Table 7.2 shows that the changes in d.c.link current for the step change in reference speeds are almost same. The transient curves obtained from the above data show that the d.c.link current also settles very fast with the change in speed. This shows the effectiveness of design approach at the selected controller parameters.

7.4 CLOSED LOOP PERFORMANCE OF CSI- FED INDUCTION MOTOR DRIVE

After studying the performance of the drive in open loop, it is operated in closed loop. In open loop as the load on the machine changes, the slip of induction motor changes; hence it is difficult to operate the machine at a set value of reference speed and at the same time it is difficult to operate the machine at rated value of flux in open loop for each operating frequency. To improve the performance of the drive it is operated in closed loop by providing the speed feed back loop and slip speed regulator loop. The speed controller processes the speed error and sets the reference slip speed (ω_{sl}^*). The slip regulator loop calculates the stator reference active current (I_{act}^*) and stator reference reactive current (I_{react}^*), needed for the determination of reference current (I_{ref}). The inner current controller adjusts the firing pulses of pulse width modulated converter to regulate the d.c.link current. The system tries to minimise the steady state error between the reference speed and actual speed.

To investigate the closed loop performance of the drive the machine is coupled with separately excited d.c. generator and loaded exactly in the same manner as in the case of transient investigation. The closed loop operation is controlled by implementing the software through the personal computer. The various tests were performed to determine the steady state performance of the modified CSI-fed induction motor drive in

239

closed loop condition. The steady state performance of the drive is determined experimentally at the selected value of controller parameters. The reference speed is varied through keyboard of personal computer. When the speed of the machine settles in the tolerance limit of $\pm$ 5% the various performance parameters such as speed, power output, stator voltage, stator current, efficiency, power factor of the machine, d.c.link voltage, d.c.link current are noted and plotted with respect to torque as shown in Figs 7.54 to 7.61. The analytical performance curves are obtained by putting the different reference speed, in the simulation program and when the actual speed is equal to the reference speed the various performance parameters are noted. At each set of reference speed the steady state error is found to be zero. The analytical performance curves are also shown in the same figure for comparison. The different experimental and analytical performance characteristics are discussed below.

(i)   Speed vs torque

The closed loop speed vs torque curves determined experimentally for load torque varying linearly with speed on the machine and analytically obtained speed vs torque curve for the same load are shown in Fig 7.54.As obvious the performance of the experimentally determined speed vs torque curve in closed loop is found to be better than the open loop. The experimental and analytical curves are quite close to each other. The slight difference in two curves is because of instrumental error and assumptions made in the simulation model.

(ii)   Power output vs torque

The power output vs torque curves determined experimentally and obtained analytically are shown in Fig 7.55 for same load on the machine. The power output in
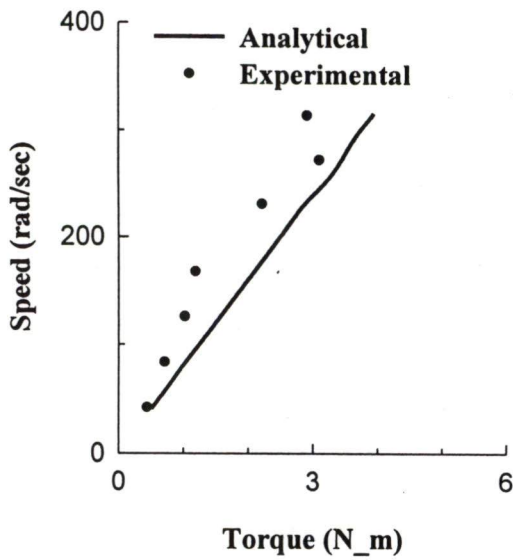
Fig 7.54. Speed vs. torque characteristics
$(c = 150 \ \mu\text{F/phase}, \ t_l = t_L * (\omega_r/\omega_b))$
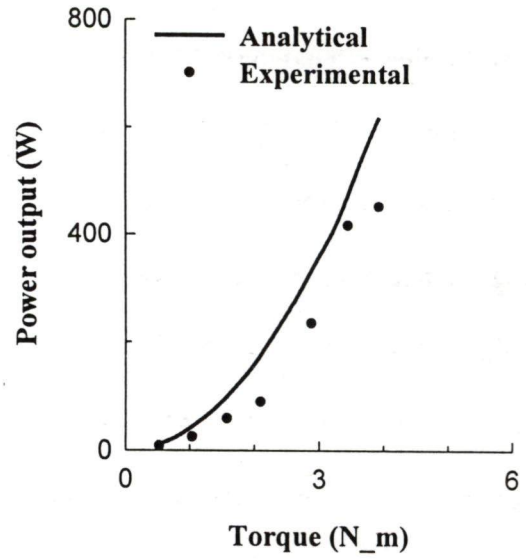
Fig 7.55. Power output vs. torque characteristics
$(c = 150 \ \mu\text{F/phase}, \ t_l = t_L * (\omega_r/\omega_b))$
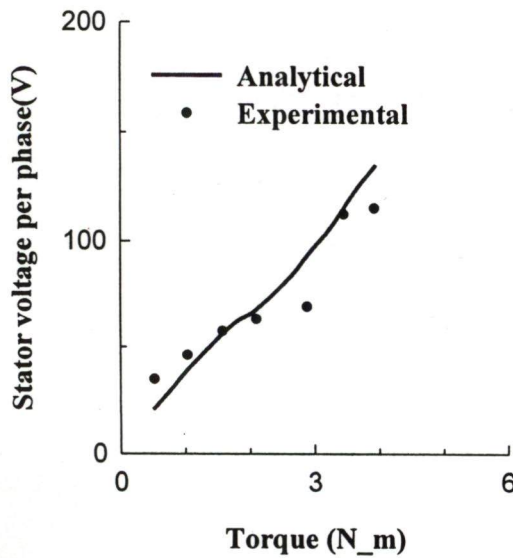
Fig 7.56. Stator voltage vs. torque characteristics
$(c = 150 \ \mu\text{F/phase}, \ t_l = t_L * (\omega_r/\omega_b))$
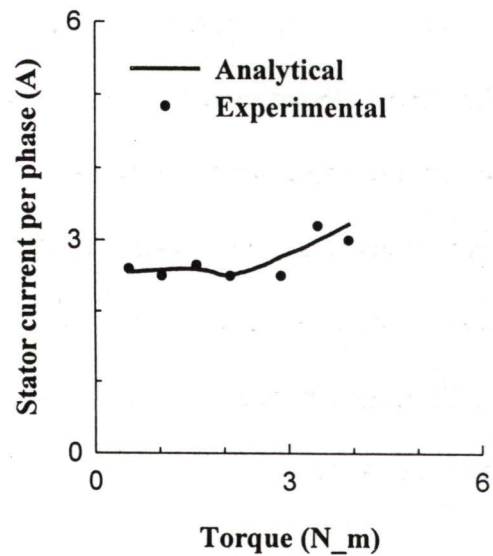
Fig 7.57. Stator current vs. torque characteristics
$(c = 150 \ \mu\text{F/phase}, \ t_l = t_L * (\omega_r/\omega_b))$

241
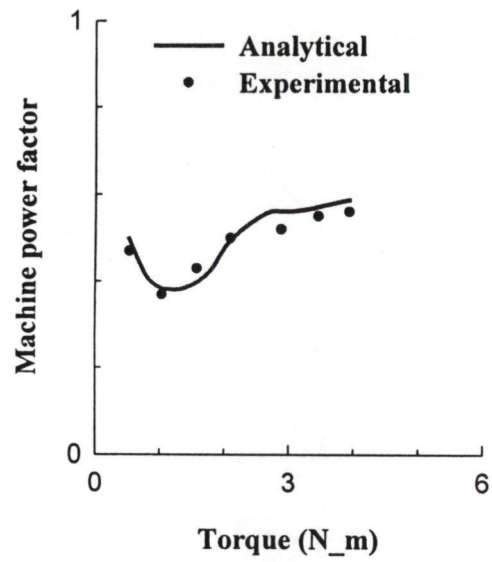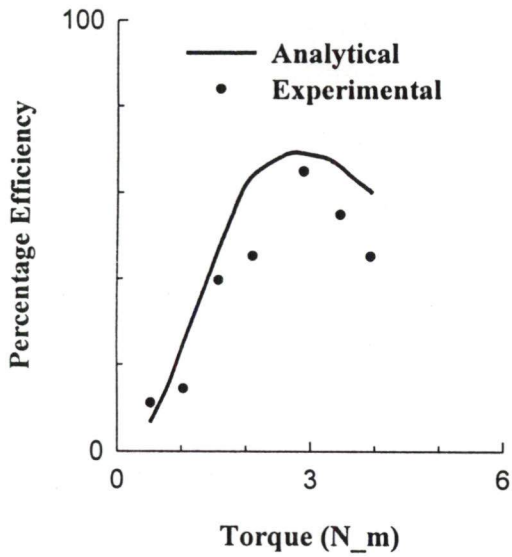
Fig 7.58. Efficiency vs. torque characteristics
$(c = 150 \ \mu F/phase, t_l = t_L^*(\omega_r/\omega_b))$

Fig 7.59. Power factor vs. torque characteristics
$(c = 150 \ \mu F/phase, t_l = t_L^*(\omega_r/\omega_b))$
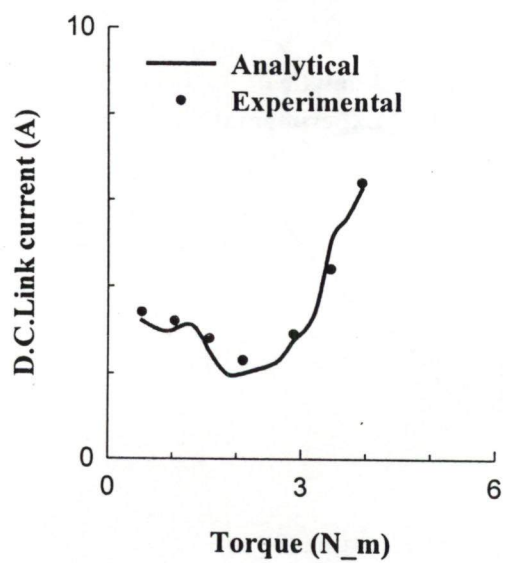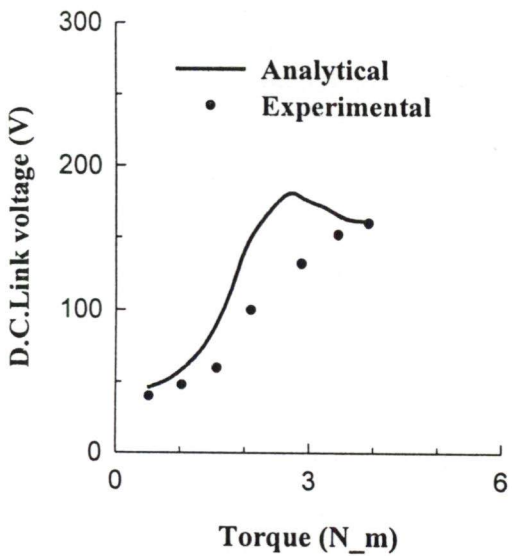
Fig 7.60. D.C.Link voltage vs. torque characteristics
$(c = 150 \ \mu F/phase, t_l = t_L^*(\omega_r/\omega_b))$

Fig 7.61. D.C.Link current vs. torque characteristics
$(c = 150 \ \mu F/phase, t_l = t_L^*(\omega_r/\omega_b))$

closed loop found experimentally is higher than the power output in open loop and motor is able to deliver the rated power output. The power output corresponding to each value of torque found experimentally is less than the power output obtained analytically because of negligence of core loss and other losses in the estimation of analytical curves. In both the cases power output increases with the increase in torque.

(iii)   Stator voltage per phase vs torque

The stator voltage vs torque characteristics determined experimentally and obtained analytically are shown in Fig 7.56. With the increase in speed of the drive, load on the motor increases because load is varying linearly with the speed, resulting in higher reference voltage and rectifier output voltage. Hence stator voltage of the induction motor increases. The experimental and analytical characteristics are quite close to each other. In both the cases with the increase in torque demand, stator voltage increases.

(iv)   Stator current per phase vs torque

The stator current vs torque characteristics determined experimentally and obtained analytically are shown in Fig 7.57. Both the characteristics are quiet close to each other. With the increase in the load torque load on the motor the stator current is near constant at low value of torque and then slowly increases with the load torque.

(v)   Percentage efficiency vs torque

Experimentally determined and analytically obtained percentage efficiency characteristic curves are shown in Fig 7.58. Both the curves are almost same for most values of torque. Practically obtained efficiency is found to be poor than analytically obtained efficiency because of negligence of the core loss and other assumptions in the

estimation of analytical curves. In both the cases efficiency increases till maximum efficiency is not achieved.

(vi)   Power factor vs torque

The power factor vs torque characteristics determined experimentally and obtained analytically are shown in Fig 7.59. Both the curves are quiet close to each other. The power factor initially decreases with the torque because of resonance effect. The moment, the effect of resonance dies out the power factor of the machine increases with the increase in torque just like an ordinary induction motor.

(vii)   D.C.Link voltage vs torque

Experimentally determined and analytically obtained d.c.link voltage vs torque characteristic curves are shown in Fig 7.60. Both the curves are almost matching at most of the values of torque. The practically obtained d.c.link voltage increases almost linearly with the increases in torque, while the analytically obtained d.c.link voltage is not linear in the resonance affected region. The analytically obtained curves show that in the resonance affected region, the d.c.link current decreases with the increase in torque, while power demand increases with the increase in torque. To meet out the power demand d.c.link voltage increases with the increase in torque in the resonance affected region. Once the effect of resonance dies out d.c.link voltage increases with the increase in torque just like an ordinary CSI-fed induction motor drive.

(viii)   D.C.Link current vs torque

The d.c.link current vs torque characteristics determined experimentally and obtained analytically are shown in Fig 7.61. Both the curves are almost identical at each

operating torque. Initially with the increase in torque the d.c. link current decreases. This is because of resonance effect. Once the effect of resonance dies out the d.c.link current increases with the increase in torque like an ordinary CSI – fed induction motor drive.

7.5   CONCLUSION

The steady state performance of the modified CSI-fed induction motor in open and closed loop is investigated experimentally for designed controller parameters (using continuous data approach) experimentally. An exhaustive experimentation has been carried out in both open and closed loop conditions. The open loop experiment is carried out by employing only the inner current PI controller loop. Open loop experiment is carried out by varying the load on the induction motor, at a fixed value of d.c.link current and for the variable operating frequency. The change in operating frequency is done via the computer keyboard. The closed loop experiment is carried out by employing both the speed and current PI regulators. The closed loop experiment is carried out at different reference speeds for load torque varying linearly with the speed. The reference speed is given via the keyboard of the personal computer. The various performance parameters are noted and performance characteristics are plotted with respect to torque in all the cases. To verify the experimentally determined open and closed loop performance characteristics of the drive, analytical performance characteristics of the drive are also obtained for the same operating conditions using computer simulation of the drive with the help of developed computer program. A comparison of the two sets of characteristics shows a close match between them at each operating frequency. It confirms the validity of the analytical approach for modeling and design of the drive.

The transient performance of the drive for step change in reference speed is also examined experimentally for designed value of the controller parameters. The experimental transient performance of speed and current loop is recorded by X-Y recorder. The speed transient is recorded by coupling a 3- phase a.c. tacho- generator at the shaft of the motor, and the output of the 3-phase a.c. tacho-generator is rectified using diode bridge rectifier and filtered, using R-C filter. The current transient is recorded by recording the d.c.link current. The transient performance of the controller is also determined from computer simulation for changes in reference speed. The experimental and analytical transient response of both the controllers are almost matching for step changes in reference speed. The settling time corresponding to step changes in reference speed is very small. Corresponding to step changes in reference speed d.c.link current of the drive also settles fast. This confirms the satisfactory performance of the drive and the validity of the analytical approach for modeling and design of the drive.

CONCLUSIONS AND SCOPE FOR FURTHER WORK

8.1   CONCLUSIONS

Variable and smooth speed control is the mandatory requirement of any industrial drive. Over the years, the d.c.motor fed from converter or chopper have been used for the industrial applications. The d.c.motor is having decoupled field and armature winding. Therefore by controlling the armature or field voltages only, the speed of the machine can be controlled. Because of mechanical commutators and carbon brushes, the motor is bulky in comparison with induction motor of same rating and is not suitable for dusty and explosive atmosphere. The motor is also not suitable for high-speed applications and high power ratings .On the other hand the induction motor, specially cage rotor induction motors, having robust constructions, high power/weight ratio, no mechanical commutators and carbon brushes are more efficient and reliable. With the latest development in the power semiconductor technology these motors are preferred as a variable speed drive over d.c. in industrial applications. Variable and step- less speed control of the induction motor is possible by supplying it with the variable frequency power supply through voltage source and current source inverters. Due to controlled current operation of the current source inverter, it protects the power semiconductor devices and machine from over currents. The current source inverter is having another advantage of natural regeneration capability. Therefore the current source inverter is a better alternative to supply the induction motor than the voltage source inverter for speed control. Inspite of the above advantages, conventional current source inverter fed induction motor drive suffers with some of the disadvantages such as: low speed torque

pulsation due to non sinusoidal current, large value of d.c.link inductor, large commutating capacitor, sluggish response and stability problem at light load.

Lots of research work has been carried out to overcome these problems, such as implementation of PWM techniques, incorporation of self – commutating devices, PWM techniques in front-end converter, digital control using fast processor, stability and transient analysis.

In the light of the above work, it was felt to develop a CSI fed induction motor drive with sinusoidal current and voltage. The present thesis deals with the design, analysis, development and performance investigation of the modified self-commutating current source inverter fed induction motor drive. The modified CSI-fed drive is having capacitor bank at the terminals of the motor, which supplies the reactive power demand of the motor at almost each operating frequency, therefore the motor line voltage and currents are almost sinusoidal at each operating frequency of operation. The drive also employs PWM techniques to control both front-end and converter, motor-end inverter. The steady state and transient performance of the drive are investigated experimentally and determined analytically in open and closed loops.

The modified self-commutating current source inverter consists of two converters connected through d.c.link inductor. The front-end converter is a three-phase pulse width modulated converter and acts as a current source with d.c.link current feedback. It provides a controllable d.c. link current. Equal pulse width modulation technique is employed to control the output of the front-end converter and input power factor. The other converter at load end is a three-phase pulse width modulated current source inverter.

At the terminals of the inverter three-phase capacitor bank is connected. Space vector PWM technique is employed in the current source inverter.

In the CSI-fed induction motor, air gap flux saturates at a very low value of slip; motor can not be operated in this region because of excess iron loss. To operate the machine at a normal value of air gap flux, the motor is operated in statically unstable region of torque-slip characteristics. Hence closed loop operation of the drive is mandatory. The closed loop operation is also required for fast and stable operation of the drive as well as better speed regulation. The closed loop scheme employs two PI controllers, one in outer speed feed back loop and other in inner current feed back loop. The outer speed controller compares the reference speed and actual rotor speed and processes the speed error to obtain the reference slip speed. The reference slip speed is used to obtain the reference stator active and reactive currents and hence the reference d.c.link current. The speed PI processing is done at every 10 ms. The speed PI controller makes the steady state speed error zero. The inner current PI controller processes the current error in reference d.c.link current and actual d.c.link current and adjusts the turn on period of PWM pulses and hence the output voltage of the converter. The inner current PI processes the current error at every 1 ms. The synchronous speed of the machine is obtained by adding the actual rotor speed and the reference slip speed. The synchronous speed decides the operating frequency of the inverter and the number of switching of the devices over a cycle for the PWM operation of the inverter. At low and medium values of the switching frequencies the number of switching of the devices per cycle are more as compared to the high values of the switching frequencies.

The mathematical modeling of the complete drive system has been developed in synchronously rotating q^e- d^e reference frame. Modeling of the complete drive system has been done considering certain assumptions. This mathematical model is developed in terms of the machine parameters and the value of capacitance per phase connected across machine terminals. The developed mathematical is used later to design the parameters of speed and current PI controllers. The steady state performance characteristics of the drive are determined by computing the various parameters such as torque, slip, power factor, power output, power loss, stator voltage, stator current, efficiency and d.c.link voltage. The steady state performance characteristics are drawn with respect to torque. The performance characteristics of the drive is determined for the different operating conditions, namely (i) fixed frequency, constant d.c. link current, variable capacitance per phase (ii) variable frequency, constant d.c. link current, fixed capacitance per phase (iii) variable d.c. link current, fixed frequency, fixed capacitance per phase (iv) constant load torque, fixed capacitance per phase, fixed d.c. link current (v) linearly varying load torque, fixed capacitance per phase, fixed d.c. link current. The value of capacitor to be connected across the machine terminals for the different operating conditions is determined by observing the steady state behavior of the drive at different values of capacitance connected across the machine terminals and its open loop performance investigated experimentally at different values of capacitance.

The steady state analysis shows that in the unstable region the efficiency of the drive is poor in comparison to the stable region at each operating condition. The power factor of the motor is unaffected by the values of capacitor connected across motor terminals. The phenomenon of resonance is observed in a definite frequency range of

operation. The performance of the drive is not described in the frequency range, where resonance is occurring.

The performance of the current source inverter depends upon the number of switching commands per cycle. As the number of switching commands increases per cycle, the output current of the PWM inverter is near to sinusoidal. But due to switching frequency limitations of the devices, nine switching commands per 90 degree is employed in a cycle at the low and medium values of the operating frequencies, i.e. from 5 Hz to 40 Hz, At high values of the operating frequencies, the five switching commands per 90 degree is employed in a cycle. The modulation index of the inverter also changes with the change in operating frequencies. Its minimum value is kept at 0.82 and the maximum value is limited to 1.0.

The Hall effect current sensor is used to sense the actual d.c.link current. A low pass R-C filter is used to filter the ripples from the output current. The actual speed of the machine is measured through the rotatory incremental type pulse encoder. The closed loop response of the drive depends upon the properly designed PI controller parameters of the speed and the current feed back loop. The D- partitioning technique is applied for designing of the speed and current controller parameters. This technique is based on the linearized characteristic equation in terms of the controller parameters. The mathematical model of the developed drive in $q^e - d^e$ reference frame is highly non-linear. Therefore to design the controller parameters using D – partitioning technique, the system equations are linearized around a steady state operating point by applying small perturbation theory. The current loop is designed first because the current loop is faster than the speed loop. While designing the parameter of the current loop, the perturbation in the speed is

neglected. Once the parameters of the current loop are finalized, designing of the parameters of the speed controller loop is done. The linearized characteristic equations of the current and the speed loop are used to plot the stability curves in the parametric plane. By shading the D – partition contours the most probable stable region is found in each case. A point check for the stability of this most probable region is carried out by frequency scanning technique and by selecting the parameters from this region. For fast and stable operation of the drive, the D- partition curves are plotted for different values of degree of stability (σ) and damping ratio (ξ), and the parameters are selected from the region having higher degree of stability and good damping ratio. The final selection of the current and speed PI controller parameters of both the loops are carried out by determining the transient response of the drive for 5% change in reference current and speed respectively. The system equations are expressed in terms of state variables to obtain the transient response of the current loop and the complete drive system.

The proto-type model of modified self-commutating current source inverter fed induction motor drive is developed for 1 HP induction machine. The designed parameters of the PI controllers obtained from the D- partitioning technique are incorporated to operate the drive in closed loop manner. The control of the drive system is implemented through the PC- AT computer based system based on 8088 microprocessor. Control implemented through the personal computer reduces the hardware complexity to a great extent and makes the system fast controllable, more reliable and more flexible. To implement different control schemes only software has to be changed, no change in hardware is required. The hardware of complete system includes a three phase pulse width modulated converter at the front- end, a three phase PWM inverter at motor-end, an 8031 microcontroller based system, zero crossing detection circuit, pulse amplification

circuit for the converter and inverter devices and necessary hardware for d.c.link current and speed measurement. Three phase PWM converter acts as a current source and it employs self- commutating devices (MOSFETS) in the upper legs and line commutated devices (thyristors) in the lower legs. The firing pulses for the front- end converter is generated through the 8031 micro controller. Six zero crossing signals are required each at 60° for synchronization of firing pulses of the converter. The actual speed of the induction motor is measured through the rotatory incremental pulse type encoder The d.c.link current is measured through Hall effect current sensor and it is digitized through 12 bit ADC. Use of 12 bit ADC increases the resolution. Both the PI processing is implemented through software. The complete software for open and closed loop operation of the drive is written in C language. The software for the operation of the drive in open and closed loop consists of main program, interrupt service subroutine for zero crossing signal program, serial subroutine program, initialization of port and timer subroutine, open loop program, speed and current PI processing subroutine program, closed loop program. The software enables the implementation of change in pulse widths of the firing pulses of the converter depending upon the load requirement and hence controls the output voltage of the converter. The slip regulator characteristics are stored in the memory of the personal computer, which makes the implementation of the slip regulator fast. The synchronous speed, obtained by adding the actual rotor speed and reference slip speed, decides the operating frequency of the inverter and hence the number of switching commands for the PWM operation of the inverter. The PWM firing pulses of the current source inverter is generated through the personal computer using ADD-ON card.

The performance of the three phase current source and three phase PWM inverter is checked by recording the various current and voltage waveforms of the control and

power circuit. The closed loop operation of the front-end converter maintains the d.c.link current at a set value. The actual waveforms of the converter input voltage and current, voltage across load, load current at the different duty cycles are recorded and it is found that converter input displacement factor is almost unity at different duty cycles. The actual waveform of the motor line voltages, line currents, inverter line current, d.c.link current and voltage, at the different value of the operating frequencies are recorded under steady state condition. The actual motor line voltages, line currents waveforms are also recorded without having any capacitance at the machine terminals, at an operating frequency 10 Hz, under steady state condition. The recorded line current and voltage waveforms of the motor show that, the harmonics in the output currents and voltages in presence of capacitor at the motor terminals are quite less than the harmonics present without any capacitance at the motor terminals. The output current and voltage waveforms are almost sinusoidal at each value of operating frequency in presence of capacitor at the machine terminals. An exhaustive experimentation has been carried out in open and closed loop to obtain the performance characteristics of the drive. The experimentally obtained performance characteristics are compared with analytically obtained performance characteristics. Both the performance characteristics are found to be very close to each other, thus justifying the mathematical model of the drive. The transient performance of the drive is investigated by recording the speed and d.c.link current for step change in reference speed. The transient performances obtained experimentally are compared with the analytically obtained performance characteristics. Both the characteristics are almost matching, hence justifying the designed controller parameters.

The proposed drive is designed and developed in the laboratory. The mathematical model of the drive has been developed in synchronously rotating reference d- q frame. The steady state analysis of the drive is carried out for different operating conditions. The drive is operated in closed loop using PI controller in speed and current both the loops. The control of the drive is implemented using 8088 microprocessor and 8031 microcontroller. The controller parameters are designed using D- partitioning technique, followed by frequency scanning. The steady state performance of the drive is investigated experimentally and verified by the analytical performance obtained through simulation. The transient performance of the drive is also determined experimentally, using designed value of the controller parameters and it is verified analytically. The performance of the developed drive is investigated experimentally.

The experimental results are almost matching with the analytical results obtained from simulation. The line currents and line voltages of the motor are found to be sinusoidal at each operating frequency. Therefore the performance of the developed drive is found to be satisfactory.

8.2   SCOPE FOR FURTHER WORK

The steady state analysis and transient performance of the modified self–commutating CSI-fed induction motor drive obtained analytically are in good agreement with the experimentally investigated results. However, certain gaps are observed which needs to be fulfilled for the improvement of the drive performance. The steady state and transient analysis of the drive can be carried out by considering the modeling of the power semiconductor devices, ripples in d.c.link current, saturation effect. The PI parameters of the current controller and speed controller are designed in continuous data

system. Since the implementation of the control has been done through the personal computer and the speed and current PI processing have been done at the predetermined instants of the supply period, therefore the controller parameters need be designed in the sampled data system.

The phenomenon of resonance is observed at some values of the operating frequency, at the chosen value of capacitor at the machine terminals, hence experimentation has not been possible in the entire operating region. Further research is required to avoid the resonance from the operating frequency region at the chosen value of capacitance at the terminals of the machine, so that the operation of the drive could be possible in the entire operating frequency region.

In the present work micro controller is used for the generation of firing pulses to the converter, this could be replaced by the fast processor such as DSP for entire processing.

The PI controllers are used in both the feed back loops for drive implementation. Fuzzy and ANN based control techniques may be used for the drive implementation.

1. Ward Leonhard, "Electric drives universal energy converters", Semens Review, pp. 32-37, 4/89.

2. R.G. Schieman, E.A. Wilkes and H.F. Jordan, "Solid state control of electric drives", IEEE Proceedings, Vol. 62, No. 12, pp. 1643-1660, Dec. 1974.

3. B.K. Bose, "Power electronics – An emerging technology", IEEE Transactions on Industrial Electronics, Vol. IE-36, No. 3, pp. 403-412, 1989.

4. G.K. Dubey, "Power semiconductor controlled drives", (Book), Prentice Hall, New Jersey, 1989.

5. J.M.D. Murphy, "Thyristor control of AC motors", Pergamon Press Ltd., 1973.

6. B.L. Jones and J.E. Brown, "Electrical variable speed drives", IEE Proc. Vol. 131, Pt. A, No. 7, pp. 516-558, Sept. 1984.

7. B.K. Bose, "Adjustable speed a.c. drives – A technology status review", IEEE Proceeding, Vol. 70, No. 2, pp.116-135, February 1982.

8. W. Leonhard, "Control of electrical drives", Springer-Varlag Barline Heidelberg, 1985.

9. Nelson and Radomski, "Induction motor drive systems", IEEE Trans. on IECI, pp. 141-145, May1975.

10. D. Finney, "Variable frequecy a.c. motor drive systems", Peter Peregrinus Lt., London, 1988.

11. J.M.D. Murphy and F.G. Turnbull, "Power electronic control of a.c. motor", Pergamon Press, 1988.

12. T.H. Borton, "Variable frequency variable speed ac drives", Electric Machines and Power Systems, pp. 143-163, 1987.

13. W. Leonhard, "Adjustable speed a.c. drives", IEEE Proc. Vol. 76, no. 4, pp. 455-471, April 1988.

14. R.M. Davis, "Power diode and thyristor circuits", (Book), Peter Peregrinus Ltd., 1988.

15. V. Subramanyam, "Thyristor control of electric drives", (Book), Tata McGraw-Hill Publishing Company Ltd., New Delhi, 1992.

16. E.E. Ward, "Inverter suitable for operation over a wide range of frequency", IEE Proc. Vol. 111, pp. 1423-1434, August 1964.

17. W. Lienau, A. Muller-Hellmann and H.C. Skudelny, "Power converters for feeding asynchronous traction motors of single-phase AC vehicles", IEEE Trans. on Industry Applications, Vol. IA-16, No. 1, pp. 103-110, Jan/Feb 1980.

18. S. Suzuo, T. Nakagawa, A. Hirata and M. Miyazaki, "New application of current-source type inverter", IEEE Trans. on Industry Applications, Vol. 20, pp. 226-235, Jan/Feb 1984.

19. P.D. Ziogas, S. Manias and E.P. Wiechman, "Application of current source inverters in UPS system", IEEE Trans. on Industry Applications, Vol. 20, pp. 742-752, July/Aug. 1984.

20. A.K. Chattopdhayaya , " Current source inverter fed induction motor drive- A status of the art research review", Journal of Institution of Electronis and Telecommunication Engineers, vol.37, No. 1, pp. 34- 44 1991.

21. K.P. Phillips, "Current source converter for A.C. motor drive", IEEE Trans. (IA), Vol. 8, No. 6, pp. 679-683, Novl/Dec 1972.

22. W. Farrer and J.D. Miskin, "Quasi-sine wave fully regenerative inverter", IEEE Proc., Vol. 120, pp. 969-976, Sept. 1973.

23. H.B. Brennen, "Comparative analysis of two commutation circuits for adjustable current input inverter feeding induction motor", IEEE-PESC Record, pp. 201-212, 1973.

24. G.R. Slemon and S.B. DEWAN, "Induction motor drive with current source inverter", IEEE – IAS 9 th Annual Meet Conference Record, Pt. I, pp. 411- 417, Oct. 1974.

25. G.N. Revankar ,S.K. Pillai , M.C.Srisailm ,Y.R. Shah and J. Zoha " Effect of feed inductance on current source inverter operation", Journal of the Institution of Electronics and Telecommunication Engineers, vol.28, pp. 30 –34 , Jan.1982

26. F.W. Fuchs and A.M. Callmann, "Control methods for reducing the inductance in the d.c. link of current source inverter", IEEE Trans. on Industry Applications, Vol. 19, pp. 699-707, Sept./Oct. 1983.

27. K. Venkatesan and J. Lindsay, "Comparative study of the losses in voltage and current source inverter fed induction motors", IEEE Trans. on Industry Applications, Vol. 18, No. 3, pp. 240 -246, May/June 1982.

28. T.A. Lipo, "State-variable steady- state analysis of a controlled current induction motor drive", IEEE Transactions on Industry Applications, Vol. IA-11, No.6, pp. 705-712, Nov/Dec 1975.

29. N. Sawaki and N.Sato, "Steady-state and stability analysis of induction motor driven by current source inverter", IEEE Transactions on Industry Applications, Vol. IA-13, No. 3, pp. 244-251, May/June 1977.

30. M. Macdonald and P.C. Sen, "Control loop study of induction motor drives using dq model", IEEE Transactions on Industrial Electronics and Control Instrumentation, Vol. IECI-26, No. 4, pp. 237-243, Nov. 1979.

31. A. Joshi and S.B. Dewan, "Modified steady-state analysis of the current-source inverter and squirrel cage motor drive", IEEE Transactions on Industry Applications, Vol. IA-17, No. 1, pp. 50-57, Jan / Feb 1981.

32. B. Singh, K.B. Naik and A.K. Goel, "Steady state analysis of an inverter-fed induction motor employing natural commutation", IEEE Transactions on Power Electronics, Vol. 5, No. 1, pp.117 –123, January 1990.

33. J.H. Song, T.W. Yoon, K.H. Kim, K.B. Kim and M.J. Youn, "Control loop study of a load commutated CSI-fed induction motor", IEE proc.-B, Vol. 139, No.3, pp. 183-190, May 1992.

34. P. Agarwal and V.K. Verma, "Performance evaluation of current source inverter-fed induction motor drive", Journals of Institution of Engineers, Vol.72, pp. 209-217, February 1992.

35. E.P. Cornell, and T.A. Lipo, "Modelling and design of controlled current induction motor drive system", IEEE Trans. (IA), Vol. 13, July/Aug. 1977, pp. 321-329.

36. J. Holtz and W. Reese, "Stability analysis of current fed inverter drive with air gap voltage feedback", Proc. ICEM , pp. 222-225, 1982.

37. A. Kawamura and R. Host, "Instantenous feedback controlled PWM inverter with adoptive hysteresis", IEEE Transactions on Industry Applications, Vol. IA-20, No.4, pp. 769-774, July/August 1984.

38. T.H. Chin, M. Nakaho and Y. Fuwa, "New PWM technique using a traingular carrier wave of saturable amplitude", IEEE Transactions Industry Applications, Vol. IA-20, No. 3, pp. 643-650, May/June 1984.

39. M. Hombu, S. Veda, A. Ueda and Y. Matsuda, "A new current source GTO inverter with sinusoidal output voltage and current", IEEE Transactions on Industry Applications, Vol. IA-21, No. 5, pp. 1192-1198, Sept /Oct 1985.

40. S. Nonka and Y. Neba, "New GTO current source inverter with pulse width modulation control techniques", IEEE Transactions on Industry Applications, Vol. IA-22, No. 4, pp. 666-672, July/Aug 1986.

41. A. Nabe, S. Ogasawara and H. Akagi, "A novel control scheme for current controlled PWM inverters", IEEE Transactions on Industry Applications, Vol. IA-22, No. 4, pp. 697-701, July/Aug 1986.

42. M. Hombu, S. Ueda and A. Ueda, "A current source GTO inverter with sinusoidal input and outputs", IEEE Transactions on Industry Applications, Vol. IA-23, No. 2, pp. 247-254, March/April 1987.

43. S. Nonka and Y. Neba, "Analysis of PWM GTO current source inverter-fed induction motor drive system", IEEE Transactions on Industry Applications, Vol. IA-23, No. 2, pp. 256-262, March /April 1987.

44. S.R. Bowes and R.I. Bullough, "Optimal PWM microprocessor controlled current-source inverter drives", IEEE proceedings, Vol. 135, Pt. B, No. 2, pp. 59-75, March 1988.

45. S. Nonka and Y. Neba, "A PWM GTO current source converter-inverter systems with sinusoidal inputs and outputs", IEEE Transactions on Industry Applications, Vol. 25, No. 1, pp. 76-84, Jan / Feb 1989.

46. P.N. Enjeti, P.D. Ziogas and J.F. Lindsay, "Programmed PWM technique to eliminate harmonics: A critical evaluation", IEEE Transactions on Industry Applications, Vol. 26, No. 2, pp. 302-315, March/April 1990.

47. T. Kataoka, K. Mizumachi, S. Miyari, "A pulse width controlled AC to DC converter to improve power factor and waveform of AC line current", IEEE transaction on Industry Applications, Vol. IA-15, No. 6, pp. 670-675, Nov /Dec 1979.

48. M.J. Kocher and R.L. Steigerwald, "An AC to DC converters with high quality input waveforms", IEEE Transaction on Industry Applications, Vol. IA-19, No. 4, July/August 1983.

49. N.R. Zargari, Y. Xiao and Bin Wu, "Near unity input displacement factor for current source PWM drives", IEEE Industry Applications Magazine, pp. 19 to 25, July/Aug. 1999.

50. Y. Xiao, B. Wu, S. Rizzo and R. Sotuden, " A Novel power factor control scheme for high power GTO current source converter" , Conference Record IEEE-IAS, pp. 865-869, 1996.

51. S.B. Han, N.S. Choi, C.T. Rim and G.H. Cho, "Modelling and analysis of static and dynamic characteristics of Buckt ype three phase PWM rectifier by circuit dq transformation", IEEE Transactions on Power Electronics, Vol.13, No. 2, pp. 323-336, March 1998.

52. T. Chin and H. Tomita, "The principles of eliminating pulsating torque in current source inverter induction motor systems", IEEE transactions on Industry Applications , vol. IA- 17, No.2, pp. 160 –166, Mar /Apr 1983.

53. J. Murphy and M. Egan, "A comparison of PWM strategies for inverter-fed induction motors", IEEE transactions on Industry Applications, Vol. IA-19, No. 3, pp. 363-368, May/June 1983.

54. M.A. Boost, P.D. Ziogas, "State-of-the-Art carrier PWM techniques: A critical evaluation", IEEE Transactions on Industry Applications, Vol. 24, No.2, pp. 271-280, March/April 1988.

55. D.G. Holmes, "A unified modulation algorithm for voltage and current source inverters based on ac-ac matrix converter theory", IEEE Transactions on Industry Applications, Vol. 28, No. 1, pp. 31-40, Jan/Feb 1992.

56. L.H. Walker and P.M. Espelage, "A high-performance controlled-current inverter drive", IEEE Transactions on Industry Applications, Vol. IA-16, No. 2, pp.193-202, Mar /Apr 1980.

57. T. Konishi, K. Kamiyama and T. Ohmae, " A performance analysis of microprocessor- based control systems applied to adjustable speed motor drives", IEEE Transactions on Industry Applications, Vol. IA-16, No.2, pp. 378-386, May/June 1986.

58. K. Kumbo, M. Watnabe, T. Ohmae and K. Kamiyama, "A Software based speed regulator for motor drives", International Power Electronics conf. Ref., Tokyo, pp. 1500-1511, 1983.

59. A.J. Pollman, "Software pulse width modulation for μp control of AC Drives", IEEE Transactions on Industry Applications Vol. IA-22, No. 4, pp. 691-696, July/Aug1986.

60. G. Chen, "Single chip micro computer based current source inverter", Electric machines and Power system, pp. 49-57, 1989.

61. P.Agarwal and V.K.Verma , "Microprocessor based firing pulse generator for PWM current source inverter", Journal of Institution of Engineers vol .71 , 1992

62. W.L. Fredrich and K.S. Swenson, "Microprocessor based converter firing pulse generator", IEEE Transactions on Industrial Electronics, Annual Meeting, pp. 439-445, 1982.

63. S. Bolojnani and G.S. Buja, "Control system design of a current inverter induction motor drive", IEEE Transaction on Industry Applications, Vol. IA-21, No. 5, pp. 1145 –1152 , Sept /Oct 1985.

64. R. Prakash and S. Vittal Rao, "Robust control of a CSI-fed induction motor drive system", IEEE Transactions on Industry Applications, Vol. IA-23, No. 4, pp. 610-616, July/Aug1987.

65. C.T. Pan and C.M. Liaw, "Design and implementation of an adaptive speed regulator for current source induction motor drive", IEEE Transactions on Energy Conversion, Vol. 4, No. 3, pp. 480-486, Sept. 1989.

66. N. Mutho, A. Ueda, K. Sakai, M. Hattori and K. Nandoh, "Stabilizing control methods for suppressing oscillations of induction motors driven by PWM inverters", IEEE Transactions on Industry Applications, Vol. 37, No. 1, pp. 48-56, February 1990.

67. S. Bolognani and G.S. Buja, "D.C. link current control for high-performance CSIM drives", IEEE Transactions on Industry Applications, Vol. IA-23, No. 6, pp. 1043-1047, Nov / Dec 1987.

68. E. Wernekinek, A. Kawammura and R. Host, "A high frequency AC/DC converter with unity power factor and minimum harmonic distortion", IEEE Transactions on Power Electronics, Vol. 6, No. 3, pp. 364-370, July 1991.

69. Y. H. Sang and B.H. Kwon, "A direct digital control for the phase-controlled rectifier", IEEE Transactions on Industrial Electronics, Vol. 38, No. 5, pp. 337-342, Oct. 1991.

70. K. Taniguchi, Y. Ogino and H. Irie, "PWM technique for power MOSFET inverter", IEEE Transaction on Power Electronics, Vol. 3, No. 3, pp. 328-334, July 1988.

71. Eric Persson, "Transient effects in applications of PWM inverters to induction motors", IEEE Transactions on Industry Applications, Vol 28, No. 5, pp. 1095-1101, Sept / Oct 1992.

72. Y. Iwaji and S. Fukuda, "A pulse frequency modulated PWM inverters for induction motor drives", IEEE Transactions on Industry Applications, Vol. 7, No. 2, pp. 404- 409, April 1992.

73. S. Nonka and Y. Neba, "Quick regulation of sinusoidal output current in PWM converter inverter system", IEEE Transactions on Industry Applications, Vol. 27, No. 6, pp. 1055-1062, Nov / Dec 1991.

74. B. Wu, G.R. Slemon and S.B. Dewan, "PWM-CSI induction motor drive with phase angle control", IEEE Transactions on Industry Applications, Vol.27, No. 5, Sept /Oct 1991.

75. B.K. Bose, "Evaluation of modern power semi conductor devices and future trends of converters", IEEE Transactions on Industry Applications, Vol. 28, No. 2, pp. 403-414, March/April 1992.

76. B. Wu, S.B. Dewan and G.R. Slemon, " PWM-CSI inverter for induction motor drives", IEEE Transactions on Industrial Applications, Vol. IA-28, No. 1, pp. 64-71, 1992.

77. G. Joos, G. Moschopoulos and P.D. Ziogas, " A high performance current source inverter", IEEE Transactions on Power Electronics", Vol. 8, No. 4, pp. 571-578, Oct. 1993.

78.   J. Holtz, W. Lotzkat, A.M. KhambadKone, "On continuous control of PWM inverters in the over modulation range including the six step mode", IEEE Transactions on Power Electronics, Vol. 8, No. 4, pp. 546-543, Oct. 1993.

79.   G. Narayanan and V.T. Ranganathan, "Sychronisation PWM strategies based on space vector approach part 1: Principles of waveform generation", IEEE Proceedings, Electric Power Applications, Vol. 146, No. 3, pp. 2657-275, 1999.

80.   G. Narayanan and V.T. Ranganathan, "Synchronized PWM strategies based on space vector approach Part 2: Performance assessment and application to V/f drives", IEEE Proceedings, Electric Power Applications, Vol. 146, No. 3, pp. 276-281, 1999.

81.   C.B. Jacobina, A.M.N. Lima and E.R.C. da Silva, "PWM space vector based digital scalar modulation", Power Electronics Specialist Conference PESC' 97, Record 28th Annual IEEE proceedings, Vol. 1, pp. 606-611, 1997.

82.   S.R. Bowes, Y.S. Lai, "The relationship between space-vector modulation and regular sampled PWM", IEEE Transactions on Industrial Electronics, Vol. 44, No. 5, pp. 670-679, Oct. 1997.

83.   H.R. Karshenas, H.A. Kojori and S.B. Dewan, "Generalised techniques of selective harmonic elimination and current control in current source inverters/converters", IEEE Transactions on Power Electronics, Vol.10, No. 5, Sept. 1995.

84.   Holmes, D. Grahame, "Significance of zero space vector placement for carrier based PWM schemes", IEEE Transactions on Industrial Applications, Vol. 32, No. 5, pp. 1122-1129, Sept / Oct 1996.

85. R. Carbone, D. Menniti, R.E. Morrison and E. Delaney, "Harmonic and inter harmonic distortion in current source type inverter drives", IEEE Transactions on Power Delivery, Vol. 10, No. 3, pp. 1576-1583, July 1995.

86. Rizzo, Steven C; Wu, Bin; Sotuden, Reza, "Symmetric GTO and snubber component characterization in PWM current sources inverters", IEEE annual Power Electronics Specialists Conference, vol .1, pp. 613- 619,1996.

87. P.A. Dahono, T. Kataoka, Y. Sato, "Dual relationship between voltage-source and current source three-phase inverters and its application", International conference on Power Electronics and Drive Systems proceedings, Vol. 2, pp. 559-565, May 1997.

88. Ide, Kozo; Tanaka, Takash; Yang, Zi-Jiang, Tsuji, "Simple adaptive control with exact linearization for CSI-fed induction motor, Proceedings of the 1995, IECON Proc., vol.1, IEEE, Los, 1995.

89. J.A. Pomilio, Leopoldo Rossetlo, P. Tenti, P. Tomasin, "Performance improvement of soft-switched PWM rectifiers with inductive load", IEEE Transactions on Power Eectronics, Vol. 12, No. 1, pp. 153-160, January 1997.

90. I. Omura and W. Fichtner, "Numerical study of reverse blocking switching devices in current source", Proceedings of the, 9th International symposium on power semi conductor devices and ICs, ISPD ,1997.

91. J.R. Espinoza and G. Joos, "Current-source converter on-line pattern generator switching frequency minimization", IEEE Transactions on Industrial Electronics, Vol. 44, No. 2, pp. 198-205, April 1997.

92. J.R. Espinoza and G. Joss, "A current-source inverter-fed induction motor drive system with reduced losses", IEEE Transactions on Industrial Applications, Vol.34, No. 4, pp. 796-805, July/Aug. 1998.

93. Y. Yin and A. Y. Wu, "A low-harmonic electronic drive system based on current source inverter", IEEE Transactions on Industrial Applications, Vol. 34, No. 1, pp. 227-235, Jan./Feb. 1998.

94. B. Wu, S.B. Dewan and G.R. Slemon, "PWM-CSI inverter for induction motor drives", IEEE Transactions on Industrial Applications, Vol. IA-28, No. 1, pp. 64-71, 1992.

95. Ashish Bendre, Ian Wallace, Jonathan Nord and Venkatran Giri, "A current source PWM inverter with actively commutated SCRs", IEEE Transactions on Power Electronics, Vol. 17, No. 4, pp. 461-468, July 2002.

96. Y. Xiao, B. Wu, S. Rizzo and R. Sotuden, " A Novel power factor control scheme for high power GTO current source converter", Conference Record IEEE-IAS, pp. 865-869, 1996.

97. S.R. Bowes and S. Grewal, "Novel harmonic elimination PWM control strategies for three phase PWM inverters using space vectors techniques", IEEE Proceedings Electric Power Applications, Vol. 146, pp. 495-514, Sept. 1999.

98. E. Cengelchi, S.U. Sulistijio, B.O. Woo, P. Enjeti, R. Tedo rescu and F. Blaabjerg, "A New medium-voltage PWM inverter topology for adjustable – speed drives", IEEE Transactions on Industry Applications, Vol. 35, No. 3, pp. 628-636, May/June 1999.

99. M.P. Kazmicrkenski and Luigi Malesani, "Current control techniques for three-phase voltage-source PWM converters: A survey", IEEE Transactions on Industrial Electronics, Vol. 45, No. 5, Oct. 1998.

100. S.Chakrabarti, M. Ramamoorthy and V.R. Kanetkar , "Reduction of torque ripplesin direct torque control of induction motor drives using space vector

modulation base pulse width modulation", Power Electronics and Drives System Proc., Vol.1, pp. 117-121, May 1997

101. P.C. Loh, D.G. Holmes, "A variable based universal flux/change modulator for VSI and CSI modulation", 36th IAS Annual meeting – Conference record of Industrial Applications, Vol. 2, pp. 999-1006, 2001.

102. M.S. Abu Khaizaran, H.S. Rajamani, P.R. Palmer, "The high power IGBT current source inverter", 36th IAS Annual meeting-conference record of the Industrial Applications, Vol. 2, pp. 879-885, 2001.

103. G. Amler, "A PWM current source inverter for high quality drives", EPE Journal, Vol. 1, ISS.1, pp. 21-30, July1991.

104. J.F.Martins, J.F.Silva and A.J. Pires, " A novel and simple current controller for three phase IGBT PWM Power inverters" , IEEE Transactions on Industrial Electronics, Vol.45, No.5, pp. 802-804, Oct 1998

105. G. Kim, I. Ha and M. Ko, "Control of induction motors for both high dynamic performance and high efficiency", IEEE Transactions on industrial electronics, Vol. IE-39, pp.323-333, Aug. 1992.

106. J.G. Deland, V.E. McCrormick and M.W. Turner, "Design of Efficiency Optimization Controller for inverter fed ac induction motors", Proceedings IAS, pp. 16-21, 1995.

107. C.B.Jacobina, A.M.Lina and E.R.C.D da Silva, " PWM space vector based in digital scalar Modulation" Power Electronics Specialist System Conference 1997, PESC'S 97 Record 28 th Annual IEEE Vol, pp. 606-611, 1997

108. D.C. Lee, D.H. Kim and D.W. Chung, "Control of PWM current source converter and inverter system for high performance induction motor drives", 22nd

International Conference on Industrial Electronics, Control and Instrumentation, Vol. 2, pp. 1100-1105, 1996.

109. A Dakir, R. Barlik, M. Novak and P. Grochal, "Computer simulations for two angular speed control system of a current source inverter feeding and induction machine", Proceedings of the IEEE International Symposium on Industrial Electronics, pp. 940-945, Vol. 2, 1996.

110. Yen-Shin Lai and S.R.Bowes, " A novel high frequency universal space vector modulation control technique", International conference on Power Electronics and drive system, Proc., Vol.1, pp.117-121, May 1997

111. D.W. Novotny and R.D. Lorentz, "Introduction to field orientation and high performance ac drives", Tutorial course presented at IEEE Industry Application Society Annual Meetings, 1985.

112. C.C. Chan, K.T. Chau, Y. Li and D.T.W. Chau, "A Unifield analysis of d.c. link current in space-vector PWM drives", International Conference on Power Electronics and drive system proceedings, Vol. 2, pp. 762-768, June 1997.

113. N. Mohan, T.M. Underland and W.P. Robbins, "Power Electronics: Converters, Applications and design", John wiley and Sons Publications, 1994.

114. M.H. Rasid, "Power electronics circuit devices and applications"(Book), Prentice Hall Publications, 1993.

115. A.M. Hava, R.J. Kerkman, T.A. Lipo, "Simple analytical and graphical tools for carrier based PWM methods", IEEE Transactions on Power Electronics, Vol. 14, No. 1, pp. 49-61, Jan. 1999.

116. S. Chakrabarti, M. Ramamoorthy, V.R. Kanetkar, "Reduction of torque ripple in direct torque control of induction motor drives using space vector modulation

based pulse width modulation", Conference on Power Electronics and drive systems, Proceeding, Vol. 1, pp. 117-121, 1997.

117. S. Vaiz and M.A.Rahman, "Adaptive loss minimization control of inverter-fed IPM motor drives", 28th Annual Power Electronics, Specialist Conference, Vol. 2, pp. 861-868, June 1997.

118. S.M.R. Sadriyeh, M.R. Zolghadri and J. Mahadevi, "Application of a current source inverter for a linear Piezoelectric step", Proceedings of the International Conference on Power Electronics and drive 2001.

119. M.R. Stojic, "Design of the microprocessor based digital system for d.c. motor speed control", IEEE Transaction on Industrial Electronics, Vol. 31, No. 3, pp. 245-248, Aug. 1988.

120. H.C. Wang, "Sampling period and stability analysis for the microcomputer based motor control systems", IEEE Transaction on Industrial Electronics and control instrumentation Vol. 28, No. 2, pp. 98-102, May1981.

121. P. Agarwal, and V.K. Verma, "Parameter plane synthesis of variable speed d.c. motor drive", Electrical Machines and Power Systems, pp. 57-68, Vol. 1987.

122. J. Nanda, "Analysis of steady state stability of a two machine system by the D-Decomposition technique", IEEE Transaction of Power Apparatus and System, Vol. 90, pp. 1848-1855, July/Aug. 1971.

123. M.A. Aizerman, "Theory of Automatic Control", Pergamon pren, New York, 1963, Chapter-3.

124. Siljack, D.D., "Non Linear Systems : The parameter analysis and design", Johnwiley and Sons., U.S.A., 1969.

PARAMETER PLANE SYNTHESIS METHOD

Any control system is said to be stable, if for any small disturbance in the steady state condition of the system, it restores steady state operating condition which it was having before the occurrence of the disturbance. For a linear system, if the system is stable for small disturbance, than it is stable for any disturbance. The necessary and sufficient condition for the stability of a linear control system is that all the real roots of the characteristic equation of the system, must be negative while the complex roots of the characteristic equation should have a negative real part.

The conventional control techniques, normally used in the control systems such as Routh. Harwitz's criterion, Nyguist method and root locus are used to study the effect of only one parameter on the effect of system performance. D-partition method [121, 122] an improved technique is used to study the effect of two parameters on the control system on stability and transient performance. with regard to stability analysis, the method provides a possibility of defining the relative stability of control system with the roots of the characteristic equation lying within a specified p- plane contour of general shape. The p plane with the two adjustable parameters as coordinate axis is termed as 'parameter plane'. The parameter plane method can also be extended in case of non-linear and sample data system.

PARAMETER MAPPING

Parameter plane method is based on mapping procedure that transform points from the complex p (σ, ω) plane to the parameter γ-δ plane. Considering a general mapping of nth degree algebraic equation.

$$D(p) = a_0 p_0 + a_1 p_1 + a_2 p_2 + \dots\dots\dots\dots\dots\dots\dots\dots\dots + a_n p_n = 0$$

where,

$\quad$ p is a complex variable defined as $p = -\sigma + j\omega$

and $\quad a_0 \dots\dots\dots a_n$ are $\quad$ the function of two real parameters γ, δ i.e.

$$a_k = a_k(\gamma, \delta) \qquad k = 0,1,2,3,4,\dots\dots\dots\dots\dots.n$$

If for a given pair of number (σ_1, ω_1) there corresponds a pair of parameter (γ_1, δ_1). So that the mapping equation $D(p) = 0$ is satisfied, then for γ_1 and δ_1, the equation has a root pair.

$$p_1 = -\sigma_1 + j\omega_1$$

Therefore, the defined mapping can be regarded as a transformation of the points (σ, ω) for the complex p-plane, which represent the root values of the algebraic equations where $D(p) = 0$, to certain points of parameters of γ - δ plane. The same theory is applicable to other complex plane defined as $p = -\xi\omega_n + j\omega_n \sqrt{1-\xi^2}$ in (ξ, ω_n) plane.

Consider that the two parameters γ, δ entering linearly into the characteristic equation so that the characteristic equation can be reduced to the form.

$$D(p) = \gamma S(p) + \delta Q(p) + R(p) \qquad\qquad (A.1)$$

Substituting $p = -\sigma + j\omega$, in equation (A.1)

$$D(-\sigma + j\omega) = \gamma S(-\sigma + j\omega) + \delta Q(-\sigma + j\omega) + R(-\sigma + j\omega) \qquad (A.2)$$

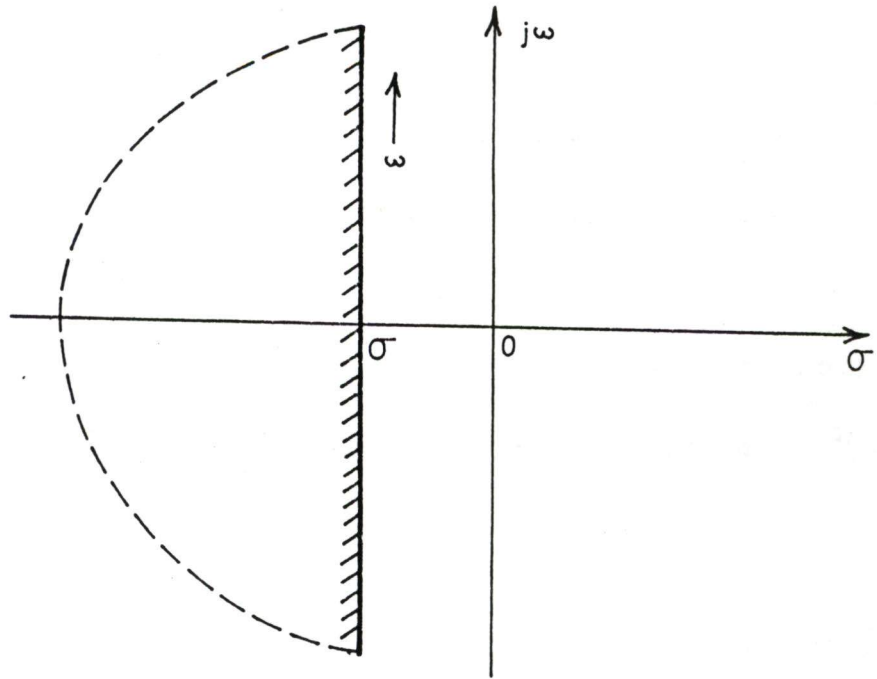The equation (A.2) is a function of σ, ω, γ, δ and can be expressed as:
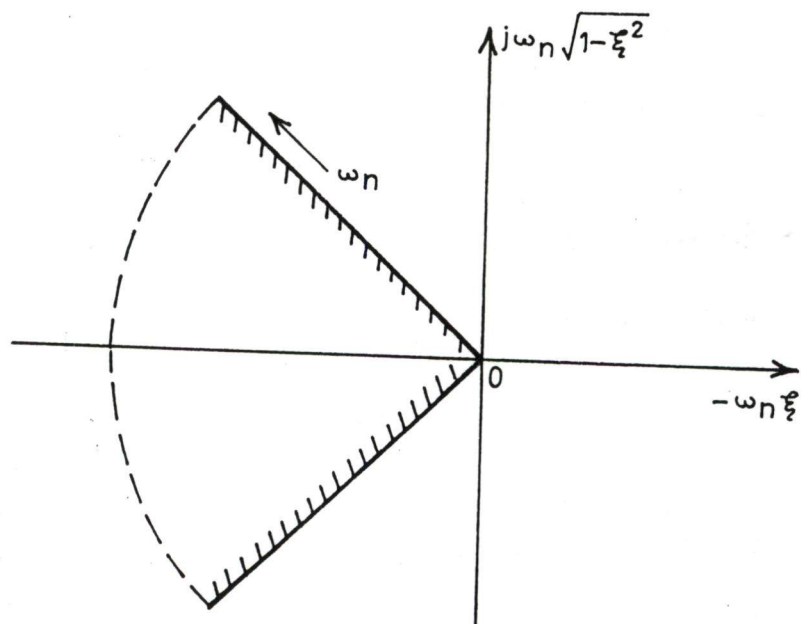
Fig. A.1. p-Plane contour for constant σ.

Fig. A.2. p-Plane contour for constant ξ.

$$U(\sigma, \omega, \gamma, \delta) + j\, V(\sigma, \omega, \gamma, \delta) \;=\; 0 \tag{A.3}$$

Separating the real and imaginary parts of the above equation results in.

$$U(\sigma, \omega, \gamma, \delta) \;=\; 0 \tag{A.4}$$

$$V(\sigma, \omega, \gamma, \delta) \;=\; 0 \tag{A.5}$$

For the determination of D-partition boundary, the value of γ, δ is required for each value of ω, therefore, separating the term containing γ, δ. Results in the following equations.

$$U(\sigma, \omega, \gamma, \delta) \;=\; \gamma\, S_1(\sigma, \omega) + \delta\, Q_1(\sigma, \omega) + R_1(\sigma, \omega) = 0 \tag{A.6}$$

$$V(\sigma, \omega, \gamma, \delta) \;=\; \gamma\, S_2(\sigma, \omega) + \delta\, Q_2(\sigma, \omega) + R_2(\sigma, \omega) = 0 \tag{A.7}$$

Solving A.6, A.7 for the determination of γ, δ, for each ω give.

$$\gamma = \frac{Q_1 R_2 - Q_2 R_1}{S_1 Q_2 - S_2 Q_1} \tag{A.8}$$

$$\delta = \frac{S_2 R_1 - S_1 R_2}{S_1 Q_2 - S_2 Q_1} \tag{A.9}$$

Equation (A.6) and (A.7) give one value of γ, δ as given by (A.8) and (A.9) for each ω, only if they are linearly independent.

If for any value of ω, say ω_c, the numerator and denominator becomes, zero, then for this value of ω, the two equations are linearly dependant to each other and a straight line is obtained in the γ - δ plane. This line is known as a spatial line. In this case, any of the two equation (A.6) and (A.7) is the equation of straight line, this value of ω, is

substituted. If the coefficient of the highest term of the characteristic equation depends on the parameter γ, δ, then by equating this coefficient to zero a spatial line at $\omega = \infty$ is obtained. Similarly a similar line at $\omega = 0$ is obtained by equating the coefficient of the lowest (free) term of the characteristic equation to zero.

In order to find the number of roots in the various regions obtained in the parameter plane by the plotted boundaries it is necessary to know whether a root is leaving or entering the p-plane contour as shown in Fig. (A.1) and (A.2) at the instant that point goes over a boundary in the parameter plane. In order to know whether the roots are leaving on entering the p-plane contour, the boundary to be shaded is determined according to sign of the denominator of Δ where $\Delta = S_1 Q_2 - S_2 Q_1$.

Facing the direction in which ω is increasing the boundary curve in the γ - δ plane is shaded on the left side if $\Delta > 0$ and on the right side if $\Delta < 0$. Usually, the curve is traversed twice, once when ω goes from $-\infty$ to 0 and next when it changes from 0 to $+\infty$. It is shaded both the times on the same side, as the sign of Δ changes with change in sign of ω (Δ is an odd function of ω). After the complex root boundaries are shaded, the spatial lines (for $\omega \neq 0$ or ∞) are simply oriented in accordance with the shading of complex boundaries. The shading of such a spatial line must be done twice on the same side as that on the complex root boundary at their point of intersection. The spatial lines at $\omega = 0$ and $\omega = \infty$ are also shaded with this rule but they are shaded only once. The root leaves the contour if it goes from a shaded region to the unshaded region and enters the contour if it goes from unshaded to shaded region. After the boundaries are appropriately shaded, the relative number of roots in each bounded region is easily determined. The region with maximum number of roots on the left side in the p-plane is established by

inspection of the plot. For ascertaining stable region a point in the region with maximum number of roots is selected and the stability of the system is checked by the Frequency Scanning Technique. If the system is stable at this point then this entire enclosed region is also stable region.

FREQUENCY SCANNING TECHNIQUE

The frequency scanning test is used to confirm the stability region, obtained from the parametric plane. Let $D(p) = 0$ be the characteristic equation of the system, where $D(p)$ may be polynomial in p or may include terms which are functions of p. Frequency trajectories which are the result of plotting the imaginary part of $D(j\omega)$ against its real part as frequency is varied from zero to infinity, are drawn. The frequency trajectory along with its mirror image is shaded on the left side for $\omega = -\infty$ to $\omega = \infty$. If the origin is contained in the inner-most region (in the sense of shading), the system is stable.

SPECIFICATIONS OF SYSTEM ELEMENTS

B.1 INDUCTION MOTOR SPECIFICATION

Vol. 400/230   connection : star/delta

H.P. : 1   phase 3

Frequency :   50 Hz

RPM   :   1400

B.2 INDUCTION MACHINE PARAMETERS

r_s = $3.52\ \Omega$

r_r = $2.78\ \Omega$

l_{ss} =   0.165 H

l_{rr} =   0.165 H

l_m =   0.15 H

J = $0.01289\ \text{kg-m}^2$

B.3 D.C. LINK PARAMETERS

r_f = $0.250\ \Omega$

l_f =   0.04 H

B.4 D.C. MACHINE SPECIFICATION

Volt   =   220 V   H.P. = 1

Current =   4A   RPM = 1500   Connection: shunt

B.5   DEVICE SPECIFICATIONS

(a)   THYRISTOR

Grade : Converter   PIV : 1200 V

Current : 16A

(b)   MOSFET

Voltage : 500 V

Current : 20/13 Amp

B.6   PROTECTION CIRCUIT SPECIFICATION

(a)   SNUBBER CIRCUIT FOR THYRISTOR

R   =   50 Ω, 5W

C   =   0.1 μF, 1 kW

(b)   SNUBBER CIRCUIT FOR MOSFET

R   =   33 Ω, 10 W

C   =   0.1 μf, 1 kW

B.7   CAPACITOR SPECIFICATION

Capacitance =   50 μF

Voltage   =   600 V

Type   =   Electrolytic